

GIScience and Geo-environmental Modelling

Biswajeet Pradhan
Pravat Kumar Shit
Gouri Sankar Bhunia
Partha Pratim Adhikary
Hamid Reza Pourghasemi *Editors*


Spatial Modelling of Flood Risk and Flood Hazards

Societal Implications


 Springer

GIScience and Geo-environmental Modelling

Series Editors

Biswajeet Pradhan , School of Information, System and Modelling, Building 11, University of Technology Sydney, Sydney, Australia

Pravat Kumar Shit, Postgraduate Department of Geography, Raja N. L. Khan Women's College, Autonomous, Midnapore, West Bengal, India

Gouri Sankar Bhunia , GIS, Randstad India Pvt Ltd, New Delhi, India

Partha Pratim Adhikary, Groundwater Management, ICAR Indian Institute of Water Management, Bhubaneswar, Odisha, India

Hamid Reza Pourghasemi, Resources and Environmental Engineering, Shiraz University, Department of Natural, Shiraz, Iran

The “GIScience and Geo-environmental Modelling” book series seeks to publish a broad portfolio of scientific books addressing the interface between geography and the environment. The aim of the book series is to present geospatial technology approaches to data mining techniques, data analytics, modeling, risk assessment, visualization, and management strategies. The series includes peer-reviewed monographs, edited volumes, textbooks, and conference proceedings. The focus of Geo-environmental is on geospatial modelling in the frontier area of earth-environment related fields, such as urban and peri-urban environmental issues, ecology, hydrology, basin management, geohazards, estuarine-ecology, groundwater, agriculture, climate change, land-water, and forest resources, and related topics.

Geo-environmental modelling techniques have enjoyed an overwhelming interest in recent decades among the earth environmental and social sciences research communities for their powerful ability to solve and understand various complex problems and develop novel approaches toward sustainable earth and human society. Geo-environmental modelling using data mining, machine learning, and cloud computing technology is focused on spatiotemporal data analysis and modeling for sustainability in our environment.

More information about this series at <https://link.springer.com/bookseries/16663>


Biswajeet Pradhan • Pravat Kumar Shit •
Gouri Sankar Bhunia •
Partha Pratim Adhikary •
Hamid Reza Pourghasemi
Editors

Spatial Modelling of Flood Risk and Flood Hazards

Societal Implications

Editors

Biswajeet Pradhan 
CAMGIS
University of Technology Sydney
Ultimo, NSW, Australia

Gouri Sankar Bhunia 
Geography
Seacom Skills University
Birbhun, India

Hamid Reza Pourghasemi
Department of Natural Resources
and Environmental Engineering, College
of Agriculture
Shiraz University
Shiraz, Iran

Pravat Kumar Shit
PG Department of Geography
Raja N. L. Khan Women's College
(Autonomous)
Midnapore, West Bengal, India

Partha Pratim Adhikary
Department of Groundwater
Management, ICAR – Indian Institute
of Water Management
Chandrasekharapur, Bhubaneswar,
Odisha, India

ISSN 2730-7506 ISSN 2730-7514 (electronic)
GIScience and Geo-environmental Modelling
ISBN 978-3-030-94543-5 ISBN 978-3-030-94544-2 (eBook)
<https://doi.org/10.1007/978-3-030-94544-2>

© The Editor(s) (if applicable) and The Author(s), under exclusive license to Springer
Nature Switzerland AG 2022

This work is subject to copyright. All rights are solely and exclusively licensed by the Publisher, whether the whole or part of the material is concerned, specifically the rights of translation, reprinting, reuse of illustrations, recitation, broadcasting, reproduction on microfilms or in any other physical way, and transmission or information storage and retrieval, electronic adaptation, computer software, or by similar or dissimilar methodology now known or hereafter developed. The use of general descriptive names, registered names, trademarks, service marks, etc. in this publication does not imply, even in the absence of a specific statement, that such names are exempt from the relevant protective laws and regulations and therefore free for general use.

The publisher, the authors and the editors are safe to assume that the advice and information in this book are believed to be true and accurate at the date of publication. Neither the publisher nor the authors or the editors give a warranty, expressed or implied, with respect to the material contained herein or for any errors or omissions that may have been made. The publisher remains neutral with regard to jurisdictional claims in published maps and institutional affiliations.

Disclaimer: The authors of individual chapters are solely responsible for the ideas, views, data, figures, and geographical boundaries presented in the respective chapters of this book, and these have not been endorsed, in any form, by the publisher, the editor, and the authors of forewords, preambles, or other chapters.

This Springer imprint is published by the registered company Springer Nature Switzerland AG
The registered company address is: Gewerbestrasse 11, 6330 Cham, Switzerland

*Dedicated to
Young Scholars in the field of Geomorphology
and Environment*

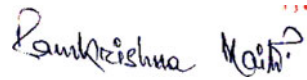
Foreword



I am happy to introduce this impressive volume on *Spatial Modeling of Flood Risk and Hazard: Societal Implication* edited by a group of hard-working geographers. This volume is the collection of excellent articles which are distributed in thirteen chapters and contributed by esteemed researchers. The articles are technically sound and put emphasis on the applications of GIS modeling and machine learning algorithms in predicting flood areas, their magnitude, and frequency. Contributors generated and assimilated huge data set in spatial modeling of floods in the river basins, understanding the role of humans in intensifying flood vulnerability, and examining community preparedness for flood and their long-practiced mitigation strategies. The articles are cautiously selected and carefully arranged by the editors in an orderly sequence that helps the readers to have a complete understanding on the topic covered.

Floods are the most effective formative events for landscape shaping or reshaping in a drainage basin depending on event size and distribution of magnitude frequency. Flood occurs when the input of water exceeds output from the river basin and storage capacity surpasses. Recently, global climate change and intensification of rain trigger high magnitude floods more frequently than before. Economically and socially marginalized people, especially those who live in third world countries suffer more out of this flood hazard. Millions of people in Bangladesh, India, and other South and Southeast Asian countries are internally displaced due to flood hazards.

From this perspective, the present effort is socially relevant and academically important in endorsing rigorous research pursuit, progressing geomorphic-hydrologic understanding, and fostering the applications of modern techniques to address the potential flood risk.

A handwritten signature in black ink, reading "Ramkrishna Maiti". The signature is written in a cursive style. To the right of the signature, there are three small red dots arranged in a horizontal line.

Prof. Ramkrishna Maiti
Department of Geography
Vidyasagar University
Midnapore, India

Preface

Floods and flash floods with hydrometeorological are the most devastating natural disasters causing massive damages to natural and man-made features. Flood hazards are a major threat to human life (injure or death of man and animal life), properties (agricultural area, yield production, building, and homes), and infrastructures (bridges, roads, railways, urban infrastructures). The damage that can occur due to such disasters leads to huge economic loss and bring pathogens into urban environments that cause microbial development and diseases. The natural and social hazards are discontinuing the development of human society and sustainability. Therefore, flood hazards susceptibility mapping (risk assessment), modeling is an essential step for the early warning system, emergency services, prevention and mitigation of future environmental and social hazards, and implementation of risk management strategies.

This book is composed of 13 chapters associated with spatial modeling of floods and flash floods hazards in basin drainage scale, human interference and flood vulnerability, and community preparedness for flood mitigation strategies. The contemporary researches in this field have been amalgamated to comprehend the various modern geospatial methods for the prediction of floods, hazards, and mitigation strategies.

We are very much thankful to all the authors who have meticulously completed their documents on a short announcement and played a vital role in building this edifying and beneficial publication. We do believe that this will be a very convenient book for river scientists, geographers, ecologists, economists, and others working in the field of water resources management including research scholars, environmentalists, and policymakers. We also acknowledge our deep gratitude to the Springer Publishing House especially to Doris Bleier and her team for contracting with us for such timely publication.

Ultimo, NSW, Australia
Midnapore, India
Birbhun, India
Chandrasekharpur, Bhubaneswar, India
Shiraz, Iran

Biswajeet Pradhan
Pravat Kumar Shit
Gouri Sankar Bhunia
Partha Pratim Adhikary
Hamid Reza Pourghasemi

Acknowledgments

The preparation of this book has been guided by several geomorphologic pioneers. We are obliged to these experts for providing their time to evaluate the chapters published in this book. We thank the anonymous reviewers for their constructive comments that led to substantial improvement to the quality of this book. Because this book was a long time in the making, we want to thank our family and friends for their continued support. This work would not have been possible without constant inspiration from our students, knowledge from our teachers, enthusiasm from our colleagues and collaborators, and support from our family. Finally, we also thank our publisher and its publishing editor, Springer, for their continuous support in the publication of this book.

Contents

1	Introduction to Spatial Modeling of Flood Risk and Hazard: Societal Implication	1
	Biswajeet Pradhan, Pravat Kumar Shit, Gouri Sankar Bhunia, Partha Pratim Adhikary, and Hamid Reza Pourghasemi	
2	Flood Susceptibility Mapping Using Morphometric Parameters and GIS	15
	Md. Hasanuzzaman, Aznarul Islam, Biswajit Bera, and Pravat Kumar Shit	
3	Palaeohydrologic Estimates of Flood Discharge of Lower Ramganga River Catchment of Ganga Basin, India, Using Slackwater Deposits	33
	Rameswar Mukherjee	
4	Flood Risk Zone Identification Using Multi-criteria Decision Approach	51
	Raja Majumder and Gouri Sankar Bhunia	
5	Dynamics River Networks and Determination of the Flood Potential in Lower Brahmaputra Valley Using Geoinformatics	77
	Asraful Alam, Rajat Kumar Paul, Amir Khan, Lakshminarayan Satpati, and Nilanjana Ghosal	
6	Flood Vulnerability Assessment Using AHP and Frequency Ratio Techniques	91
	Md. Hasanuzzaman, Partha Pratim Adhikary, Biswajit Bera, and Pravat Kumar Shit	
7	Application of Hybrid Machine Learning Algorithms for Flood Susceptibility Modeling	105
	Swapan Talukdar, Sujit Kumar Roy, Showmitra Kumar Sarkar, Susanta Mahato, Swades Pal, Atiqur Rahman, Bushra Praveen, and Tanmoy Das	
8	Flash Flood Susceptibility Mapping Using GIS-Based AHP Method	119
	Subhasish Choudhury, Amiya Basak, Sankar Biswas, and Jayanta Das	

9	GIS-Based Hydrological and Hydraulic Models to Forecast River Flood Risks and Proposition of Management Measures	143
	Gisele Icyimpaye and Chérifa Abdelbaki	
10	Large-Scale Human Intervention and Estimation of Flood Susceptibility Applying Frequency Ratio Model	161
	Meelan Chamling, Biswajit Bera, and Sudipa Sarkar	
11	Flood-Induced Transport Infrastructural Losses in India: Regional Assessments	185
	Suwendu Roy	
12	Rural–Urban Differential in Flood Vulnerability and Community Preparedness for Flood Management Strategies	203
	Aznarul Islam, Susmita Ghosh, and Suman Deb Barman	
13	Application of Geospatial Techniques for Urban Flood Management: A Review	225
	Biraj Kanti Mondal and Satiprasad Sahoo	
	Index	237

Editors and Contributors

About the Editors



Prof. Dr. Biswajeet Pradhan is an internationally established Scientist in the field of Geospatial Information Systems (GIS), remote sensing and image processing, complex modeling/geo-computing, machine learning and soft-computing applications, natural hazards and environmental modeling, and remote sensing of Earth observation. He is the Director of the Centre for Advanced Modelling and Geospatial Information Systems (CAMGIS) at the Faculty of Engineering and IT. He is also a distinguished professor at the University of Technology, Sydney. He is listed as the World's most Highly Cited researcher by Clarivate Analytics Report in 2019, 2018, 2017, and 2016 as one of the world's most influential minds. In 2019 and 2018, he has been awarded as World Class Professor by the Ministry of Research, Technology, and Higher Education, Indonesia. He is a recipient of the Alexander von Humboldt Research Fellowship from Germany. In 2011, he received his habilitation in "Remote Sensing" from Dresden University of Technology, Germany. Since February 2015, he is serving as "Ambassador Scientist" for Alexander Humboldt Foundation, Germany. Professor Pradhan has received 55 awards since 2006 in recognition of his excellence in teaching, service, and research. Out of his more than 450 articles, more than 400 have been published in science citation index (SCI/SCIE) technical journals. He has written eight books and thirteen book chapters. He is the Associate Editor and Editorial Member in more than 8 ISI journals. Professor Pradhan has widely traveled abroad visiting more than 52 countries to present his research findings.



Dr. Pravat Kumar Shit is an Assistant Professor at the PG Department of Geography, Raja N. L. Khan Women's College (Autonomous), West Bengal, India. He received his M.Sc. & Ph.D. degrees in Geography from Vidyasagar University and PG Diploma in Remote Sensing & GIS from Sambalpur University. His research interests include applied geomorphology, soil erosion, groundwater, forest resources, wetland ecosystem, environmental contaminants & pollution, and natural resources mapping & modeling. He has published 16 books (Springer-12, Elsevier-02, CRC Press-01, and others) and more than 70 papers in peer-reviewed journals. He is currently the Editor of the GIScience and Geo-environmental Modelling (GGM) Book Series, Springer-Nature.



Dr. Gouri Sankar Bhunia received Ph.D. from the University of Calcutta, India in 2015. His Ph.D. dissertation work focused on environmental control measures of infectious disease using Geospatial technology. His research interests include environmental modeling, risk assessment, natural resources mapping and modeling, data mining, and information retrieval using Geospatial technology. Dr. Bhunia is Associate Editor and on the editorial boards of three international journals in Health GIS and Geosciences. Dr. Bhunia has published more than 70 articles in various journals in Scopus indexed. He is currently the Editor of the GIScience and Geo-environmental Modelling (GGM) Book Series, Springer-Nature.



Dr. Partha Pratim Adhikary is a renowned Scientist in the field of GIScience and simulation modeling. He is presently at ICAR—Indian Institute of Water Management, Bhubaneswar, India. He has a brilliant career and experience of more than 15 years on research, teaching, and training in the field of Spatial Variability, Soil and Water Conservation, Groundwater Pollution, and Solute Transport Modelling. He has been bestowed with various scholarships, fellowships, and awards by various scientific societies, universities, and Government as recognition of his contribution to science and the society. He is the member of several national and state-level professional scientific bodies. Dr. Adhikary has more than 120

publications to his credit which include research papers in SCI journals, books, book chapters, popular articles, technology brochures, technical reports and bulletins, etc. He is the Associate Editor of the Indian Journal of Soil Conservation. Currently, he is the Editor of Springer-Nature book series “GIScience and Geo-environmental Modeling.”



Hamid Reza Pourghasemi is an Associate Professor of Department of Natural Resources and Environmental Engineering in the College of Agriculture, Shiraz University, Iran. He has a B.Sc. in Watershed Management Engineering from the University of Gorgan (2004), Iran; an M.Sc. in Watershed Management Engineering from Tarbiat Modares University (2008), Iran; and a Ph.D. in Watershed Management Engineering from the same University (Feb 2014). His main research interests are GIS-based spatial modeling using machine learning/data mining techniques in different fields such as landslide, flood, gully erosion, forest fire, land subsidence, species distribution modeling, and groundwater/hydrology. Also, Hamid Reza works on multi-criteria decision-making methods in natural resources and environment. He has published more than 130 peer-reviewed papers in high-quality journals and three books in Springer and Elsevier as Editor. Also, he is an active Reviewer in more than 60 international journals.

Contributors

Partha Pratim Adhikary Department of Groundwater Management, ICAR – Indian Institute of Water Management, Chandrasekharpur, Bhubaneswar, Ordisa, India

Chérifa Abdelbaki Pan-African University Institute for Water and Energy Sciences (PAUWES), Tlemcen, Algeria;
Laboratoire EOLE, Université de Tlemcen, Tlemcen, Algeria

Asrafal Alam Department of Geography, Serampore Girls’ College, University of Calcutta, Serampore, West Bengal, India

Suman Deb Barman Department of Geography, The University of Burdwan, Burdwan, West Bengal, India

Amiya Basak Department of Geography and Applied Geography, University of North Bengal, Darjeeling, India

Biswajit Bera Department of Geography, Sidho Kanho Birsha University, Puruliya, India

Gouri Sankar Bhunia Department of Geography, Seacom Skills University, Kendradangal, Santiniketan, Birbhum, West Bengal, India

Sankar Biswas Department of Geography and Applied Geography, University of North Bengal, Darjeeling, India

Meelan Chamling Department of Geography, Sidho-Kanho-Birsha University, Purulia, India

Subhasish Choudhury Centre for Himalayan Studies, University of North Bengal, Darjeeling, India

Jayanta Das Department of Geography, Rampurhat College, Birbhum, India

Tanmoy Das Faculty of Natural Science, Department of Geography, Jamia Millia Islamia, New Delhi, India

Nilanjana Ghosal CAD, Jadavpur University, Kolkata, West Bengal, India

Susmita Ghosh Department of Geography, Aliah University, Kolkata, India

Md. Hasanuzzaman PG Department of Geography, Raja N. L. Khan Women's College (Autonomous), Gope Palace, Midnapore, West Bengal, India

Gisele Icyimpaye Pan-African University Institute for Water and Energy Sciences (PAUWES), Tlemcen, Algeria

Aznarul Islam Department of Geography, Aliah University, Kolkata, India

Amir Khan Department of Geography, University of Calcutta, Kolkata, West Bengal, India

Susanta Mahato Special Centre for Disaster Research, Jawaharlal Nehru University, New Delhi, India

Raja Majumder Department of Geography, Seacom Skills University, Kendradangal, Santiniketan, Birbhum, West Bengal, India

Biraj Kanti Mondal Department of Geography, Netaji Subhas Open University, Kolkata, West Bengal, India

Rameswar Mukherjee Department of Geography, Samsi College, Samsi, Malda, West Bengal, India

Swades Pal Department of Geography, University of Gour Banga, Malda, India

Rajat Kumar Paul Department of Geography, University of Calcutta, Kolkata, West Bengal, India

Hamid Reza Pourghasemi Department of Natural Resources and Environmental Engineering, College of Agriculture, Shiraz University, Shiraz, Iran

Biswajeet Pradhan Faculty of Engineering and IT, Centre for Advanced Modelling and Geospatial Information Systems (CAMGIS), University of Technology, Sydney, NSW, Australia

Bushra Praveen School of Humanities and Social Science, Indian Institute of Technology Indore, Madhya Pradesh, India

Atiqur Rahman Faculty of Natural Science, Department of Geography, Jamia Millia Islamia, New Delhi, India

Sujit Kumar Roy Institute of Water and Flood Management (IWFM), Bangladesh University of Engineering and Technology (BUET), Dhaka, Bangladesh

Suwendu Roy Department of Geography, Kalipada Ghosh Tarai Mahavidyalaya, Bagdogra, Darjeeling, WB, India

Satiprasad Sahoo Department of Geography, Jadavpur University, Jadavpur, India

Showmitra Kumar Sarkar Department of Urban and Regional Planning, Khulna University of Engineering and Technology, Khulna, Bangladesh

Sudipa Sarkar Department of Geography, Sidho-Kanho-Birsha University, Purulia, India

Lakshminarayan Satpati Department of Geography and HRDC, University of Calcutta, Kolkata, West Bengal, India

Pravat Kumar Shit PG Department of Geography, Raja N. L. Khan Women's College (Autonomous), Gope Palace, Midnapore, West Bengal, India

Swapan Talukdar Faculty of Natural Science, Department of Geography, Jamia Millia Islamia, New Delhi, India



Introduction to Spatial Modeling of Flood Risk and Hazard: Societal Implication

Biswajeet Pradhan, Pravat Kumar Shit,
Gouri Sankar Bhunia, Partha Pratim Adhikary, and
Hamid Reza Pourghasemi

Abstract

Spatial Modeling of Flood Risk and Hazard: Societal Implication offers a flexible medium for the study of the prediction and assessment of flood risk, human interference, infrastructure loss, damages of properties, and management strategies. The main aim of this book is to highlight the applications of remote sensing (RS), GIS modeling, and machine learning algorithms to predict and estimate the flood

and mapping of flash flood's hazards susceptibility. All these aspects were covered by 13 chapters, where special emphasis was given on spatial modeling of floods and flash floods' hazards in river basin scale, human interference and flood vulnerability, and community preparedness for flood reduction and mitigation strategies. This valuable edited volume will definitely benefit and help the students, researchers, scholars, academicians and policy-makers for acquiring adequate knowledge and integrated sustainable river basin flood management.

B. Pradhan
Faculty of Engineering and IT, Centre for Advanced Modelling and Geospatial Information Systems (CAMGIS), University of Technology, Sydney, NSW, Australia
e-mail: Biswajeet.Pradhan@uts.edu.au

P. K. Shit (✉)
Department of Geography, Raja N.L. Khan Women's College (Autonomous), Gope Palace, Medinipur 721102, West Bengal, India

G. S. Bhunia
Department of Geography, Seacom Skill University, Kolkata, West Bengal, India

P. P. Adhikary
Department of Groundwater Management, ICAR – Indian Institute of Water Management, Chandrasekharpur, Bhubaneswar, Ordisa 751023, India
e-mail: Partha.Adhikary@icar.gov.in

H. R. Pourghasemi
Department of Natural Resources and Environmental Engineering, College of Agriculture, Shiraz University, Shiraz, Iran

Keywords

Flash floods hazards · Floods risk · GIS modeling · Machine learning algorithms · Sustainable basin management

1.1 Concept of Floods

Flooding is probably the most common weather-related hazard in the world. It can happen almost everywhere. Floods occur when the water is overflowing on river banks and dry lands, and is the most frequent kind of natural disaster (Mills 2005). Flooding is frequently causing unmixed damage, especially in countries with lower wealth, where infrastructure systems, particularly drainage and flooding, tend to be less advanced (IPCC 2012). The vast majority of the world's

flood vulnerable countries (88%) are low- and medium-income nations, although countries of all stages of development are exposed to flood risks. More than 2 billion people worldwide were impacted by floods over 1998–2017. Both beneficial and bad effects might be expected from floods (Talbot et al. 2018). They can provide relief to long-drowned individuals and ecosystems but are also considered to be the most costly natural disaster. Flooding most frequently occurs when severe rainfall does not allow natural watercourses to absorb excessive water. However, excessive rainfall is not always responsible for floods. They can be the result of various events, especially in coastal locations, where floods may be triggered by a tropical cyclone, tsunami, or high tide, which corresponds to greater levels than usual levels of the river (Kumar et al. 2014; Samanta et al. 2018; Majumder et al. 2019). River floods are one of the most common natural disasters, wreaking havoc around the world. When a river or stream overflows its natural banks and inundates normally dry land, it is called a river flood. River flooding is most common in the late winter and early spring, and it can be caused by heavy rainfall, rapidly melting snow, or ice jams. Coastal flooding occurs when winds from a coastal storm, such as a hurricane or nor'easter, push a storm surge—a wall of water—from the ocean onto land, affecting more than 8.6 million Americans. Storm surge has the potential to cause widespread devastation. Higher sea levels are also causing an increase in shallow, non-life-threatening floods. There are extreme events (heavy or prolonged rains, storm surge, and rapid snowmelt), and then there are human-driven facets, such as how we manage our waterways (via dams, levees, and reservoirs) and land changes. Increased urbanization, for example, adds pavement and other impervious surfaces, alters natural drainage systems, and frequently results in more homes being built on floodplains. Under-maintained infrastructure in cities can result in flooding. Flooding is becoming increasingly linked to climate change. Climate change may also increase the frequency or severity of flooding (Hirabayashi et al. 2013;

Arnell and Lloyd-Hughes 2014). A warmer atmosphere retains more water and then dumps it. Since 1901, the country has warmed by an average of 1.8 °F, becoming about 4% wetter, with the eastern half of the country becoming the wettest. The most severe storms in the Northeast now produce about 27% more moisture than they did a century ago. Mainly, when it rains, it pours more because of global warming. Hotter temperatures, on the other hand, can cause more rain-on-snow events in areas where seasonal snowmelt plays a significant role in the annual runoff, with warm rains causing faster and often earlier melting. Global sea levels are rising as ocean temperatures rise and the world's glaciers and ice sheets melt (both of which are exacerbated by climate change). Our oceans are about seven to eight inches higher than they were in 1900 (with about three of those inches added since 1993 alone)—a faster rate of rising per century than any other century in the past 2,000 years.

Flooding during the monsoon is a regular activity, and some natural processes such as the introduction of alluvial soils into areas, groundwater refueling, or water bodies have also happened (Rubinato et al. 2019). The floods have become unexpected and intractable due to variable weather conditions and the growing volume of severe precipitation. In recent years, the number of incidences and the intensity of floods have increased dramatically and professionals believe that efficient and organized flood control is needed quickly to address this challenge.

Inland floods (river floods, flash floods, and drainage floods) killed 175,000 people and affected more than 2.2 billion people between 1975 and 2002, according to global statistics (Jonkman 2005). 2.2 billion people, or 29% of the world's population, live in areas that are expected to be flooded at some point during a once-in-a-100-year flood event (Rentschler and Salhab 2020). Such an occurrence has a one percent chance of occurring in any given year, a ten percent chance in a decade, and a fifty percent chance in a lifetime (68 years). According to (Alfieri et al. 2018), flood losses in Asia and Africa account for 95% of floods worldwide each

year and 73% of total direct economic damage. Due to the vast limited extend of flood-prone areas in congested areas, flooding from large rivers is responsible for a lot of people being affected by floods annually (Pesaresi et al. 2017). Around 1.47 billion people, or 19% of the global population, are directly affected by inundation depths of more than 0.15 m. Furthermore, flooding could be even worse for over half of this vulnerable population, with life-threatening consequences, particularly for children and the disabled (Zischg and Bermúdez 2020). Almost half of the 132 million people living in extreme poverty and high flood risk live in just three countries. With over 35 million people are at risk of flooding, the largest number of exceedingly poor people in the world, accounting for 2.5% of the country's total population. The top ten countries in terms of the number of poor people are exposed at \$1.90 account for 65% of all poor people worldwide who are vulnerable to flooding. Temperatures are rising throughout South Asia, with all conceivable climate scenarios anticipated to continue to grow for decades to come (Muthukumara et al. 2018). These changes will lead to more floods, higher demand for water, and increasing health problems. South Asian towns like Kolkata, Mumbai, Dhaka, and Karachi, where 50 million people live, pose a significant risk of flood devastation in the next century. India is among the most susceptible to climate change in the world. The frequency of drops and gaps between rainy days during the monsoon has been enhanced. As India's temperature warms, it is projected that extreme weather would worsen, such as heavy rain and floods. The recent World Bank report predicted that Chhattisgarh and Madhya Pradesh would be the worst-hit states by 2050. The population at danger from catastrophic flooding might increase sixfold in India by 2040, from 3.7 million to 25 million from 1971 to 2004. Satellite technology has changed the way we deal with large-scale floods over the course of the disaster management cycle, from preparedness to recovery. Numerical Weather Predictions (NWP) have reaped significant benefits from satellite data in terms of improving forecast skills over the

oceans, in areas not covered by traditional measurement networks, and in general, in extending their predictability in time and for extreme events (Bouttier and Kelly 2001). Moreover, various sensors mounted on satellites have demonstrated core elements in detecting and identifying surface water extent (Pekel et al. 2016), river, and lake height (Calmant et al. 2008), and large-scale flooding (Pekel et al. 2016).

1.2 Impact of Flood—Global Scenario

About 2.2 billion people or 29% of the world's population, live in places where flooding occurs at an estimated rate of 1 in 100 years. This event is 1% likely to happen in a certain year, which is 10% likely in a decade or 50% in a lifetime (68 years). Approximately, 1.47 billion or 19% of the world's population is exposed directly to flood depths of more than 0.15%. Since 1960, the number of floods documented in the database for EM-DAT catastrophes has increased. Many occurrences which comply with the criterion are nonetheless often not recorded in the EM-DAT. For example, in the EM-DAT, the country of floods was less than 50, climbing approximately 80 by the middle of the 1980s. The frequency of flood events in low-income nations documented, in particular, was quite low before the mid-1990s (Fig. 1.1).

As the overall global modeling area in flood mitigation measures are not being taken into consideration, this increasing trend is not the cause of a growing percentage of flood hazards internationally; this implies that advancement in improving transparency and data collection is one of the main driving forces for the increasing number of flood reports (Fig. 1.2). Additional factors may also contribute (socioeconomic changes, including population expansion). The annual total of fatalities recorded and the measure of economic losses reported by flooding in the EM-DAT indicate an increased tendency between 1960 and 2013 (1.5% per year for annual reported deaths, and 6.3% per year for reporting financial losses).

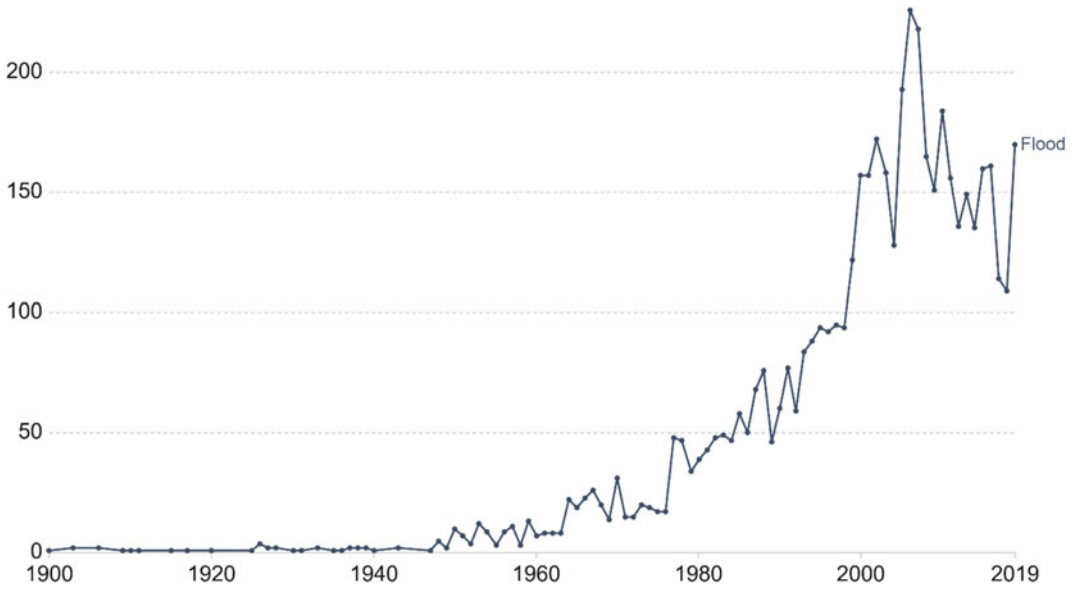


Fig. 1.1 Number of recorded flood disasters from 1900 to 2019 (EMDAT (2020); OFDA/CRED International Disaster Database, Université catholique de Louvain—Brussels—Belgium)

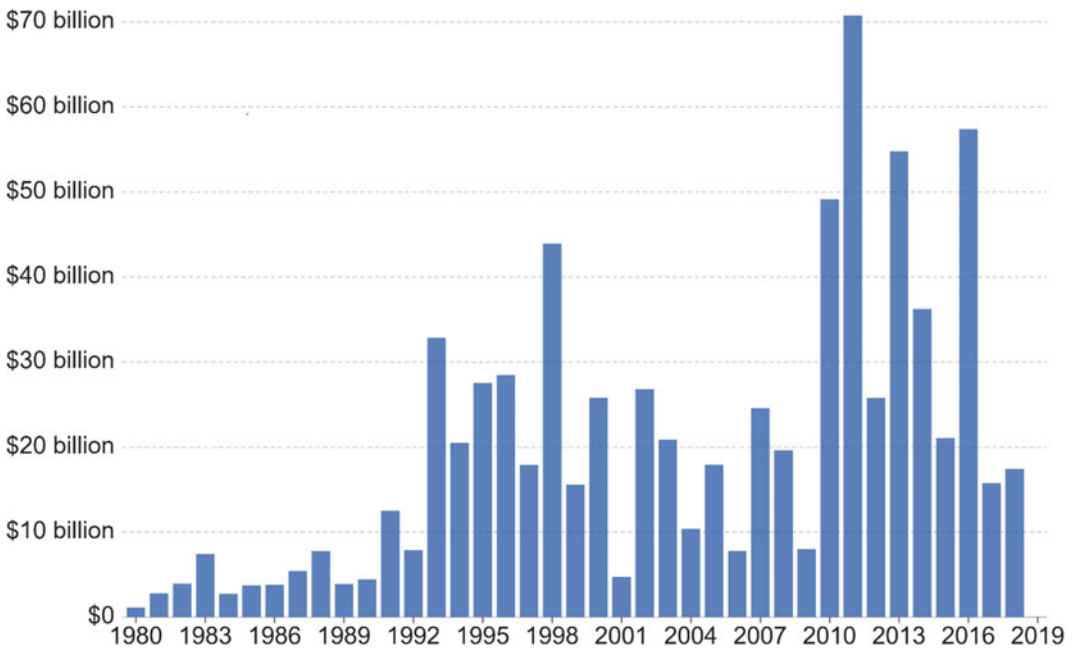


Fig. 1.2 Global damage cost from flood (Source EMDAT (2020); OFDA/CRED International Disaster Database, Université catholique de Louvain—Brussels—Belgium)

In developing countries, the impact of flooding is more damaging because of low flood protection. In India and Nepal, for example, 6648

fatalities from floods occurred in 2013, while repeated floods in the Philippines caused more than 100 deaths per year between 2011 and 2013

(Fig. 1.3), and persistent flooding in Thailand caused severe economic losses in 2011 (EMDAT 2019). In Europe, the Danube flooded in 2013 just as the Kinu River flooded in Japan in 2015. Developed countries also suffered from floods. But, as a consequence of historical attempts to reduce flood impacts, loss of flooding and damage, particularly in terms of deaths, is generally not as serious in developed countries compared to underdeveloped countries (Doocy et al. 2013).

There is some evidence that climate change will increase the risk of flooding. Based on the outputs of 11 climate models, Hirabayashi et al. (2013) present regionally disaggregated flood risk estimates for the year 2100. They show that a high-concentration climate change scenario could result in a large increase in flood frequencies in Southeast Asia, India, East and Central Africa, and large parts of Latin America by modeling the changes in river discharge and inundation areas.

1.3 Floods in India—A Case Study

In spite of the fact that July was the driest in the past five years, several portions of India, particularly the Assam and Bihar provinces, are still flooded. It was projected that more than 10 million people have suffered and, until the first week of August this year, at least 125 have passed away as a result of floods (Hunt and Menon 2020). Moreover, hundreds of Uttar Pradesh villages have been flooded, Maharashtra's metropolis, Mumbai has been waterlogged and there's imminent flooding in Kerala and West Bengal. The majority of deaths (11,316) were reported due to flood/heavy rain in India in 1977 and the least in 1953 (37). In the wake of flooding, more than 1600 people die each year, affecting around 32 million. There is a yearly loss of more than 92,000 cattle, an impact of seven million hectares, and damage exceeding Rs 5,600 crore (Fig. 1.4). In 2009, there was a loss of Rs. 32,541 crores in

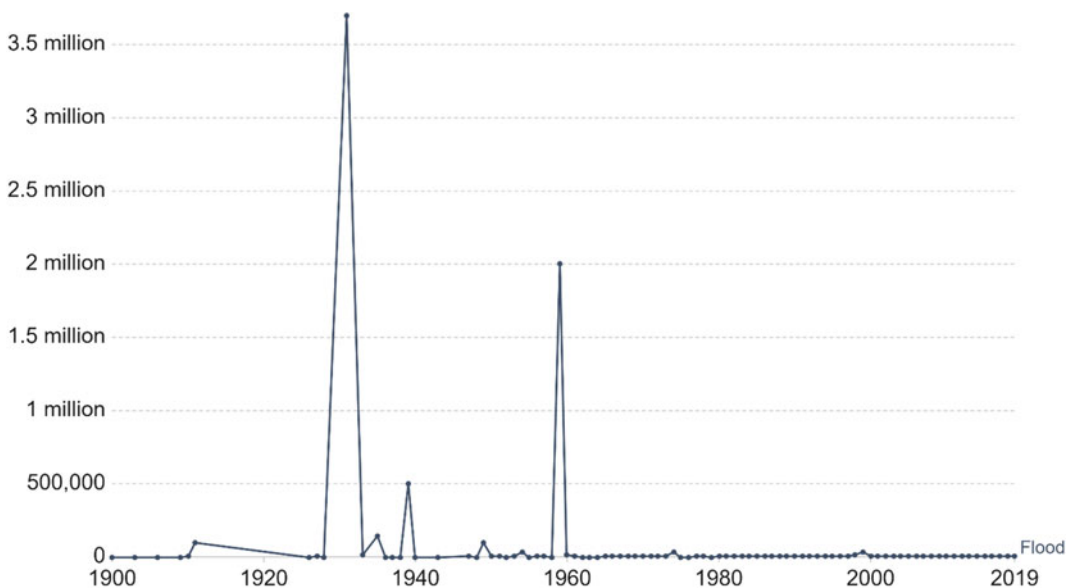


Fig. 1.3 Global deaths due to flood, 1900–2019 (Source EMDAT (2020): OFDA/CRED International Disaster Database, Université catholique de Louvain—Brussels—Belgium)

crops, homes, and utilities, the greatest for any one year. In 2003, flooding destroyed crops worth Rs. 7,298 in 2009 with the largest damage caused by flooding to residences exceeding Rs 10,000 in 2009. West Bengal, Orissa, Andhra Pradesh, Kerala, Assam, Bihar, Gujarat, Uttar Pradesh, Haryana, and Punjab are flood-prone countries. In the 20 states, the country has 226 flood prediction plants, 2 union territories, and 19 river basins for flood monitoring.

Their geographical position is one explanation for the repeated floods in many parts of India. For example, in the Terai region, at the foot of the Himalayas and with the help of hundreds of watercourses, states like Bihar, Uttar Pradesh, West Bengal, Assam, and Bihar are prone to flood hazard. Apart from Ganga, river basins that are prone to flooding other flood-prone basins are also scattered across the states such as Kosi, Gandak, Damodar, Brahmaputra, and Mahanadi. There are several powerful affluents in these rivers, which produce huge flooding water during the wet season. According to information presented in the Rajya Sabha, India lost an estimated Rs. 957 billion in 2018 and lost 1,808 lives due to floods across the country. Government information reveals an incidence of yearly flood losses—comprising damage to the home, public property, and crop—of Rs. 3612 billion on average between 1953 and 2011. More than

125,000 households have lost their residential or agricultural land as a result of floods since 1947, according to the Assam government. Over the previous ten years, some of the biggest flood catastrophes have been in 2013 at Uttarakhand, 2014 in Chennai, 2015, 2018 at Kerala, 2019 at Patna, as well as the periodic floods in Northeast India. The Central Water Commission said that the flood management expenditure in the 10th Five-Year Plan (2002–2007) was increased from 43,44 billion Rs. (4,344 crores) to 171,30 billion Rs. (17,130 crores) (2007–2012).

Officially, India's overall flood-prone territory comprises around 40 million hectares, representing 12% of the country's total area. This statistic for the flood-prone region is really old; for at least the last two and a half decades, we have heard this figure of 40–50 million hectares. This number is actually related to the flood zones reported by the river. The shape and scope of the floods have changed a lot in recent years and our communities are flooded now. The flood was previously mostly restricted to the river basin areas such as Brahmaputra, Kosi, Gandak, Damodar, and Mahanadi. In addition, the flood time was limited to rainy seasons, with the floods in typical ways being managed by rural inhabitants. But new cities and towns grew and existing ones expanded with the rise of people. Often without a correct master strategy, this change

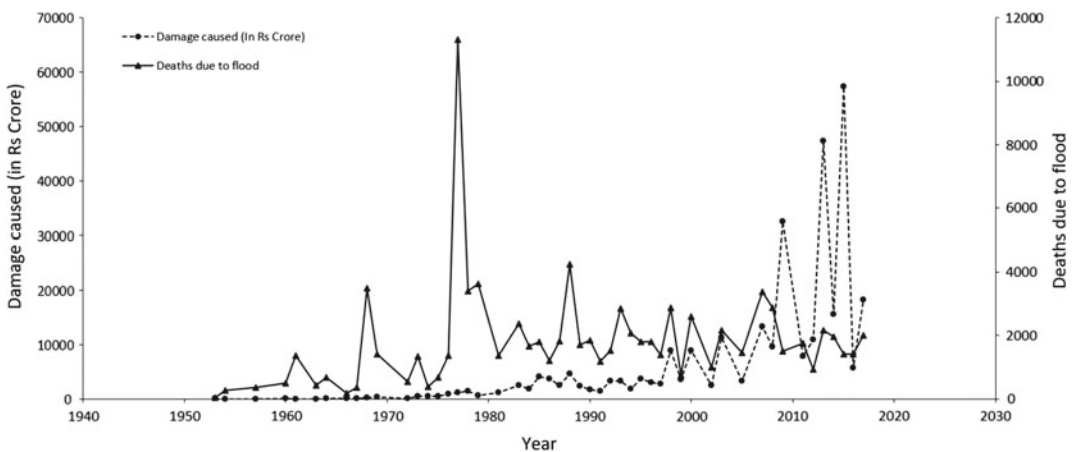


Fig. 1.4 Impact of flood in India, 1953–2017 (Source Central Water Commission)

was badly accomplished. This led in 2005 to urban flooding, 2015 to Chennai, and 2019 to Patna. Many water and weather experts emphasize the importance to detect vulnerable flood hotspots. They think it can give the administrators a tiny image to map these locations and maintain a thorough record. Many experts have also questioned the construction of unneeded banks and structures at the banks for “river flow control”. Rashtriya Barh Aayog (National Flood Commission) was established in the 1970s and suggested that these structures should not be fully evaluated for their “efficiency”.

The river broke the banks of Bihar in 2007 during the terrible Kosi inundations in over 30 sites and the national highways were broken at hundreds of locations. Today, though, we are raising the terrain embankment. This water (in 2007 from Kosi floods) had spread throughout and remained stuck for two and a half months in northern Bihar. It means the water could not get out. Extreme precipitation events have increased over recent decades and in a short time caused rough and heavy rain. Nevertheless, factors such as poor drainage, excessive ground cementation, and invasive water bodies such as lakes and pools and unplanted waste disposal have compounded the situation. There are several water bodies in this entire area of the terai at the foot of the Himalayas. Such bodies (rivers, lakes, and ponds) supplied water by saving it during the heavy rainfall but these sites were either invaded for building or filled with solid trash and garbage in the past few years. The natural cushion or buffer for rainwater in urban areas was thereby destructed.

1.4 Need for Floods Prediction Map

The purpose of a floods warning service is to detect and anticipate threatening flood occurrences in order to warn the public in advance and to respond adequately to minimize the impact of the event. In developing countries, flooding causes massive loss of lives or property. Flood alerts are particularly significant when protection is not desirable or attainable through huge, hard

defences. This may occur if defences generate harmful societal or environmental concerns or if the expenses of building defences are prohibitive. The flood alert phase demands continual weather observation. This enables dangerous occurrences to be detected and evaluated before they reach a community. Prognoses can also be made to help policy-makers model how an event will develop; how important it will be when it arrives and which segments of the population will be likely to be vulnerable. This is required, as simply detecting an occurrence does not give enough time to respond. In order to achieve monitoring and forecasting, a flood warning system would probably integrate meteorological, mare, and river and coastal flood prediction models. When an incident surpasses a specific threshold, a warning is generated. The message will likely be distributed over a number of channels to the ‘at-risk’ population. Media, police and fire departments, and simple signs like sirens and flags all play significant roles. The second stage of the flood warning service, which was launched after the people, was notified of the risk. Hazardous Zone communities must take efforts to minimize their hazardous exposure and mitigate flood impacts. It is necessary to communicate suitable activities to the public in advance of a disaster through awareness-raising efforts. That means that measures can be done quickly to mitigate the effects of floods to the greatest extent.

Flood risk management has a number of objectives that span a wide range of time and spatial scales. The advancement and implementation of relevant portfolios of measure (where one’s advantages reimburse for the drawbacks of another) are required to achieve these goals, a process made more difficult by the changing the nature of the flooding system (through climate, geomorphologic and socio-economic influences). As a result, a number of new strategies, concepts, and initiatives have been proposed, including flood protection, evacuation, environmentally friendly solutions, river denaturalization, fool-proof structural measures, nonstructural measures, soft measures, hard measures, river room, flood fighting, resilient approach, sustainable flood management, integrated approach, risk-

based flood management, nature-based solutions, dykes, floodwalls, warning systems, and more. Efficient management of flooding was also not in keeping with developing countries' land strategy. There have been several causes for it, politically, socially, and economically. The WMO research stated that modern land use, which gradually interferes with the natural environment, has an effect on all three dimensions: hazard, vulnerability, and exposure to flooding risks. Removal of vegetation, soil, surface gradation, and drainage structures interrupt the patterns of natural drainage and watercourses. The river-runoff rate and the entire river's volume increase as a consequence of the decline in natural water storage capacity when natural surfaces change to less or less prevalent artificial surfaces. Seashore mangroves serve as a protective wall during any coastal flood, especially when a strong cyclonic storm causes the floods. We also know that cyclones become more frequent and strong owing to global warming effects, thus conservation and the protection of mangroves against destruction or degradation is vitally crucial.

Hydrological and hydraulic engineers have been developing numerous approaches in the past decades to delineate the borders of the plains. Manual, arduous, and labor-intensive are the most common ways. Automated floodplain delimitation can be achieved with the advent of sophisticated computer technologies and a high-precision digital terrain model (DTM). Recently, numerous floodplain delineation management techniques have been developed and used in flood occurrence zones.

The GIS Flood Tool (GFT) uses relative DEMs, the zero point of which is referred to as the lowest point on the defined stretch of the stream channel, rather than traditional modeling. A flood region is determined by using the Manning equation at each grid cell, given a user-specified river discharge or stream stage. This determines how quickly this cell is flowing and how the water is flowing. Additional geographical information such as settlement patterns, transport networks, and land utilization/land cover might improve flood patterns. Instead of

employing more intense DEM-based approaches, flood extensions can come from the processing of aerial or satellite imaging, such as LANDSAT. During a flood, these maps can be swiftly drawn to alert officials and first respondents. Algorithms are meant to read visible spectrum pixel values or near pictures and to build a rapid flood outline. In order to achieve this strategy, modifications must be done in order to ensure clear separate water surfaces, such as rooftops or parking lots, from other large flat areas. EcoFIM is developing library resources for ecosystem studies from USGS Flood Inundation Mapping (FIM). The pilot EcoFIM supports the NRCS efforts through an assessment of flood influences on the biodiversity of flood lands (e.g., plant species, fish, and animals), biogeochemistry (e.g., nutrient cycles and fluxes), and ecosystem services (e.g., regeneration, safe water, view of the nature), with data types to conduct Eco-FIM projects related to those subjects. EcoFIM supports the efforts of the NRCS.

India has concentrated on developing a comprehensive early flood warning system in recent years. In 2015, Chennai faced catastrophic floods and was India's first smart flood warning system in 2019. In June 2020, Mumbai was equally equipped with the built-in flood alert system (IFLOWS). These flood alert systems can provide area-specific flood information during the monsoon. TERI has currently launched with the IMD and NDMA, in collaboration, a comparable flood forecasting system for Assam. The IMD also calculates the total predicted accumulation of water in any river/sub-river basin using rainfall data. The collection and exchange of this information with various entities can help to improve the management of flooding. Sampson et al. (2015) have been created to produce maps for the entire terrestrial area between 56°S and 60°N with a return period of flood risk of up to 90 m resolution, and data are validated for high-resolution government-based data set on flood risk from the UK and Canada (HRSC). The global model shows that two-thirds to three-quarters of the benchmark data are risky without generating excessive false positive predictions.

1.5 Role of Geospatial Technology for Floods Prediction

Over the previous decades, in most aspects of flood catastrophe management, satellite data have effectively been utilized. It was noted in the recent literature on flood monitoring and ramification assessment schemes that the majority of the studies used satellite data to conduct their analyses. In several phases of flood mitigation, earth observations satellites can be used to map geomorphological aspects, past figures, and successive flooding, such as duration, flood depth, and current direction (Samanta et al. 2018). They used a variety of imaging modalities, such as Landsat, the Moderate Resolution Imaging Spectroradiometer (MODIS), the Canadian Radar Satellite (RADARSAT), and the Satellite Pour l'Observation de la Terre (SPOT), or a combination of modalities. NDWI (Memon et al. 2015), MLSWI (Kwak et al. 2014), OWL (Huang et al. 2012), and MNDWI (Memon et al. 2012) were used to detect flooded areas in those studies (Atif et al. 2016). MODIS has been combined with another satellite modality in some studies. Martinis et al. (2013) discovered that it fused with SAR, and Landsat (Martinis et al. 2013; Zhang et al. 2014). In some cases, using either a MODIS or a Synthetic Aperture Radar (SAR) image alone was more accurate than combining both images in identifying floods. Another set of studies focused on estimating flood damage. Evaluation thresholds, including topographic, pedologic and botanical properties have been determined in the floodplains using remotely sensed data (Dunne and Leopold 1978). Evaluating the flood impact is a complex issue that only interdisciplinary study and step-by-step methodology can resolve. Digital elevation models can be built fast or upgraded with SRTM or Aster images. In addition, the land cover, for example, permissibility, interception, evapotranspiration, surface roughness, etc. is related to all types of factors relevant for hydrological modeling. And since satellite mapping is now regular practice, the space distribution of these values may be approximated readily.

A website based on MODIS and RADARSAT data was used to visualize spatial information of flooded areas using GIS (Auynirundronkool et al. 2012). Furthermore, using MODIS satellite imagery, GIS and RS technologies were used to review previous flood incidents (Likhit 2014). Most flood monitoring systems, according to recent surveys on mobile GIS, primarily used sensed hydrological and meteorological data, including rainfalls and runoffs, etc. (Pagatpat et al. 2015; Chen et al. 2018). Information was delivered via short message service (SMS) or as descriptive text on smart connected device platforms running web or native applications (Ancona et al. 2014). Multi-Criteria Analysis (MCA) is a structured method for determining overall preferences among various policy measures, where each policy may have multiple objectives. It identifies potential policy alternatives (along with related actions) and evaluates each one against a set of criteria. MCA is frequently used in conjunction with cost-benefit analysis (CBA), and it provides a more flexible approach, particularly in situations where options are difficult to express in purely monetary terms. The most intriguing use of RS maybe its usage for the study of components at risk. High-resolution images provide tremendous possibilities for identifying particular structures. In order to determine its vulnerability, importance, and value, recognition of the functioning of these structures are vital. This provides the opportunity to evaluate the increased risks and effects and use them in the decision process, particularly in the case of cities experiencing quick and uncontrolled expansion into dangerous locations such as floodplains. Information was delivered via short message service (SMS) or as descriptive text on various smart device platforms running web or native applications (Ancona et al. 2014). A common piece of data was the current status of a specific area's water level, which could be seen in real time. Integrated prototypes were also created, which compiled relevant data and provided more analytical content (Kulkarni et al. 2014). Another GIS-based mobile application was created to report flood situations, which

included damage from the flood, water level, and photographs (Jeeramard and Tangwannawit 2014). In disaster management, GPS plays an important role, especially in locating the affected areas. Tsunami warnings (Falck et al. 2010) and landslide monitoring (Tagliavini et al. 2007) are examples of recent applications in this field. GPS has been proven to be helpful in hydrology and flood management for documenting area-specific rainfall for runoff prediction (Benevides et al. 2015), along with flood monitoring (Suparta and Ali 2012). Google Maps API is a development tool that makes it easier to integrate Google Maps as a component into application software or a web page (Liang et al. 2012). In web development, for example, the code may be written in HTML and JavaScript and interfaced with PHP or Java in the backend (Choimeun et al. 2010). According to a recent survey on the use of Google Map API in flood management, the API is most commonly used as notification and reporting agents.

The flood risk map of Evros Transboundary Watershed was generated by Mentzafou et al. (2017) using a grid-based GIS modeling method that combines major flood development factors: topography, soil use, geology, pitches, accumulation of flow, and intensity of precipitation. ArcHydro is an ESRI Product geographic and temporal water resources data model. ArcHydro has a set of related tools, which have been constructed collaboratively by the ESRI (Institute of the Environmental System Research) and CRWR (Centre for Water Research) (Maidment 2002). ArcHydro is a hydrographical simulation model supporting data structure, however, it's not a simulation model by itself. The goal of ArcHydro is to describe surface waters hydrology despite the fact that the ArcHydro groundwater data model is independent data that should allow surface and groundwater information to be integrated. HEC-HMS is a standard model for the design of drainage systems, enabling, for example, the quantification of flood effects due to land utilization changes (Singh and Frevert 2006). A hydrological model like HEC-HMS translates

a rainfall input into single-watershed streamflow output characteristics including a drainage area, pathway, land cover, and soil type. Many of these data types can be measured in a GIS database. Kraus (2000) provided an intriguing example of a small watershed in Texas, USA using GIS and HEC-RAS integration. In the 1990s, the specifically designed GIS interface was built for the delivery of geopathic data such as HEC-GeoHMS/HECGeoRAS systems, HEC-HMS, and HEC-RAS are written in object-oriented programming languages. HEC-GeoRAS allows a specialist with a small GIS training to produce geometric data in the HEC-RAS and examine the data on the water surface profile with ArcGIS (Ackerman et al. 2000). A Web Map Interface with dynamic maps of existing and anticipated flood occurrences is developed by CARIS Spatial Fusion. This Web GIS program has the capacity to allow the users to simply find their area of interest based on a 6-digit postal code (Statistics Canada 2008). The Web-GIS interface has been built to determine and display the spatial extent of the expected flood plain, allowing visualizations of the transit system, property borders, municipal infrastructure, and flood polygons (Mioc et al. 2008).

1.6 Key Aims of the Book

Geo-spatial techniques have enjoyed a rising interest in recent decades among the earth's environmental and social sciences research communities for their powerful ability to solve and understand various complex problems and develop novel approaches toward sustainable earth and human society. By linking geospatial computational intelligence techniques with societal and environmental-oriented problems, this book demonstrates the geospatial technology approach to data mining techniques, data analysis, modeling, risk assessment, and visualization, and management strategies in different aspects of flood hazards.

1.7 Individual Chapters

This book is composed of 13 chapters associated with spatial modeling of floods and flash floods hazards in basin drainage scale, human interference and flood vulnerability, and community preparedness for flood mitigation strategies. Chapter 2 deals with sub-watershed prioritization for flood susceptibility mapping based on the morphometric parameters with GIS techniques. The palaeohydrologic estimates of flood discharge using slackwater deposits (SWD) have been described in Chap. 3. In Chap. 4, Majumder and Bhunia presented the prediction of flood risk mapping using GIS-based multi-criteria decision approach. In Chap. 5, Alam et al. evaluated the flood vulnerability which is primarily based on multi-criteria evaluation (MCE) conducted in the lower the Brahmaputra River of Assam. Chapter 6 dealt with Analytical Hierarchy Process (AHP) and frequency ratio (FR) model to prepare a flood susceptibility map. In Chap. 7 written by a group of researchers under the lead of Talukdar, described the novel hybrid models by integrating machine learning algorithms with a statistical model like logistic regression (LR) for generating flood susceptibility models (FSM). This chapter also emphasizes the various machine learning algorithms, such as artificial neural network (ANN), and random forest (RF), and logistic regression (LR) and their integration with each other to generate two hybrid machine learning algorithms, such as ANN-LR, and RF-LR models for FSM. Chapter 8 dealt with the role of GIS-based AHP method to predict flash flood susceptibility mapping (FFSM) in the urban area. GIS-based hydrological and hydraulic models to forecast river flood risks and proposition of management measures have been illustrated in Chap. 9. In Chap. 10 written by a group of researchers under the lead of Chamling, discussed the large-scale human intervention and estimation of flood susceptibility applying the Frequency Ratio model. Chapter 11 analyzed and described the transport infrastructural losses in India due to floods during the past 60 years. In Chap. 12, Islam and their co-authors have

discussed rural–urban differential in flood vulnerability and community preparedness for flood management strategies. The last chapter of the book described the issues of urban flood management with the application of geospatial techniques, to provide scientific information for the city planners and policy-makers to formulate resilient urban flood management strategies.

References

- Ackerman CT, Evans TA, Brunner GW (2000) HEC-GeoRAS: Linking GIS to hydraulic analysis using Arc/Info and HEC-RAS. In: Maidmentand D, Djokic D (eds) Hydrologic and Hydraulic. Modelingsupport. ESRI Press, Redlands, pp 155–176
- Amell NW, Lloyd-Hughes B (2014) The global-scale impacts of climate change on water resources and flooding under new climate and socio-economic scenarios. *Clim Chang* 122:127–140
- Alfieri et al. (2018) A global network for operational flood risk reduction. *Environ Sci & Policy* 84: 149–158. <https://doi.org/10.1016/j.envsci.2018.03.014> June 2018
- Ancona M, Corradi N, Dellacasa A, Delzanno G, Dugelay J-L, Federici B, Gourbesville P, Guerrini G, La Camera A, Rosso P et al (2014) On the design of an intelligent sensor network for flash flood monitoring, diagnosis and management in urban areas position paper. *Procedia Comput Sci.* 32:941–946
- Atif I, Mahboob MA, Waheed A (2016) Spatio-temporal mapping and multi-sector damage assessment of 2014 flood in Pakistan using remote sensing and GIS. *Indian J Sci Technol* 9(1):1–10
- Auynirundronkool K, Chen N, Peng C, Yang C, Gong J, Silapathong C (2012) Flood detection and mapping of the Thailand Central plain using RADARSAT and MODIS under a sensor web environment. *Int J Appl Earth Obs Geoinf* 14(1):245–255
- Benevides P, Catalao J, Miranda PMA (2015) On the inclusion of GPS precipitable water vapour in the nowcasting of rainfall. *Nat Hazards Earth Syst Sci* 15 (12):2605–2616
- Bouttier F, Kelly G (2001) Observing-system experiments in the ECMWF 4D-Var data assimilation system Q. *J R Meteorol Soc* 127:1469–14
- Calmant S, Seyler F, Cretaux JF (2008) Monitoring continental surface waters by satellite altimetry *Surv. Geophys* 29:247–269. <https://doi.org/10.1007/s10712-008-9051-1>
- Chen Z, Chen N, Du W, Gong J (2018) An active monitoring method for flood events. *Comput Geosci* 116:42–52
- Choimeun S, Phumejaya N, Pomnakchim S, Chantrapornchai C (2010) Tool for collecting spatial data with

- Google Maps API. U-and E-Service. In: Kim T, Ma J, Fang W, Park B, Kang BH, Ślęzak D (eds) Science and technology. Springer, Berlin, Heidelberg, pp 107–113
- Doocy S, Daniels A, Murray S, Kirsch TD (2013) The human impact of floods: a historical review of events 1980–2009 and systematic literature review. PLOS Currents Disasters. <https://doi.org/10.1371/currents.dis.f4deb457904936b07c09daa98ee8171a>
- Dunne T, Leopold LB (1978) Water in environmental planning. Freeman, San Francisco
- EMDAT (2019) The OFDA/CRED international disaster database, University Catholic Louvain-Brussels, Belgium. <http://www.emdat.be> (December, 2019)
- Falck C, Ramatschi M, Subarya C, Bartsch M, Merx A, Hoeberechts J, Schmidt G (2010) Near real-time GPS applications for tsunami early warning systems. Nat Hazards Earth Syst Sci 10(2):181–189
- Hirabayashi Y, Mahendran R, Koirala S, Konoshima L, Yamazaki D, Watanabe S, Kim H, Kanae S (2013) Global flood risk under climate change. Nat Clim Chang 3:816–821
- Huang C, Wu J, Chen Y, Yu J (2012) Detecting floodplain inundation frequency using MODIS time-series imagery. In Agro-Geoinformatics (Agro-Geoinformatics), 2012 first international conference. IEEE, pp 1–6
- Hunt KMR, Menon A (2020) The 2018 Kerala floods: a climate change perspective. Clim Dyn 54:2433–2446. <https://doi.org/10.1007/s00382-020-05123-7>
- IPCC (2012). Managing the risks of extreme events and disasters to advance climate change adaptation (Eds Field, C. B. et al.), Cambridge Univ. Press
- Jeeramard M, Tangwannawit S (2014) A monitoring system for school flood victims using the android smart phone. The Tenth National conference on computing and information technology, pp 270–275
- Jonkman SN (2005) Global perspectives of loss of human life caused by floods. Nat Hazards 34:151–175
- Kraus RA (2000). Floodplain determination using ArcView GIS and HEC-RAS. In: Maidment D, Djokic D (eds) hydrologic and hydraulic. Modeling support. Redland: ESRI Press, pp 177–189
- Kwak Y, Park J, Fukami K (2014) Near real-time flood volume estimation from modis time-series imagery in the Indus River Basin. IEEE J Sel Top Appl Earth Obser Remote Sens 7(2):578–586
- Kumar A, Brahmanand PS, Nayak AK (2014) Management of cyclone disaster in agriculture sector in coastal areas. directorate of water management. Bhubaneswar, p 108
- Kulkarni AT, Mohanty J, Eldho TI, Rao EP, Mohan BK (2014) A web GIS based integrated flood assessment modeling tool for coastal urban watersheds. Comput Geosci 64:7–14
- Liang M, Guerra J, Brusilovsky P (2012) Building multi-layer social knowledge maps with Google Maps API. In Proceedings of workshop on semantic and adaptive social web (SASWeb 2012). University of Pittsburgh
- Likhit N (2014) Geoinformation technology for natural disaster studies in Thailand. Burapha Sci J. 19(2):179–188
- Maidment DR, Djokic D (2002) Hydrologic and hydraulic. Modeling support with geographic information systems. Redlands: ESRI. 216 p
- Majumder R, Bhunia GS, Patra P, Mandal AC, Ghosh D, Shit PK (2019) Assessment of flood hotspot at a village level using GIS-based spatial statistical techniques. Arab J Geosci 12(13):1–12. <https://doi.org/10.1007/s12517-019-4558-y>
- Martinis S, Twele A, Strobl C, Kersten J, Stein E (2013) A multi-scale flood monitoring system based on fully automatic MODIS and TerraSAR-X processing chains. Remote Sens 5(11):5598–5619
- Memon AA, Muhammad S, Rahman S, Haq M (2015) Flood monitoring and damage assessment using water indices: A case study of Pakistan flood-2012. Egypt J Remote Sens Space Sci. 18(1):99–106
- Mioc D, Nickerson BG, Anton F, Fraser D, MacGillivray E, Morton A, Tang P, Arp JP, Liang G (2008) Web-GIS application for flood prediction and monitoring. WIT Trans Ecol Environ 118:145–154
- Mills E (2005) Insurance in a climate of change. Science 309:1040–1044
- Mentzafou A, Markogianni V, Dimitriou E (2017) The use of geospatial technologies in flood hazard mapping and assessment: case study from river Evros. Pure Appl Geophys 174:679–700. <https://doi.org/10.1007/s00024-016-1433-6>
- Muthukumara M, Bandyopadhyay S, Chonabayashi S, Markandya A, Mosier T (2018) South Asia's Hotspots: impacts of temperature and precipitation changes on living standards. South Asia Development Matters; Washington, DC: World Bank. © World Bank. <https://openknowledge.worldbank.org/handle/10986/28723> License: CC BY 3.0 IGO.”
- Pagatpat JC, Arellano AC, Gerata OJ (2015) GSM & web-based flood monitoring system. In IOP Iop Conf Ser: Mater Sci Eng. 79(1):012023. 012023, IOP Publishing
- Pesaresi M, Ehrlich D, Kemper T, Siragusa A, Florczyk AJ, Freire S, Corbane C (2017) Atlas of the Human Planet
- Pekel J-F, Cottam A, Gorelick N, Belward AS (2016) High-resolution mapping of global surface water and its long-term changes Nature 540. <https://doi.org/10.1038/nature20584>
- Rentschler J, Salhab M (2020) People in Harm's way: flood exposure and poverty in 189 countries. Policy Research Working Paper. No. 9447
- Rubinato M, Nichols A, Peng Y, Zhang JM, Lashford C, Cai YP, Lin PZ, Tait S (2019) Urban and river flooding: Comparison of flood risk management approaches in the UK and China and an assessment of future knowledge needs. Water Sci Eng 12(4):274–283
- Samanta RK, Bhunia GS, Shit PK et al (2018) Flood susceptibility mapping using geospatial frequency ratio technique: a case study of Subarnarekha River

- Basin. *India Model Earth Syst Environ* 4:395–408. <https://doi.org/10.1007/s40808-018-0427-z>
- Singh VP, Frevert D (2006) *Watershed models*. Taylor & Francis. Boca Raton
- Sampson CC, Smith AM, Bates PD, Neal JC, Alfieri L, Freer JE (2015) A high-resolution global flood hazard model. *Water Resour. Res* 51:7358–7381. <https://doi.org/10.1002/2015WR016954>
- Suparta W, Ali MAM (2012) Monitoring of GPS precipitable water vapor during the severe flood in Kelantan. *Am J Appl Sci* 9(6):825–831
- Statistics Canada, Postal Code Conversion File (PCCF) (2008) Reference Guide September 2007 Postal codes, Catalogue no. 92–153-GIE, Issue number 2008001, ISSN 1708–3095, January 2008
- Tagliavini F, Mantovani M, Marcato G, Pasuto A, Silvano S (2007) Validation of landslide hazard assessment by means of GPS monitoring technique? a case study in the Dolomites (Eastern Alps, Italy). *Nat Hazards Earth Syst Sci* 7(1):185–193
- Talbot CJ, Bennett EM, Cassell K et al (2018) The impact of flooding on aquatic ecosystem services. *Biogeochemistry* 141:439–461. <https://doi.org/10.1007/s10533-018-0449-7>
- Zhang F, Zhu X, Liu D (2014) Blending MODIS and Landsat images for urban flood mapping. *Int J Remote Sens* 35(9):3237–3253
- Zischg AP, Bermúdez M (2020) Mapping the Sensitivity of Population Exposure to Changes in Flood Magnitude: Prospective Application From Local to Global Scale. *Front Earth Sci* 8:390. <https://doi.org/10.3389/feart.2020.534735>



Flood Susceptibility Mapping Using Morphometric Parameters and GIS

2

Md. Hasanuzzaman, Aznarul Islam,
Biswajit Bera, and Pravat Kumar Shit

Abstract

The present study investigates sub-watershed prioritization for flood susceptibility mapping of the Silabati River basin (India) based on morphometric parameters. This river basin is a sixth-order drainage system with an adendritic drainage pattern and traverses an area of 4247.99 km². Almost every year, the lower stretch of the Silabati river basin experiences floods due to physiographic characteristics and excessive rainfall during a short time. The present work has been conducted with an integrated outlook involving the morphometric parameters, geological, and climate data by geospatial techniques for determining the probability of spatial flood risk. A ranking method has been employed to prioritize the sub-watersheds for susceptibility to flooding. The results of this study depict that 48.18% area of the basin including 11 out of 26

sub-watersheds has a high to very high flood susceptibility area. Drainage density, basin slope, circulatory ratio, relative relief, relief ratio, stream frequency, and ruggedness number are the most important morphometric parameters for flooding in the study area. Since there were no such government or private historical flood records that are required for flood modeling, various morphometric parameters have been accurately used to measure sub-watershed-wise flood susceptibility. The performance and efficiency of this method are validated using ROC and AUC, which ensures a considerable amount of accuracy (89.2%) of the study. Moreover, this research may be used as a guideline for surface runoff harvesting and flood mitigation at the sub-watershed level.

Keywords

Flood · Geospatial technology · Silabati River basin · Morphometric parameters · Sub-basin prioritization

Md. Hasanuzzaman (✉) · P. K. Shit
PG Department of Geography, Raja N. L. Khan
Women's College (Autonomous), Gope Palace,
Midnapore 721102, West Bengal, India

A. Islam
Department of Geography, Aliah University,
Kolkata, India
e-mail: aznarul.geog@aliah.ac.in

B. Bera
Department of Geography, Sidho Kanho Birsha
University, Puruliya, India

2.1 Introduction

Floods are one of the most vital hydrological and meteorological hazards (Huang et al. 2008; Markantonis et al. 2013; Toduse et al. 2020). It has several negative and sudden impacts on human life and livelihood especially the agrarian

economy (Leskens et al. 2014; Yang et al. 2015; Bui et al. 2020; Islam and Ghosh 2021). United Nations Office for Disaster Risk Reduction (UNISDR) reported that the human life losses due to flood events were around 15 lakhs and around 11.1% mortality rate in the world during 1996–2015. Developing nations like India, Sri Lanka, and Bangladesh portray a very high impact rate. The flood scientists and organizations have predicted that annual losses up to US \$415 billion worldwide due to floods in 2030 (Grabs 2010; Karamouz and Fereshtehpour 2019; WMO 2016; UNISDR 2015). Floods of small watersheds area (less than 1,000 km²) reveal a complex and sudden response time due to the orographic nature of rainfall in the high land region (Destroet al. 2018; Obeidat et al. 2021). Some direct and indirect factors such as rainfall characteristics, drainage properties, infiltration, environmental conditions, evapotranspiration, and anthropogenic activities are the significant factors that impact the intensity of flood susceptibility (Azmeri and Vadiya 2016; Jodar-Abellan et al. 2019; Samanta et al. 2018). Identification of vulnerable areas for floods is a very important precursor to reduce the negative impact on human life and infrastructure (Ali et al. 2020).

Watershed management focuses on reducing the negative impact of surface runoff or floods, and surplus water use for various beneficial purposes such as irrigation, groundwater storage, and reduces erosion (Ratna et al. 2017; Sebastian et al. 1995). For water resource management, the optimum use of watersheds is important (Worku et al. 2020). Morphometric parameters for prioritization of sub-watersheds within a basin is necessary for the conservation of land and water resource (Aher et al. 2014). Various research studies have employed morphometric investigation for the prioritization of sub-watershed-wise flood or erosion susceptibility (Bhatt and Ahmed 2014; Abuzied et al. 2016; Ameri et al. 2018; Asfaw and Workineh 2019; Charizopoulos et al. 2019; Hussein et al. 2019; Kannan et al. 2018; Rajasekhar et al. 2020; Alam et al. 2020; Das 2020; Islam and Deb Barman 2020). These researches have employed some algorithms from

some classic works such as Horton (1945, 1932), Smith (1950), Strahler (1952), Miller (1953), and Schumm (1956). According to Strahler (1964), morphometric parameters depicted a relatively very simple method. To investigate the geomorphic history, geological and hydrological conditions of the basins, it may be employed. Morphometric features of the basin are very important parameters that influence flood intensity. Therefore, this research of the basin morphometry can provide a very significant database in relation to their hydrological responses (Borga et al. 2008). Of late, remote sensing (RS) and geographical information systems (GIS) have been extensively employed with the objective of watershed management (Chatterjee et al. 2013; Okumura and Araujo 2014; Hasanuzzaman et al. 2021). Digital elevation model (DEM) is a very high-resolution RS data and it's freely available for access. It is a very effective tool for the accurate investigation of watershed morphometric parameters (Ratnam et al. 2005; Samanta et al. 2018; Majumder et al. 2019; Hasanuzzaman and Mandal 2020).

Silabati Basin of West Bengal is also having ample water resources but very unevenly distributed in its upper, middle, and lower reaches of the basin. The western part is a drought-prone area while the eastern part faces the flood problem in years of surplus rain. In both cases, people suffer from loss of life and damage to properties. Therefore, this region is demanding to utilize the available water resources judiciously to solve the problems of water shortage as well as to prevent the misuse of water. This research work is a small effort to evaluate the flood of Silabati Basin that contributes to its present configuration in an integrated manner for scientific and judicious use and also for development watershed and sub-watershed wise surface runoff harvesting and flood management. Moreover, this type of work is relatively absent at the national level or regional level. Thus, the main objective of this research is the prioritization of sub-watersheds corresponding to flash floods or floods based on morphometric analysis using geo-spatial techniques. The output of this present research can be utilized to help the government to take the

necessary steps in those regions that are susceptible to floods and very high possibility for runoff harvesting.

2.2 Study Area

The present study is executed over the Silabati river basin situated in the southwestern part of the Bengal Basin. The Silabati or Silai River as well as Arkusa Nala and their ramifying channels have furrowed up the Dwarkeswar-Kangsabati interfluvium at Hura block and flows over three districts of Puruliya, Bankura, and West Medinipur. It is the principal tributary of the Rupnarayan River (Shit et al. 2015). The river Silabati originates at Baragram village (23°15'N and 86°39'E) of Puruliya district on Manbazar-Adra road and flows southeast for about 20 km in Puruliya district. The river leaves the district at Pancha block and enters Bankura district near Salanpur of Indpur block (Fig. 2.1).

Silabati River watershed presents a unique physical setting in the sense that hard rock plateau and fringe area, laterite covered upland, undulating tract, and flat alluvial plain, all are found in a single basin (Shit et al. 2016; Islam et al. 2020). Actually, the entire geomorphic unit is the southeastern continuation of the Chhotanagpur Plateau (Fig. 2.2). Plateau Fringe lies in the extreme northwestern part, which is the remnants of the spurs projecting from the Chhotanagpur plateau. Its elevation varies from 160 to 227 m and is characterized by high relative relief and moderate slope. Archaean rocks composed of granite, gneiss, schist occupy this area (Dolui et al. 2014; Gayen et al. 2013). The plateau slope lies in the eastern part of the plateau fringe. This part is covered by crystalline rocks of the Archaean age and characterized by hillocks, low ridges, and valleys. Passing over the plateau slope, the basin area presents a dissected upland covered by hard rocks and old alluvium with lateritic capping. The terrain is characterized by irregular, non-contiguous, and uneven tracts (Shit and Pati 2012). The central undulating and rolling plain to the east of this dissected upland presents a flattened and rolling

topography. This lateritic part is underlain by deposits of older alluvium and shows dissected badland topography at places (Shit and Maity 2012). This rolling plain gradually merges into a flat alluvial plain to the east consisting of assorted materials of sub recent to recent age. Flood plains are confined mainly along the major rivers which allow sudden discharge sometimes causing heavy floods.

Silabati River basin has got its climatic characteristics due to its tropical location. The upland tract in the west is much drier than that of the eastern part. The basin area enjoys a sub-tropical humid climate characterized by "Monsoon" conditions with marked seasonal variations. The mean annual rainfall of the basin varies from 110 cm in the west to 121 cm in the east (Fig. 2.2). The rainfall during monsoon months from June to September receives around 78% of the total annual rainfall with July and August being the rainiest months. The temperature starts rising from March and attains its extremes up to 48 °C during May. Otherwise, the basin is characterized by a mean minimum temperature of 21 °C and a maximum temperature of 33 °C. With the onset of the monsoon, the temperature drops appreciably. December and January are the cold months with mean maximum and minimum temperature as 26 °C and 11 °C, respectively.

2.3 Data and Methods

The conceptual framework of the method applied in this present study is depicted in Fig. 2.3. For the objective of watershed characterization and prioritization of sub-watersheds of the Silabati River basin, twenty-six morphometric parameters were selected (Table 2.1). According to the total weight value of sub-watersheds, the total ranking method was used for the ranking sub-watersheds (Watershed prioritization) (Biswas et al. 1999; Puno and Puno 2019). The main morphometric parameters of the basin are linear, areal, and relief aspects of watersheds (Melton 1957; Strahler 1964). For computing the morphometric indices, basic parameters of a watershed like a basin length, basin area, perimeter, lengths of streams,

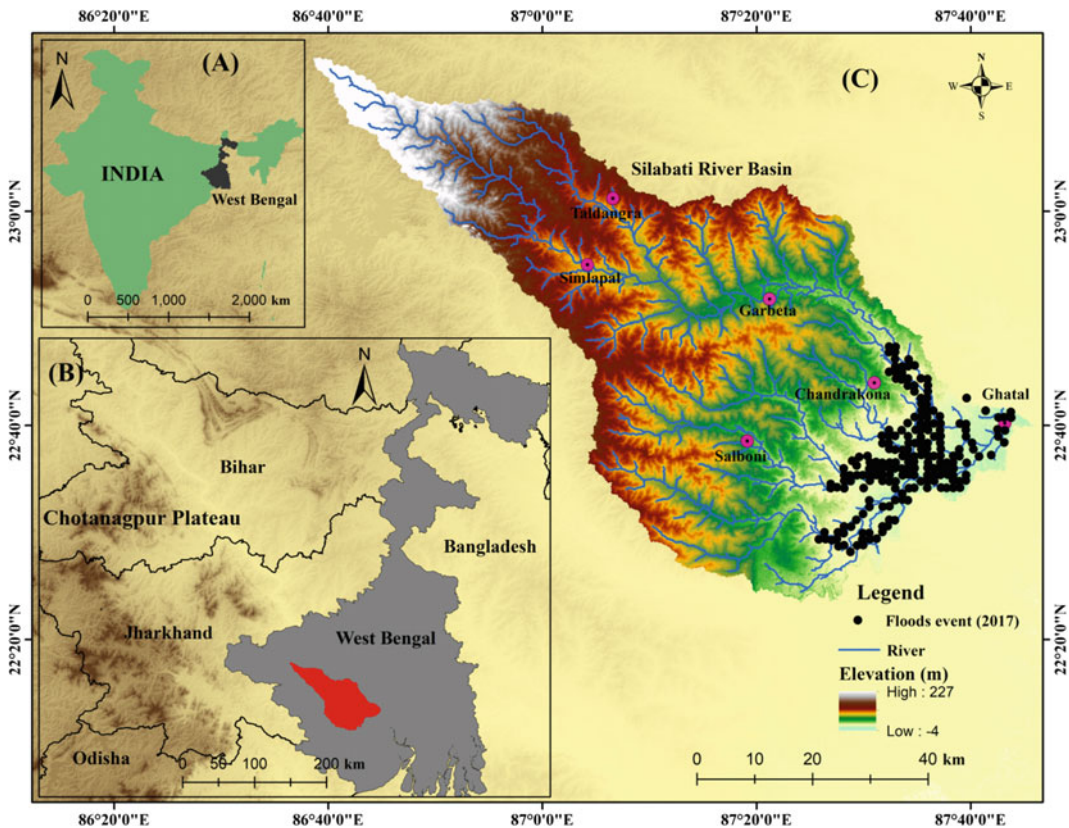


Fig. 2.1 Location of the study area

and the number of streams for each stream order have been calculated directly from the Digital Elevation Model (DEM) using GIS techniques. The DEM was downloaded from www.search.earthdata.nasa.gov and www.earthexplorer.usgs.gov with the resolution is 30 m and 12.5 m (Radar Imagery 2001–2006). First of all, filling the DEM for finding out the missing data was accomplished followed by the generation of stream network and flow accumulation map of the Silabati River Basin (SRB) and then to subdivide the SRB into sub-watersheds. Mathematical equations were used for the measurement of other morphometric parameters of the basin like drainage density, ruggedness number, circularity ratio, basin relief, length of overland flow, relative relief ratio, basin slope, hypsometric integral, elongation ratio, stream frequency, and relief ratio (Obeidat et al. 2021). These mathematical equations are depicted in Table 2.1. For the sub-

watersheds prioritization, the morphometric ranking method (Total Rank) was employed (Patel et al. 2012). According to morphometric parameters value, each sub-watershed was divided into various prioritized rank groups, where rank 1 represents the very low probability for floods risk, and so on (Obeidat et al. 2021).

The selected 12 parameters of morphometric have been employed for the sub-watersheds susceptibility map of the flood (Table 2.1). All these parameters of morphometric are related to flood either directly or indirectly. Out of twelve parameters, eight parameters (relief ratio, basin area, circularity ratio, drainage density, basin slope, ruggedness number, relative relief ratio, and stream frequency,) have a direct relationship with the surface flow or flood possibility. The higher values of eight parameters are indicating the higher degree of possibility to flood risk. So, these parameters of sub-watershed having the

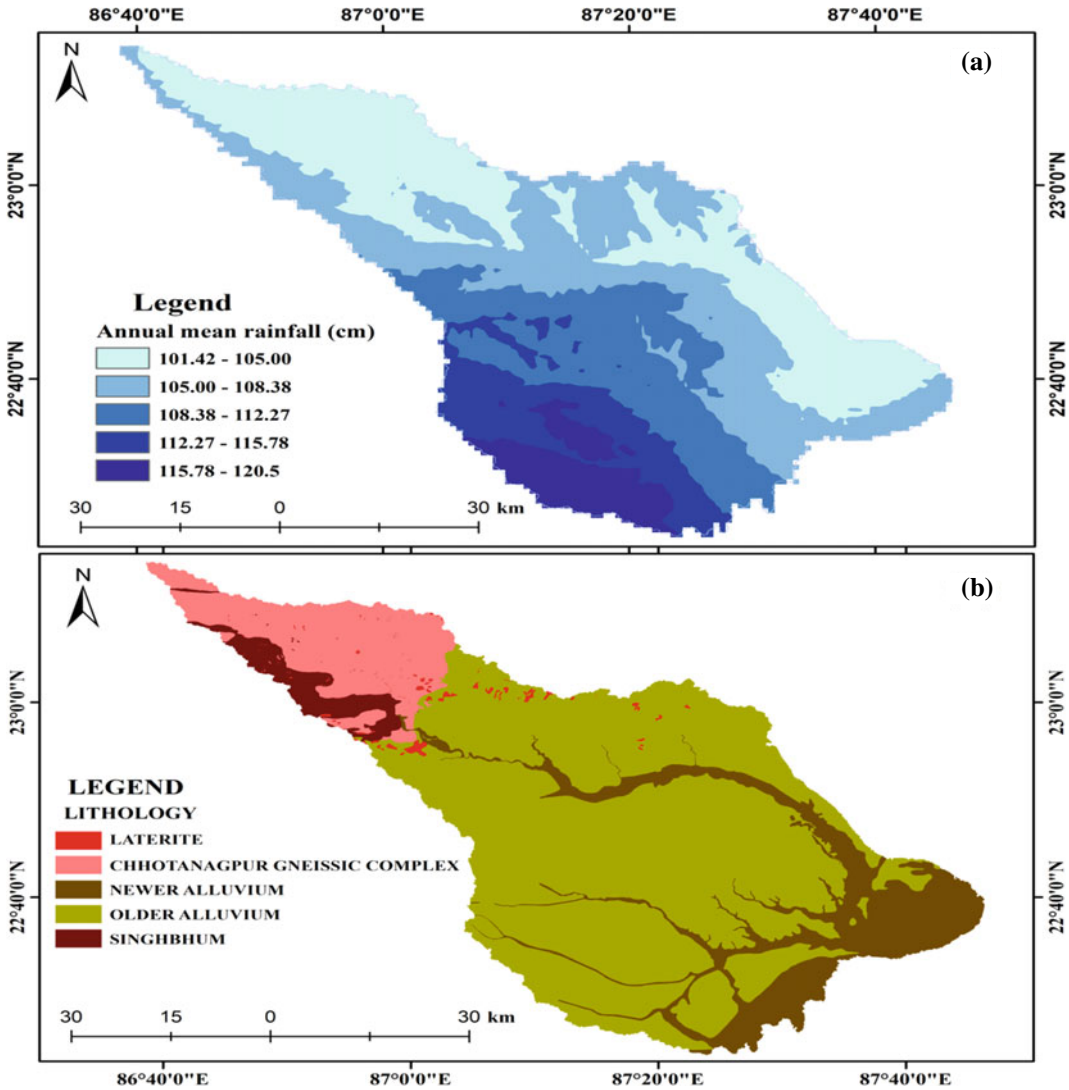


Fig. 2.2 a Climate map and b Geological map (Source Geological Survey of India) of the study area

highest values are given the top rank (5). On the opposite side, the other four parameters (shape factor, hypsometric integral, length of overland flow, and elongation ratio) have an inverse relationship to surface runoff or flood possibility. The lower values of the four parameters are indicating a higher degree of flood possibility and these parameters are given the top rank (5). Firstly, each parameter value was summed, and

normalized from 0 to 1 to find out the specific prioritized rank of the sub-watershed. The same value of sub-watershed has defined the similar ranking. After that the sub-watersheds are divided into five floods susceptibility categories (very high, high, moderate, low, very low priority) following a simple equation to demarcate the interval length that is $(\text{Maximum} - \text{Minimum}) / 5$ (Farhan and Anaba 2016).

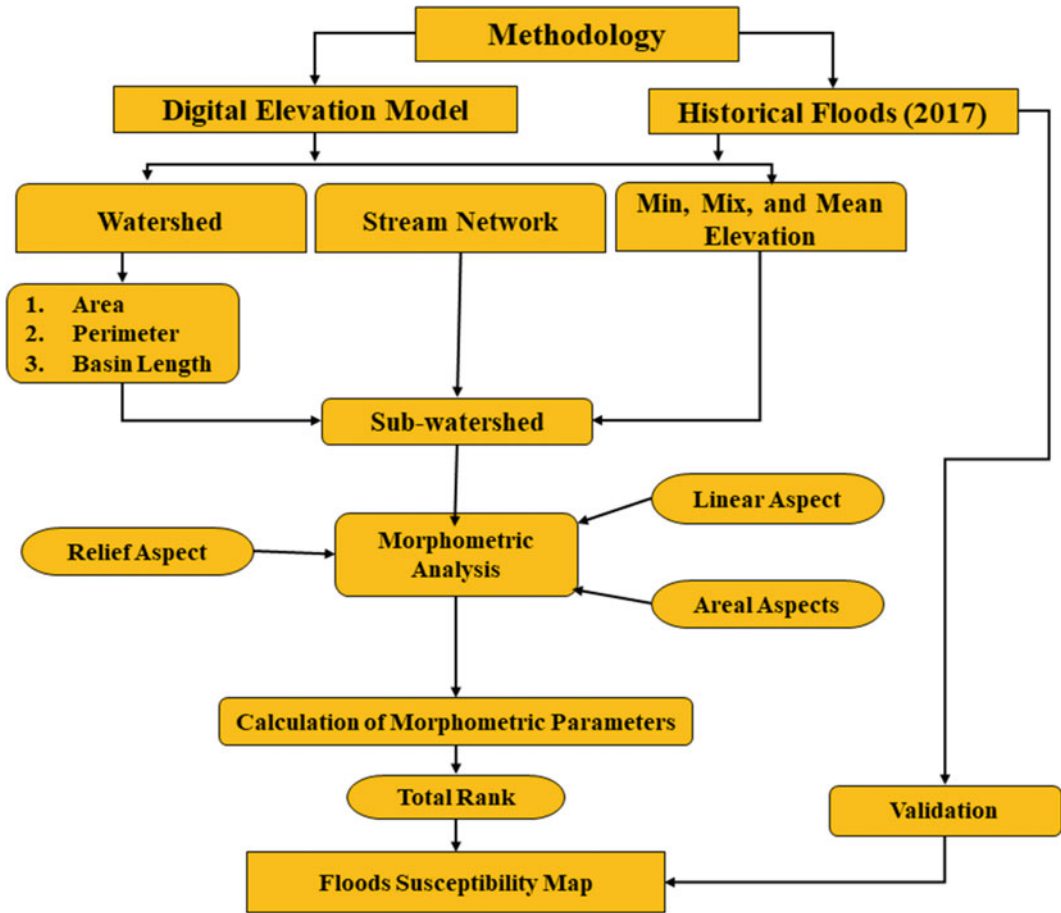


Fig. 2.3 Conceptual framework of the methodology of the study

2.4 Results and Discussion

2.4.1 Morphometric Parameters

According to the flow accumulation of the SRB, 26 sub-watersheds were demarcated using the ArcGIS 10.8 software (Fig. 2.4). The final outputs of the morphometric investigation of all sub-watersheds were depicted in Fig. 2.5 and Table 2.2. To determine the flood susceptibility map, the geomorphologic and hydrological relation in the study area was used (Fig. 2.5).

2.4.1.1 Linear Parameters

Basin perimeter is a very significant basic parameter of morphometric parameters as an

indicator of basin shape and size. The minimum perimeter value was found as 32 km (SW 5) and the maximum value was found as 176.44 km (SW 25). A strong correlation is depicted between basin perimeter and area (Obeidat et al. 2021). A significant indicator of surface runoff feature is basin length (Christopher et al. 2010; Taha et al. 2017). In the present study, basin length ranges from 5.89 km (SW 13) to 49.36 km (SW 25). Also, a strong correlation is depicted between stream length and basin length (Obeidat et al. 2021). The stream order of the SRB extends up to six orders but all sub-watersheds vary from first order to fourth order. The high stream numbers represent the high surface flow or rapid peak flow (Bhat et al. 2019). In the study river basin, the total stream number is 2559, and 1285

Table 2.1 Detailed information of morphometric parameters

Parameter no	Morphometric parameter	Formula/definition	References	
Linear	1	Basin perimeter (P)	Perimeter of the watershed (km)	Horton (1945)
	2	Basin length (L_b)	Length of the basin (km)	Horton (1945)
	3	Stream order (U)	Hierarchical rank	Strahler (1952)
	4	Total number of streams (N_u)	Total no. of streams of all orders	Strahler (1952)
	5	Stream length (L_u)	Length of the stream (km)	Horton (1945)
	6	Total number of streams (N_u)	Total no. of streams of all orders	Strahler (1952)
	7	Stream length (L_u)	Length of the stream (km)	Horton (1945)
Areal	8	Basin area (A)	Plan area of the watershed (km ²)	Horton (1945)
	9	Drainage density (D_d)	$(D_d = L_u / A$, where L_u = total stream length of all orders (km) A = area of the watershed (km ²)	Horton (1945)
	10	Length of overland flow (L_o)	$L_o = 1/(2 * D_d)$, where D_d = drainage density	Horton (1945)
	11	Stream frequency (F_s)	$F_s = N_u / A$, where N_u = Total number of streams of all orders A = area of the basin (km ²)	Horton (1945)
	12	Elongation ratio (R_e)	$R_e = 1.128 * (A^{0.5}) / L_b$, where A = area of the basin (km ²) L_b = basin length (km)	Strahler (1957)
	13	Circularity ratio (R_c)	$R_c = 4 \times \pi \times A / P^2$, where $\pi = 3.14$ A = area of the basin (km ²) P = perimeter (km)	Schumm (1956)
	14	Shape factor (S_f)	$S_f = L_b^2 / A$, where L_b = basin length (km) A = area of the basin (km ²)	Miller (1953)
Relief	15	Basin relief (H)	$H = h - h_1$, where h = maximum height (m) h_1 = minimum height (m)	Horton (1945)
	16	Relief ratio (R_r)	$R_r = H / L_b$, where H = total relief (km) L_b = basin length (km)	Malik et al. (2011)
	17	Relative relief ratio (R_v)	$R_v = H / P$, where H = total relief (km) P = perimeter of the basin (km)	Schumm (1956)
	18	Basin slope (B_s)	$B_s = H / L_b * 60$, where H = total relief (km) L_b = basin length (km)	Melton (1957)
	19	Ruggedness number (R_n)	$R_n = D_d * H$, where H = basin relief (km) D_d = drainage density	Farhan and Anaba (2016)
	20	Hypsometric integral (HI)	$HI = (E_{mean} - E_{min}) / (E_{max} - E_{min})$, where E_{mean} = the weighted mean elevation E_{max} = maximum elevation E_{min} = minimum elevation	Schumm (1956)

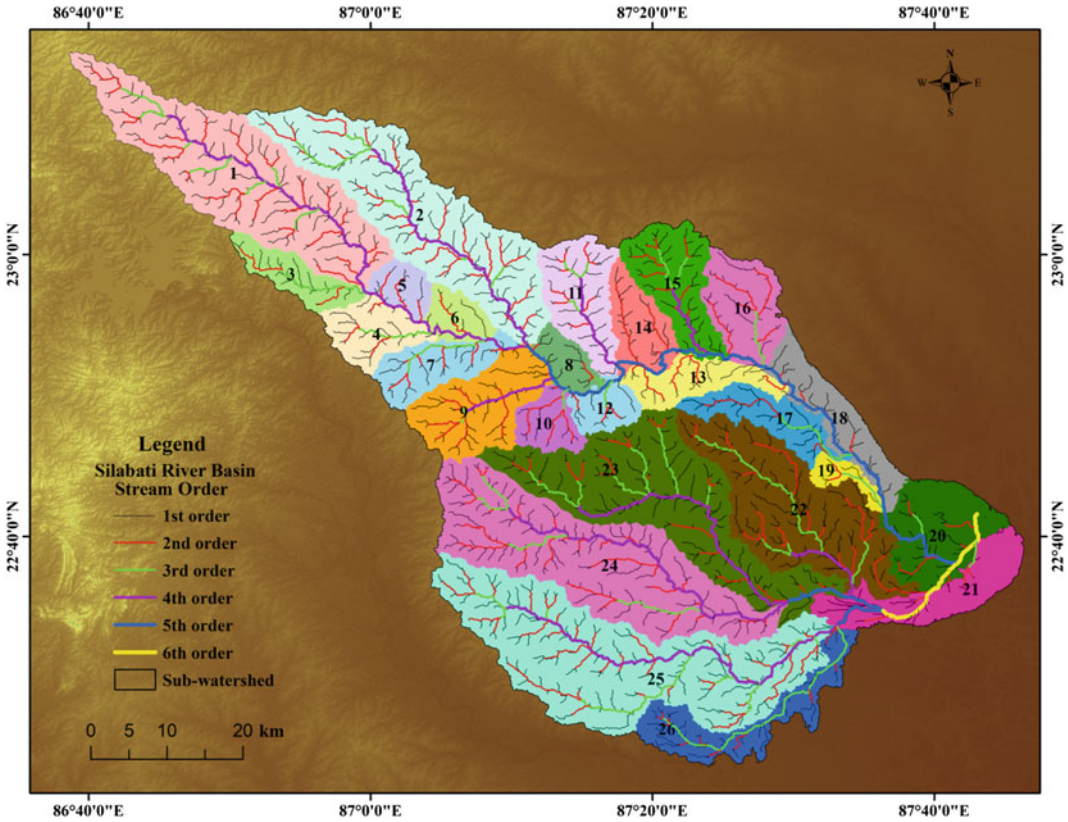


Fig. 2.4 Sub-watershed of the Silabati River basin with drainage pattern and stream order

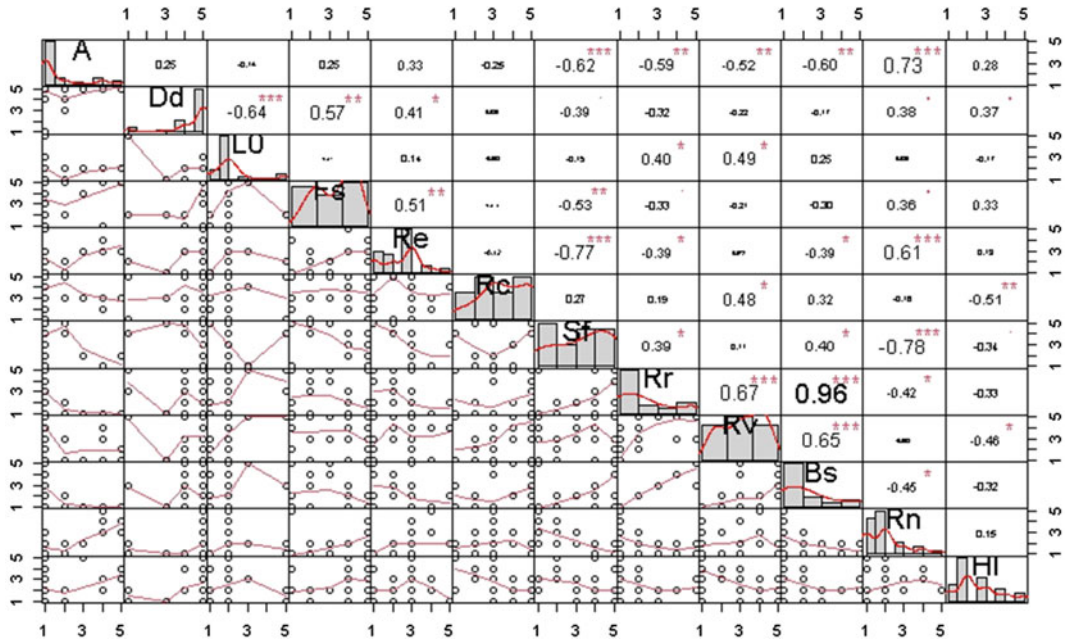


Fig. 2.5 The matrix of the Pearson correlation coefficient for all twelve morphometric parameters weight value

streams are first-order streams (50.2%) in all sub-watershed. Among the 26 sub-watersheds, SW 25 has the highest total number of the stream (320) and SW 8 has the minimum total number of the stream (18 streams). Stream length indicates the contributing area of a basin of a certain order (Magesh et al. 2011). According to Strahler (1952), the higher the stream length the lower the infiltration, and the greatest runoff-producing power of the basin. The SRB's total stream length of all orders is 3274.96 km.

2.4.1.2 Areal Parameters

The sub-basin area of the SRB ranges from 26.26 km² (SW 19) to 543.42 km² (SW 25). These sub-watersheds are located at the maximum rainfall area of the basin. Drainage density is controlled mainly by two factors, such as relative relief and slope of the basin (Magesh et al. 2011). So, it is directly correlated with flood or flash flood. The drainage density is high which means minimum infiltration rate and maximum surface runoff of the watershed (Kelson and Wells 1989). In the current study, maximum drainage density was found as SW 3, and the minimum was found as SW 5. According to Horton (1945), length of overland flow denotes the length of water flow over the land surface before it becomes concentrated into defined stream channels. Climate conditions, rocks, soil material, relief, and vegetative are the main influential factors of the length of overland flow (Youssef et al. 2009). The length of the overland flow value of the SRB is 0.77 and it varies from 0.06 (high probability to flood) for SW 5 to 0.88 for SW 18. Therefore, sub-watersheds 5 and 6 were given the top rank (5) that these sub-basins have high susceptibility for the flood. According to Horton (1932), stream frequency denotes the ratio between the total number of streams and area. If the stream frequency value is high, maximum surface flow and minimum infiltration are recorded (Melton 1957). The highest stream frequency of the SRB is found for SW 3 and the lowest for SW 1. SW 3 with the high vulnerability of sub-watershed for flooding with low infiltration capacity. According to Schumm (1956), the bifurcation ratio is the

ratio between the number of stream segments of a given order to the number of segments of the next higher order. Its low value means that it is structurally less disturbed watersheds (Strahler 1964) and the maximum value represents the high runoff producing capability of a basin in a short lag time (Howard 1990). The SRB has found a mean bifurcation ratio value of 2.52, and it varies from 1.64 to 4.75 across the sub-watersheds.

According to Horton (1932), the elongation ratio signals about the basin shape. The elongation ratio ranges between 0.6 and 0.8, which means basin characteristics have steep slopes and high relief. Another side, its value is close to 1 which means that the basin characteristic has very low relief (Dar et al. 2013). In this work, SW 12, 13, 18, 19, 20, and 21 have the lowest sensitivity to flooding, whereas SW 7 has the highest indicating more susceptibility to flooding. According to Miller (1953), the circulatory ratio is the proportion of the watershed area to the area of the circle having the same perimeter of the watershed. Geological structures, roughness, slope, climate, frequency of stream, and length of stream are controlled by the circulatory ratio (Bisht et al. 2018). Its value is directly correlated with flash floods. Its higher value indicates the minimum time taken to surface runoff and maximum time taken to infiltration. In this research, SW 6 has the lowest circulatory ratio value, and SW 12 to have the highest value (high potential for flooding). Sub-watersheds 4, 5, 8, 9, 10, 12, and 16 are given the highest rank (5) due to the high circulatory ratio value, whereas sub-watersheds 6 and 26 are referred to the least rank (1). The shape factor determines the rate of sediment and water yield (Farhan et al. 2017). The low value of the shape factor represents maximum relief and steep slopes that indicate a high probability of flood. The shape factor values of the SRB vary from 0.93 (SW 12) to 5.83 (SW 23). Sub-watersheds 1, 2, 3, and 23 with high shape factor values are denoted by the lowest rank (1), and sub-watersheds 10, 12, 13, 18, 19, 20, and 21 with the low values are denoted by the highest rank (5).

2.4.1.3 Relief Parameters

The difference between the highest elevation and lowest elevation is called basin relief. It plays an important role in various aspects such as drainage development, erosional properties of the terrain, landforms development, surface and subsurface water (Magesh et al. 2011). In this study, sub-watershed 21 is determined as the minimum and sub-watershed 3 as the maximum. It depicts that the basin has the maximum potentiality to produce floods. In the present study, SW 12 is the most sensitive sub-watershed for floods, whereas SW 20 is the least sensitive one. Sub-watersheds 6, 12, and 13 are found to have a high value of relief ratio values. According to Macka (2001), the relative relief ratio has a direct relationship with the probability of floods. In the present study, sub-watersheds 20, 21, 22, 23, 25, and 26 with low relative relief ratio value has been given the lowest rank (1) and sub-watersheds 3, 4, 5, 6, 8, 12, and 14 with high values are denoted by the highest rank (5). Basin slope has an impact on the hydrological processes such as the amount of surface runoff and speed, and the time (Meraj et al. 2013). Steep slope and high relief of the basin increase the probability of flash floods. In the present study, sub-watersheds 1, 2, 20, 21, 22, 23, 24, 25, and 26 with the lowest basin slope values are denoted by the lowest rank (1). Sub-watersheds 3, 12, and 13 with the highest values are denoted by the highest rank (5). Ruggedness is the nature of the surface undulations of the basin (Selvan et al. 2011). If the ruggedness number is maximum, there is a high possibility for erosion and flash floods (Patton and Baker 1976). It is directly related to flooding (Obeidat et al. 2021). Sub-watersheds of the study areas 8, 12, 13, 18, 19, 20, 21, and 26 with the lowest ruggedness number are denoted by the lowest rank (1). Sub-watershed 1 with the highest ruggedness number are denoted by the highest rank (5). Hypsometric Integral is a very important parameter to determine the interrelations existing among the lithology, climate, erosion, and tectonic uplift (Pavano et al. 2018). Hypsometric integral value is lowest for SW 22 and SW 26 and hence these

watersheds are given top rank (5) while SW 5, SW 7, SW11, and SW 21 with the highest hypsometric integral are given the lowest rank (1).

The eight direct morphometric parameters (basin slope, basin area, circularity ratio, ruggedness number stream frequency, relief ratio, drainage density, and relative relief ratio) and four indirect parameters (length of overland flow, shape factor, hypsometric integral, and elongation ratio) weights are employed for the Pearson correlation coefficient matrix in Fig. 2.5. This matrix revealed that the correlation of the all-morphometric parameters are correlated to each other. According to the result of the correlation analysis, the strongest correlation has been found between the basin relief and basin slope ($r = 0.96$). Moreover, the circularity ratio to other morphometric parameters has been found as the weakest correlation.

2.4.2 Prioritization of the Sub-basin for Flood Susceptibility

The morphometric total ranking method was used for assessing the flood hazard. Table 2.2 and Fig. 2.6 illustrate the results of this study. The total ranking method was used for the total score of twelve factors for each sub-watershed. The flood prioritization map of the SRB represents two sub-watersheds (18, and 21) with very high flood probability. About 5.61% of the total area is under this category and this area is also the same as that of the historical flood. Around 42.57% of the total area encompassing nine sub-watersheds (12, 13, 17, 19, 20, 22, 24, 25, and 26) are under the high flood susceptibility zone. The results of the study represent that this is a high flood-prone area. Around 27.65% of the total basin area distributed over ten sub-watersheds (5, 6, 7, 8, 9, 10, 11, 15, 16, and 23) are included in the moderate class flood risk category. Sub-watersheds 1 and 14 are fall under the low flood risk class with around 11.60% of the total basin area. Sub-watersheds 2, 3, and 4 with around 12.68% of the total area of the basin are included under very low flood risk areas. The

Table 2.2 Details description of the results of the study with weight values

SW	A	D_d	L_o	F_s	R_e	R_c	S_f	R_r	R_v	B_s	R_n	HI	Total rank	Normalization	Prioritized rank	Priority
1	1	5	2	5	3	1	4	1	1	1	1	5	30	0.40	3	Low
2	2	4	1	2	1	5	5	1	1	1	1	2	26	0.20	2	Very low
3	2	3	1	2	1	3	5	1	1	1	1	1	22	0	1	Very low
4	1	4	1	1	1	2	5	2	2	2	1	4	26	0.20	2	Very low
5	1	1	5	2	2	5	4	3	5	3	1	1	33	0.55	7	Moderate
6	1	1	5	2	2	1	4	5	5	3	2	2	33	0.55	7	Moderate
7	4	5	2	1	4	3	1	1	4	1	5	2	33	0.55	7	Moderate
8	1	3	2	2	3	5	3	3	5	3	1	2	33	0.55	7	Moderate
9	2	5	2	5	2	5	2	2	2	2	2	2	33	0.55	7	Moderate
10	1	5	2	2	2	3	5	2	5	2	2	2	33	0.55	7	Moderate
11	1	5	2	5	3	4	3	2	3	2	2	1	33	0.55	7	Moderate
12	1	4	2	1	1	5	5	5	5	5	1	2	37	0.75	9	High
13	1	5	2	3	1	3	5	5	3	5	1	2	36	0.75	9	High
14	1	4	1	2	1	3	5	4	3	4	1	2	31	0.45	4	Low
15	1	5	2	4	3	2	2	2	3	2	2	4	32	0.50	5	Moderate
16	3	5	2	4	3	3	2	1	1	1	2	5	32	0.50	6	Moderate
17	1	5	2	5	3	4	3	2	4	2	3	2	36	0.75	9	High
18	1	5	2	4	3	5	4	3	5	3	2	2	39	0.85	10	Very high
19	1	5	2	4	3	4	3	2	5	2	2	3	36	0.75	9	High
20	4	5	2	5	3	3	1	1	3	1	4	3	35	0.65	8	High
21	1	5	3	5	3	4	1	5	5	5	2	3	42	1.00	11	Very high
22	1	5	2	5	2	5	4	2	4	2	2	3	37	0.75	9	High
23	4	5	2	5	4	2	1	1	1	1	3	3	32	0.50	6	Moderate
24	5	5	2	5	3	3	2	1	2	1	3	3	35	0.65	8	High
25	5	5	2	5	3	3	2	1	1	1	4	4	36	0.65	8	High
26	1	5	2	4	5	4	3	2	4	2	2	1	35	0.65	8	High

upper part of the basin is a very low flood risk area. The lower-middle segment of the river basin is observed to be in a vulnerable condition since it belongs to the very high to high flood susceptible category. Also, these results are the same as that of the rainfall active area and geology. Current research represents that rainfall has a strong relationship with flood susceptibility. This work will be helpful for the authorities to take appropriate measures for reducing flood risk or surfaces runoff harvesting. Moreover, this work may be employed in other areas, when the historical flood data and validation are not available.

2.4.3 Validation

In the present context, accurately measuring and preparing the flood susceptibility map with validation is a very crucial and difficult task. The present study used success and prediction rate methods to validate the model by comparing predicted hazard areas to existing hazard locations (Zare et al. 2013). To do this, a total number of 200 known flood sites are demarcated from the flood map of 2017 (Figs. 2.1 and 2.6) published by the National Remote Sensing Centre (bhuvan.nrsc.gov.in). Therefore, an area under curve (AUC) method evaluated the

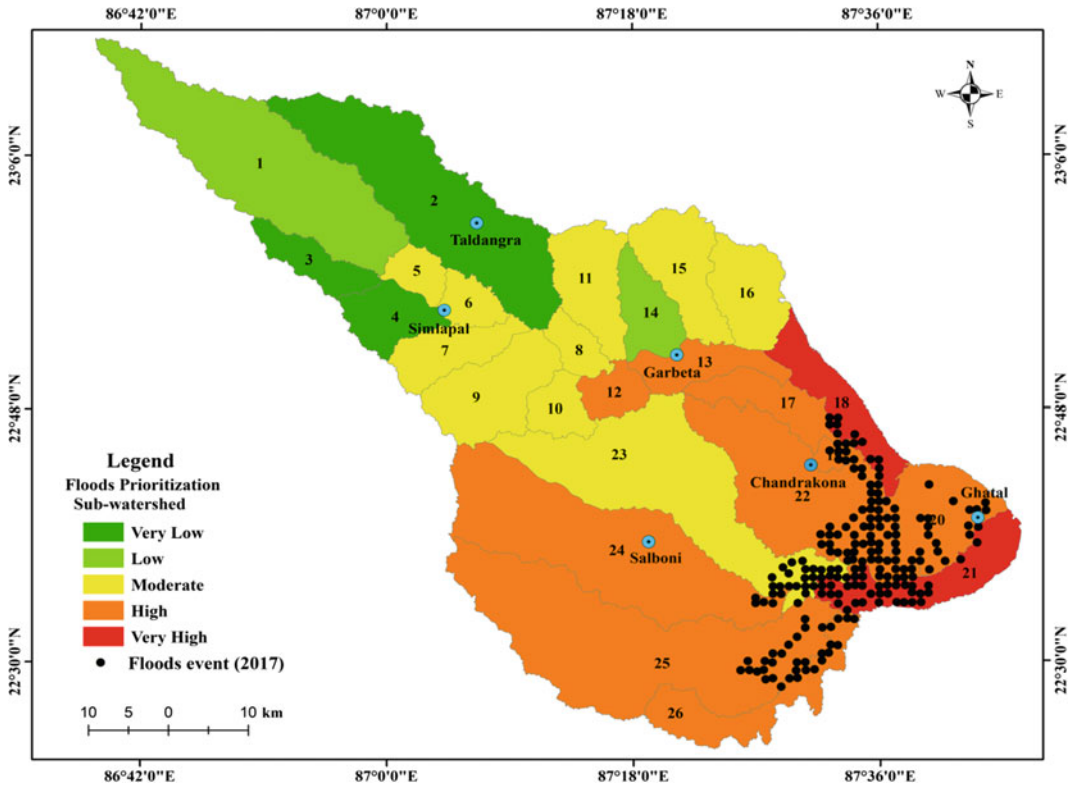


Fig. 2.6 Sub-watersheds-wise final flood susceptibility map

prediction capabilities of validation of the model (Swets 1988; Hong et al. 2015). In this work, the AUC is considered to evaluate the performance and efficiency of this morphometric method. In order to assess the validity of the flood susceptibility map, the AUC is computed, and the output value, i.e., 89.2% depicts that the accuracy level of the flood map prepared to adopt the morphometric analysis technique is well acceptable (Fig. 2.7). Also, different field photos during the flood also validate this work (Fig. 2.8).

2.5 Conclusion

Hydro-morphometric analysis and GIS techniques are employed to predict flood vulnerable areas of the SRB. Since there were no such

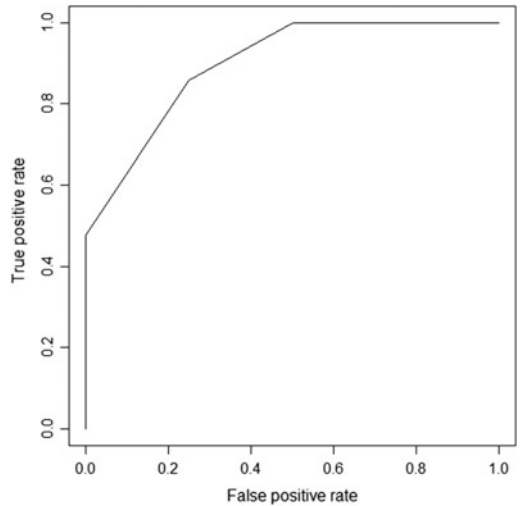


Fig. 2.7 Area under curve for validation of flood susceptibility map



Fig. 2.8 a Flood water spill over the area near Ghatal, b flood water spill over the road near Ghatal, c flood water spill over the bridge near Chandrakona, d flood water spill

over the area near Chandrakona, e flood water spill over the area near Salboni, f flood water spill over the road near Salboni (Source Field Photographs 2020)

government or private historical flood records that are required for flood modeling, sub-watershed-wise flood susceptibility analysis has been done using the morphometric investigation. The current study result depicts that around 48.18% of the total basin area is included under the high to very-high-flood susceptibility category. Basin slope, relative relief ratio, drainage density, circulatory ratio, relief ratio, stream frequency, and

ruggedness number are the most important morphometric parameters for flooding in the study area. The performance and efficiency of this method are validated using the AUC model that ensures a considerable amount of accuracy (89.2%) of the study. The flood prioritization map of the SRB represents two sub-watersheds (18 and 21) with very high flood probability. About 5.61% of the total area is under this category and

this area is also the same area as the area of the historical flood. Around 42.57% of the total area over nine sub-watersheds (12, 13, 17, 19, 20, 22, 24, 25, and 26) are under the high flood susceptibility zone. The result of the study represent that this is a high flood-prone area. Therefore, the current study depicts that managing the flood of the area is much needed. It should be the main focus of the government to protect human lives and agricultural land. Moreover, this study carried out using the combination of morphometric analysis with GIS may act as an important tool to understand sub-watersheds parameters related to flooding management.

References

- Abuzied S, Yuan M, Ibrahim S, Kaiser M, Saleem T (2016) Geospatial risk assessment of flash floods in Nuweiba area. *Egypt J Arid Environ* 133:54–72
- Aher PD, Adinarayana J, Gorantiwar SD (2014) Quantification of morphometric characterization and prioritization for management planning in semi-arid tropics of India: a remote sensing and GIS approach. *J Hydrol* 511:850–860
- Ali SA, Parvin F, Pham QB, Vojtek M, Vojtekova J, Costache R, ... Ghorbani MA (2020) GIS-based comparative assessment of flood susceptibility mapping using hybrid multi-criteria decisionmaking approach, nave Bayes tree, bivariate statistics and logistic regression: a case study of Topl'a basin, Slovakia. *Ecol Indicators* 117:106620. <https://doi.org/10.1016/j.ecolind.2020.106620>
- Alam A, Ahmed B, Sammonds P (2020) Flash flood susceptibility assessment using the parameters of drainage basin morphometry in SE Bangladesh. *Quat Int*. <https://doi.org/10.1016/j.quaint.2020.04.047>
- Ameri AA, Pourghasemi HR, Cerda A (2018) Erodibility prioritization of sub-watersheds using morphometric parameters analysis and its mapping: a comparison among TOPSIS, VIKOR, SAW, and CF multi-criteria decision-making models. *Sci Total Environ* 613–614:1385–1400
- Asfaw D, Workineh G (2019) Quantitative analysis of morphometry on Ribb and Gumara watersheds: implications for soil and water conservation. *Int Soil Water Conser Res* 7:150–157
- Azmeri HIK, Vadiya R (2016) Identification of flash flood hazard zones in mountainous small watershed of Aceh Besar Regency, Aceh Province, Indonesia. *Egyptian J Remote Sens Space Sci* 19:143–160
- Bhatt S, Ahmed SA (2014) Morphometric analysis to determine floods in the Upper Krishna basin using Cartosat DEM. *Geocarto Int* 29(8):878–894
- Biswas S, Sudhakar S, Desai R (1999) Prioritization of sub watersheds based on morphometric analysis of drainage basin—a remote sensing and GIS approach. *J Indian Soc Remote Sens* 27(3):155–166
- Bisht S, Chaudhry S, Sharma S, Soni S (2018) Assessment of flash flood vulnerability zonation through geospatial technique in high altitude Himalayan watershed, Himachal Pradesh India. *Remote Sens Appl Soc Environ* 12:35–47
- Borga M, Gaume E, Creutin JD, Marchi L (2008) Surveying flash floods: gauging the ungauged extremes. *Hydrol Process* 22:3883–3885
- Bui DT, Hoang ND, Martínez-Álvarez F, Ngo PTT, Hoa PV, Pham TD, Samui P, Costache R (2020) A novel deep learning neural network approach for predicting flash flood susceptibility: a case study at a high frequency tropical storm area. *Sci Total Environ* 701:134413
- Bhat MS, Alam A, Ahmad S, Farooq H, Ahmad B (2019) Flood hazard assessment of upper Jhelum basin using morphometric parameters. *Environ Earth Sci* 78:54. <https://doi.org/10.1007/s12665-019-8046-1>
- Charizopoulos N, Mourtziou P, Psilovikos T, Psilovikos A, Karamotsou L (2019) Morphometric analysis of the drainage network of Samos Island (northern Aegean Sea): insights into tectonic control and flood hazards. *Comptes Rendus-Geosci* 351:375–383
- Chatterjee S, Krishna AP, Sharma P (2013) Geospatial assessment of soil erosion vulnerability at watershed level in some sections of the Upper Subarnarekha river basin. *Environ Earth Sci* 71(1):357–374
- Christopher O, Idowu A, Olugbenga A (2010) Hydrological analysis of Onitsha North East drainage Basin using Geoinformatic techniques. *World Appl Sci J* 11(10):1297–1302
- Dar RA, Chandra R, Romshoo SA (2013) Morphotectonic and lithostratigraphic analysis of intermontane Karewa Basin of Kashmir Himalayas. *India. J Mountains Sci* 10(1):1–15
- Destro E, Amponsah W, Nikolopoulos EI, Marchi L, Marra F, Zoccatelli D, Borga M (2018) Coupled prediction of flash flood response and debris flow occurrence: application on an alpine extreme flood event. *J Hydrol* 558:225–237
- Das S (2020). Flood susceptibility mapping of the Western Ghat coastal belt using multi-source geospatial data and analytical hierarchy process (AHP). *Remote Sens Appl Soc Environ* 20:100379. <https://doi.org/10.1016/j.rsase.2020.100379>
- Dolui G, Chatterjee S, Das Chatterjee N (2014) Weathering and mineralogical alteration of granitic rocks in Southern Purulia District, West Bengal, India. *Int Res J Earth Sci* 2(4):1–12

- Farhan Y, Anaba O (2016) Flash flood risk estimation of WadiYutum (southern Jordan) watershed using GIS based: morphometric analysis and remote sensing techniques. *Open J Modern Hydrol* 6:79–100
- Farhan Y, Anbar A, Al-Shaikh N, Mousa R (2017) Prioritization of semi-arid agricultural watershed using morphometric and principal component analysis, remote sensing, and GIS techniques, the Zerqa River Watershed, Northern Jordan. *Agric Sci* 8:113–148
- Gayen S, Bhunia GS, Shit PK (2013) Morphometric Analysis of Kangshabati-Darkeswar Interfluvies Area in West Bengal, India using ASTER DEM and GIS techniques. *J Geol Geosci* 2:133. <https://doi.org/10.4172/2329-6755.1000133>
- Grabs WE (2010) Regional flash flood guidance and early warning system. Associated Programme on flood management. WMO, Switzerland
- Hasanuzzaman M, Mandal S (2020) A morphology-independent methodology to assess erosion, accretion and lateral migration of an alluvial channel using geospatial tools: a study on the Raidak-I river of Himalayan Foothills. *Sustain. Water Resour Manag* 6:35. <https://doi.org/10.1007/s40899-020-00393-9>
- Hasanuzzaman M, Gayen A, Shit P (2021) Channel dynamics and geomorphological adjustments of Kalgani River in Himalayan foothills. *Geocarto Int*, 1–28. <https://doi.org/10.1080/10106049.2021.1882008>
- Horton R (1932) Drainage basin characteristics. *Trans Am Geophys Union* 13:350–361
- Horton RE (1945) Erosional development of streams and their drainage basins; hydrophysical approach to quantitative morphology. *Bull Geol Soc Amer* 56:275–370
- Howard AD (1990) Role of hypsometry and planform in basin hydrologic response. *Hydrol Process* 4(4):373–385
- Hong H, Pradhan B, Xu C, Bui DT (2015) Spatial prediction of landslide hazard at the Yihuang area (China) using two-class kernel logistic regression, alternating decision tree and support vector machines. *CATENA* 133:266–281
- Huang X, Tan H, Zhou J, Yang T, Benjamin A, Wen SS, Li S, Liu S, Liu A, Li X et al (2008) Flood hazard in Hunan province of China: an economic loss analysis. *Nat Hazards* 47:65–73
- Hussein S, Abdelkareem M, Hussein R, Askalany M (2019) Using remote sensing data for predicting potential areas to flash flood hazards and water resources. *Remote Sens Appl Soc Environ* 16:100254. <https://doi.org/10.1016/j.rsase.2019.100254>
- Islam A, Deb Barman S (2020) Drainage basin morphometry and evaluating its role on flood-inducing capacity of tributary basins of Mayurakshi River, India. *SN Appl Sci* 2:1–23. <https://doi.org/10.1007/s42452-020-2839-4.pdf>
- Islam A, Ghosh S (2021) Economic transformation in the wake of flood: a case of the lower stretch of the Mayurakshi River Basin, India. *Environ Dev Sustain*, 1–41. <https://doi.org/10.1007/s10668-021-01310-6>
- Islam A, Sarkar B, Das BC, Barman SD (2020) Assessing gully asymmetry based on cross-sectional morphology: a case of Gangani Badland of West Bengal, India. In: *Gully erosion studies from india and surrounding regions* (pp 69–92). Springer, Cham. https://link.springer.com/chapter/10.1007%2F978-3-030-23243-6_5
- Jodar-Abellan A, Valdes-Abellan J, Pla C, Gomariz-Castillo F (2019) Impact of land use changes on flash flood prediction using a sub-daily SWAT model in five Mediterranean ungauged watersheds (SE Spain). *Sci Total Environ* 657:1578–1591
- Karamouz M, Fereshtehpour M (2019) Modeling DEM errors in coastal flood inundation and damages: a spatial nonstationary approach. *Water Resour Res* 55(8):6606–6624
- Kannan R, Venkateswaran S, Vijay Prabhum M, Sankar K (2018) Drainage morphometric analysis of the Nagavathi watershed, Cauvery river basin in Dharmapuri district, Tamil Nadu, India using SRTM data and GIS. *Data Brief* 19:2420–2426
- Kelson KI, Wells SG (1989) Geologic influences on fluvial hydrology and bed load transport in small mountainous watersheds, northern New Mexico, USA. *Earth Surf Proc Land* 14:671–690
- Leskens JG, Brugnach M, Hoekstra AY, Schuurmans W (2014) Why are decisions in flood disaster management so poorly supported by information from flood models? *Environ Modell Softw* 53:53–61. <https://doi.org/10.1016/j.envsoft.2013.11.003>
- Markantonis V, Meyer V, Lienhoop N (2013) Evaluation of the environmental impacts of extreme floods in the Evros River basin using contingent valuation method. *Nat Hazards* 69:1535–1549
- Melton MA (1957) Correlations structure of morphometric properties of drainage systems and their controlling agents. *J Geol* 66:442–460
- Malik MI, Bhat MS, Kuchay NA (2011) Watershed based drainage morphometric analysis of Lidder catchment in Kashmir valley using Geographical Information System. *Recent Res Sci Technol* 3(4):118–126
- Magesh NS, Chadrasekar N, Soundranagyagam JP (2011) Morphometric evaluation of Papanasam and Manimuthar watersheds, part of Western Ghats. Tirunelveli District, Tamil Nadu, India: a GIS approach. *Environ Earth Sci* 64:374–381
- Macka Z (2001) Determination of texture of topography from large scale contour maps. *Geografski Vestnik* 73(2):53–62
- Majumder R, Bhunia GS, Patra P, Mandal AC, Ghosh D, Shit PK (2019) Assessment of flood hotspot at a village level using GIS-based spatial statistical techniques. *Arab J Geosci* 12(13):1–12. <https://doi.org/10.1007/s12517-019-4558-y>
- Meraj G, Yousuf AR, Romshoo SA (2013) Impacts of the geo-environmental setting on the flood vulnerability at

- watershed scale in the Jhelum basin. M Phil dissertation. India: University of Kashmir. <http://dspace.uok.edu.in/jspui/handle/1/1362>
- Miller VC (1953) A quantitative geomorphic study of drainage basin characteristics on the Clinch Mountain area, Virginia and Tennessee, Proj.NR 389–402, Tech Rep 3. New York: Columbia University, Department of Geology, ONR
- Obeidat M, Muheeb A, Farah A-H (2021) Morphometric analysis and Prioritisation of watersheds for flood risk management in WadiEasal Basin (WEB), Jordan, Using Geospatial Technologies. *J Flood Risk Manag* 14 (2). <https://doi.org/10.1111/jfr3.12711>.
- Okumura M, Araujo AG (2014) Long-term cultural stability in hunter–gatherers: a case study using traditional and geometric morphometric analysis of lithic stemmed bifacial points from Southern Brazil. *J Archaeol Sci* 45:59–71
- Patel D, Dholakia M, Naresh N, Srivastava P (2012) Water harvesting structure positioning by using geo-visualization concept and prioritization of mini-watersheds through morphometric analysis in the Lower Tapi Basin. *J Indian Soc Remote Sens* 40:299–312
- Patton PC, Baker VR (1976) Morphometry and floods in small drainage basins subject to diverse hydrogeomorphic controls. *Water Resour Res* 12:941–952
- Pavano F, Catalano S, Romagnoli G, Tortorici G (2018) Hypsometry and relief analysis of the southern termination of the Calabrian arc, NE Sicily (southern Italy). *Geomorphology* 304:74–88
- Puno GR, Puno RCC (2019) Watershed conservation prioritization using geomorphometric and land use-land cover parameters. *Global J Environ Sci Manag* 5 (30):279–294
- Ratna Reddy V, Saharawat YS, George B (2017) Watershed management in South Asia: a synoptic review. *J Hydrol* 551:4–13
- Rajasekhar M, Sudarasanaraju G, SiddiRaju R (2020) Morphometric analysis of the Jilledubanderu River Basin, Anantapur District, Andhra Pradesh, India, using geospatial technologies. *Groundwater Sustain Dev* 11:100434. <https://doi.org/10.1016/j.gsd.2020.100434>
- Ratnam KN, Rao VV, Amminedu E (2005) Check dam positioning by prioritization of micro-watersheds using SYI model and morphometric analysis. *Remote Sens GIS Perspect* 33(1):25–38
- Samanta RK, Bhunia GS, Shit PK et al (2018) Flood susceptibility mapping using geospatial frequency ratio technique: a case study of Subarnarekha River Basin. *India Model Earth Syst Environ* 4:395–408. <https://doi.org/10.1007/s40808-018-0427-z>
- Sebastian M, Jayaraman V, Chandrasekhar MG (1995) Space technology applications for sustainable development of watersheds. Technical report. Bangalore: Indian Space Research Organization
- Smith K (1950) Standards for grading texture of erosional topography. *Am J Sci* 248(9):655–668
- Strahler A (1952) Hypsometric (area–altitude) analysis of erosional topography. *Geol Soc Am Bull* 63:1117–1142
- Strahler A (1957) Quantitative analysis of watershed geomorphology. *Trans Am Geophys Union* 38:913–920
- Strahler A (1964) Quantitative geomorphology of drainage basins and channel networks. In Chow V (Ed), *Handbook of applied hydrology* (pp 439–476). New York: McGraw Hill
- Schumm S (1956) Evolution of drainage systems and slopes in badlands at Perth Amboy, New Jersey. *Geol Soc Am Bull* 67:597–646
- Selvan MT, Ahmad S, Rashid SM (2011) Analysis of the geomorphometric parameters in high altitude glacierised terrain using SRTM DEM data in central Himalaya, India. *ARPN J Sci Technol* 1(1):22–27
- Shit PK, Maity R (2012) Rill Hydraulics—an experimental study on gully basin in lateritic upland of PaschimMedinipur, West Bengal. *India. J Geogr Geol* 4(4):1–11
- Shit PK, Pati CK (2012) Non-timber forest products for livelihood security of tribal communities: a case study in PaschimMedinipur District, West Bengal. *J Hum Ecol* 40(2):149–156. <https://doi.org/10.1080/09709274.2012.11906533>
- Shit PK, Paira R, Bhunia G et al (2015) Modeling of potential gully erosion hazard using geo-spatial technology at Garbheta block, West Bengal in India. *Model Earth Syst Environ* 1:2. <https://doi.org/10.1007/s40808-015-0001-x>
- Shit PK, Bhunia GS & Maiti R (2016) Spatial analysis of soil properties using GIS based geostatistics models. *Model Earth Syst Environ* 2:107. <https://doi.org/10.1007/s40808-016-0160-4>
- Swets JA (1988) Measuring the accuracy of diagnostic systems. *Science* 240:1285–1293
- Taha MMN, Elbarbary SM, Naguib DM, El-Shamy IZ (2017) Flash flood hazard zonation based on basin morphometry using remote sensing and GIS techniques: A case study of Wadi Qena basin, Eastern Desert, Egypt. *Remote Sens Appl: Soc Environ* 8:157–167
- Toduse NC, Ungurean C, Davidescu S, Clinciu I, Marin M, Nita M D, ...Davidescu A (2020) Torrential flood risk assessment and environmentally friendly solutions for small catchments located in the Romania Natura 2000 sites Ciucas, Postavaru and Mare. *Sci Total Environ* 698:134271. <https://doi.org/10.1016/j.scitotenv.2019.134271>
- UNISDR (2015) Making development sustainable: the future of disaster risk management. In: *Global assessment report on disaster risk reduction*. Geneva, Switzerland: United Nations Office for Disaster Risk Reduction (UNISDR)

- WMO (2016) World meteorological organization: flash flood guidance system (FFGS) with global coverage Brochure
- Worku G, Teferi E, Bantider A, Dile YT (2020) Prioritization of watershed management scenarios under climate change in the Jemma sub-basin of the Upper Blue Nile Basin, Ethiopia. *J Hydrol Regional Stud* 31:100714. <https://doi.org/10.1016/j.2020.100714>
- Yang YCE, Ray PA, Brown CM, Khalil AF, Yu WH (2015) Estimation of flooddamage functions for river basin planning: a case study in Bangladesh. *Nat Hazards* 75:2773–2791
- Youssef AM, Pradhan B, Gaber AFD, Buchroithner MF (2009) Geomorphological hazards analysis along the Egyptian Red Sea Coast between Safaga and Quseir. *Nat Hazard* 9:751–766
- Zare M, Pourghasemi HR, Vafakhah M, Pradhan B (2013) Landslide susceptibility mapping at vaz watershed (Iran) using an artificial neural network model: a comparison between multilayer perceptron (mlp) and radial basic function (rbf) algorithms. *Arab J Geosci* 6:2873–2888



Palaeohydrologic Estimates of Flood Discharge of Lower Ramganga River Catchment of Ganga Basin, India, Using Slackwater Deposits

Rameswar Mukherjee

Abstract

Conventional statistical methods for estimating recurrent intervals of the flood are less reliable due to the unavailability of recorded discharge data for a longer period. It can only be possible through palaeohydrological analysis along with sedimentological and geomorphic investigations. In the palaeohydrological study, palaeodischarge is calculated using slackwater deposits (SWD). These are the natural records of overbank megaflood deposits. In the present study, the SWD remain preserved in a natural levee section of the lower Ramganga river catchment wherein seven discrete megaflood events were identified. According to the calculated palaeodischarge stage (top elevation of each slackwater deposits layer), the palaeofloods events were reconstructed. The palaeodischarge of these floods was estimated which ranged from 2664.72 m³/s to 4121.46 m³/s. From recorded discharge data, the flood frequency was calculated by using Log Pearson type III distribution. The grain size analysis was carried out through the Malvern Mastersizer-S analyser.

The slackwater deposits were differentiated clearly with slope clastic deposits by the grain size distribution.

Keywords

Palaeohydrology · Slackwater deposits · Palaeoflood events · Palaeostage · Discharge reconstruction

3.1 Introduction

Flood frequency analysis (FFA) using historical or gauging discharge records is considered as quite insufficient for the precise estimation of flood frequency and its magnitude. The longest gauging records (usually much less than 100 years) are also too short to provide trustworthy prediction for extreme flood events. Therefore, in order to understand the flood behaviour of any channel it is necessary to receive long-term records of the floods. It can only be possible from the sedimentary archives preserved in the flood plain region (Yang et al. 2000). The palaeoflood data provides long-term natural records of the flood histories (Baker 2008). By using this data, palaeoflood hydrological estimation can be made a long with sedimentological and geomorphological investigations. The flood frequency, magnitude and recurrent interval of mega floods spanned over the decades to thousands of years preserved as palaeoflood deposits can improve the FFA by

R. Mukherjee (✉)
Department of Geography, Samsi College, Samsi,
Malda, West Bengal, India

enhanced fitting of the probability functions (Webb et al. 1988; Thorndycraft et al. 2003; Benito et al. 2004).

The palaeoflood hydrology is the interdisciplinary science of reconstructing past flood events (Baker 1987, 2008). It plays an important role in the temporal analysis of flood and channel response to palaeoenvironmental change, planning for mitigation of flood hazard and protection of hydraulic engineering construction (Zha et al. 2009a, 2015; Zhou et al. 2016). According to Baker and Kochel (1988), *'Palaeoflood hydrology combines a multidisciplinary approach (stratigraphy, sedimentology, geomorphology and hydraulics) in the study of past or ancient floods, to decipher, quantitatively, past flood discharges, extending the record of extreme floods from centuries to thousands of years'*. Benito and Thorndycraft (2005) opined that in the palaeofloods study, the term palaeo has promoted to common fallacy that it is only used for estimating very old floods that occurred in the geological period. However, most of the palaeoflood hydrological analyses encompasses the study of prehistoric, historic or modern floods in ungauged basins. This study has been popularized widely around the world since the past four decades because of long-term natural records of high magnitude floods that provide better insight on the following issues: (i) risk assessment of extreme flood events; (ii) determination of extreme limit of flood magnitude; (iii) channel responses of flood in various hydroclimatic settings; (iv) assessing the sustainability of floodwater in dry climatic region (Knox 2000; Benito et al. 2003; Benito and Thorndycraft 2005; Baker 2006; Zha et al. 2009b).

The techniques for palaeohydrological analysis do not incorporate the direct measurement or observation of the flood. Instead, by applying numerous flood-induced marks on the landscape which are derived from channel features associated with floods or flood deposits, various indirect indices can be implied. These indices are applied to measure the palaeoflood, e.g., flood velocity, discharge and flood stage levels (Stokes et al. 2012). It is very useful for ungauged

drainage systems or where the documentation of systematic records is short or not properly maintained.

Over the past four decades, the palaeoflood slackwater deposits (SWD) have been utilized as a robust tool for palaeohydrological research. This study has been successfully conducted in the United States (Baker 1983; Ely and Baker 1985; Enzel et al. 1994; O'connor et al. 1986, 1994; Wang and Leigh 2012; Greenbaum et al. 2014); Spain (Benito et al. 1998, 2003) China (Yang et al. 2000; Huang et al. 2012; Fan et al. 2015; Li et al. 2015; Zha et al. 2015; Mao et al. 2016) and in India (Kale et al. 1994, 1997, 2000, 2003, 2010; Sridhar 2007).

Although slackwater deposits are found in all climatic conditions at different geomorphic settings, most specifically its presence is marked in the arid and semi-arid region (Baker and Kochel 1988; O'Connor et al. 1994; Baker 2006). The rivers located in these regions are often experienced with very high rainfall for a short span of time. The heavy torrential rainfall generates a high flood situation, accompanied by heavy sediment load coming from the unconsolidated and uncovered sediment deposits (Hirschboeck 1988). During high flood situations, the sediment loads were deposited at or near the channel margin. These deposits were reworked by the channel with the passage of time. The rainfall, runoff, bioturbation, human and animal interference also cause damage to the primary sedimentary deposits. Apart from the arid and semi-arid regions, the SWDs are quite well preserved in the tropical region also (Ely et al. 1996; Kale et al. 2003, 2010; Kale 2008). It has been found that low to medium magnitude overbank flood deposits are more susceptible for undercutting and subsequent flow. Only the deposits of megaflood events remain in situ and probably preserved for a longer period (Ely et al. 1996).

According to Kale (2008), there is a low to moderately low chance of getting palaeoflood slackwater deposits in the Gangetic Plain region. This region is heavily populated and large-scale agricultural practices are going on since ~5000 years near the river. Apart from that, the incidence of high magnitude flow causes frequent

channel migration which brings inconsistencies in the successive records of flood deposits. In spite of such hindrances, if the researchers conduct a thorough field survey along the probable locations specifically in the Western Gangetic plain region, they may definitely get the well-preserved SWD data (Mukherjee 2019). The rivers located in the Western Gangetic plain region are incisional in nature and less dynamic than the Eastern Gangetic plain rivers (Sinha et al. 2005). In the incised channel, the flood deposits can be easily traced than the aggrading channel. Besides, there is a preponderance of partly confined channels in the western Gangetic plain region from where one can archive recurrent flood deposits. In the present study, palaeodischarge has been estimated on the lower Ramganga river, located in the Western Gangetic plain. The uncontrolled and unscientific growth of the human population in this river catchment has increasingly been posing the risk of flood on the human habitation as well as in the infrastructural development. Therefore, palaeoflood hydrological analysis can be fruitful for flood assessment, risk analysis, flood plain planning and management. The aims of the present study are as follows:

- i. to describe and quantify extreme flood events using historical flood data;
- ii. to discuss pedo-stratigraphic characteristics of palaeoflood slackwater deposits;
- iii. to reconstruct extreme flood events using stratigraphic records of palaeoflood slackwater deposits;
- iv. to estimate palaeoflood peak discharge by employing slope-area method.

3.2 Study Reach

The Ramganga river catchment is located in the Lesser and Outer Himalayas as well as in the Western Gangetic plain (Fig. 3.1). It drains an area of 30,635.1 km² (Mukherjee et al. 2017). The river originates from the Lesser Himalaya,

near Gairsen, Uttarakhand. After flowing ~167.91 km in the Himalayas, the Ramganga river debouches the Western Gangetic plain. The total length of this river is ~649.11 km and it is a right-bank tributary of the Ganga river. The present study reach is located in Western Gangetic Plain locally known as *Rohilkhand Plain*. The study area is comprised of quaternary alluvium, namely: (i) Varanasi older alluvium (ii) Ramganga terrace alluvium and (iii) Ramganga recent alluvium, (Khan and Rawat 1992; Khan et al. 2016).

The Varanasi older alluvium is found in upland interfluvial surface, sandy alluvial ridges, and older terrace surface (Fig. 3.2). The older and dissected terrace plain, inactive floodplains are composed by the Ramganga terrace alluvium and the Ramganga recent alluvium closely corresponds with active and younger floodplains (Mukherjee et al. 2017). The lower reach of the Ramganga river is unconstrained as a result of that frequent channel migrations are more common. The channel pattern alternates between meandering to partly braided types. At several places, high-curvature meandering channels are observed. The river is also characterized by higher stream power (Sinha et al. 2005; Mukherjee 2019). The fluvial regime of this river is largely controlled by the monsoon climate. This river catchment receives more than 80% of annual rainfall in the monsoon season (June to September). During this period, large floods are more common in the lower reaches of the catchment area (Fig. 3.3). Because of higher stream power, presence of easily erodable bank materials and fragile foundation of the natural levees, the floods become extremely hazardous in this study reach.

3.3 Database and Methodology

The present analysis has been done by using extreme flood discharge data and palaeoflood slackwater deposits (Fig. 3.4). The sources of data collection are given in Table 3.1.

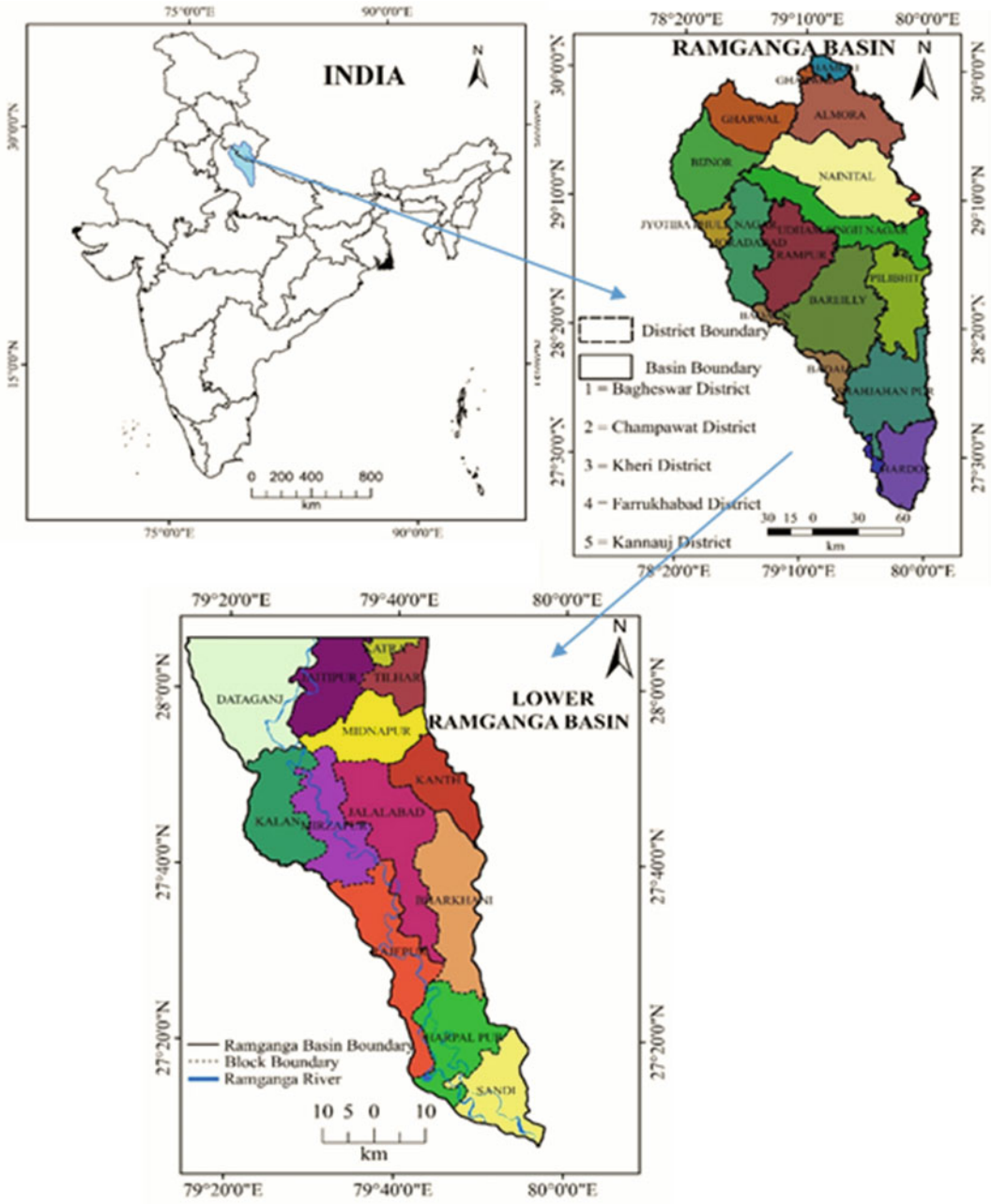
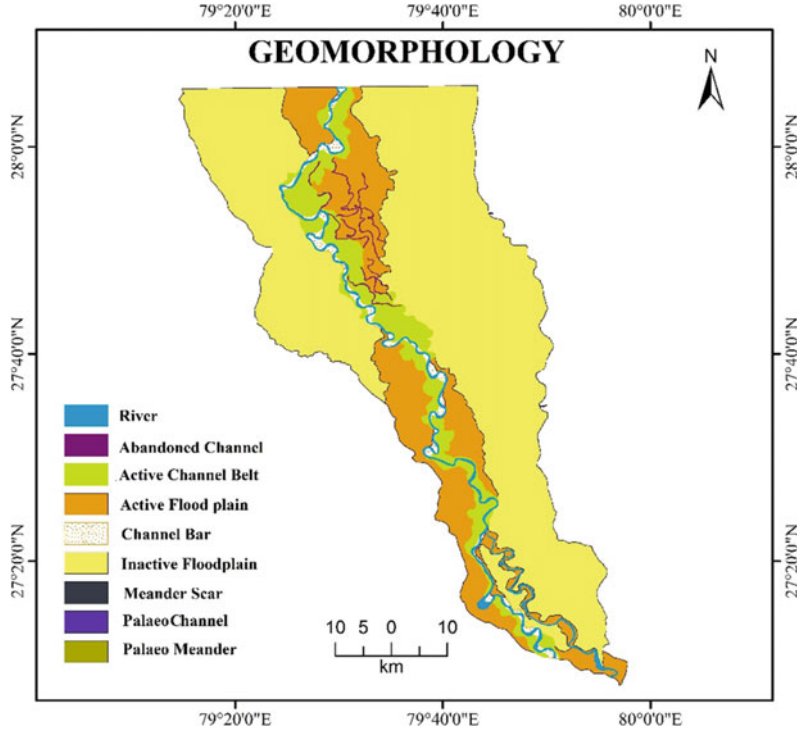


Fig. 3.1 Study reach

Fig. 3.2 Geomorphological map of the study reach



3.3.1 Flood Frequency Analysis by Log-Pearson Type III Distribution

For flood frequency analysis, the annual extreme discharge value was taken into consideration. The Log Pearson III distribution was used to estimate probable extreme flood frequencies of the Ramganga river. This measure is extensively applied for FFA to the major tropical rivers as it fits most appropriately to estimate flood peaks. This method involves first converting the variate into logarithmic form and then analyzing the transformed data (Subramanya 2013). Mukherjee and Bilas (2019) assessed the flood frequency of the lower Ramganga river by applying Gumbel’s, Log-Pearson Type III, and Weibul’s method, where it has been found that the Log-Pearson Type III is the most appropriate measure for FFA.

For calculating flood frequency of the lower Ramganga river by using Log-Pearson Type III distribution, the following steps were followed.

- (i). At first, all the annual maximum flood discharge value was transformed into logarithms by using Eq. 3.1:

$$Y = \log x \tag{3.1}$$

- (ii). Then, the mean (\bar{y}), standard deviation (σ_y), and skewness coefficient (C_s) of y series were estimated as

$$\bar{y} = \frac{1}{n} \sum y_i \tag{3.2}$$

$$\sigma_y = \sqrt{\sum (y - \bar{y})^2 / (N - 1)} \tag{3.3}$$

$$C_s = \frac{N \sum (y - \bar{y})^3}{(N - 1)(N - 2)(\sigma_y)^3} \tag{3.4}$$

- (iii). The logarithms of extreme flood discharge were computed using the equation

$$5Y_T = \bar{y} + K_T \sigma_y \tag{3.5}$$

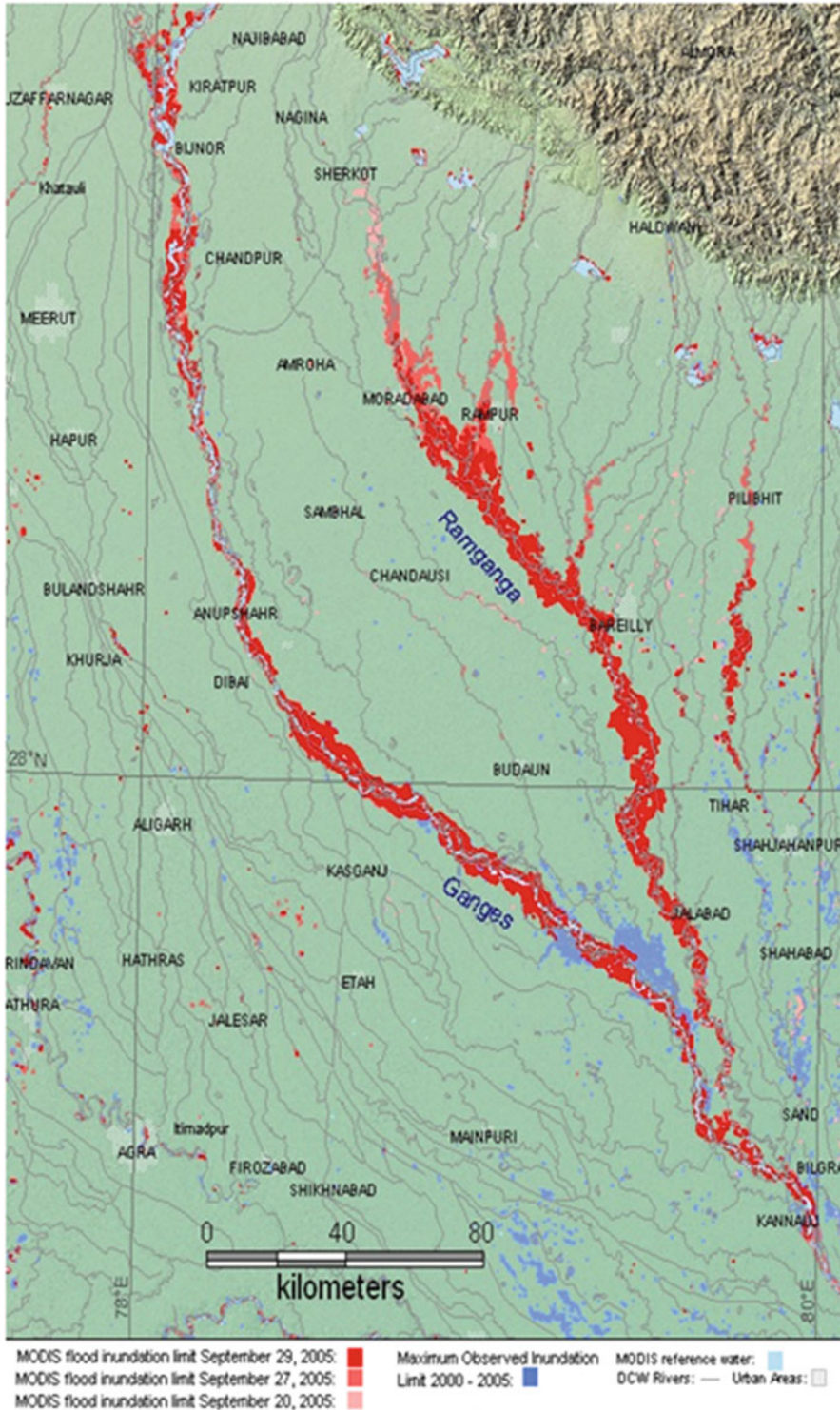


Fig. 3.3 Inundation map derived from MODIS Data (Dartmouth Flood Observatory 2014)

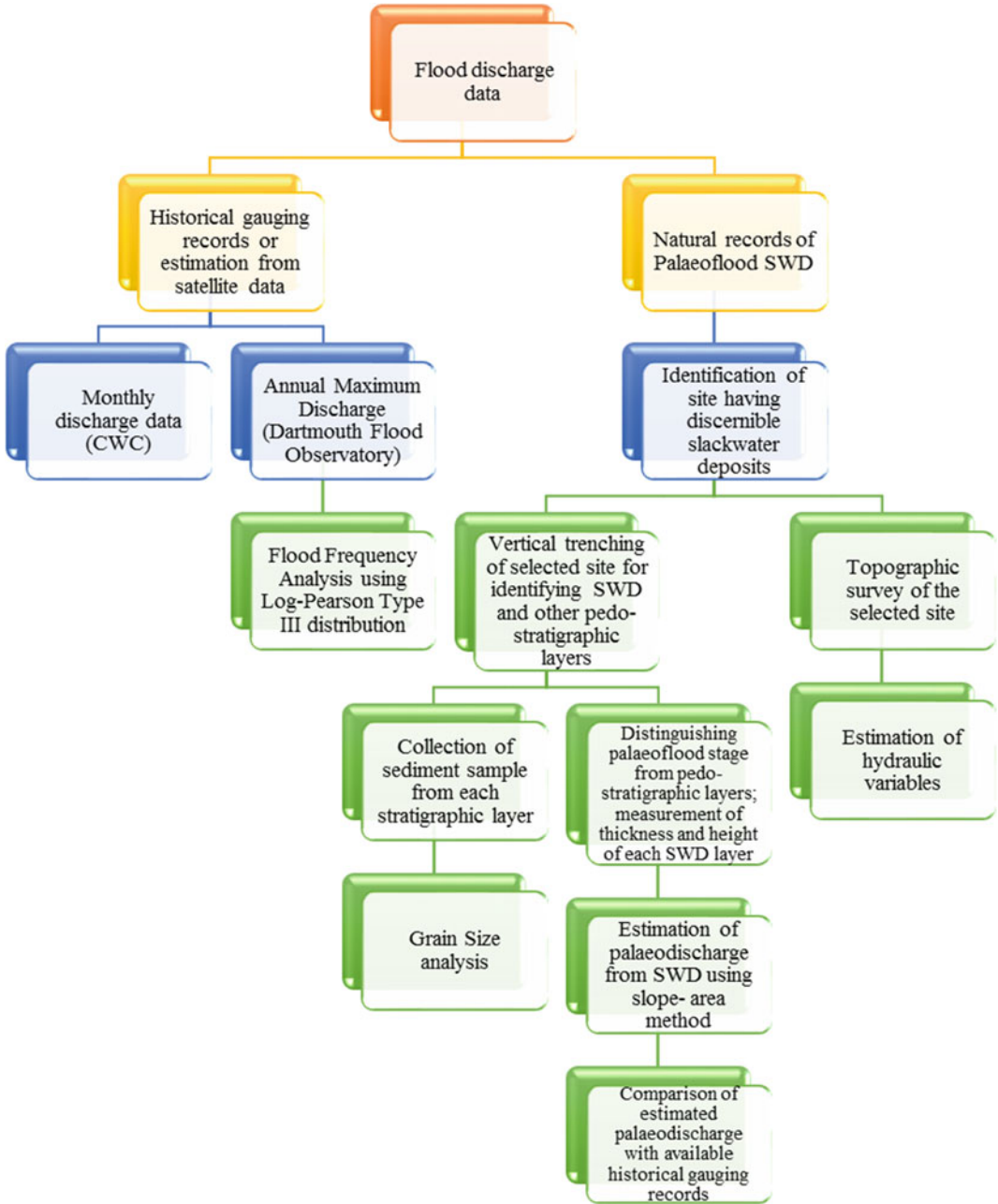


Fig. 3.4 Methodological Workflow

Table 3.1 Sources of data

Data types	Gauging site/survey site	Duration	Source
Maximum annual discharge	Dandi, Badaun District, UP	1998–2020	Dartmouth flood observatory Website (floodobservatory.colorado.edu)
Monthly annual discharge	Dabri, Shahjahanpur district, UP	1998–2002	Central Water Commission, Govt. of India
Slackwater deposit sample	Rampur Bajhera Village, Hordoi district, UP	20–26 March 2016	Personal Field Survey

The frequency factor K_T is a frequency factor that is a product of the return period and skewness coefficient

$$K_T = f(C_s, T) \quad (3.6)$$

- (iv) After calculating y_T by Eq. (3.5), the extreme flood discharge value was obtained by antilogarithm of Y_T is

$$X_T = \text{antilog}(y_T) \quad (3.7)$$

descriptions were made on the identified palaeoflood slackwater deposits.

- (iv) The samples of flood deposits were collected for sedimentological analysis.
- (v) A topographic survey was conducted on the selected SWD site and river reaches.
- (vi) Estimation of hydraulic variables and palaeodischarge was carried out on the selected site.
- (vii) A comparison was made with available historical or gauging records of the flood discharge
- (viii) Flood frequency analysis was done.

3.3.2 Palaeoflood Hydrological Investigations

For palaeohydrological estimates of the lower Ramganga river, the methodological steps instructed by Benito and Thorndycraft (2005) were followed, which includes the following:

- (i) For selecting suitable sites for palaeoflood slackwater deposits, a detailed study of topographical maps and satellite images of the lower Ramganga river catchment was carried out.
- (ii) On the basis of that study, the most suitable sites of SWD were marked. A detailed field survey was conducted on those sites for identifying the presence of stratigraphic layers of slackwater deposits or other flood indicators.
- (iii) The most prominent site was identified on a natural levee section where pedological and stratigraphic characteristics remain well preserved. The stratigraphic

In the present study, a geomorphic and sedimentological investigations were carried out in order to identify palaeoflood stage and estimate the frequency and magnitude of past megaflood events. In this study, the main objective of the fieldwork was to identify the palaeoflood stage (PFS). Then the PFS was converted into palaeoflood peak discharge. The reconstruction of PFS is dependent on the evolution, thickness, and attitude of the palaeoflood slackwater deposits (SWD) (Li et al. 2015). Basically, the top of the slackwater deposits can be extrapolated to estimate the PFS. Various river scientists used the elevation of the endpoints of palaeoflood SWD, which is in contact with the upper slope as PFS (Yang et al. 2000; Zha et al. 2009b; Wang et al. 2014).

The palaeodischarge was calculated by using slackwater deposits. These deposits were identified on the field based on several sedimentological criteria: (i) sediment deposits consisting silt, and silty-sand; (ii) abrupt vertical change in

sediment grain size, colour, texture, and structure; (iii) clear division between successive stratigraphic layers; (iv) clay cap over the bed; (v) bioturbation which indicates exposure of sediment surface; (vi) existence of anthropogenic remains; (vii) presence of slope wash with angular clastic alluvial deposits between stratigraphic layers (Baker and Kochel 1988; Kale et al. 2000; Benito et al. 2003; Benito and Thorndycraft 2005; Thorndycraft et al. 2005; Sridhar 2007; Zhang et al. 2013, 2015).

After extensive field investigation, the most prominent SWD was found near Rampur Bajhera village in the Hardoi district of Uttar Pradesh (Fig. 3.5). Here a well-developed natural levee is present whose deposits did not get disturbed by burrowing animals or by anthropogenic activities. The natural levee Sect. (27° 29' 26", 79° 43' 00") has ~3.5 m elevation above the normal level of Ramganga. After observing the multi-temporal satellites and topographical maps it becomes evident that the region has remained relatively stable for the past 100 years. The stratigraphic records that remain preserved at the natural levee section were measured accurately.

For palaeohydraulic investigation, the cross-section was measured in the field by using theodolite.

The palaeopeak discharge was reconstructed by using the slope area method of streamflow measurement (Manning, 1889). It was calculated as

$$Q = \frac{1}{n} (AR^2 S^{\frac{1}{2}}) \quad (3.8)$$

where Q = Palaeoflood peak discharge (m^3/s),

n = Manning's n value or roughness value,

A = Cross-sectional area of the stream at the flood stage,

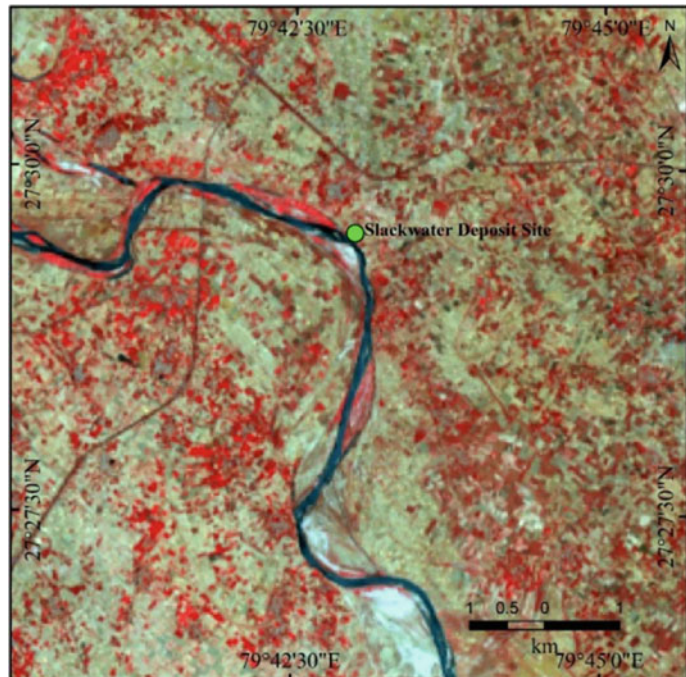
R = Hydraulic radius,

S = Water surface slope.

3.3.3 Grain Size Measurement

The sediment samples collected from a stratigraphic layer of the natural levee were measured using the Krumbein and Pettijohn (1938) standard pipette method. The size of the sand, silt and clay particles were measured using a Malvern Mastersizer-S analyser. But before that CaCO_3

Fig. 3.5 Slackwater deposit Site (Natural Levee Section)



and organic matter contents were removed from the collected samples by providing pre-treatment with 10% HCl and 10% H_2O_2 solution.

3.4 Result and Discussion

3.4.1 Hydrological Characteristics

The Ramganga river is a spring-fed river and most of its tributary channels are either spring or groundwater fed. Hence, a majority of the water discharge of Ramganga and its tributary channels derives from the monsoon rainfall (Mukherjee and Bilas 2019). The monthly average discharge data (2003–2012) of Lower Ramganga river at Dabri gauging station ($27^{\circ} 53' 1''$ N and $79^{\circ} 54' 44''$ E) has been plotted in Fig. 3.6. It depicts the typical monsoon discharge of a river. It starts to rise from July and reaches a maximum in September and then declines from October. Every year, July to October is designated as the period of higher water discharge and it reaches an extreme level in August and September.

3.4.2 Estimation of Probable Flood Discharge and Flood Recurrence Interval

The flood frequency analysis is a statistical technique used to understand flood behaviour of any river. On the basis of that flood, forecasting can be made for a longer time period. This analysis involves the use of peak annual discharge to calculate probable flood discharge and its recurrent interval. The average of the observed peak discharge data is $1603.05 \text{ m}^3/\text{s}$ and the standard deviation (SD) is $383.11 \text{ m}^3/\text{s}$. For Log-Pearson type III distribution, the mean and SD values of peak discharge are 3.193 and 0.105, respectively. For Log-Pearson III methods, frequency factor (K_T) has been used for measuring the peak flow. The calculation of various parameters for peak flow measurements at various recurrent intervals has been given in Table 3.2. It shows $2128.54 \text{ m}^3/\text{s}$ for 10 years recurrent intervals, $2739.7 \text{ m}^3/\text{s}$ for 100 years, and $3295.51 \text{ m}^3/\text{s}$ for every 1000 years recurrent intervals.

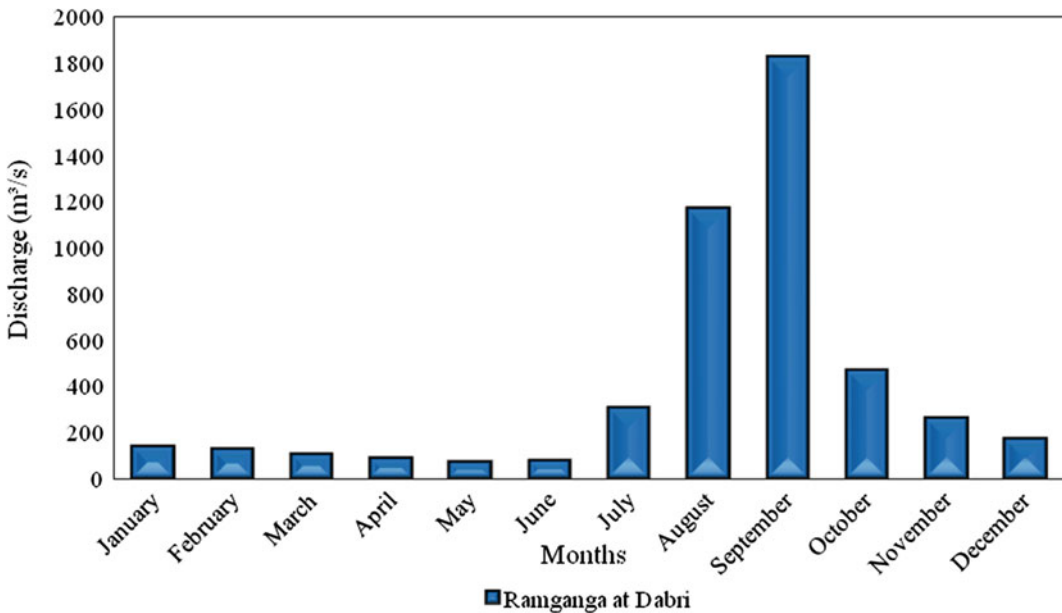


Fig. 3.6 Average monthly water discharge (2003–2012) of the Ramganga river at Dabri gauging station

Table 3.2 Calculation of probable peak discharge by using log-Pearson III method

Recurrent interval	Cs	K_T	y_T	x_T
5	0.48075	0.4852	3.243946	1753.66
10	1.282	1.2865	3.3280825	2128.54
20	1.595	1.5995	3.3609475	2295.87
25	1.751	1.7555	3.3773275	2384.12
50	2.054	2.0585	3.4091425	2565.34
100	2.326	2.3305	3.4377025	2739.7
200	2.576	2.5805	3.4639525	2910.42
500	2.769	2.7735	3.4842175	3049.42
1000	3.09	3.0945	3.5179225	3295.51

3.4.3 Estimation of Palaeohydraulic Flood Discharge Using Slack Water Deposits

For palaeoflood studies, the palaeodischarges of the basin have been calculated by marking the palaeostage indicators (PFS) (Baker et al. 1979). Flood exceeding a certain threshold has been registered through sedimentary records or other 'palaeostage indicators erosional landforms (stripped soils, flood scarps, high flow channels), and high-water marks (e.g., drift wood, tree impact scarps, silt lines)' (Benito et al. 2003). The slackwater deposits (SWD) are formed by the material brought by flood and vertically accrete overbank. The top elevation of each slackwater deposit is considered as a palaeostage (Kochel and Baker 1982; Baker et al. 1983; Baker 1989). During the period of flood, fine-grained suspended sediments accumulate rapidly in a vertical sequence, where an abrupt drop of flow velocity occurs. When such a phenomenon occurs at the recurrent interval, a series of subsequent stratigraphic layers of slackwater deposits have been formed. These layers are generally separated by slope clastic deposits.

In the natural levee section, seven major palaeoflood events were recorded (Figs. 3.7 and 3.8). The PFS of each palaeoflood event was measured. Along with that, channel cross-sectional area, wetted perimeter, river gradient and hydraulic radius of the channel on both sections were measured most accurately. By using the slope-area method, the maximum

palaeoflood discharge was estimated as 4121.46 m³/s whereas the minimum value was recorded as 2664.72 m³/s (Table 3.3).

3.4.4 Stratigraphy and Grain Size Analysis of Slackwater Deposits

In the natural levee section, total of 17 stratigraphic layers are observed. The pedo-stratigraphic descriptions have been given in Table 3.4. Out of which seven layers are designated as palaeoflood slackwater deposits. These layers are clearly visible and distinguishable from other layers. The colour of these deposits varies from yellow to orange. The concentration of silt to silty sand particles is higher, parallel to wavy laminations are found.

The grain size analysis was done in order to differentiate slackwater deposits from other sediments, to identify the proportion of sandy silt and clay deposits and also to distinguish the nature of their frequency distribution and degree of sorting. In the present stratigraphic section, all of the palaeoflood slackwater deposits are characterized by a higher degree of silty-sand concentration and they are well sorted (Table 3.5). The mean grain size of these deposits is ranged between 28.10 µm and 39.71 µm. The deposits of silty sand to coarse sand are predominantly higher in B2, B4 and D2 slackwater deposit layers. It demonstrates high energy flow and vertical accretion of the larger particles. The

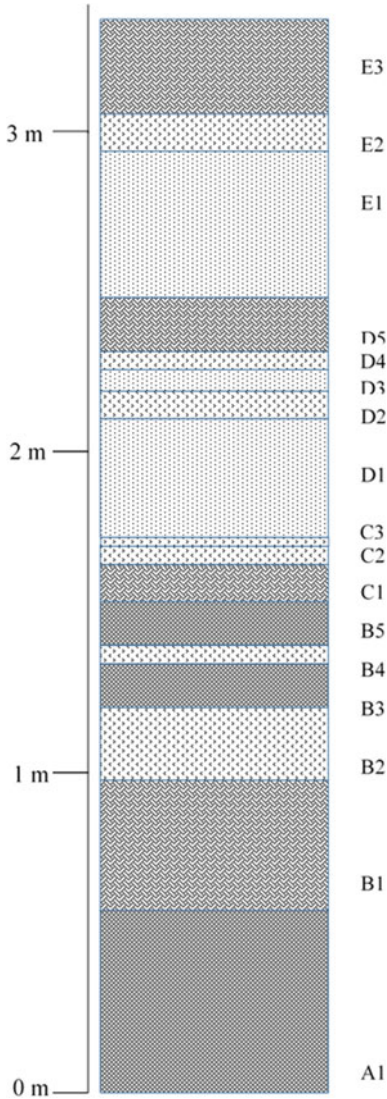


Fig. 3.7 Facies of natural levee section

concentration of the coarser and unconsolidated materials is relatively higher in the upper stratigraphic section. The palaeosols are characterized by clay to clayey-silt deposits. On the other hand, in the recent soil deposits coarser silt and sand deposits predominate. The mean grain size increases in the upper section. The largest concentration of the clay and clayey-silt is found in the lowermost part of the stratigraphic section. Apart from that, the concentration of such materials is higher in B3, B5 and D3 layers,0



Fig. 3.8 Natural levee section near Rampur Bajhera village, Hordoi district, UP (2016)

which are lying just above the layers of slack-water deposits. It depicts the period of low magnitude flood deposits. The values of kurtosis reveal that all of the deposits are characterized by platykurtic distribution. Its value increases in the upper layer deposits. All of the sediment distributions are positively skewed.

3.4.5 Accuracy Assessment

Based on present-day channel geometry and flood stage indicator the peak discharge of the 2011 megaflood has been estimated by applying the slope area method, i.e., 4396.81 m³/s. The extreme flood discharge recorded as 4650.78 m³/s in Dabri gauging site on 23 August 2011. On that day, the water level reached 138.515 m. It is

Table 3.3 Reconstructed peak discharges of the holocene paleofloods (Natural Levee Section)

SWD layer	Cross section area (m ²)	Wetted perimeter (m)	River gradient	Hydraulic radius (m)	Roughness coefficient	Palaeoflood peak discharge (m ³ /s ⁻¹)
E2	5217.62	1534.8	0.0001	3.399	0.032	4121.46
D4	4713.75	1396.8	0.0001	3.375	0.032	3705.29
D2	4567.67	1318.1	0.0001	3.465	0.032	3654.48
C3	4478.23	1301.5	0.0001	3.441	0.032	3566.01
C2	4003.89	1280.9	0.0001	3.126	0.032	2990.7
B4	3964.95	1265	0.0001	3.134	0.032	2966.86
B2	3709.45	1258.2	0.0001	2.948	0.032	2664.72

Table 3.4 Pedo-stratigraphic description of natural levee section

Symbol	Pedo-stratigraphic Subdivision	Depth(cm)	Pedo-stratigraphic description
E3	Modern soil	0–030	Top soil, slope wash, granular soil structure, porous, upper part grass concentration is higher, abundant bio pores
E2	SWD	30–41.6	Palaeoflood slack water deposit, parallel lamination, yellow and light brown recent flood deposits
E1	Modern soil	41.6–87.4	Coarse to medium sand intermixed with silt, parallel to wavy lamination, high root density
D5	Modern soil	87.4–98.3	Slope wash deposits intermixed with coarse to medium sand and silt deposits parallel to the wavy lamination
D4	SWD	98.3–104.1	Slack water deposits, yellow-orange colour, parallel lamination, higher concentration of silty sand particles
D3	Modern soil	104.1–110.9	Parallel lamination sandy layer intermixed with silty layer
D2	SWD	110.9–119.6	Slack water deposits, yellow orange colour, silt to silty sand deposits
D1	Palaeosol	119.6–157.7	Sand deposits, medium to coarse size, white to light yellow colour, cross bedding with climbing ripples, numerous silty lenses, presence of wavy lamination
C3	SWD	147.7–160.4	Palaeoflood slackwater deposits, parallel lamination, yellow to orange colour
C2	SWD	160.4–167.25	Palaeoflood slack water deposits, lamination-cross lamination-pale to yellow-orangecolour, friable medium-grained sandy-silt
C1	Palaeosol	167.25–178.1	Slope clastic deposits, medium to coarse-grained sand, unsorted, higher concentration of silty lenses, wavy lamination, high plant root density.
B5	Palaeosol	178.1–191.6	Clay layer dark grey, high plant root density
B4	SWD	191.6–197.5	Dull yellow-orange colour, soft silty-sands, parallel to wavy lamination bounded by clay layer in up and bottom
B3	Palaeosol	197.5–211.5	Dark clay layer-granular structure

(continued)

Table 3.4 (continued)

Symbol	Pedo-stratigraphic Subdivision	Depth(cm)	Pedo-stratigraphic description
B2	SWD	211.5–234.5	Slack water deposits, dominance of silt to silty clay, pale yellow orange colour, light brown medium grain sand in bottom and clay in top visible stratigraphic break, parallel to wavy lamination
B1	Palaeosol	234.5–275.5	Slope wash, sandy silt deposits, whitish to light yellowish colour, presence of plant roots, bears the deposits of low magnitude flood, higher concentration of silty lenses
A1	Palaeosol	275.5–332.5	Dark clay and clayey silt deposits predominate, grey to greyish brown color

Table 3.5 Particle-size distribution of the natural levee section

Symbol	Pedo-stratigraphic subdivision	Thickness (cm)	Grain Size (%)				Mean (μm)	Sorting	Skewness	Kurtosis
			<2 μm	2–16 μm	16–63 μm	>63 μm				
E3	Modern soil	30	6.98	34.3	39.10	19.62	44.32	0.29	1.05	1.12
E2	SWD	11.60	7.05	28.85	47.36	16.74	39.71	0.47	1.01	1.19
E1	Modern soil	45.8	10.1	31.4	40.7	17.80	47.51	0.30	0.89	0.98
D5	Modern soil	10.9	9.37	29.35	39.56	21.72	39.56	0.431	1.07	1.23
D4	SWD	5.8	6.59	27.81	42.93	22.67	46.74	0.28	0.81	0.91
D3	Modern soil	6.8	18.82	37.71	28.81	14.66	41.26	0.27	0.83	1.35
D2	SWD	8.7	7.26	26.05	43.59	23.1	37.89	0.23	0.77	0.83
D1	Palaeosol	38.1	13.48	26.73	38.71	21.08	50.73	0.39	1.08	1.01
C3	SWD	2.7	13.74	33.95	38.25	14.06	28.16	0.27	0.91	0.97
C2	SWD	6.85	11.84	37.21	35.73	15.22	29.4	0.20	0.99	0.64
C1	Palaeosol	10.85	8.09	32.06	42.79	17.06	39.88	0.29	0.87	0.74
B5	Palaeosol	13.5	19.09	38.16	31.50	11.25	30.47	0.26	1.02	0.93
B4	SWD	5.9	8.74	27.91	43.59	19.76	33.21	0.17	0.74	0.69
B3	Palaeosol	14.0	24.91	34.48	32.49	8.12	34.66	0.16	0.66	0.81
B2	SWD	23.0	10.8	32.75	41.87	14.58	28.10	0.18	0.48	0.59
B1	Palaeosol	41.0	18.21	36.93	35.26	9.60	29.89	0.31	0.63	0.71
A1	Palaeosol	57	37.33	40.81	20.7	1.16	22.85	0.14	0.55	0.57

considered that such magnitude of flood has never been experienced since the past 100 years (Mukherjee 2019). This gauging station of the lower Ramganga river, lying ~ 1.80 km upstream of the present surveyed section. The gauging record of extreme discharge of the 2011 flood closely corresponds to the present estimation.

3.5 Conclusion

The research on the palaeohydrological events has been carried out for temporal analysis of extreme flood behaviour in terms of its magnitude and recurrent interval and also to explain channel responses to such extreme floods in a

particular reach of the river catchment. This kind of research might be very effective for floodplain planning and flood risk management, because if we know the extreme flood magnitudes, the flood inundation zone can be designated. On the basis of that long-term effective measures for flood adaptation and community resilience can be made. In the present paper, the magnitude and frequency of palaeofloods and historical flood events were reconstructed using palaeoflood slackwater deposits combined with a hydrographic survey, sedimentological analysis and instrumental records of floods.

The hydrological characteristics of the Ramganga river are largely governed by the monsoon climate. For flood frequency analysis, annual peak discharge data has been used. To observe the chance of peak discharge of a certain magnitude of flood for lower Ramganga river Log-Pearson III distribution has been attempted. For 10–50 years of the recurrent interval of the flood, the peak discharge ranged from 2128.54 m³/s to 2565.34 m³/s for Log-Pearson III. Whereas for 100 years, it is estimated as 2739.70 m³/s. A careful investigation for palaeoflood study was carried out in the alluvial reaches of the lower Ramganga in a ~3.5 m natural levee section (near Rampur Bajhera village, Hordoi district, UP). The study was based on identifying and marking Slack water deposits. On the basis of seven available SWD layers, palaeostage was measured on the field. By applying these palaeostage data, the palaeodischarges were extrapolated by using the slope-area method. The estimated palaeo peak discharge is ranged from 2664.72 m³/s to 4121.46 m³/s. The accuracy of the discharge estimation is dependent on the stability of the channel geometry over time. Such conditions may exist in stable bedrock confined channel reach. In the alluvial plain region, the instability of the channel is inherent, therefore, the possibility of uncertainty in the palaeodischarge may significantly arise. Although in the Western Gangetic plain region, partly confined channels are widely observed, where due to local resistance the river course remains stable over the period of time. If one can explore those places and trace out the palaeoflood deposits, the

reconstruction of palaeohydraulic discharge and the time of flood occurrence would be possible. This kind of research will help to understand the nature and intensity of the past flood event accurately than the analysis of historical or gauging data. Hence, on the basis of palaeodischarge data, the future predictions can be made more efficiently.

References

- Baker VR (1983) Palaeoflood hydrologic techniques for the extension of stream flow records. *Transp Res Rec* 922:18–23
- Baker VR (1987) Palaeoflood hydrology and extraordinary flood events. *J Hydrol* 96:79–99
- Baker VR (2006) Palaeoflood hydrology in a global context. *CATENA* 66:161–168. <https://doi.org/10.1016/j.catena.2005.11.016>
- Baker VR (2008) Palaeoflood hydrology: origin, progress, prospects. *Geomorphology* 101:1–13
- Baker VR, Kochel RC (1988). Flood sedimentation in bedrock fluvial systems. In Baker VR, Kochel RC, Patton PC (eds) *Flood geomorphology*. NY Wiley, pp 123–137
- Baker VR, Kochel RC, Patton PC (1979) Long-term flood frequency analysis using geological data. The hydrology of areas of low precipitation. *IAHS Publ* 128:3–9
- Benito G, Sopen'a, A., Sánchez-Moya Y, Machado MJ, Pérez-González A (2003) Palaeoflood record of the Tagus River (central Spain) during the late Pleistocene and Holocene. *QuatSci Rev* 22:1737–1756
- Benito G, Thorndycraft VR (2005) Palaeoflood hydrology and its role in applied hydrological sciences. *J Hydrol* 313:3–15
- Benito G, Lang M, Barriendos M, Llasat MC, Francés F, Ouarda T, Thorndycraft VR, Enzel Y, Bardossy A, Coeur D, Bobée B (2004) Use of systematic palaeoflood and historical data for the improvement of flood risk estimation: review of scientific methods. *Nat Hazards* 31:623–643
- Benito G, Machado MJ, Perez-Gonzalez A, Sopena A (1998) Palaeoflood hydrology of the Tagus River, Central Spain. In Benito G, Baker VR, Gregory KJ (eds), *Palaeohydrology and environmental change*. Wiley: London, pp 317–333
- Dartmouth Flood Observatory. Accessed on 01/02/2016 from <http://www.dartmouth.edu/~floods/hydrography/E80N30.html>
- Ely LL, Baker VR (1985) Reconstructing Paleoflood hydrology with Slackwater deposits-Verde River, Arizona. *Phys Geogr* 6:103–126
- Ely LL, Enzel Y, Baker VR, Kale VS, Mishra S (1996) Changes in the magnitude and frequency of late

- Holocene monsoon floods on the Narmada River, central India. *Geol Soc Amer Bull* 108:1134–1148
- Enzel Y, Ely LL, Martinez J, Vivian RG (1994) Paleofloods comparable in magnitude to the catastrophic 1989 dam failure flood on the Virgin River, Utah and Arizona. *J Hydrol* 153:291–317
- Fan L, Huang CC, Pang J, Zha X, Zhou Y, Li X (2015) Sedimentary records of palaeofloods in the Wubu Reach along Jin-Shaan gorges of the middle Yellow River, China. *Quatern Int* 380–381:368–376
- Greenbaum N, Harden TM, Baker VR, Weisheit J, Cline ML, Porat N, Halevi R, Dohrenwend J (2014) A 2000 year natural record of magnitudes and frequencies for the largest Upper Colorado River floods near Moab, Utah. *Water Resour Res* 50.<https://doi.org/10.1002/2013WR014835>
- Hirschboeck KK (1988) Flood hydroclimatology. In: Baker VR, Kochel RC, Patton PC (Eds), *Flood geomorphology*. N.Y:Wiley, pp 27–49
- Huang CC, Pang J, Zha X, Zhou Y, Su H, Zhang Y, Wang H, Gu H (2012) Holocene palaeoflood events recorded by slackwater deposits along the lower Jinghe River valley, middle Yellow River Basin, China. *J Quat Sci* 27(5):485–493
- Kale VS (2008) Palaeoflood hydrology in the Indian context. *J Geol Soc India* 71:56–66
- Kale VS, Achyuthan H, Jaiswal MK, Sengupta S (2010) Palaeoflood records from Upper Kaveri River, Southern India: Evidence for discrete floods during Holocene. *Geochronometria* 37:49–55
- Kale VS, Mishra S, Baker VR (1997) A 2000-Year palaeoflood record from Sakarghat on Narmada, central India. *J Geol Soc India* 50:283–288
- Kale VS, Singhvi AK, Mishra PK, Banerjee D (2000) Sedimentary records and luminescence chronology of late Holocene palaeofloods in the Luni River, Thar Desert, northwest India. *CATENA* 40:337–358
- Kale VS, Ely LA, Enzel Y, Baker VR (1994) Geomorphic and hydrologic aspects of monsoon floods on the Narmada and Tapi Rivers in central India. *Geomorphology* 10:157–168
- Kale VS, Mishra S, Baker VR (2003) Sedimentary records of palaeofloods in the bedrock gorges of the Tapi and Narmada Rivers, central India. *Current Sci* 84:1072–1079
- Khan MYA, Daityari S, Chakrapani GJ (2016) Factors responsible for temporal and spatial variations in water and sediment discharge in Ramganga River, Ganga Basin, India. *Environ Earth Sci* 75:283
- Khan AU, Rawat BP (1992) Quaternary geology and geomorphology of a part of Ganga basin in parts of Bareilly, Badaun, Shahjahanpur and Pilibhit district, Uttar Pradesh. Hyderabad: G.S.I
- Knox JC (2000) Sensitivity of modern and Holocene floods to climate change. *Quatern Sci Rev* 19:439–457
- Kochel RC, Baker VR (1982) Paleoflood hydrology. *Science* 215:353–361
- Krumbein WC, Pettijohn FJ (1938) *Manual of sedimentary petrography*. Appleton Century-Crofts Inc., New York, pp 230–233
- Li X, Huang CC, Pang J, Zha X, Ma Y (2015) Sedimentary and hydrological studies of the Holocene palaeofloods in the Shanxi-Shaanxi Gorge of the middle Yellow River, China. *Int J Earth Sci (geol-rundsch)* 104:277–288
- Manning R (1889) On the flow of water in open channels and pipes. *Trans InstCivEnglrel* 20:161–207
- Mao P, Pang J, Huang C, Zha X, Zhou Y, Guo Y, Zhou L (2016) A multi-index analysis of the extraordinary paleoflood events recorded by slackwater deposits in the Yunxi Reach of the upper Hanjiang River, China. *Catena* 145:1–14
- Mukherjee R (2019) Ramganga River Basin- a geomorphological study of channel dynamics and palaeofloods, Unpublished PhD thesis, Dept. of Geography, Institute of Science, Banaras Hindu University, UP, India
- Mukherjee R, Bilas R (2019) Flood frequency analysis of Ramganga River Basin in Western Gangetic Plain, India. *NGJI Int Peer Rev J* 65(3):286–299
- Mukherjee R, Bilas R, Biswas SS, Pal R (2017) Bank erosion and accretion dynamics explored by GIS techniques in lower Ramganga river, Uttar Pradesh, India. *Spatial Inform Res*, 23-38.<https://doi.org/10.1007/s41324-016-0074-2>
- O'Connor JE, Webb RH, Baker VR (1986) Palaeohydrology of pool-and-riffle pattern development: Boulder Creek, Utah. *Geol Soc Amer Bull* 97(4):410–420
- O'Connor JE, Ely LL, Wohl EE, Stevens LE, Melis TS, Kale VS, Baker VR (1994) A 4500-year record of large floods on the Colorado river in the Grand Canyon, Arizona. *J Geol* 102:1–9
- Sinha R, Jain V, Babu GP, Ghosh S (2005) Geomorphic characterization and diversity of the fluvial systems of the Gangetic Plains. *Geomorphology* 70(3–4):207–225
- Sridhar A (2007) A mid-late Holocene flood record from the alluvial reach of the Mahi River, western India. *CATENA* 70:330–339
- Stokes M, Griffiths JS, Mather A (2012) Palaeoflood estimates of Pleistocene coarse grained river terrace landforms (Río Almanzora, SE Spain). *Geomorphology* 149–150:11–26
- Subramanya K (2013) *Engineering hydrology*. McGraw Hill Education (India) Private Limited: New Delhi
- Thorndycraft VR, Benito G, Llasat MC, Barriendos M (2003) Palaeofloods, historical data and climatic variability: applications in flood risk assessment. In: Thorndycraft VR, Benito G, Barriendos M, Llasat MC (eds), *Palaeofloods, historical data and climatic variability: applications in flood risk assessment*. Madrid: CSIC, pp 3–9
- Thorndycraft VR, Benito G, Rico M, Sopena A, Sanchez-Moya Y, Casa A (2005) A long-term flood discharge

- record derived from slackwater flood deposits of the Llobregat River, NE Spain. *J Hydrol* 313:16–31
- Wang L, Leigh DS (2012) Late-Holocene paleofloods in the Upper Little Tennessee River Valley, Southern Blue Ridge Mountains, USA. *The Holocene* 22(9):1061–1066
- Wang L, Huang CC, Pang J, Zha X, Zhou Y (2014) Palaeofloods recorded by slackwater deposits in the upper reaches of the Hanjiang River valley, middle Yangtze River basin, China. *J Hydrol* 519:1249–1256
- Webb R, O'Connor FE, Baker VR (1988) Paleohydrologic reconstruction of flood frequency on the Es'calante River. In Baker VR, Kochel RC, Patton PC (eds), *Flood geomorphology*: New York: John Wiley, pp 403–418
- Yang D, Yu G, Xie Y, Zhan D, Li Z (2000) Sediment records of large Holocene floods from the middle reaches of the Yellow River, China. *Geomorphology* 33:73–88
- Zha X, Huang C, Pang J (2009a) Palaeofloods recorded by slackwater deposits on the Qishuihe River in the Middle Yellow River. *J Geog Sci* 19(6):681–690
- Zha X, Huang C, Pang J (2009b) Palaeofloods recorded by slackwater deposits on the Qishuihe River in the Middle Yellow River. *J GeogrSci* 19:681–690
- Zha X, Huang C, Pang J, Liu J, Xue X (2015) Reconstructing the palaeoflood events from slackwater deposits in the upper reaches of Hanjiang River, China. *Quatern Int* 380–381:358–367
- Zhang YZ, Huang CC, Pang JL, Zha XC, Zhou YL, Gu HL (2013) Holocene paleofloods related to climatic events in the upper reaches of the Hanjiang River valley, middle Yangtze River basin, China. *Geomorphology* 195:1–12
- Zhang YZ, Huang CC, Pang JL, Zha XC, Zhou YL, Wang XQ (2015) Holocene palaeoflood events recorded by slackwater deposits along the middle Beiluohe River valley, middle Yellow River basin, China. *Boreas* 44:127–138. <https://doi.org/10.1111/bor.12095>. ISSN0300-9483
- Zhou L, Huang CC, Zhou Y, Pang J, Zha X, Xu J, Zhang Y, Guo Y (2016) Late Pleistocene and Holocene extreme hydrological event records from slackwater flood deposits of the Ankang east reach in the upper Hanjiang River valley, China. *Boreas*. <https://doi.org/10.1111/bor.12181>



Flood Risk Zone Identification Using Multi-criteria Decision Approach

4

Raja Majumder and Gouri Sankar Bhunia

Abstract

Flooding phenomenon is deliberated as the world's vilest comprehensive risk in terms of scale, existence, geographical extent, forfeiture of life and goods along with dislodgment of people and demographic events. A flood risk map of the Bongaon sub-division was generated using multi-criteria decision approach (MCDA) through geographical dataset, viz. rainfall, elevation, slope, soil, geomorphology, distance of river to the main channel, vegetation vigor, fractional impervious surface, road density, land use/land cover. Fifty-five validation points are used to evaluate the flood hazard risk map. The validation result proposes that MCDA and geospatial technology are very influential approaches in flood risk analysis and mapping. The derived flood risk map was reclassified into five categories through manual classification methods in ArcGIS software, such as very low risk, low risk, medium risk, high risk, and very high risk. The flood risk map portrays that probably 74.70 km² (8.96%) of the area comes under very high flood risk areas. The medium flood risk areas are calculated as

242.02 km² (29.02%), distributed in the central north, north-west and south-west part of the study site. The overall user accuracy and producer accuracy of the flood risk map was calculated as 69% and 72%, respectively. Choosing suitable factors may be useful to planners and developers for future development and land use planning.

Keywords

Flood hazard · Multi-criteria decision approach · GIS · Flood control

4.1 Introduction

Flood hydrology covenants with the functionality of time and space reliant developments of waters and are engrossed on hydraulic and engineering magnitudes of floods. Flood in association with climate change and meteorological variability in the recent past in India have already been analyzed and discussed by several researchers (Guhathakurta et al. 2011; Nandargiand and Dhar 2003). Moreover, there is a substantial chronological dissimilarity in the monsoon rainfall connected to climatic erraticism in India. To generate the flood hazard map, numerous issues are required for accurate mapping under circumstances of data and other constituents' inadequacies that epitomize the condition in most of

R. Majumder (✉) · G. S. Bhunia
Department of Geography, Seacom Skills
University, Kendradangal, Santiniketan, Birbhum,
West Bengal 731236, India

the countries. In general, computable data of the flood predisposing factors derived through a number of specialists accordingly, the format and spatial resolution of the data illustration differs between various sources. Earlier several research studies were conducted using remote sensing and GIS technique to generate the flood inundation areas (Haq et al. 2012; Patel and Srivastava 2013; Ouma and Tateishi 2014; Kazakis et al. 2015; Roy and Sarker 2016; Dhruvesh et al. 2016). For the past two to three decades, researchers were elaborating on evolving dissimilar approaches and facsimiles for flood risk mapping using Remote Sensing and Geographical Information System (Dandapat and Panda 2018). Fuzzy logic (Nugraha et al. 2018), logistic regression (Lim and Lee 2018), analytical hierarchy process (Matori et al. 2014), artificial neural networks (Elsafi 2014), frequency ratio (Cao et al. 2016), multi-criteria decision support system (Samanta et al. 2016) and weights-of-evidence (Rahmati et al. 2016) are limited eminent and satisfactory approaches in natural hazard modelling for investigating the multifaceted difficulties in different parts of the world.

Floods are perhaps the most frequent, pervasive calamitous and recurrent natural hazards in India. North 24 Parganas are one of the most flood-prone regions in West Bengal (India) due to heavy rainfall in monsoon season, highly silted Ichamati River system, inadequate capacity to carry the high flood discharge (http://www.wbiwd.gov.in/uploads/ANNUAL_FLOOD_REPORT-2016.pdf), improper drainage, land use/land cover characteristics, geomorphology, etc. (Majumder et al. 2017). The human interferences subsidizing to flood events are principally in the practice of repossession of wetlands and surface water bodies, modification in land use configuration, creation of impenetrable linkages of roads, formation of extensive built-up areas, deforestation etc. Ajin et al. (2011) conducted a study to generate the flood risk maps of the Vamanapuram River basin reliant upon multi-criteria assessment using geospatial technologies. Ismail and Saanyol (2013) have conducted a research for the flood vulnerability

mapping in the Kaduna River of Nigeria using a digital elevation model (DEM) and hydrological analysis. Getahun and Gebre (2015) carried out the study on flood hazard assessment and mapping of flood inundation area of the Awash River Basin in Ethiopia using GIS and HEC-GeoRAS/HEC-RAS Model.

The flood vulnerability mapping demarcates risk areas in the Gangetic plain by assimilating local acquaintance, hydrological, climatological, and geomorphological data using various methods. Consequently, hazards hypothetically detrimental physical extent, the phenomenon for the feature of life or injury, property impairment, ecological dilapidation, socio-economic commotion (Getahun and Gebre 2015). The creation of a very high spatial resolution GIS database is costly and time-consuming. Recently, several investigations have been done to evaluate flood hazards using geospatial technology (Mandal and Mandal 2015). Frequency ratio (Tehrany et al. 2015), analytical hierarchy process (Stefanidis and Stathis 2013), fuzzy logic (Pradhan 2011), logistic regression (Fustos et al. 2017), artificial neural networks (Abdellatif et al. 2015), and weights of evidence (Tehrany et al. 2017) and multi-criteria decision support systems are few well known and acceptable methods in flood hazard modelling for analysing complex problems different regions.

Correct and up-to-date floodplain maps can be the most cherished tackles for evading unadorned social and fiscal victims from floods. One of the flood risk management against flood impact at the regional scale is the identification of vulnerable areas to provide early warning, facilitate quick response and decrease the impact of possible flood events. The aims of the present research work are to find out the appropriate conditioning factor of flood susceptibility of the Bongaon Sadar sub-division and its applicability in various regions. Therefore, the flood risk map of Bongaon Sadar sub-division was generated through multi-criteria decision approach (MCDA) based on the integration of remotely sensed products and secondary datasets.

4.2 Study Area

Bangaon subdivision is part of the Ichamati–Raimangal Plain, located in the North of the North 24 Parganas (West Bengal, India). Figure 4.1 shows the location of the map of the Bongaon subdivision. The sub-division is divided into 3 blocks, namely Bagda, Bongaon and Gaighata. Bongaon subdivision is particularly susceptible to flooding because of its physiography and tropical monsoon climate characterized by drenching rainfall and unplanned management of floods (Ghosh and Mistri 2015). The sub-division is a part of the lower Gangetic delta and is also remarkable on the vast gradational surface (Saha 2015). Bhagirathi and Hooghly River flow over the western side of the sub-division (Mondal and Bandyopadhyay 2014). Ichamati River flows through the center. Surface expression of normal fault is running through the Burdwan–Debagram–Jalangi area (Sengupta 1966), flowing through the eastern part of the North 24 Parganas (north and south) districts eventually exits in the Raimangal River *vis-à-vis* the Bay of Bengal. The annual temperature of the study area ranges between 8 and 41°C in January and May, respectively. The highest relative humidity of the study area is recorded as 80% in July. The annual average rainfall of the study area is calculated as 1,579 mm. The major crop of the study area is recorded as rice, wheat, pulses and other oil seeds. As per the 2011 census, the total population of the study area was recorded as 1,063,028, with a population density of 838.17 km². Bongaon subdivision had a literacy rate of 80.57%.

The dwindling of this Ichamati River can be accredited to extreme sedimentation load, lessening headwater supply, tidal interference, growth of cultivated land and numerous instinctive interferences into the river regime like the creation of bridges, road on the riverbed by intruding its natural flow (Saha 2015). Around 50% of the total population in Bongaon and almost 75% of its properties are placed in flood susceptible extents (http://cgwb.gov.in/documents/Bhujal_News_24_1.pdf). Several

number of life-threatening flood measures befell during the past two decades and instigating substantial mutilation to life and stuff acme the inevitability for suitable flood administration trials in the sub-division.

4.3 Materials and Method

4.3.1 Collection of Secondary Data

Quantitative methods are employed for the exploration of geometric data to inaugurate spatial associations stuck between causative factors and floods. To classify a flood risk zone, a multi-parametric dataset encompassing satellite data, conformist maps containing Survey of India (SOI) topographical sheets has been employed for the generation of thematic maps, like drainage density, built-up areas, road density and surface waterbody, etc.

4.3.2 Analysis of Flood Frequency

The most important factor for determining the flood hazard is flood frequency. Available data of flood occurrences for the decade 1996–2016 was obtained from the sub-divisional office of Bongaon, North 24 Parganas in West Bengal (India). This information was used to generate the frequency of flood occurrence in the study area. The flooded areas for each year were integrated into a single layer of the GIS database and polygon shapefile were prepared for each year.

4.3.3 Satellite Data Acquisition and Preprocessing

Landsat8 Operational Land Imager (OLI) data of two different time periods (Month of October and February) were acquired from the United States of Geological Survey (USGS) Earth Explorer community. The satellite data was radiometrically and geometrically corrected using ERDAS

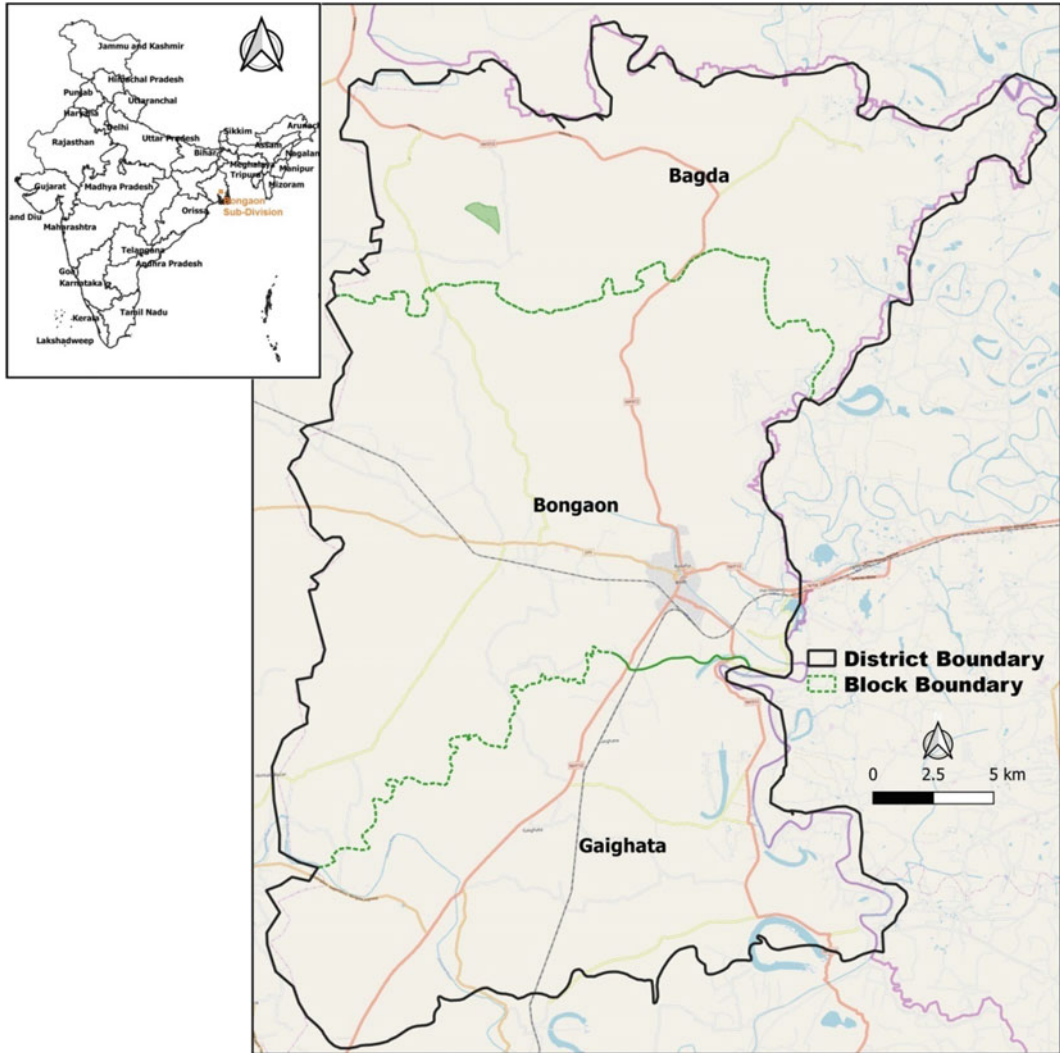


Fig. 4.1 Location map of Bongaon sub-division

Imagine software version 9.0. The Satellite data was geo-referenced in Universal Transverse Mercator (UTM) projection system and World Geodetic System (WGS) 84 datum. Advanced Space Thermal Emission Radiometer (ASTER) Global Digital Elevation Model (GDEM) data (2010) with a spatial resolution of 30 m was used for the topographical analysis, collected through the Earth Remote Sensing Data Analysis Center (ERSDAC) and the NASA Land Processes Distributed Active Archive Center (LP DAAC).

4.3.4 Rainfall Distribution

The rainfall data of the Bongaon sub-division and its surrounding station were collected from the IMD station. A total of five station data rainfall data of the past 10 years (2006–2016) were collected. The annual average rainfall data was calculated for each station. Finally, the rainfall distribution map of the study area was prepared using the radial basic function (RBF) method using ArcGIS spatial analyst tool.

4.3.5 Soil Characteristics

The soil map of the study area was acquired from the National Atlas Thematic Mapping Organization (NATMO), Kolkata, West Bengal, India, and finally validated with the published literature. The vector layer of the soil map of the Bongaon sub-division was prepared after geoprocessing operation in ArcGIS software v9.3.

4.3.6 Distance of River to Main Channel and Drainage Density

Areas located close to the main river channel and flow accumulation path are more likely to get flooded (Islam and Sado 2000). Therefore, the polygon buffer of the main channel is created as 500 m, 1000 m, 1500 m, 2000 and more than 2500 m in ArcGIS software v9.3. Drainage network is first digitized from the SOI toposheet. After that, the drainage network has been validated with the Landsat8 Operational Land Imager (OLI) satellite data. The drainage density of the study area is calculated as follows:

$$D_d = \frac{\text{Total length of drainage channel in sq km}}{\text{Area (within 5sq km)}}$$

4.3.7 Surface Elevation and Slope:

Surface elevation is another natural factor that causes flood. In areas of higher elevation, the probability of flood occurrence is relatively lower than that of the lower elevation. In areas of lower elevation, the terrain is generally gentle, and the flow of water remains slow and holds the water for a long duration of time. The elevation map of the study area is derived through ASTER digital elevation model data. A slope map of the study areas is prepared from ASTER Digital Elevation Model (DEM) Data. The slope angle of each pixel is generated from ArcGIS software v9.3.

4.3.8 Geomorphology

By a combination of spectral band7 (SWIR 1.55–1.75 μm), band10 (TIR 10.40–12.50 μm) and band6 (NIR 0.77–0.90 μm) of Landsat8, image analysis was performed to identify the geomorphic characteristics like river/stream, abandoned channel, old and new alluvial plain, ox-bow lake, paleochannel, natural depressions, back swamps and meander scar. The geomorphological map was prepared with the evidence used by Chaturvedi and Mishra (2015) and Mukherjee (2006). After that, the selective field checks were performed to assess the validity of the pre-field image interpretation.

4.3.9 Analysing of Land Use/Land Cover and Vegetation Characteristics

The land use classes derived are often not satisfactory because of the limitation of spatial resolution in remote sensed imagery and the heterogeneity of urban landscapes. A range of impervious surfaces may be mixed with other land cover types such as forest, soils and pastures. Land use/land cover is an additional imperative persuading factor of flood hazard (Alexakis et al. 2014).

The vegetation characteristic of the study area was derived using a near-infrared and red band of OLI sensor data of Landsat8. The normalized difference vegetation index (NDVI) was calculated using channel 5 and channel4 of the landsat8 OLI sensor using the following equation:

$$NDVI = \frac{(\text{Near infrared}_{\text{Channel5}} - \text{Red}_{\text{Channel4}})}{\text{Near infrared}_{\text{channel5}} + \text{Red}_{\text{channel4}}}$$

4.3.10 Fractional Impervious Surface Area (FIS)

Impervious surface is demarcated as the surface avert water penetrates the soil and is mainly associated with conveyance and building

rooftops. FIS can be perceived and enumerated because of their massive topographical coverage and chronological occurrence of data collection, thus deciphered numerous ecological disputes such as land cover for hydrological and eco-friendly mockups. In this study, to calculate the FIS following equation has been followed:

$$FIS = 1 - FVC$$

where FVC refers to Fractional Impervious Surface Area.

FVC can be calculated using the following equation proposed by Calson and Ripley (1997):

$$FVC \approx (NDVI_s)^2$$

whereas, NDVI refers to normalized difference vegetation index. ND0VIs can be calculated using the following equation proposed by Basarudin and Adnan (2014).

$$NDVI_s = \frac{NDVI - NDVI_{low}}{NDVI_{high} - NDVI_{low}}$$

FVC ranges between 0 and 1.

4.3.11 Population Density

Population pressure is another important factor of the hazard map. A village-based vector layer is prepared from the entire sub-division and integrated with the GIS database based on 2011 census data. The population density of the study area is calculated as

$$\text{Population density} = \frac{\text{Total number of population in a village}}{\text{Area in km}^2}$$

4.3.12 Road Density

In this research, all the metalled, unmetalled and pucca village roads of the study area were digitized. All the roads were extracted primarily from the SOI topographical sheet and improved using Google Earth image in shapefile format. The

density is calculated as the length of the road per sq km. After that using the spatial analyst tool of ArcGIS software, the road density map was generated.

4.3.13 Multi-criteria Analysis

GIS-based multi-criteria decision analysis (MCDA) can be thought of as a process that combines and transforms spatial and aspatial data into a resultant decision. This practice is an arithmetical scheme reliant upon biophysical aspects, which are directly or circuitously associated with the event of floods. In this study, elevation, slope, drainage density, the distance of river to the main channel, vegetation vigour, fractional impervious surface, road density, land use/land cover were taken as the most important elements for appraising the flood hazard. Weights were consigned to the rasterized data layers and using map algebra in the spatial analyst tool to run a multi-criteria analysis. Subsequently, among the weighting measures, each aspect was segregated into five sub-factors, each of which was specified a ranking cost for the analogous sub-factor. For every aspect, the weighted influence ranking was attained by bourgeoning its burden by the ranking value for the analogous sub-types. The entire assessed threat, attained by tallying the weighted flood statuses of all the features were categorized into five classes—very low, low, moderate, high and very high. The overall methodology of the study area is illustrated in Fig. 4.2.

4.3.14 Verification and Observation

Finally, flood hazard risk maps were composed in the GIS platform and the maps were endorsed in the field to evaluate its exactitude. The procedure has been completed through a field visit to describe how meticulously the flood risk map settles with the concrete field condition. For the field justification, 55 GPS ground truth data of flood pretentious areas delineated organized with

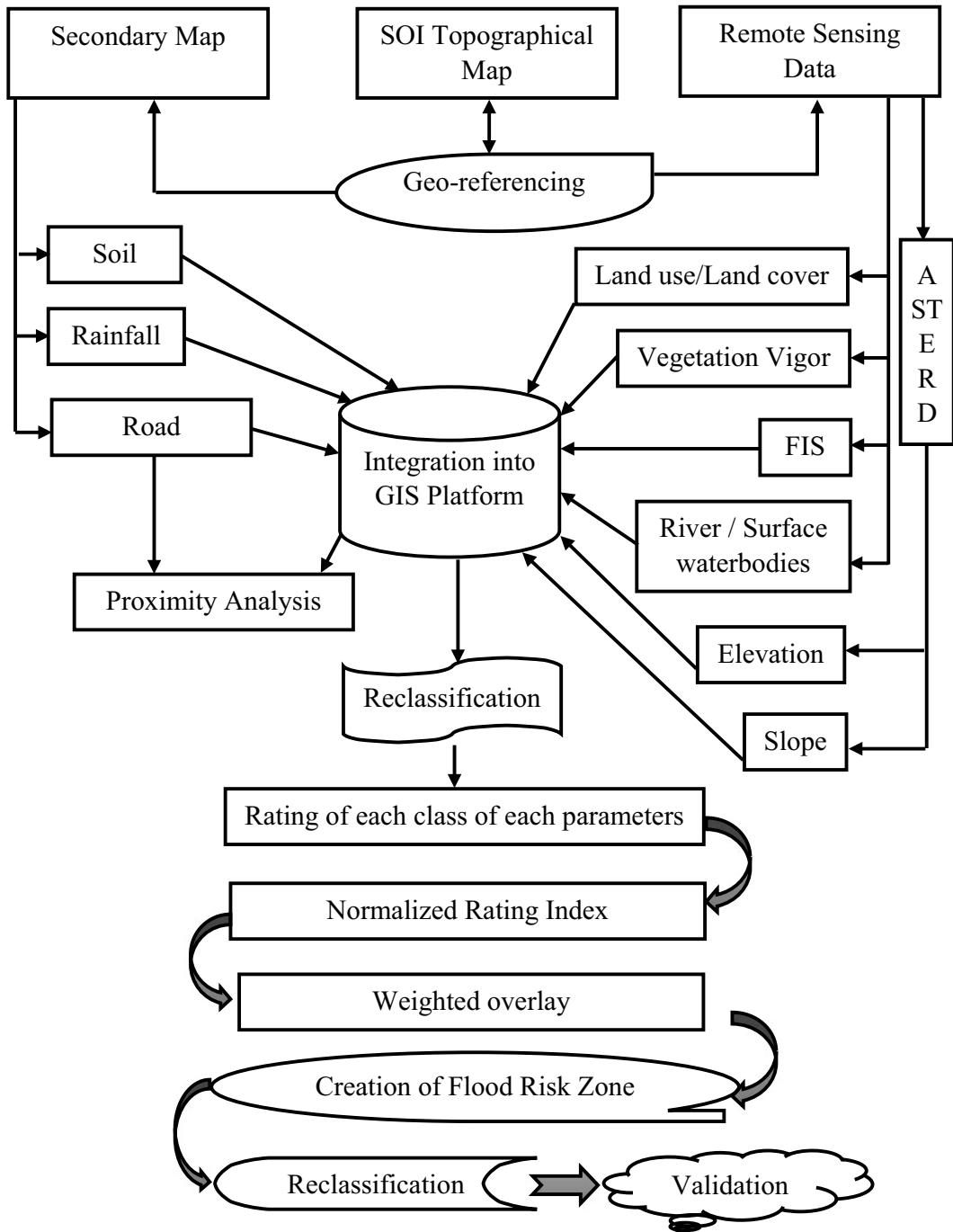


Fig. 4.2 Overall methodology of the research work

their corresponding LULC types were demarcated and a point shapefile has been generated. The LULC features that are set up within flood-

affected areas (e.g. built-up areas, cultivated land, agricultural fallow and landscapes located in a hazardous area) are confirmed at the field,

considered as a flood risk indicator. This point shapefile was superimposed with flood hazard and risk maps and then the flood hazard risk maps were verified with the actual field situations.

4.4 Results

The details of the flood pre-disposing factors were described in chapter VI, which are directly or circuitously associated with the happening of floods. All the features governing flood hazard layers were rehabilitated into raster format. Furthermore, these raster maps were reclassified. Weighted sum operation in spatial analysis extension of ArcGIS v9.3 was charted to assimilate all Normalized Rating Index (NRI) and Normalized Weight Index (NWI) and to produce a pixel by pixel (15 m spatial resolution) flood hazard and/or vulnerability database (Tables 4.1 and 4.2). The weights of the selective themes were consigned on a scale of 1 to 5 reliant upon

their impact on the flood menace. Apposite weights were allocated to the eleven aspects and their discrete aspects after understanding their importance in causing flood hazard occurrence in the sub-division. Among the elevation factors, LULC weighted the highest with 21%, followed by rainfall with 15%, slope with 13%, elevation with 8%, soil with 8%, road density with 8%, distance from the river by 7.5%, geomorphology by 7.5%, vegetation vigour by 7% and fractional impervious surface by 5%, respectively. The factors were weighted based on their virtual prominence to each other and to their estimated significance in initiating floods in the Bongaon sub-division. For every aspect, the subjective menace ranking was attained by multiplying its burden by the ranking worth for the conforming sub-factor.

Monthly rainfall data of five meteorological stations within the Bongaon sub-division for a period of (2005–2016) were obtained from the meteorological department. Monthly data were then converted to annual mean rainfall. The

Table 4.1 Rate, normalized rating index, weight index based on MCDA of flood hazard assessment of Bongaon sub-division

Parameters	Category/class	Rate	Normalized rating index (NRI) [Individual/total]	Weight (W)	Normalized weight index (NWI)
Rainfall (mm)	Less than 1450	5	0.33	15	1.5
	1451–1500	4	0.27		
	1501–1520	3	0.20		
	1521–1543	2	0.13		
	More than 1543	1	0.07		
Elevation (m)	<5.0 m	5	0.38	8	0.8
	5.1–7.5	4	0.31		
	7.6–10.0	3	0.23		
	>10.1	1	0.08		
Slope (degree)	Less than 1.0°	5	0.33	13	1.3
	1.1–1.5°	4	0.27		
	1.6–2.0°	3	0.20		
	2.1–4.0°	2	0.13		
	More than 4.1°	1	0.07		

(continued)

Table 4.1 (continued)

Parameters	Category/class	Rate	Normalized rating index (NRI) [Individual/total]	Weight (W)	Normalized weight index (NWI)
Land use/land cover	River/surface waterbodies	5	0.28	21	2.1
	Low laying area	4	0.22		
	Moist fallow	3	0.17		
	Built-up area	1	0.06		
	Agricultural fallow	2	0.11		
	Crop land	3	0.17		
Vegetation vigour (NDVI)	<0.0098	5	0.33	7	0.7
	0.0099–0.16	4	0.27		
	0.17–0.23	3	0.20		
	0.24–0.50	2	0.13		
	>0.50	1	0.07		
Fractional impervious surface	<20	1	0.10	5	0.5
	21–35	2	0.20		
	36–50	3	0.30		
	>51	4	0.40		

Table 4.2 Rate, normalized rating index, weight index based on MCDA of flood hazard assessment of Bongaon sub-division

Parameters	Category/class	Rate	Normalized rating index (NRI) [Individual/total]	Weight (W)	Normalized weight index (NWI)
Geomorphology	Abandoned channel	3	0.07	7.5	0.75
	Active river channel	5	0.12		
	Back swamp	3	0.07		
	Channel bar	5	0.12		
	Deep depression	4	0.09		
	Meander scar	5	0.12		
	Newer alluvial plain	4	0.09		
	Older alluvial plain	2	0.05		
	Older alluvial plain- type ii	1	0.02		
	Ox-bow lake	4	0.09		
	Paleochannel	4	0.09		
	Shallow depression	3	0.07		

(continued)

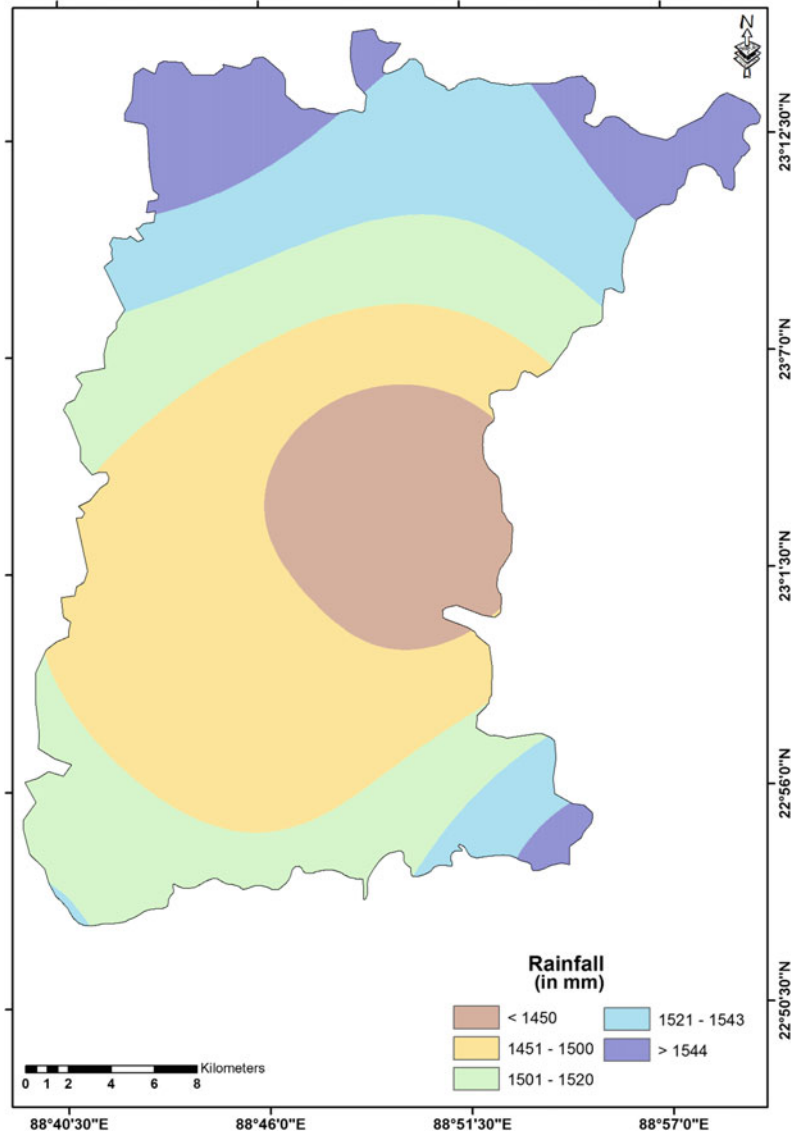
Table 4.2 (continued)

Parameters	Category/class	Rate	Normalized rating index (NRI) [Individual/total]	Weight (W)	Normalized weight index (NWI)
Soil Type	Very deep to deep, poorly drained, fine loamy to fine	5	0.25	8	0.8
	Very deep, fine loamy, poorly to imperfectly drained	4	0.2		
	Very deep, fine loamy, poorly to moderately well drained, fine loamy	2	0.1		
	Very deep, moderately well to poorly drained, coarse loamy to fine	2	0.1		
	Very deep, poorly drained, fine loamy	3	0.15		
	Very deep, poorly to moderately well drained, fine to coarse loamy	3	0.15		
	Very deep, poorly to well drained, fine to sandy	1	0.05		
Distance from the river (m)	Less than 500	5	0.33	7.5	0.75
	501–1000	4	0.27		
	1001–1500	3	0.20		
	1501–2000	2	0.13		
	More than 2001	1	0.07		
Road density (km ²)	<0.59	1	0.07	8	0.8
	0.60–0.76	2	0.13		
	0.77–0.92	3	0.20		
	0.93–1.1	4	0.27		
	>1.2	5	0.33		

average annual rainfall map was prepared through radial basis function and the rainfall map was divided into five categories (Fig. 4.3). In the classification process, the sub-division with higher rainfall (mm) is assigned 1 as it would be very extremely pretentious by a flood. The elevation map of the study area was prepared through ASTER satellite data and the Bongaon sub-division was categorized into 4 sub-categories of elevation zone (Fig. 4.4). Areas with the lowest elevation zone were considered as most vulnerable to flooding, thus ranked 1 which is less than 5.0 m. Following the flood hazard classes, there were the class high (5.1 m–7.5 m) ranked 2, class moderate (7.6 m–10.0 m)

ranked 3 and class low (>10.1 m) very low ranked 4. The slope layer of the Bongaon sub-division was prepared from the ASTER Digital Elevation Model (DEM) data and reclassified into five sub-categories in the order of flood hazard rating. The ASTER DEM was downloaded from USGS Earth Explorer Community (<https://earthexplorer.usgs.gov/>). The pixel resolution of ASTER DEM data is 30 m considered for this analysis. In the present research, less than 1° slope is considered as high risk for flood hazard (Fig. 4.5). LULC characteristics of the sub-division were reclassified into a common scale permissible of their rainwater intellection capabilities for the flood hazard examination into

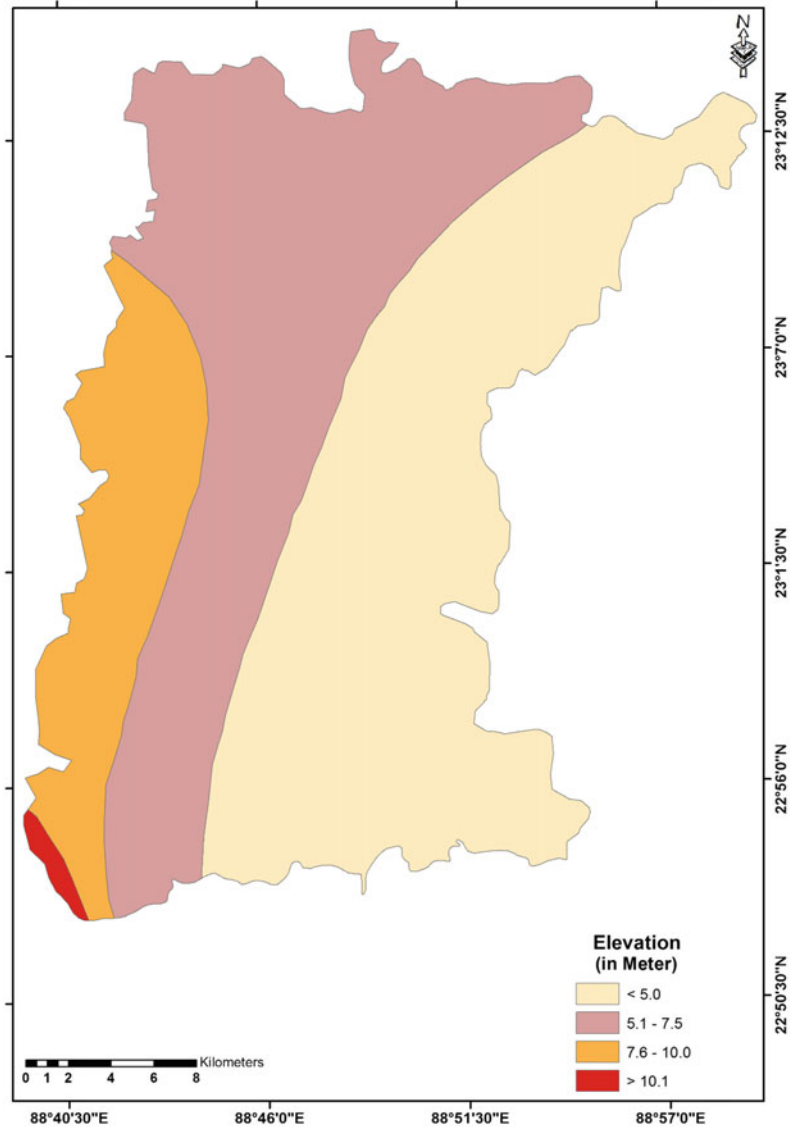
Fig. 4.3 Reclassified rainfall map of Bongaon sub-division



flood evaluation outcomes for land cover element map (Fig. 4.6) Based on the flood causing physiognomies of the LULC types, river and/or surface water bodies as a very high rating, low laying area was assigned high flooding, moist fallow and crop land were assigned as moderate class, agricultural fallow was demarcated as low rating and the built-up area was assigned as very low rating. Vegetation characteristics designate the presence of the landscapes and are commonly categorized by the amount and form of vegetation, which reflects its usage, milieu, agronomy

and cyclic phenology. The vegetation characteristics of the Bongaon sub-division have been classified into five sub-zones (Fig. 4.7). The low-density vegetation cover was assigned as a high rating for flood vulnerability and the high-density vegetation cover was demarcated as a low rating for flood hazard. The reclassified map of fractional impervious surface (FIS) of the Bongaon sub-division is illustrated in Fig. 4.8. The lower FIS value implies a higher permeability, whereas the higher FIS value indicated lesser permeability. The geomorphological characteristics of the

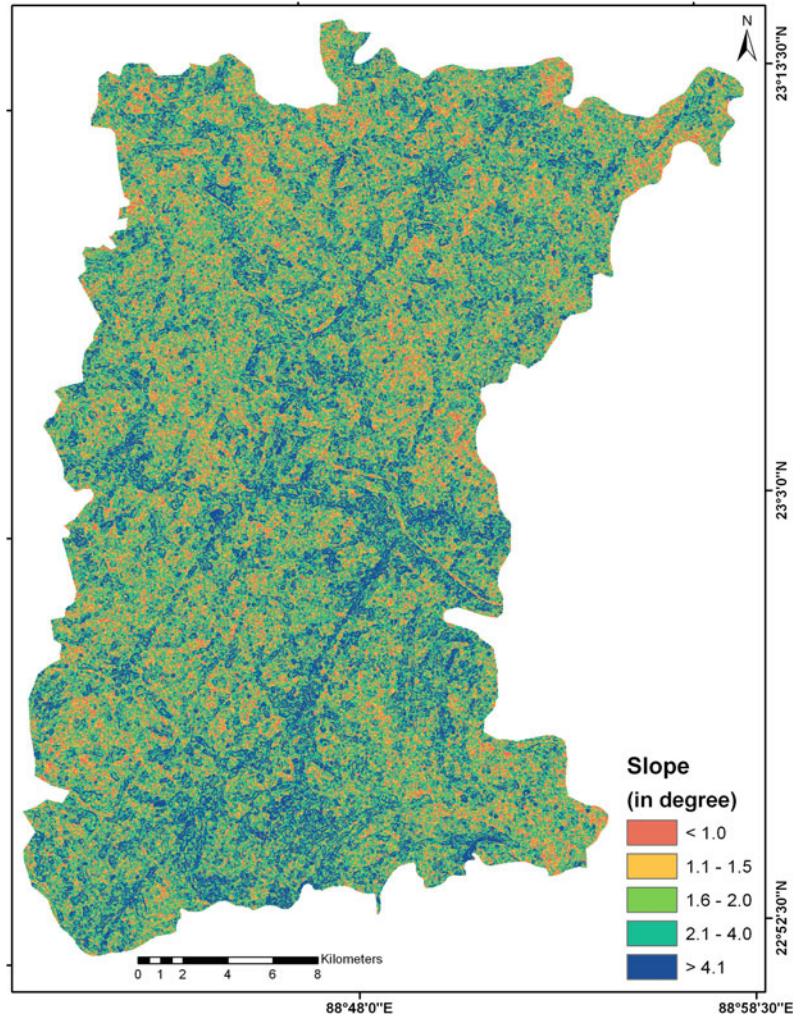
Fig. 4.4 Reclassified elevation map of Bongaon sub-division



sub-division play an important role in flood hazard susceptibility. In the Bongaon sub-division, new alluvial plain zones, channel bar and meander scar were providing a high rating for flood risk (Fig. 4.9). High to moderate flood vulnerability areas were demarcated as abandoned river channel, paleochannel, ox-bow lake, back swamp and deep depression due to the location adjacent to the very high susceptibility zone. Moreover, the low flood susceptibility zone was assigned as an older alluvial plain and shallow depression (Table 4.2). In this research,

very deep to deep, poorly drained, fine loamy to fine soil has been assigned higher weightage and the very deep, poorly to well drained, fine to sandy has been assigned the lower rating (Fig. 4.10). Moreover, very deep, poorly to well drained, fine to sandy soil was demarcated as a low rating of flood hazard. Finally, the soil map was transformed into raster format and reclassified based on their water infiltration capacity into flood rating results for the soil factor map (Table 4.2). Less than 500 m distance from the active river channel is considered as more prone

Fig. 4.5 Reclassified slope map of Bongaon sub-division (Slope map was generated from ASTER DEM Data; Spatial resolution—30 m)



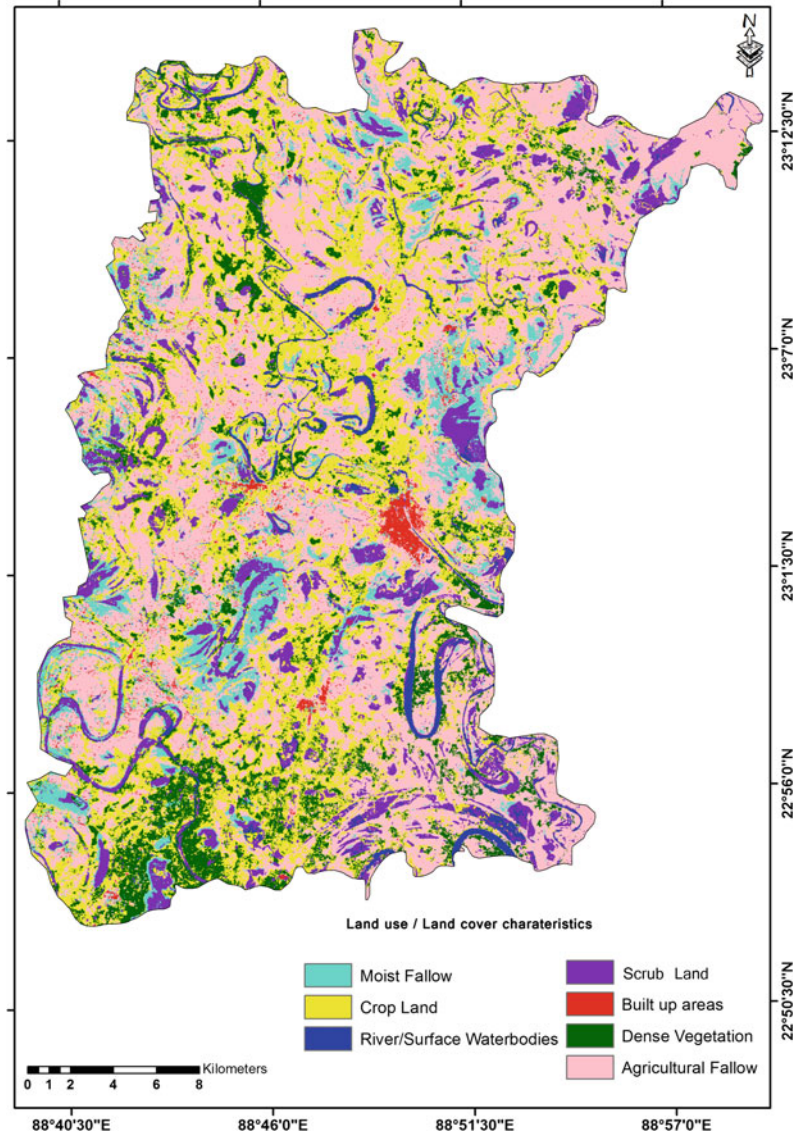
to flood hazards in the Bongaon sub-division. The rating has been decreased with the increasing distance from the river channel due to a decrease in ferocity (Fig. 4.11).

The road densities played a significant role in flood hazards as it is disturbing the free flow of water and restrict the passage of flood discharge. The road density of the Bongaon sub-division has been categorized into 5 sub-zones (Fig. 4.12). The higher road density was assigned a low rating and the lower road density region was demarcated as a higher rating for flood hazard. Following the very high susceptibility to flooding class, there was a class very high (<0.59 per km^2), $0.60\text{--}0.76$ per km^2 graded

as class 2, $0.77\text{--}0.92$ per km^2 placed as class 3, $0.93\text{--}1.1$ per km^2 ranked as class 4 and very low ranked as >1.2 per km^2 .

The calculated flood risk index values of the output database vary from 0.05 (Low) to 0.68 (High) (Table 4.3). The derived flood risk map was reclassified into five categories through manual classification methods in ArcGIS software, such as: (i) very low risk (less than 0.15), low risk (0.16–0.26), medium risk (0.27–0.33), high risk (0.34–0.48), and very high risk (more than 0.49) (Fig. 4.13). The ‘medium risk’ is measured along the areas that might be seasonally overwhelmed in the wet season. The ‘very low risk’ refers to the areas prone to very low

Fig. 4.6 Reclassified land use/land cover map of Bongaon sub-division

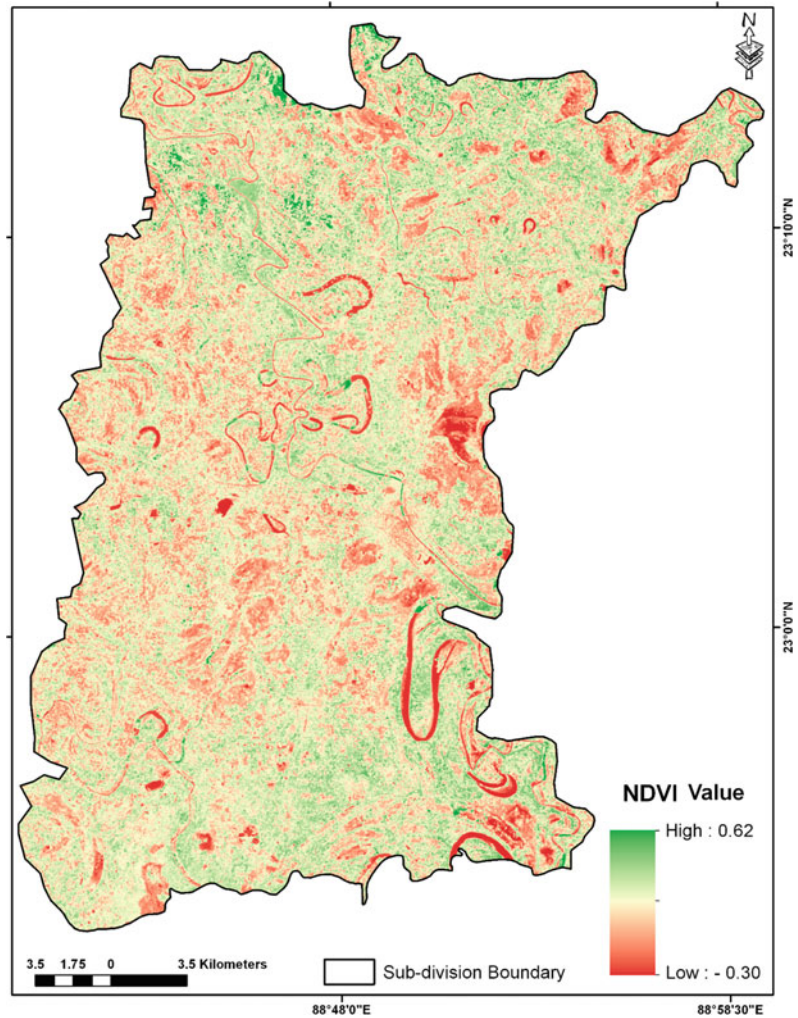


occurrences of floods, almost nil. Moreover, the ‘very high risk’ and ‘high risk’ zones of flood denote the conceivable areas of flood that can eventuate because of the periodic as well as intermittent heavy rainfall.

Zonal statistical tool of ArcGIS software v9.3 was used to determine the areal distribution of flood risk areas of the Bongaon sub-division. The flood risk map portrays that probably 74.70 km² (8.96%) of the area comes under very high flood risk areas (Table 4.3). These areas were mostly distributed in the south-east, north, north-east

and some small pockets of the central part of the Bongaon sub-division. Approximately, 19.36% (161.45 km²) of the area falls under high risk, distributed in the eastern and northern part of the sub-division. The medium flood risk areas are calculated as 242.02 km² (29.02%), distributed in the central north, north-west and south-west part of the study site. About 28.33% (236.33 km²) of the Bongaon sub-division falls under the low flood risk areas which are disseminated in the central, southern and western part of the sub-division (Fig. 4.13).

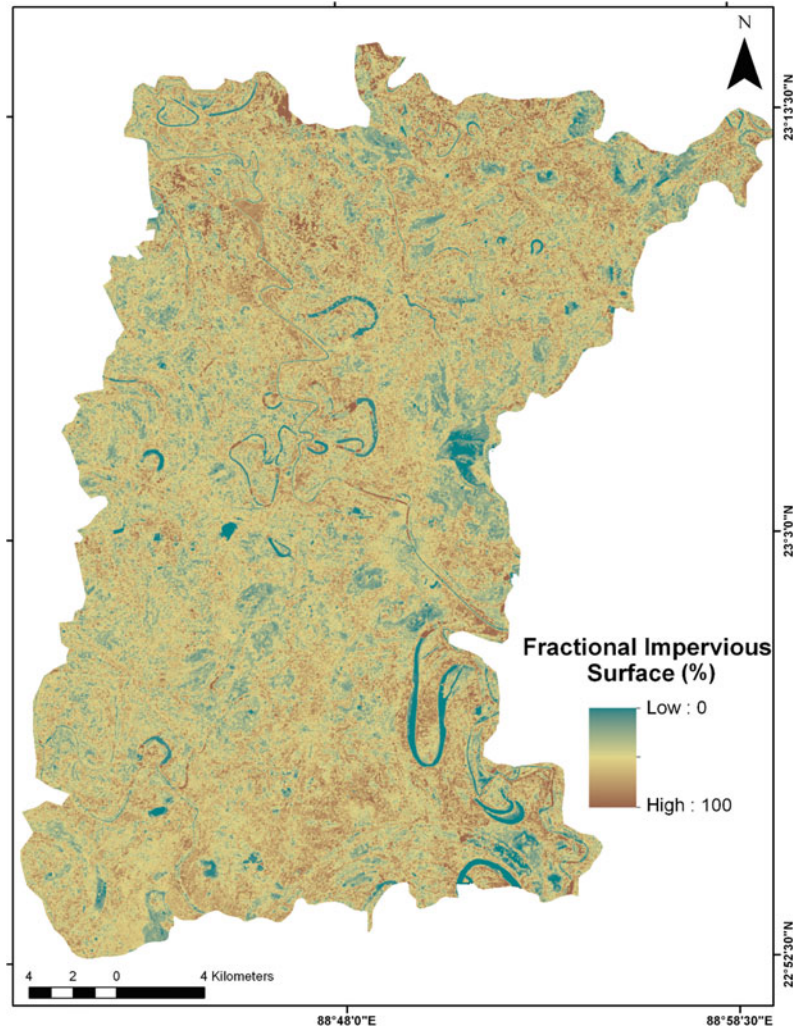
Fig. 4.7 Reclassified vegetation characteristics (NDVI) map of Bongaon sub-division



A total of 55 sites were designated to measure the flood substantiations events (Table 4.4). These points are distributed in different directions of the sub-division and distributed in the entire region of the sub-division. Chronological floods events were used as verifications sites. There were 13 sites (VP1, VP2, VP4, VP12, VP17, VP18, VP19, VP20, VP37, VP43, VP44, VP45 and VP46) of 'very high' risk of flood events and eight sights (VP6, VP14, VP25, VP30, VP31, VP42, VP5 and VP55) of 'high' risk for flood events were checked. The medium flood risk validation points are demarcated as VP10, VP13, VP16, VP23, VP27, VP29, VP36 and VP52. These areas are usually waterlogged

for 3 to 4 days or a short duration of the flood because of the concentrated rainfall events. The low flood risk validation points are designated as VP3, VP7, VP8, VP21, VP26, VP32, VP39, VP40, VP49 and VP51. The user accuracy and producer accuracy of low flood risk areas were calculated as 89% and 80%, respectively. Moreover, VP5, VP9, VP11, VP15, VP22, VP28, VP33, VP34, VP35, VP38, VP41, VP47, VP48, VP50 and VP53 are considered as very low risk. These areas were not also inundated since 2005 and mostly characterized by high elevation, far from the river channel, dense vegetation cover, protected from the flood by anthropogenic activities. The user's accuracy and

Fig. 4.8 Reclassified Fractional Impervious Surface (FIS) map of Bongaon sub-division



producer's accuracy of the predictive map of flood hazard in the Bongaon sub-division were calculated as 69% and 72%, respectively. Hence, the result of the analysis indicated that the methodology is satisfactorily consistent for substitute response.

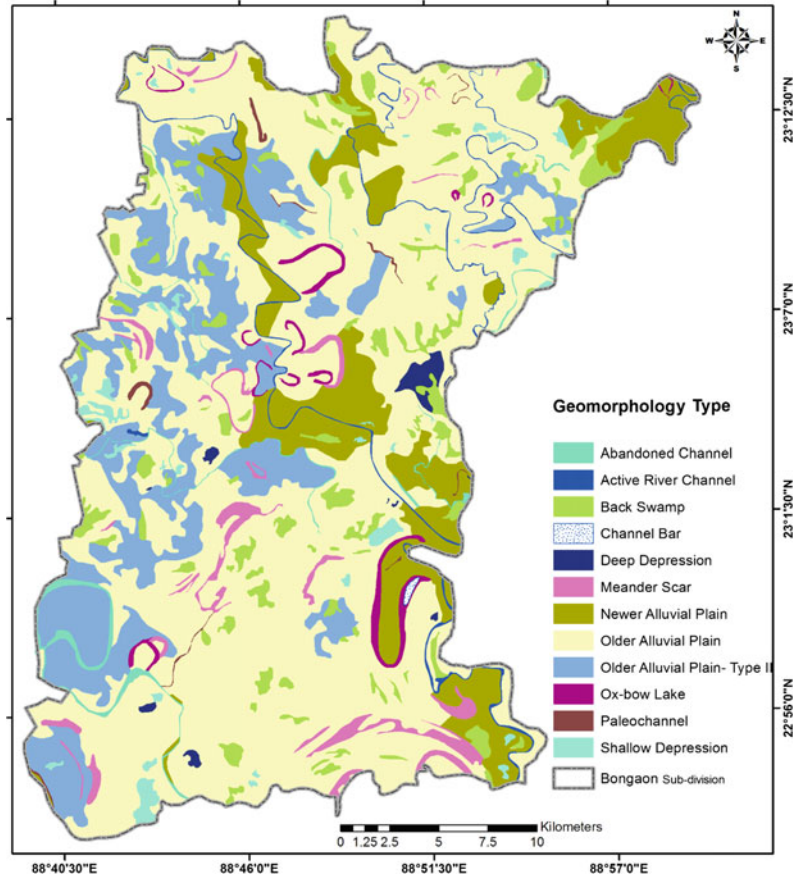
4.5 Discussion

Due to geographical characteristics, unplanned infrastructure and land use planning have a high level of flood risk. Flooding has become a regular phenomenon and continues to threaten the vulnerable social and economic infrastructure of the

sub-division. A flood risk map is a vivacious constituent for apposite land use forecasting in flood susceptible spaces. It produces easily read, quickly reachable graphs and diagrams which assists the superintendents and architects to categorize the extents of threat and highlight their vindication exertions (Gitikaand Ranjan 2016). Moreover, the flood vulnerability maps are intended to proliferate cognizance of the possibility of the drowning among the civic, indigenious specialists and other establishments by endorsing greater sentience of the risk of flooding.

The spatial variability of slope in the Bongaon sub-division is less, however, it plays an

Fig. 4.9 Reclassified geomorphological map of Bongaon sub-division

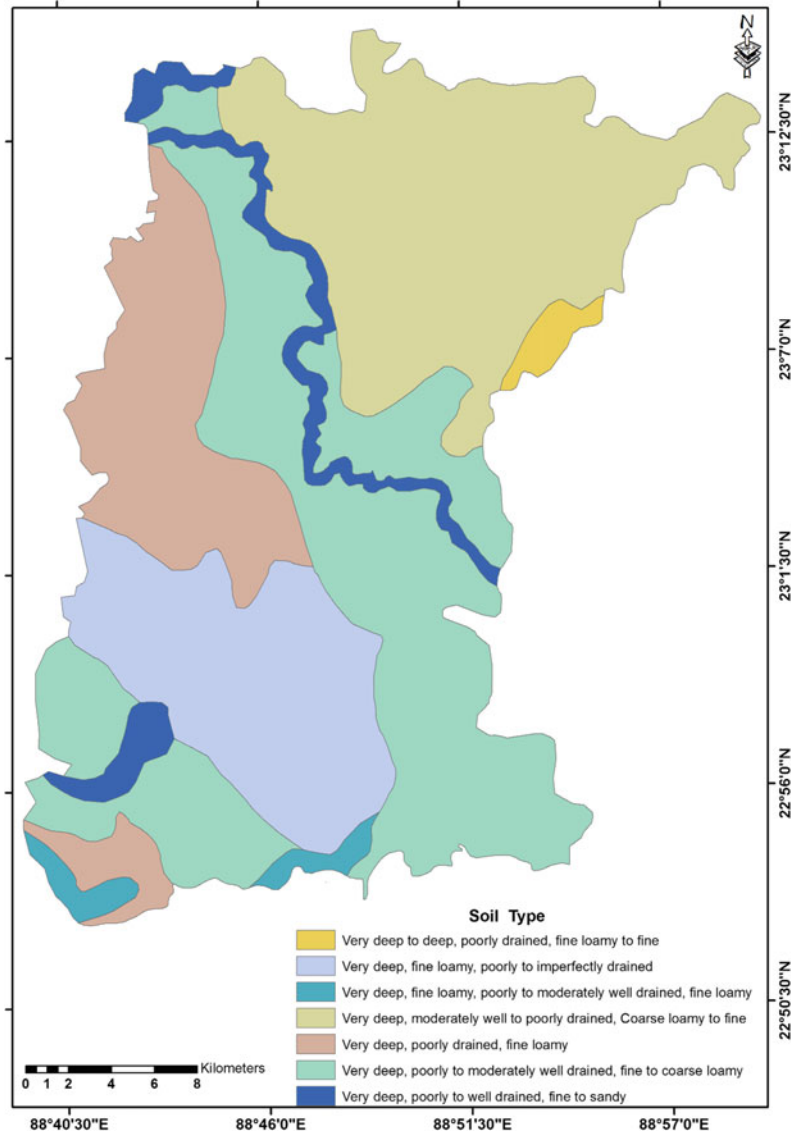


important role in hydrodynamic friction for flash flood simulation. The amount of water infiltration is reliant upon the peripheral aspects and soil properties, which differ based on the form of soil (Tejedor et al. 2013), types and texture (Nyarko 2002). Loamy soil water permeation is a factor that prerequisites to explain the processes of runoff, soil loss and aquifer recharge in addition to irrigation management and plant water convenience (Rimba et al. 2017). Population density is higher in lower elevated and flat areas and these areas have a very high liability to flash flooding. Additionally, descending areas should also be a focus as these are predisposed to descend during flood events (Cao et al. 2016). So,

the increase of sedimentation in river water caused loss of navigation which is also a great threat to the ecological balance of the river basin (Adel 2012).

The relationship between the occurrence of flooding and the classes of each conditioning factors was analysed. The elevation analysis outcomes designate that the lowest elevation was most persuasive on flooding. Moreover, results also showed that lower slopes along the eastern and northern parts of the sub-division inferred greater occurrence of flooding. Due to the lower slope, the speed of water flow has been lessened and upsurges the time for absorption and infiltration of water into the ground (Alemayehu

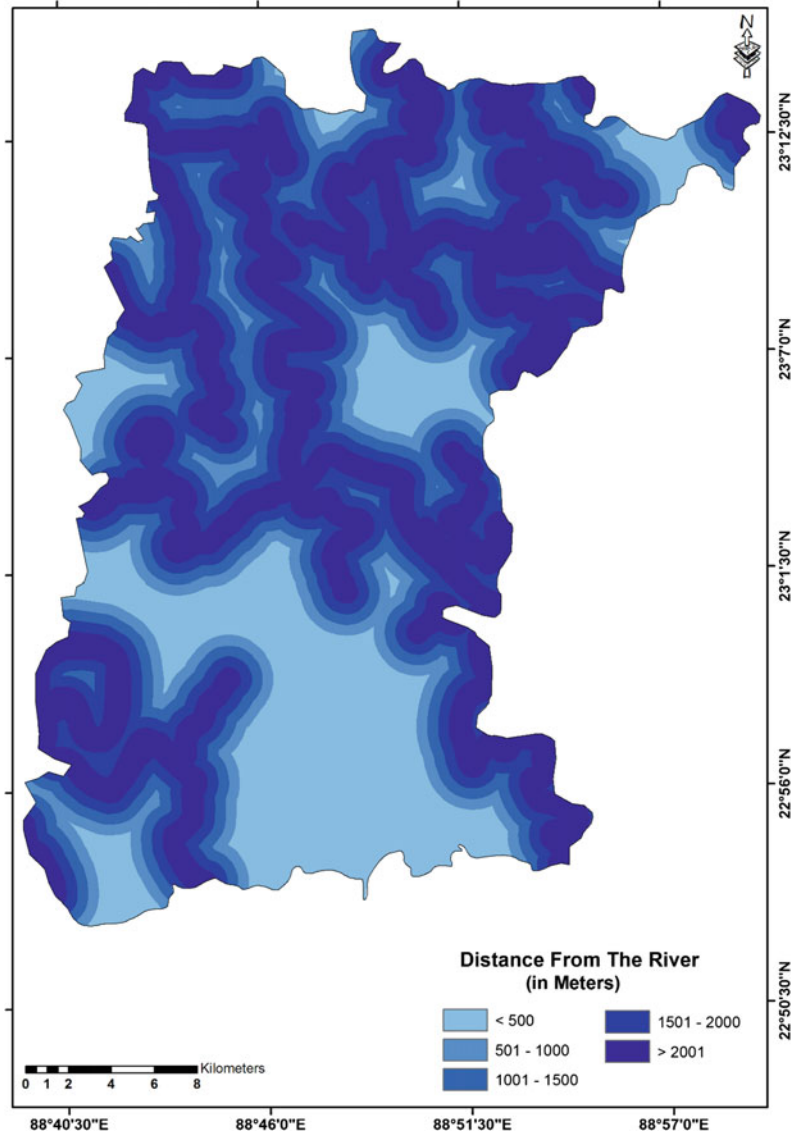
Fig. 4.10 Reclassified soil map of Bongaon sub-division



2007). The slope encourages the direction of the amount of surface runoff (Dai et al. 2002), and have a leading effect on the impact of rainfall to streamflow (Sawyer et al. 2004). According to Krumbein (1965), a flat surface is disposed to waterlogging; whereas, the steeper slope allows water to flow speedily. In the Bongaon sub-division, a high grade is consigned to less than 1° slope for the gentle gradient of the flood plain;

whereas, a little score is apportioned for the slope of more than 4.1°. Due to the heavier rainfall during flooding, river levels will increase and causing an overflow of water into areas closest to the riverbank. Road density is also a major factor of flood susceptibility mapping as it decreased the infiltration capacity of the terrain and is a source of runoff (Tehrany et al. 2017). The physical properties of the soil were considered to

Fig. 4.11 Reclassified distance from the river map of Bongaon sub-division



develop soil type factors. In the Bongaon sub-division, sandy soil has greater hydraulic conductivities than better-textured soils because of the great pore space between the soil elements. An earlier study also reported that the infiltration rate of the sandy soils is much higher than the clayey soil (Wondim 2016). Moreover, the areas situated adjacent to the main river channel and flow accumulation path are prone to

flood (Islam and Sado 2000). Mojaddadi et al. (2017) suggested that soil types have a straight influence on water stowage, penetrability and drainage.

LULC plays an important role in recognizing the sensitive regions prone to flooding. Areas covered with the vegetation compromise the levels of protecting appliances, creating land less lying to flooding and a negative relationship

Fig. 4.12 Reclassified road density map of Bongaon sub-division

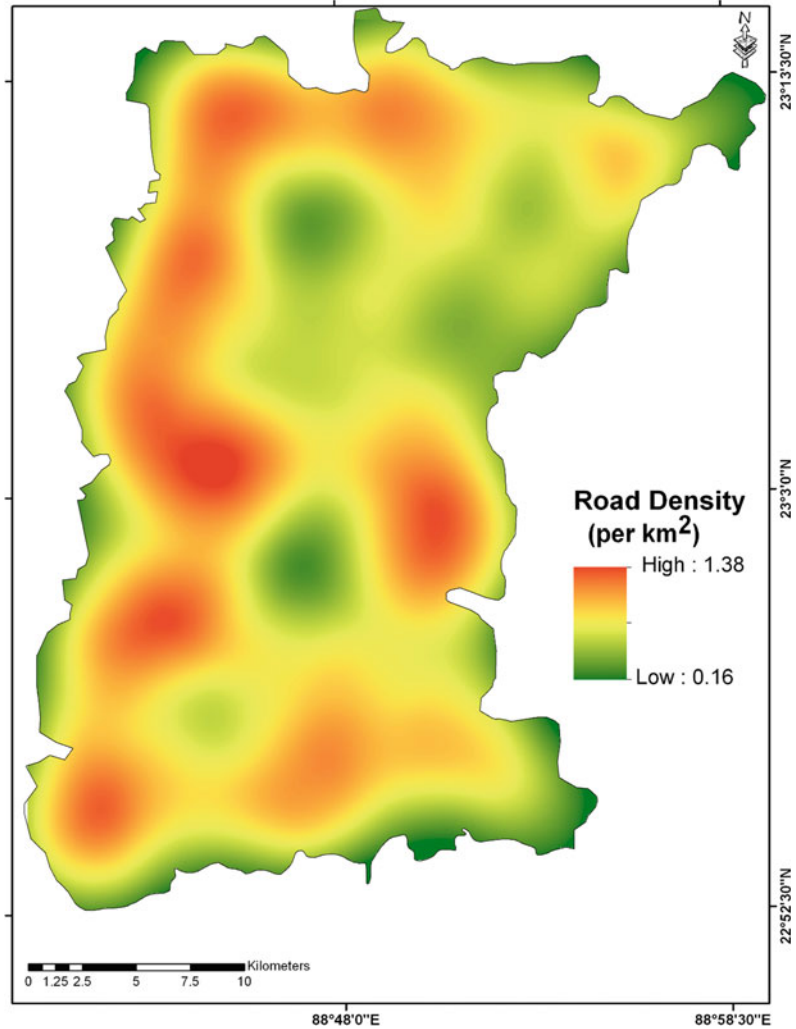


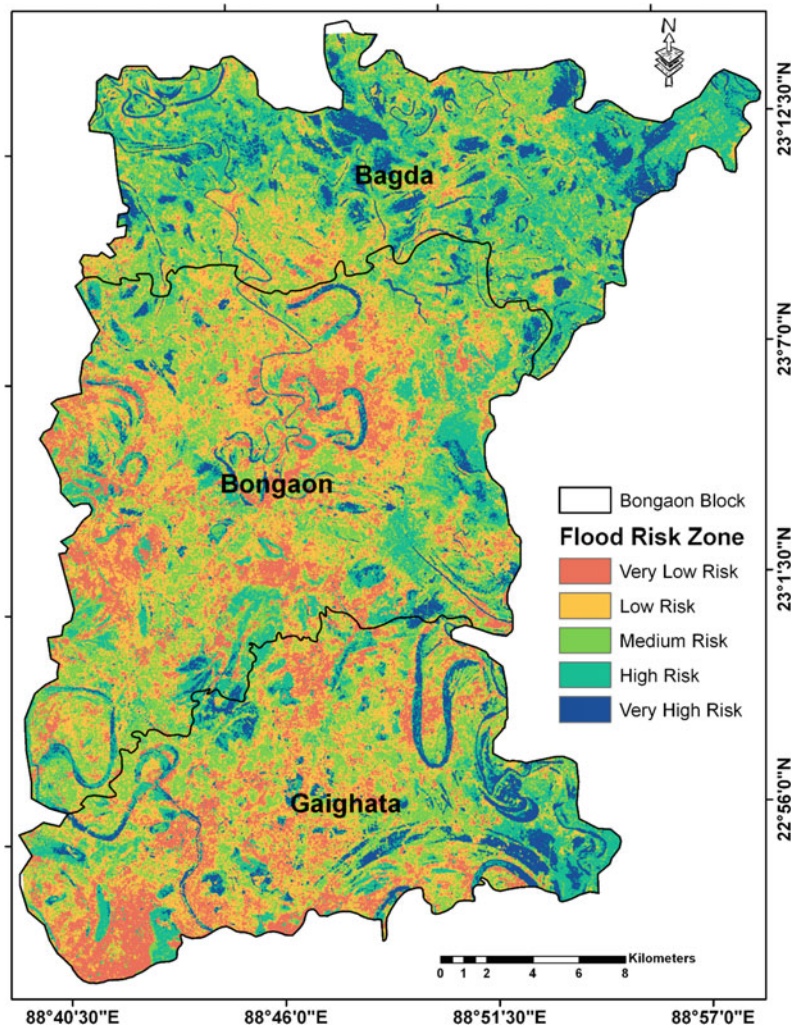
Table 4.3 Areal distribution of flood risk index map of the Bongaon sub-division

Flood risk index	Area (km ²)	Percent
Very low	119.55	14.33
Low	236.33	28.33
Medium	242.04	29.02
High	161.45	19.36
Very high	74.70	8.96

exists between a flood event and vegetation density (Al-Zahrani et al. 2016). LULC characteristics are a significant environment scheming the hazards as its solidities designate the appearance of the landscape and its geotechnical

chattels (Pareta 2004). The infringement of the areas are responsible for floods by human settlements and infrastructural development (Njoku et al. 2017). Results derived in this study also indicated that all NDVI classes of more than 0.24

Fig. 4.13 Flood risk map of Bongaon sub-division



have minimal impact on flood occurrence. The spatial extent of regional geomorphic features like new and old alluvial plain, meander scar, paleochannel, ox-bow lake, active river channel, abandoned river channel, natural depression, etc., are largely helpful in delineating flood susceptibility zone (Majumder et al. 2017).

However, the population density is very high in the sub-division due to its fertile alluvial plain (Paul and Chatterjee 2012; Jana et al. 2011). A huge chunk of settlements is observed in the sub-division and make some barriers (Saha 2015). Residents are using the riverbed as agricultural land for many decades. So, the increase of sedimentation in river water caused loss of

navigation, which is also a great threat to the ecological balance of the river basin (Adel 2012). Consequently, by the construction of a railway bridge at Majdia (Nadia District, West Bengal), a water barrier has been developed. The road is an important anthropogenic factor inducing flood hazards. Versini et al. (2010) stated that road network and traffic monitoring are a major cause for flood event managers. Consequently, by the construction of a railway bridge at Majdia (Nadia District, West Bengal), a water barrier has been developed. Valdiya (2004) reported that the obstructions caused by the construction of artificial infrastructures, considerably encumber the free flow of water.

Table 4.4 Assessment of the validation point of flood risk map of Bongaon Sub-division

Validation point (VP)	Ground observation/existing data base (2005–2016)	Flood risk index	Validation point (VP)	Ground observation/existing data base (2005–2016)	Flood risk index
VP1	2006–2009, 2011, 2013–2016	Very high	VP29	2007, 2008	Medium
VP2	2006–2009, 2011, 2013, 2015, 2016	Very high	VP30	2006–2009, 2015, 2016	High
VP3	Nil	Low	VP31	2007, 2011, 2015, 2016	High
VP4	2007, 2008, 2015, 2016	Very high	VP32	2007, 2008	Low
VP5	Nil	Very low	VP33	Nil	Very low
VP6	2007, 2008, 2015, 2016	High	VP34	Nil	Very low
VP7	2015	Low	VP35	Nil	Very low
VP8	2007, 2008	Low	VP36	2011, 2015, 2016	Medium
VP9	Nil	Very low	VP37	2006–2009, 2011, 2013–2016	Very high
VP10	2007, 2008	Medium	VP38	Nil	Very low
VP11	Nil	Very low	VP39	Nil	Low
VP12	2006–2009, 2015, 2016	Very high	VP40	Nil	Low
VP13	2006–2009, 2011, 2013, 2015, 2016	Medium	VP41	Nil	Very low
VP14	2007, 2008, 2015, 2016	High	VP42	2006 -2009, 2015, 2016	High
VP15	Nil	Very low	VP43	2006–2009, 2011, 2013–2016	Very high
VP16	2007, 2008, 2015	Medium	VP44	2006–2009, 2011, 2013–2016	Very high
VP17	2006–2009, 2011, 2013–2016	Very high	VP45	2006 -2009, 2015, 2016	Very high
VP18	2006–2009, 2011, 2013–2016	Very high	VP46	2007, 2008, 2015, 2016	Very high
VP19	2006–2009, 2011, 2013–2016	Very high	VP47	Nil	Very low
VP20	2006–2009, 2011, 2013–2016	Very high	VP48	Nil	Very low
VP21	2006–2009, 2011, 2013, 2015, 2016	Low	VP49	2007, 2008	Low
VP22	Nil	Very low	VP50	Nil	Very low
VP23	2007, 2008, 2015, 2016	Medium	VP51	2007, 2008	Low
VP24	Nil	Very low	VP52	2011, 2015, 2016	Medium
VP25	2007, 2008, 2015, 2016	High	VP53	Nil	Very low
VP26	2015	Low	VP54	2006 -2009, 2015, 2016	High
VP27	2007, 2008	Medium	VP55	2007, 2008, 2015, 2016	High
VP28	Nil	Very low			

4.6 Conclusion

The flood risk map of the Bongaon sub-division was generated through MCDA based on the integration of remotely sensed products and secondary datasets. The substantiation report advocates that remote sensing and GIS techniques are very influential approaches in flood risk exploration and planning. Eleven flood acclimatizing features were nominated and a flood inventory map was exploited to generate the flood dichotomous reliant layer. The MCDA method exposed in this research can be enriched further by counting these constraints, likewise rainfall, elevation, slope, distance from the river, road density, land use/land cover, etc. Hence, the extenuation actions can be accurately completed, and the controlling of flood menace is made easy. The generated flood risk map may be beneficial to proposers and creators for selecting an appropriate place for the forthcoming expansions and land use forecasting, and also to trace assemblies in the rickety regions. It could be of practice for specialists of the area for confirming security to the people of pretentious areas. This research also ropes the accompanying of the outmoded hydrological, with the contemporary geospatial tools, hence augmenting the assemblage, storage, analysis, management and demonstrating of flood data, along with being more cost, period and manpower competent.

References


- Adel MM (2012) Downstream ecocide from upstream water piracy. *Am J Environ Sci* 8(5):528–548
- Ajin RS, Krishnamurthy RR, Jayaprakash M, Vinod PG (2013) Floodhazard assessment of Vamanapuram River Basin, Kerala, India: An approach using Remote Sensing and GIS techniques. *Adv Appl Sci Res* 4(3):263–274
- Alemayehu Z (2007) Modeling of flood hazard management for forecasting and emergency response of 'Koka'rea within Awash River basin using remote sensing and GIS method. Unpublished Msc Thesis, AddisAbaba University, Ethiopia
- Alexakis DD, Grillakis MG, Koutroulis AG, Agapiou A, Themistocleous K, Tsani IK, Michaelides S, Pashiardis S, Demetriou C, Aristeidou K, Retalis A, Tymvios F, Hadjimitsis DG (2014) GIS and remote sensing techniques for the assessment of land use changes impact on flood hydrology: the case study of Yialias Basin in Cyprus. *Nat Hazards Earth Syst Sci* 14:413–426
- Al-Zahrani M, Al-Areeq A, Sharif HO (2016) Estimating urban flooding potential near the outlet of an arid catchment in Saudi Arabia. *Geomat Nat Hazards Risk* 1:1–17
- Basarudin Z, Adnan NA (2014) Impervious surface detection and mapping via digital remotely sensed techniques. In: *International Conference on Civil, Biological and Environmental Engineering (CBEE-2014)*, pp 27–28
- Cao C, Xu P, Wang Y, Chen J, Zheng L, Niu C (2016) Flash flood hazard susceptibility mapping using frequency ratio and statistical index methods in coalmine subsidence areas. *Sustainability* 8: 948. <https://doi.org/10.3390/su8090948>
- Chaturvedi R, Mishra SD (2015) Geomorphic features and flood susceptibility zones: A study for Allahabad district, Uttar Pradesh, India, using Remote Sensing and GIS technique. *Trans Inst Indian Geographers* 37(2):259–268
- Dai FC, Lee CF, Ngai YY (2002) Landslide risk assessment and management. An overview. *Eng Geol* 64:65–87
- Dandapat K, Panda GK (2018) A geographic information system-based approach of flood hazards modelling, Paschim Medinipur district, West Bengal, India. *Jamba (potchefstroom, South Africa)* 10(1):518. <https://doi.org/10.4102/jamba.v10i1.518>
- Dhruvesh KM, Praful MU, Aditya MV (2016) Flood hazard vulnerability mapping using remote sensing and GIS: a case study of Surat. *Res Rev: J Pure Appl Phys* 4(3):38–42
- Elsafi SH (2014) Artificial neural networks (ANNs) for flood forecasting at Dongola Station in the River Nile. Sudan. *Alexandria Eng J* 53(3):655–662
- Fustos I, Abarca-del-Rio R, Ávila A, Orrego R (2017) A simple logistic model to understand the occurrence of flood events into the Biobío River Basin in central Chile. *J Flood Risk Manag* 10(1):17–29
- Getahun YS, Gebre SL (2015) Flood hazard assessment and mapping of flood inundation area of the Awash river basin in Ethiopia using GIS and HEC-GeoRAS/HEC-RAS Model. *J Civil Environ Eng* 5:179. <https://doi.org/10.4172/2165-784X.1000179>
- Ghosh S, Mistri B (2015) Geographic concerns on flood climate and flood hydrology in monsoon-dominated Damodar river basin, Eastern India. *Geogr J Article ID* 486740, 16. <https://doi.org/10.1155/2015/486740>
- Gitika T, Ranjan S (2016) GIS-based flood hazard mapping: a case study in Krishnai river basin, India. *Res J Recent Sci* 5(ISC-2015):50–59
- Guhathakurta P, Menon PA (2011) Impact of climate change on extreme rainfall events and flood risk in India. *J Earth Syst Sci* 120(3):359–373
- Haq M, Akhtar M, Muhammad S, Paras S, Rahmatullah J (2012) Techniques of remote sensing and GIS for flood

- monitoring and damage assessment: a case study of Sindh province, Pakistan. *Egypt. J Remote Sens Space Sci* 15:135–141
- Islam M, Sado K (2000) Flood hazard map and land-development priority map developed using AVHRR data with geographical information system. *Hydrol Process* 14:605–620
- Ismail M, Saanyol IO (2013) Application of remote sensing (RS) and geographic information systems (GIS) in flood vulnerability mapping: case study of River Kaduna. *Int J Geomat Geosci* 3(3):618–627
- Jana A, Ghorai D, Bhunia GS, Pal DK (2011) Demographic pressure in transforming of land use/ land cover over four decades in Nadia District of West Bengal province India using multi-temporal Landsat data. *Niugini Agrisaiens* 3:59–74
- Kazakis N, Kougias I, Patsialis T (2015) Assessment of flood hazard areas at a regional scale using an index-based approach and analytical hierarchy process: application in Rhodope-Evros region, Greece. *Sci Total Environ* 538:555–563
- Krumbein WC, Graybill FA (1965) *An introduction to statistical models in Geology*. Mc Graw Hill, New York, p 475
- Lim J, Lee K (2018) Flood mapping using multi-source remotely sensed data and logistic regression in the heterogeneous mountainous regions in North Korea. *Remote Sens* 10(7):1036
- Majumder R, Ghosh DK, Mandal AC, Patra P, Bhunia GS (2017) An appraisal of geomorphic characteristics and flood susceptibility zone using remote sensing and GIS: a case study in Bongaon Subdivision, North 24 Parganas (West Bengal). *India. Int J Res Geogr (IJRG)* 3(4):32–40
- Mandal S, Mandal B (2015) Assessment and prediction of slope instability in the Lish River Basin of Eastern Darjiling Himalaya using RS and GIS. *Int Res J Earth Sci* 3(12):9–20
- Matori AN, Lawal DU, Yusof KW, Hashim MA, Balogun A (2014) Spatial analytic hierarchy process model for flood forecasting: an integrated approach. In: 7th IGRSM international remote sensing and GIS conference and exhibition, IOP conference series: earth and environmental science, vol 20, p 012029
- Mukherjee A (2006) Deeper groundwater flow and chemistry in the arsenic affected Western Bengal Basin, West Bengal, India. University of Kentucky Doctoral Dissertations, Paper 368. http://uknowledge.uky.edu/gradschool_diss/36
- Nandargi S, Dhar ON (2003) High frequency floods and their magnitudes in the Indian rivers. *J Geol Soc India* 61(1):90–96
- Nugraha AL, Awaluddin M, Sasmito B (2018) Modelling multi hazard mapping in Semarang city using GIS-fuzzy method. In: 2nd geoplanning-international conference on geomatics and planning. IOP conference series: earth and environmental science, vol 123, p 012002. <https://doi.org/10.1088/1755-1315/123/1/012002>
- Ouma YO, Tateishi R (2014) Urban flood vulnerability and risk mapping using integrated multi-parametric AHP and GIS: methodological overview and case study assessment. *Water* 6(6):1515–1545
- Pareta K (2004) Hydro-geomorphology of Sagar District (M.P.): a study through remote sensing technique. In: *Proceeding in XIX M. P. Young Scientist Congress*, Madhya Pradesh Council of Science & Technology (MAPCOST), Bhopal
- Patel DP, Srivastava PK (2013) Flood hazards mitigation analysis using remote sensing and GIS: correspondence with town planning scheme. *Water Resour Manag* 27:2353–2368
- Paul S, Chatterjee K (2012) Urbanisation and consistency measurement: a study on district of north 24 Parganas, West Bengal. *India. Arch Appl Sci Res* 4(5):2052–2067
- Pradhan B (2011) Use of GIS-based fuzzy logic relations and its cross application to produce landslide susceptibility maps in three test areas in Malaysia. *Environ Earth Sci* 63:329–349
- Rahmati O, Pourghasemi HR, Zeinivand H (2016) Flood susceptibility mapping using frequency ratio and weights-of-evidence models in the Golastan Province. *Iran. Geocarto Int* 31(1):42–70
- Limba AB, Setiawati MD, Sambah AB, Miura F (2017) Physical flood vulnerability mapping applying geospatial techniques in Okazaki City, Aichi Prefecture, Japan. *Urban Sci* 1:7. <https://doi.org/10.3390/urbansci1010007>
- Roy SK, Sarker SC (2016) Integration of remote sensing data and GIS tools for accurate mapping of flooded area of Kurigram, Bangladesh. *J Geogr Inf Syst* 8:184–192
- Saha M (2015) Human interference in the resource utilization of Bongaon sub-division in north 24 Parganas district of West Bengal. *RJSSM* 5(8):120–129
- Samanta S KC, Pal DK, Palsamanta B (2016) Flood risk analysis in lower part of Markham river based on multi-criteria decision approach (MCDA). *Hydrology* 3(29):1–13. <https://doi.org/10.3390/hydrology3030029>
- Sawyer CF, David RB (2004) Landslide aspect: a methodological approach to circular data for hazard analysis. In: *Proceedings of the Applied Geography Conference*, 27, St. Louis, M.O, pp 67–74
- Sengupta S (1966) Geological and geophysical studies in western part of Bengal Basin, India. *Bull Am Assoc Petrol Geol* 150:1001–1017
- Stefanidis S, Stathis D (2013) Assessment of flood hazard based on natural and anthropogenic factors using analytic hierarchy process (AHP). *Nat Hazards* 68:569–585
- Tehrany MS, Pradhan B, Mansor S, Ahmad N (2015) Flood susceptibility assessment using GIS-based support vector machine model with different kernel types. *Catena* 125:91–101
- Tehrany MS, Shabani F, Jebur MN, Hong H, Chen W, Xie X (2017) GIS-based spatial prediction of flood

- prone areas using standalone frequency ratio, logistic regression, weight of evidence and their ensemble techniques. *Geomat Natl Hazards Risk* 8(2):1538–1561. <https://doi.org/10.1080/19475705.2017.1362038>
- Tejedor M, Neris J, Jiménez C (2013) Soil properties controlling infiltration in volcanic soils (Tenerife, Spain). *Soil Sci Soc Am J* 77:202–212
- Valdiya KS (2004) Lessening the ravages of floods. In: *Geology, Environment and society*. Universities Press, India, pp 112–115
- Versini PA, Gaume E, Andrieu H (2010) Assessment of the susceptibility of roads to flooding based on geographical information—test in a flash flood prone area (the Gard region, France). *Nat Hazards Earth Syst Sci* 10:793–803
- WMO (World Meteorological Organization) (2013) Integrated flood management tools series flood mapping. Issue 20, November 2013. https://library.wmo.int/pmb_ged/ifmts_20.pdf
- Wondim YK (2016) Flood hazard and risk assessment using GIS and remote sensing in lower Awash sub-basin, Ethiopia. *J Environ Earth Sci* 6(9):69–86



Dynamics River Networks and Determination of the Flood Potential in Lower Brahmaputra Valley Using Geoinformatics

Asraful Alam , Rajat Kumar Paul, Amir Khan, Lakshminarayan Satpati, and Nilanjana Ghosal

Abstract

The river Brahmaputra majorly bears the characteristics of excessive flow, an enormous volume of sediment load, and frequent changes in channel morphology, rapid bed aggradations, bank line recession, and erosion as well. Floods are considered to be the most common natural disaster that affects the major regions of Northeast India. The objective of this paper is majorly to evaluate the flood vulnerability, which is primarily based on multi-criteria evaluation (MCE) conducted in the lower Brahmaputra River of Assam. The important contributing factors selected for flood hazard include Drainage Density, Flow Accumulation, Slope and Elevation, LULC, Micro-Watershed, Rainfall Distribution, Population Density, and Proximity to River.

Remote Sensing (RS) and Geographical Information System (GIS) have been used to derive, integrate, and analyze the geographic layers of each of the themes. Four classes of flood hazard vulnerability—ranging as very high, high, moderate, and low—have been categorized on the basis of the estimation. It is noted that more than about 50% of the total area of the watershed is under acute risk of flood and some places of the study area, namely Barpeta, Lakhipur, Agia, Bongaigaon, and Joytigaon are highly affected regions. On the other hand, Ujanpara, Sarbhog, and Dudhnoi areas are moderately affected by the flood during flood time.

Keywords

Flood intensity · Brahmaputra river · LULC and AHP

A. Alam (✉)
Department of Geography, Serampore Girls' College, University of Calcutta, Serampore, West Bengal, India

R. K. Paul · A. Khan
Department of Geography, University of Calcutta, Kolkata, West Bengal, India

L. Satpati
Department of Geography and HRDC, University of Calcutta, Kolkata, West Bengal, India

N. Ghosal
CAD, Jadavpur University, Kolkata, West Bengal, India

5.1 Introduction

Assam for ages has been a riverine civilization (Nayak et al. 2016). The river Brahmaputra has always acted as the lifeline for Northeastern India. The Brahmaputra stretches up to 2880 km. running through China, India, and Bangladesh. It is to be noted that in Upper Assam, near Dibrugarh, the river is 16 km wide whereas in lower Assam, at Pandu, a river port near Guwahati, the

river is 1.2 km wide. However, in the immediate downstream, the mighty Brahmaputra is nearly 18 km wide (Thakkar et al. 2013). The River majorly bears the characteristics of excessive flow, enormous volume of sediment load, frequent changes in channel morphology, rapid bed aggradations, bank line recession, and erosion as well. It also consists of braided channels in its course majorly in the alluvial plains of Assam. The lateral changes in channels cause extreme erosion along the banks leading to a considerable loss of good fertile land each year (Sharma et al. 2012). With its extensive network of rivers, Assam is much prone to natural disasters for which a negative impact gets created on the state's overall development (Government of Assam 2021).

Floods are considered to be the most common natural disaster that affects major regions of Northeast India. Flood as a natural catastrophe has caused lots of economic, social, and human changes and in general destroys the infrastructure of the affected areas (Nath et al. 2020). The Brahmaputra valley is deluged by the floods of the Brahmaputra River and its tributaries. It is to be remembered that the highly braided Brahmaputra River is both a snow-fed and rain-fed river and as a result, is perennial in nature. As a consequence, Brahmaputra experiences the highest water levels and strongest flows during the times of summer monsoon season (Sharma et al. 2016). Experts are also in the opinion that the rise of anthropogenic factors in recent times has resulted in catastrophic floods in the Northeastern region. Occurrence of floods in the Brahmaputra River basin are an annual event (Hazarika et al. 2016). Being majorly prone to flash floods, some of the worst flash floods have occurred in the Brahmaputra river basin in the new millennium (Thakkar et al. 2013). Northeast India is tectonically active and rivers are avulsive in nature, as evidenced by the presence of many palaeochannels (Hazarika et al. 2016). The Brahmaputra and Barak Rivers with more than 50 numbers of tributaries feeding them, causes severe flood devastation in the monsoon period each year (Government of Assam 2021). Flood hazard encompasses many particulars that mainly

include structural and erosional damages, contamination of water, damages of roads and houses, disruption of socio-economic activities, losses of life and property, etc. (Nath et al. 2020).

During the post-independence period of India, Assam faced severe floods in the years 1954, 1962, 1972, 1977, 1984, 1988, 1998, 2002, 2004, and 2012, respectively. Almost every year, three to four waves of flood wrecked the flood-prone areas of Assam. Average annual loss due to flood in Assam can be estimated up to Rs. 200.00 Crores. Particularly in 1998, the loss suffered in the state was about Rs. 500.00 Crores and during the year 2004 it was about Rs. 771.00 Crores. In the years 2004 and 2014, the south bank tributaries of Brahmaputra in lower Assam experienced flash floods of high magnitude due to cloud bursts. These flash floods caused large-scale destruction in vast areas including losses of human lives (Government of Assam 2021).

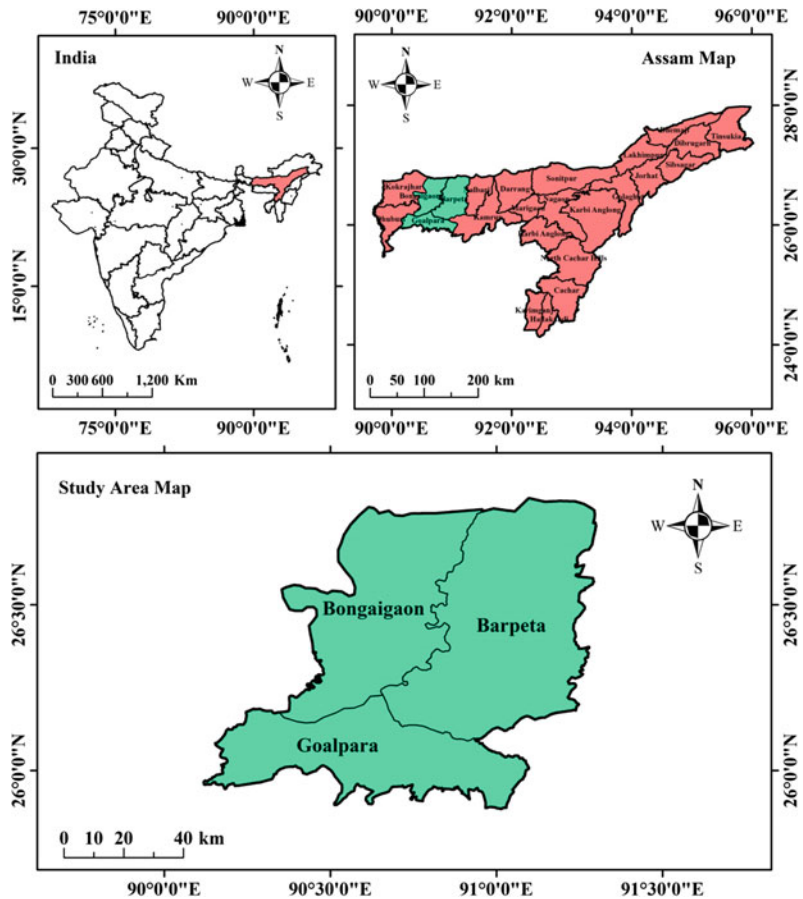
Therefore, to reduce or control the damages it is necessary to have proper and special planning for the flood-affected areas and the very first step to control flood is to identify the flooding areas and flood risk zone so as to reduce flood to its minimal level. In the present era, modern techniques and tools such as Remote Sensing and GIS are used widely to investigate hazardous areas affected by extreme events (Nath 2020). These software along with other datasets have best immense possibilities for identification, monitoring, and assessment of flood disaster and assists in interpreting images in the shortest period of time (Haq et al. 2012). Satellite observations also facilitate regular monitoring of the extent of floods and mapping of flood risk zones (Irimescu et al. 2009). With the application of Remote Sensing and GIS, analysts also get fast economic solutions to recognize and classify hazardous risk areas. These techniques are successfully used to envisage the extent of flooding and also study the flood maps in order to produce flood damage maps as well as flood risk maps (Nath 2020).

It is to be noted that the Decision Support Centre (DSC) of National Remote Sensing Centre (NRSC), ISRO has prepared Flood Hazard Atlas for Assam State using more than 90

satellite datasets acquired from Indian Remote Sensing (IRS) and Radarsat satellites during flood season over Assam region for the past 10 years, i.e., 1998–2007 (Sharma et al. 2012). Hence, this paper mainly focuses on the analysis of river networks to analyze the flood density majorly in the lower Brahmaputra plains of Assam with the application of GIS and Remote Sensing techniques, to derive the flood hazard risk zones and also determine reallocation of facilities as well as strategies for future emergency necessities (Ajin et al. 2013). The major objective of the study has been taken to analyze the network flow of rivers in the lower plains of Assam and to determine the intensity and vulnerability of floods in the lower Brahmaputra plains.

Study Area: The three districts of the lower Brahmaputra valley of Assam have been selected as a study area, these three districts are Goalpara, Bongaigaon, and Barpeta (Fig. 5.1). The selected study area is geographically located in between latitude 25°53' and 26°54' North and longitudes 89°00' to 91°30' East. The tropical monsoon climate of the study area provides two distinct features—summer and winter. It rains from June to September after the summer season from March to May. This is followed by the winter season from October to February. The study area covers an area of 5562 sq km., the western and eastern Garo Hills districts of the state of Meghalaya in the south and Kamrup and Nalbari districts in the east, Kokrajhar and Dhubri districts in the west, and Bhutan in the north.

Fig. 5.1 Study area

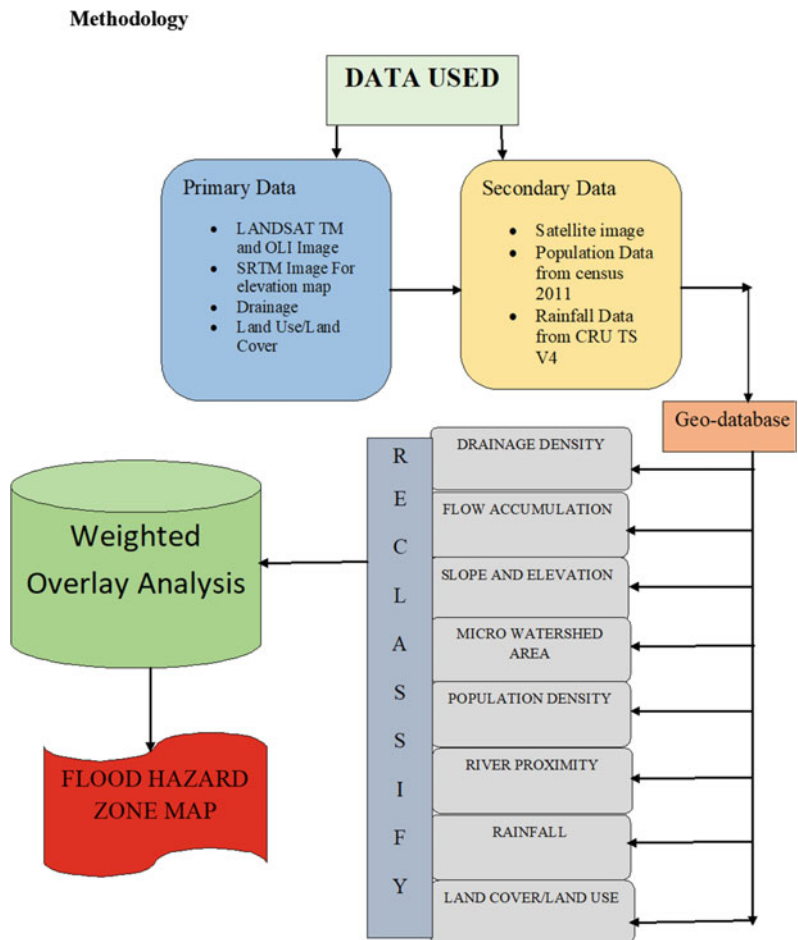


5.2 Database and Methods

The present research study has been executed through the application of GIS and Remote Sensing. The relevant maps are created using ArcGIS 10.5 and ERDAS Imagine 13.0.2 software tools. Satellite imagery is used as the primary data source. The Land use/Land cover map for proper analysis is extracted from Thematic Mapper (TM) of LANDSAT-5 and OLI (Operational Land Imager) of LANDSAT-8 and then is classified with the help of ERDAS 13.0.2 software. The DEM for analysis of slope and elevation map has been taken from Shuttle Radar Topography Mission (SRTM) digital elevation of 30 m. The rainfall data for the preparation of rainfall distribution map is collected from

CRU TS V4 (Climatic Research Unit gridded Time Series) is a widely used climate dataset on a 0.5° latitude by 0.2° longitude grid for different stations (Harris et al. 2020), and population density was calculated from village directory, census data of 2011. The present study is conducted using multi-criteria evaluation methods (Fig. 5.2). A personal geodatabase has been set in Arc Catalog. A dataset was generated for the study area with the spatial reference of GCS_WGS_1984. The thematic maps of drainage density, flow accumulation, micro-watershed area map, population density map, slope elevation map, and map of proximity have been prepared with the help of ArcGIS tools. The data layers have been integrated into the GIS environment by Weighted Overlay Analysis

Fig. 5.2 Flowchart of the methodology



using Spatial Analyst Tools from Arc Toolbox. To develop a sound base of the problem, relevant secondary sources like books, journals, magazines, newspapers, articles, maps, satellite images, etc., have also been used.

5.3 Satellite Image Processing

Satellite image processing plays an important role in research and development. It consists of images of the earth and satellites taken by means of artificial satellites. The photographs are taken in The satellite image, i.e., LANDSAT TM of the lower plains of Assam has been taken from Earth Explorer. The satellite image processing technique (Fig. 5.3) has majorly gone under the following processes (Asokan et al. 2020):

In this work, the satellite imageries are brought to a common projection of Universal Transverse Mercator (UTM) with zone-46 N, in World Geodetic System (WGS)-84 ellipsoid and WGS-84 datum. Radiometric corrections in the form of noise removal, haze removal, and histogram equalization for all satellite images have

been carried out. The raster images are brought to an equivalent resolution of 30 m along with Landsat TM images for removal of any resolution issues (Sect. 5.3.1). Delineation of rivers and drainage confluence has been executed by using Multispectral Landsat TM images. Information regarding elevation and direction of the slope has been erected out from DEM. The DEM has been extracted from SRTM of 30 m of elevation. The raw DEM is processed to undo the basic errors by generating contours. After that, manually the missing values have been corrected. The vector layers are produced after weighing the buffers are converted to raster layers with the help of a cell resolution of 30 m. A similar cell resolution actually eradicates the possibility of derangement among different raster data. Thereby, this helps out in reducing errors. In order to calculate approximately the significance of each criterion for the model of aggregation, we have applied the Analytic Hierarchy Process (AHP) to take out standard weights. The AHP method is well recognized as a multi-criteria technique (Saini et al. 2015; Alam et al. 2021) which is suitable for GIS-based “rank sum” weighted overlay analysis to find out the area or region from where flood effect is high to low. Initially, seven spatial indicators have been identified and given weightage and categorized into different layers. All output vector layer maps have been reclassified and converted into raster grids. The weightage is given on the basis of field knowledge and experience of each parameter and their sub-categories (Table 5.1) Multi-criteria analysis using AHP has been applied for the prioritization of flood-affected areas. So as to set a hazard score for each factor, the rank sum method (Janssen and Van Herwijnen 1994) has been used, where “ w_j ” is the normalized weight for the “ j th” criterion, “ n ” is the number of criteria ($j = 1, 2, \dots, n$) under consideration, and “ r_j ” is the rank position of the criterion. Each criterion is weighted as “ $n - r_j + 1$ ” and then normalized by the sum of weights, that is, $\sum (n - r_j + 1)$ (Saini and Kaushik 2012).

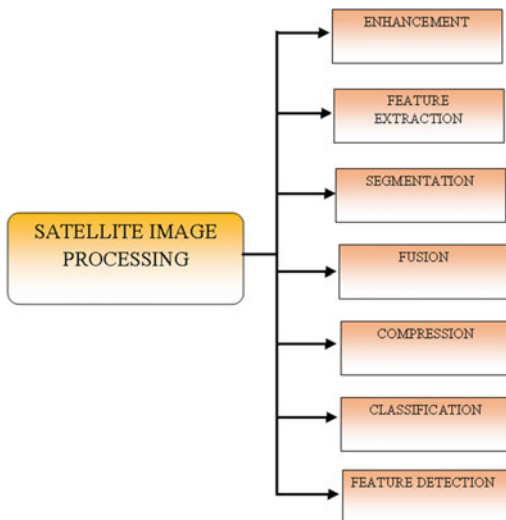


Fig. 5.3 Satellite image processing

Table 5.1 Evaluation criteria of flood hazard assessment and analytic hierarchy process weights

Sl no.	Factors	Descriptive level	Value	Weightage	%
1	Drainage density	High		7	25
		Medium		5	
		Low		3	
		Very low		2	
2	Flow accumulation	High		5	11
		Medium		4	
		Low		3	
		Very low		2	
3	Slope and elevation	High		1	21
		Medium		2	
		Low		4	
		Very low		6	
4	Lulc map	River		6	6
		Dense forest		2	
		Agricultural land		3	
		Settlement		4	
		Open forest		3	
5	Micro-watershed	Large		3	7
		Medium		4	
		Low		5	
6	Rainfall distribution	High	>2190 mm	5	14
		Medium	2140–2190 mm	3	
		Low	<2140 mm	2	
7	Population density	High		3	4
		Medium		2	
		Low		1	
8	Proximity to river	0 to 1 km		4	12
		1 to 2 km		2	
		2 to 3 km		2	
		3 to 4 km		1	
		4 to 5 km		1	
Total				100	100

5.3.1 List of Satellite Data Used in the Present Study

Satellite	Acquisition date	Path/Row/Tile Name	Sensor/Payload	No. of Bands	Spatial Resolution	Projection/Spheroid / Datum	Source/Organisation
Landsat 8	27-12-2020	137/042	OLI-TIRS	11	30 × 30 m	UTM-WGS84-46	NASA/USGS, U.S
Cartosat-1 DEM	29-04-2015	G46N	PAN-AFT, PAN-FORE	-	2.5 × 2.5 m	GCS, WGS-1984	ISRO/ NRSC, India
	29-04-2015	G46M					
	29-04-2015	G46G					
	29-04-2015	G46H					

5.4 Results and Discussion

5.4.1 Assisting Criteria Weights

Drainage density is defined as the total length of channels per unit area. It actually describes the spacing and dispersal of the drainage ways in a catchment. It can be said that the ratio which defines drainage density also represents the quantity of rivers in the catchment that is required to drain the basin (Dragicevic and Maibach 2018). Drainage density map can be derived from the drainage map. The drainage map is overlaid on a watershed map to figure out the ratio of the total length of the watershed to the total area of the watershed. After the completion of this procedure, it is categorized accordingly (Fig. 5.4). The drainage density of the watershed is calculated by using the following formula i.e., $Dd = L/A$; where, Dd = drainage density of watershed, L = total length of the drainage channel in the watershed (km), A = total area of the watershed (km^2). It is to be noted that drainage density is an inverse function of infiltration. According to the given map, major areas of the lower Brahmaputra plains of Assam experience low drainage density (<25) which indicates that the rate of runoff is low for which these areas are always prone to floods. Only a few pockets in this area have high drainage density (>75) and experiences favorable runoff

rates. Thereby, there are low flood chances in these regions (Ajin et al. 2013).

A drainage accumulation function is defined as an operator that gives the drainage direction (Tarboton et al. 1991). The highly braided Brahmaputra River is both a snow-fed and rain-fed river. Hence, the river is perennial in nature. It is also to be noted that the river experiences the

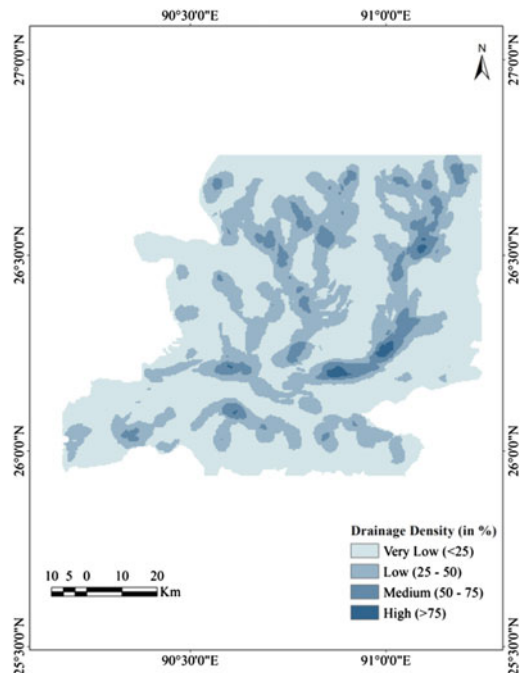


Fig. 5.4 Drainage density map

highest water levels and strongest flows during the summer monsoon season. From the above map, it can be studied that the lower Brahmaputra plains of Assam comprises very little accumulation flow. Consequently, high intensity of rainfall and peaking of tributaries at the confluence takes place which in due course give rise to high flood levels of Brahmaputra (Fig. 5.5). The flooding of tributaries during the rains aggravates the overall flood situation in the lower plains (Sharma et al. 2016).

Micro-watersheds with larger drainage areas require runoff of longer duration for consequential rise in water levels to become a flood. Thereby, it can be interpreted that micro-watersheds with the smaller area are greatly affected by floods (Fig. 5.6). From the given map, it can be interpreted that the majority of the Lower Assam plains comprises large (>6000 Sq. km) and medium sized (>1000 Sq. km) micro-watershed areas. This depicts that these zones are likely to be less affected by floods. However, some lower areas of our study of interest

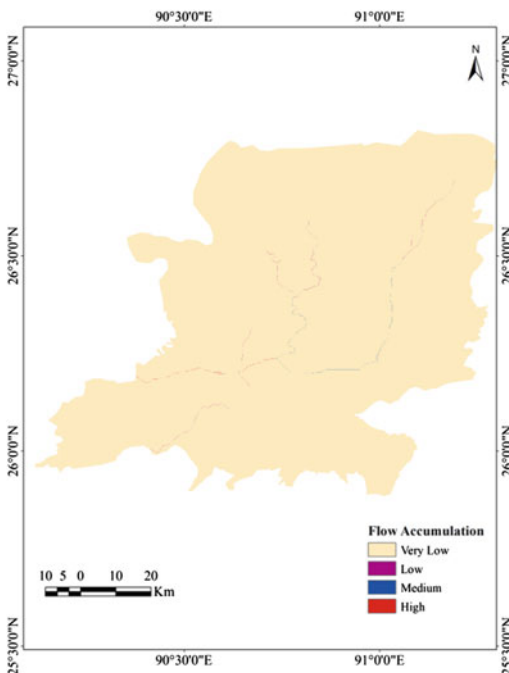


Fig. 5.5 Flow accumulation map

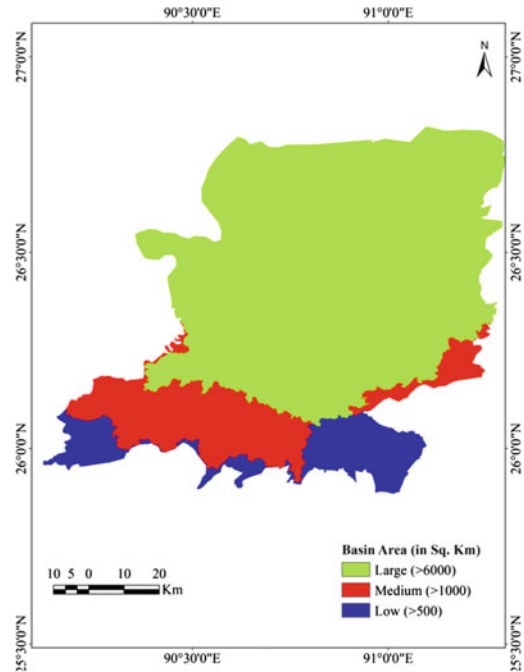


Fig. 5.6 Micro-watershed map

comprise small-sized basin areas (>500) from which it can be deciphered that these zones are largely affected by floods (Ajin et al. 2013).

Population is one of the most basic indices. Population density is normally obtained by dividing population and land area (Fujimoto et al. 2017). From the given map, it can be studied that in the lower Brahmaputra plains of Assam, high population density is observed in Borpeta, i.e., > 700 persons/Sq. km whereas the moderate and low density of population can be studied in Bongaigaon (600–700 persons/Sq. km) and Goalpara (600 persons/Sq. km), respectively (Fig. 5.7). The variation in density of population mainly assists in determining the physical condition of a particular region (Nath 2020).

Slope and elevation play a pivotal role in determining the steadiness of a terrain. The slope influences the direction and amount of surface runoff or subsurface drainage reaching a particular zone. The slope has a dominant effect on the contribution of rainfall to streamflow. Determining slope and level of elevation majorly

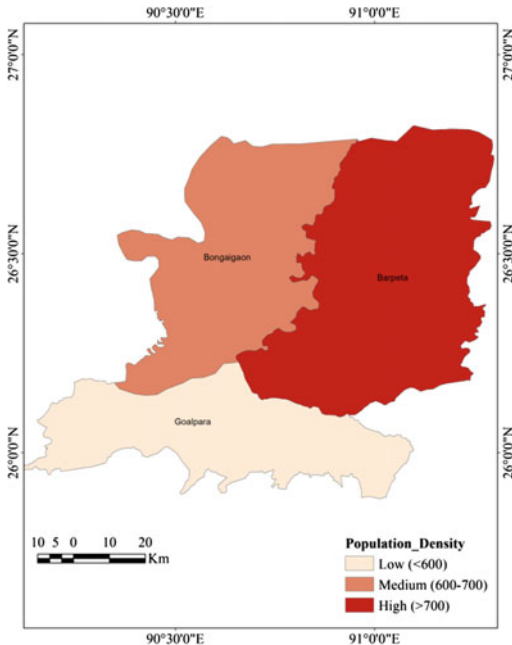


Fig. 5.7 Population density map

controls the duration of overland flow, infiltration and subsurface flow as well (Fig. 5.8). It has to be remembered that slope angles majorly define the form of the slope and its relationship with the lithology, structure, type of soil, and drainage (Ajin et al. 2013). In the above-given map, the slope angle and level of elevation have been analyzed with the application of DEM. From the given map, it can be studied that major parts of the lower Brahmaputra plains bear a medium level of slope elevation, i.e., 5° to 10° , which depicts that area of our study bears almost flat terrains and thus faces the problem of waterlogging during times of heavy rainfall while a few patches consist of slope elevation of $> 15^{\circ}$. This indicates the rate of surface runoff increases in these areas during times of rainfall as no longer water can infiltrate in soil rapidly and as a result overland flow begins (Balasubramaniam, A. 2017).

Proximity to the river is one of the important factors that help an individual in shaping flood risks of an area (Nath et al. 2020). For the analysis of the proximity of the river, various distances from the river are determined taking the

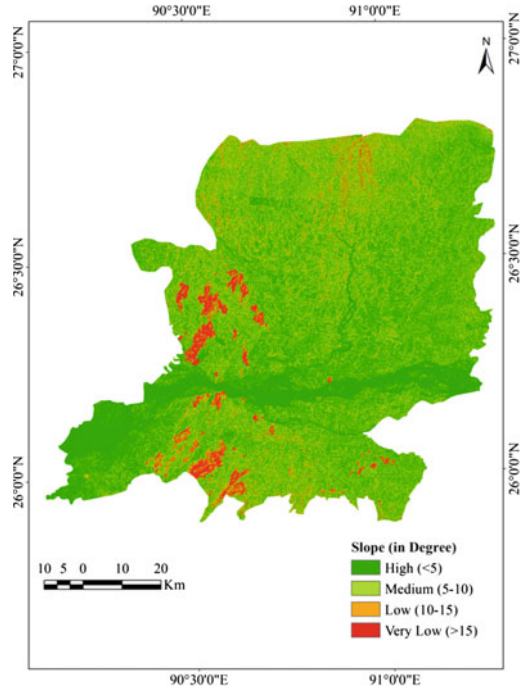


Fig. 5.8 Slope and elevation map

buffer as 0 km, 1 km, 2 km, 3 km, 4 km, and 5 km, respectively. From the above map, it can be studied that places belonging to the lower Brahmaputra plains are in a close proximity to the river i.e., 0 to 2 km are more prone to flood risks than places that are comparatively at a farther distance (4–5 km) from the river (Fig. 5.10).

Assam is battling a flood of epic proportions (Chaturvedi et al. 2020). Falling in the category of natural disasters, floods cannot be prevented. However, human activities are also contributing to a rise in untoward impacts of extreme flood events. The scale and frequency of floods are anticipated to rise due to climate change as well for which a number of local residents and economic assets located in flood-risk zones are possible to increase (Ajin et al. 2013). In this study, the flood hazard zone map has been prepared by using ArcGIS and ERDAS Imagine software tools. From the above map, it can be interpreted that major areas of the Lower Brahmaputra plains of Assam belongs to moderate and low risk zones. There are few zones that are likely to experience very low risks during

floods while some areas are much prone to high risks during the time floods in the lower Assam plains.

Flood occurs most commonly from heavy rainfall. It also happens when natural water-courses do not have the capability of holding excess water. The level of water in rivers or lakes rises due to the occurrence of heavy rain (Ajin et al. 2013). The study area of our interest experiences a tropical monsoon type of climate with high levels of humidity and heavy rainfall. Here, the area receives rains from the southwest monsoons that begin from the third week of June and continue up to the middle of September (Rahman et al. 2021). According to the above-given map, the highest amount of rainfall (>2,190 mm) can be seen in Bongaigaon, Patkijuli, Goalpara, and Lakhimpur while amount of rainfall is found to be less (<2,140 mm) at Barpetta in Assam (Fig. 5.11). When the level of water rises above the river banks or dams, the water starts to overflow causing floods. This flood water causes huge destruction and great wreckage in the areas where it flows (Ajin et al. 2013).

5.4.2 Dynamics in Land Use/Land Cover

Changes in land cover are motored by land use that can be majorly classed into two types: modification and conversion (Fig. 5.9). Modification can be defined as a change of condition within a cover type (Rajat et al. 2021). For example, unmanaged forest was modified into a forest by selective cutting. Conversion on the other hand can be defined as a change from one cover type to another. For example, deforestation to create settlement areas (Bishaw 2012). The most important changes observed in the lower Brahmaputra plains in recent years are widespread fragmentation and rapid degradation of forest areas leading to the development of settlements and agricultural lands. These changes in the backdrop have given rise to the occurrence of annual floods in these areas (Sinha et al. 2012).

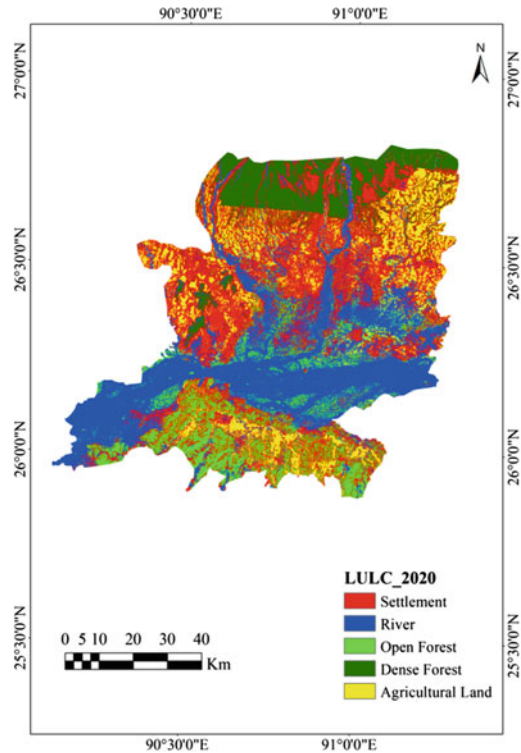


Fig. 5.9 Land use and land cover map

5.4.3 Flood Hazard

The primary concern of this area is land use/land cover. Land use/land cover not only reflects the current use of the land pattern and type of its use but also the necessity of its use in relation to the living population and the existing development (Ajin et al. 2013). The land use/land cover map of the study area is prepared from the Landsat TM image. A supervised classification method has been applied by using ERDAS Imagine 13.0.2 software and later analyzed using ArcGIS spatial analyst tool. The land use/land cover has been classified mainly in five categories, i.e., Settlement, river, open forest, dense forest, and agricultural land, respectively. From the given map, it can be interpreted that much of the area in the lower Brahmaputra plains is enveloped with agricultural land and settlements. A small part in the upper region is covered with dense forests while there are small patches in the

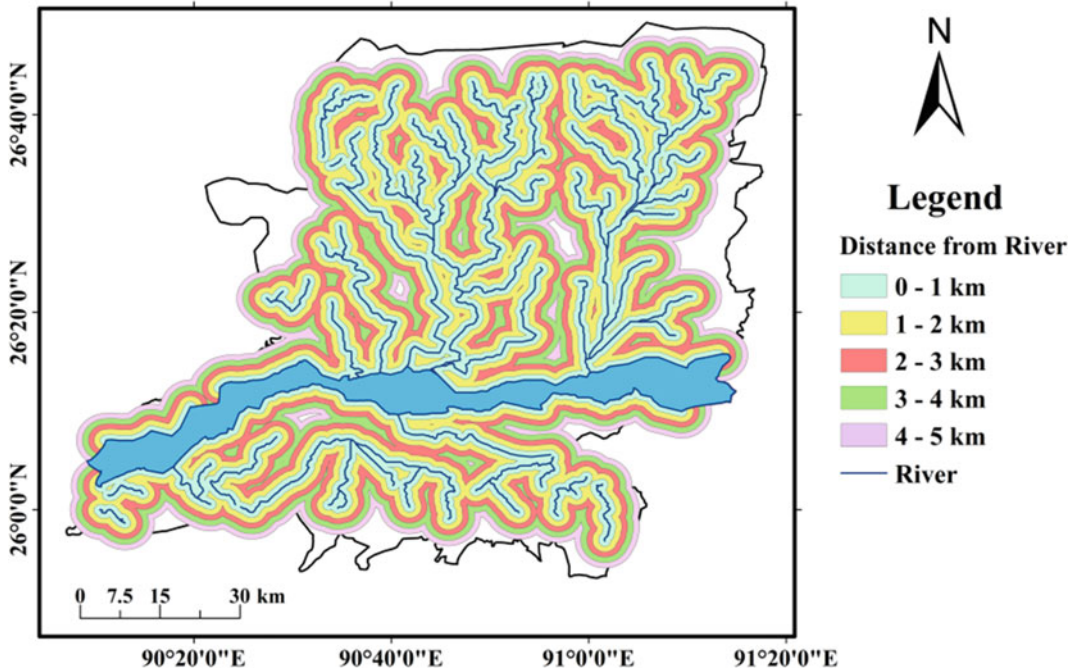


Fig. 5.10 Proximity to river

lower area of the plains covered with open forests. The mighty Brahmaputra River flows in this region and during times of heavy rainfall runoff is expected here (Fig. 5.11). The impermeable surfaces such as concretes are also expected to absorb almost no water at all. For the past years, as there has been a degradation of forest areas, leading to expansion of agricultural lands and settlements, high risks during the occurrence of annual floods have also increased in the backdrop simultaneously (Sinha et al. 2012).

Assam is battling floods of epic proportions (Chaturvedi 2020). From the above analysis, it can be said that major areas of the lower Brahmaputra Plains belong to moderate and low risks of floods. However, our study also indicates that most areas experience low drainage density for which the runoff rate is also found to be less and as a result flood occurs. The flooding of river tributaries during the times of rain actually aggravates the situation more. The places that receive maximum amount of rainfall in the lower plains are Bongaigaon, Patkijuli, Goalpara, and

Lakhimpur, respectively. The overflowing of water creates a huge havoc in whichever areas it flows (Ajin et al. 2013). As the areas almost bear a flat terrain, hence they also face problems of waterlogging during times of heavy rainfall. In further analysis with the help of land use and land cover map, it is furthermore studied that degradation of forest lands and encroachment of human settlements have also created high risks in the areas during the occurrence of the annual floods (Fig. 5.12). The impermeable surfaces such as the concrete are expected to absorb no rainwater. Hence, the use of technological tools such as remote sensing and GIS is required as these tools help in identifying the flood-prone areas in a very short time and also assist in taking appropriate strategies for accurate developmental works. In this study area some places like Barpeta, Lakhimpur, Agia, Bongaigaon, and Jyoti-gaon are highly affected regions. On the other hand, Ujanpara, Sarbhog, and Dudhnoi areas are moderately affected by the flood during flood time (Fig. 5.12).

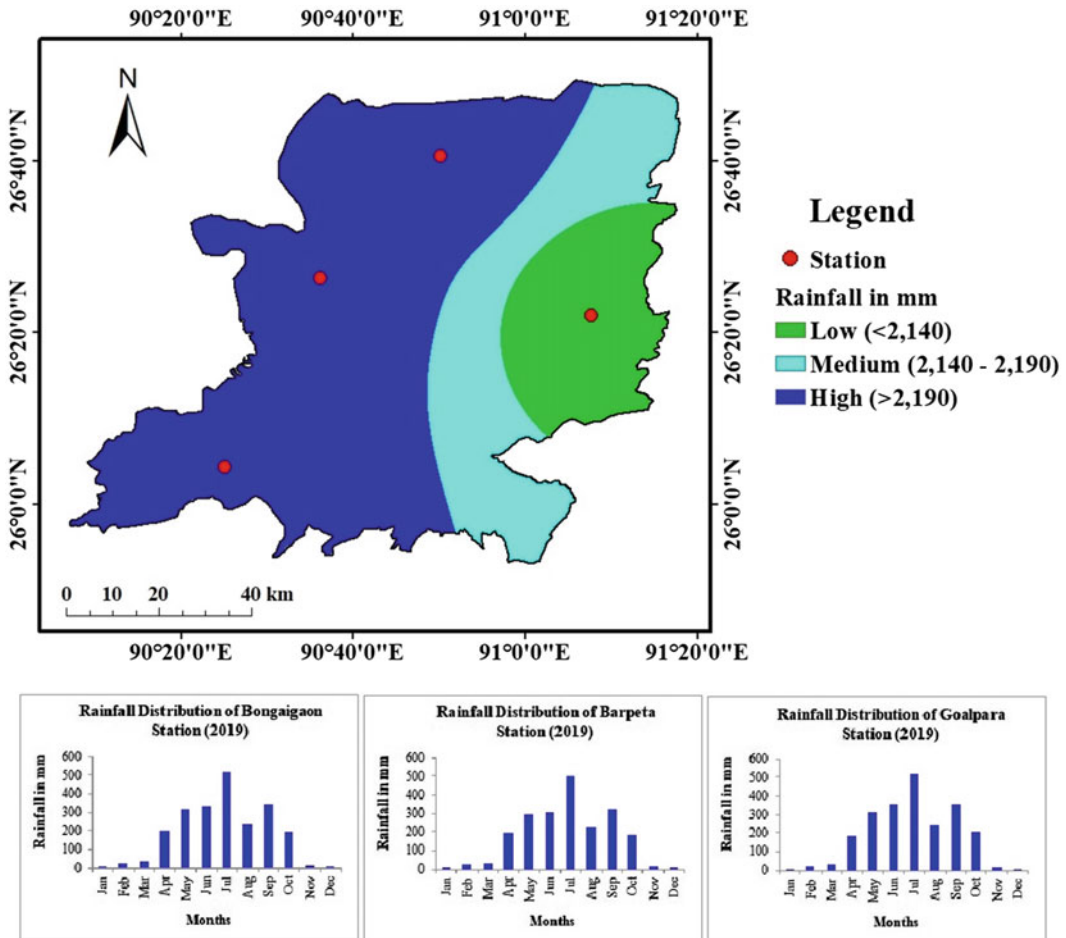


Fig. 5.11 Rainfall distribution map

5.5 Conclusion

GIS and remote sensing techniques are valuable tools that are used in various fields. These techniques are widely being used for mapping, modeling, and analysis of a variety of applications in disaster management at different levels and scales. Floods are natural phenomena that cannot be eradicated and in recent years, anthropogenic activities are contributing more to the surge in the likelihood and unfavorable impacts of extreme flood events (Ajin et al. 2013). In the lower Brahmaputra plains of Assam, its location and other physical and

climatic elements are responsible for the genesis of these natural hazards. People in these areas are adjusting to the incident of floods to a certain extent by accepting the losses (Nath et al. 2020). Along with the natural factors, man-made causes such as habitation, deforestation, population growth in catchment areas have also contributed towards higher flood risks. To curb the flood-related hazards, the Brahmaputra Board has suggested building dams and reservoirs (Agarwal 2019). Even to attain sustainability in the socioeconomic environment of the area, the government, NGOs, and communities as well are taking some preventive measures. The present study shows a simple and cost-effective way of

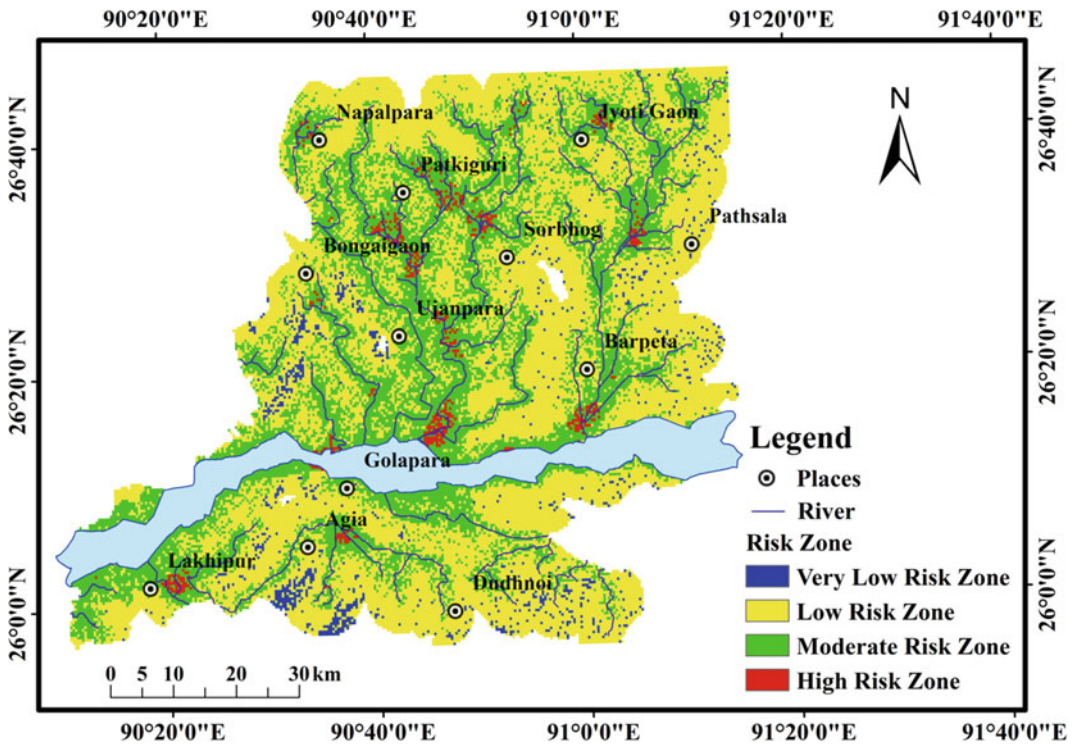


Fig. 5.12 Flood hazard zone map

using GIS and remote sensing in order to create a flood hazard map from the obtained database (Ajin et al. 2013). It may also be considered as the first step to be undertaken for better and effective flood management in the state of Assam (Sharma et al. 2012). Flood hazard zonation should be carried out based on flood recurrence intervals of different magnitudinal extensions and depth of flood inundation (Nath et al. 2020). The technology intervention coupled with flood risk mapping at the micro-level is expected to count as a major input towards effective flood mitigation strategies. It has to be understood that remote sensing data provides very useful information in vulnerable areas as terrestrial data are always not available. Therefore, it can be said that both remote sensing and GIS techniques are very useful for interpreting images in the shortest time. These tools also assist in bringing out fast economic solutions while the risk areas are classified during the time of analysis.

References

- Ajin RS, Krishnamurthy RR, Jayaprakash M, Vinod PG (2013) Flood hazard assessment of Vamanapuram River basin, Kerala, India: an approach using remote sensing & GIS techniques. *Adv Appl Sci Res* 4 (3):263–274
- Alam AR, Satpati LN (2021) Assessment of food security using geospatial techniques in rural India: a study from Koch Bihar, West Bengal. In: Rukhsana AA (eds) *Agriculture, food and nutrition security*. Springer, Cham. https://doi.org/10.1007/978-3-030-69333-6_8
- Asokan A, Anitha J, Ciobanu M, Gabor A, Naaji A, Hemanth DJ (2020) Image processing techniques for analysis of satellite images for historical maps classification—an overview. *Appl Sci* 10(12):4207
- Balasubramanian A (2017) *Surface water runoff*. Centre for Advanced Studies in Earth Science, University of Mysore, India
- Bishaw K (2012) Application of GIS and remote sensing techniques for flood Hazard and risk assessment: The case of Dugeda Bora Woreda of Oromiya Regional State, Ethiopia
- Chaturvedi R, Das B, Banerjee S, Bhattacharjee CR (2020) Ground water quality characterization of North Brahmaputra Basin using positive matrix

- factorization. In: Proceedings of the national academy of sciences, India Section A: Physical Sciences, pp 1–12
- Dragicevic N, Maibach H (2018) Combined use of nanocarriers and physical methods for percutaneous penetration enhancement. *Adv Drug Deliv Rev* 127:58–84
- Fujimoto S, Mizuno T, Ohnishi T, Shimizu C, Watanabe T (2017) Relationship between population density and population movement in inhabitable lands. *Evolution Inst Econ Rev* 14(1):117–130
- Government of Assam (2021) Water resource, flood and erosion problems. <https://waterresources.assam.gov.in/portlets/flood-erosion-problems> (Accessed on 30 May 2021)
- Haq M, Akhtar M, Muhammad S, Paras S, Rahmatullah J (2012) Techniques of remote sensing and GIS for flood monitoring and damage assessment: a case study of Sindh province, Pakistan. *Egyptian J Remote Sens Space Sci* 15(2):135–141. <https://doi.org/10.1016/j.ejrs.2012.07.002>
- Harris I, Osborn TJ, Jones P, Lister D (2020) Version 4 of the CRU TS monthly high-resolution gridded multivariate climate dataset. *Sci Data* 7(1):1–18
- Irimescu A, Stancalie G, Craciunescu V, Flueraru C, Anderson E (2009) The use of remote sensing and GIS techniques in flood monitoring and damage assessment: a study case in Romania. In: Threats to global water security, pp 167–177. https://doi.org/10.1007/978-90-481-2344-5_18
- Janssen RVH (1994) Multi-objective decision support for environmental management +DEFINITE Decisions on an FINITE set of alternatives: demonstration disks and instruction, 232
- Nath SR (2020) Changing landuse pattern in Sipajhar Development Block of Darrang District, Assam, India: a GIS based approach. *J Crit Rev* 7(11):3626–3635
- Nayak P, Panda B (2016) Brahmaputra and the socio-economic life of people of Assam. Published by Flood and River Management Agency of Assam, Guwahati, Assam, The Mahabahu Brahmaputra, pp 77–85
- Paul RK, Baidya A, Alam A, Satpati L (2021) An assessment of cyclone-induced vulnerability and change in land use and land cover (LULC) of G-Plot in Patharpratima C. D. Block of South 24 Parganas district, West Bengal, Indian. *J Geography Environ Manag*, pp 1–13
- Rahman MA, Hashem MA, Sheikh MHR, Bari AF (2021) Quality assessment of harvested rainwater and seasonal variations in the southwest coastal area. Bangladesh. *Environ Earth Sci* 80(8):1–12
- Saini SS, Kaushik SP (2012) Risk and vulnerability assessment of flood hazard in part of Ghaggar Basin: a case study of Guhla block, Kaithal, Haryana, India. *Int J Geomat Geosci* 3(1):42–54
- Saini SS, Jangra R, Kaushik SP (2015) Vulnerability assessment of soil erosion using geospatial techniques- a pilot study of upper catchment of markanda river. *Int J Adv Remote Sens, Gis Geogr* 3(1):9–21
- Sharma SSV, Roy PS (2017) Extraction of detailed level flood hazard zones using multi-temporal historical satellite data-sets—a case study of Kopili River Basin, Assam, India. *Geomat, Nat Hazards Risk* 8(2):792–802
- Sharma SSP, Rao GS, Bhanumurthy V (2012) Development of village-wise flood risk index map using multi-temporal satellite data: a study of Nagaon district, Assam, India. *Current Sci* 705–711
- South Asia Network on Dams, Rivers and People (SANDRP) (2013) Brahmaputra – the beautiful river or the battleground? (Accessed on 30 May 2021)
- Tarboton DG, Bras RL, Rodriguez-Iturbe I (1991) On the extraction of channel networks from digital elevation data. *Hydrol Process* 5(1):81–100
- Thakkar H, Saikia PJ (2013) Brahmaputra—the beautiful river or the battleground? SANDRP, 2013. <https://sandrp.in/2013/07/17/brahmaputra-the-beautiful-river-or-the-battleground/> (Accessed on 2 January 2021).



Flood Vulnerability Assessment Using AHP and Frequency Ratio Techniques

Md. Hasanuzzaman, Partha Pratim Adhikary, Biswajit Bera, and Pravat Kumar Shit

Abstract

Among all-natural disasters, flood is the most common and devastating, causing extensive disruption to the environment, socio-economy, infrastructure, and many other aspects of human life. Almost every year, the Torsa- Raidak River integrated basin area of the Himalayan foothill experiences flood due to physiographic characteristics and excessive rainfall over a short period of time. The current study uses Analytical Hierarchy Process (AHP) and Frequency Ratio (FR) model to prepare a flood susceptibility map. According to their contributions of selected factors (elevation, rainfall, topographic wetness index, slope angle, distance from rivers, and land use land cover), weightage was given using the AHP method. Moreover, AHP and FR methods were employed to find out the flood vulnerability index (FVI). Current

research results revealed that the lower part of the basin (Alipurduar and Cooch Behar) is susceptible to high to very high flood risk. Rainfall, LULC and distance from the river are contributing the most to cause flood in this study area. A total of 156 flood points were selected from different historical flood maps and field study areas for validation. The output of validation based on ROC depicted that the prediction accuracy was 81.2%, 85.7%, and 86.6% for the FVI, FR, and AHP, respectively, which may consider the model as good and acceptable for floods prediction. This research is capable to act as a guideline for grounding flood control measures in the area of study.

Keywords

Analytic hierarchy process · Flood vulnerability index · Frequency ratio model · GIS · Raidak river · Torsa river

Md.Hasanuzzaman (✉) · P. K. Shit
PG Department of Geography, Raja N. L. Khan Women's College (Autonomous), Gope Palace, Midnapore, West Bengal 721102, India

P. P. Adhikary
Department of Groundwater Management, ICAR-Indian Institute of Water Management, Chandrasekharpur, Bhubaneswar, Odisha, India
e-mail: Partha.Adhikary@icar.gov.in

B. Bera
Department of Geography, Sidho Kanho Birsha University, Puruliya, India

6.1 Introduction

Floods are one of the most significant hydro-meteorological hazards (Toduse et al. 2020). It has a very negative and sudden impact on human life and infrastructures (Leskens et al. 2014). In recent times, the incidence of natural disasters like flood, drought, cyclones, etc., has increased significantly due to numerous factors, such as climate change, environmental degradation,

excessive population growth, and inappropriate land use (Samanta et al. 2018; Majumder et al. 2019; Chakraborty and Mukhopadhyay 2019; Dano et al. 2019; Pradhan 2010). Across the globe, around 170 million people get affected and 31% of economic loss is caused by floods every year (Dano et al. 2019; Das 2019; Lawal 2012).

Flood occurs, when there is an overflow of water from rivers, lakes, ponds, reservoirs, and estuaries causing inundation of adjacent lands (Sarkar and Mondal 2020). Two distinctive physical features that give rise to the occurrence of the flood are climatological features (rainfall type, intensity, amount, etc.) and surface features (geomorphology, geology, vegetation, etc.) of the drainage basin (Şen 2018). Moreover, anthropogenic activity also plays an important role in the severity and consequences of the flood events (Yousefi et al. 2018; Feloni et al. 2020). Different aspects associated with human life from agriculture to service, ecosystem to economy, and transport network to sociocultural infrastructure go through huge deterioration and destruction during a flood (Ali et al. 2019; Sarkar and Mondal 2020; Subbarayan and Sivaranjani 2020). The consequences are greater in developing countries, where the urbanization process is rapidly increasing along the river (Das 2018). After Bangladesh, India has around 40 million hectares of flood-prone land, and is ranked as the second largest flood-prone country in the world (Sarkar and Mondal 2020). In India, approximately 7.6 million hectares of land and 3 crores of people get affected, and 1500 people lose their lives because of flood incidents every year. During the period of 1953 to 2009, India witnessed 92,000 deaths and an economic loss of 200 billion dollars due to flood (Central Water Commission 2010; Gupta et al. 2003; Sarkar and Mondal 2020; Singh and Kumar 2017). The impact of floods will dramatically be increased in near future due to socioeconomic development, depletion in forest cover and climate change (Phrakonkham et al. 2019). Preparation of a flood susceptible map would be more fruitful, if it is made considering several influential factors responsible for flood occurrence instead of a single factor analysis (Ali et al. 2019; Das 2018).

In recent times, geo-environmental hazards can best be assessed and mapped with the help of Remote Sensing (RS) and Geographic Information System (GIS) employing different models or techniques. The analysis of RS data on the GIS platform brings out accurate output for flood susceptibility assessment (Ali et al. 2019; Sarkar and Mondal 2020). To find out the more acceptable, logical, and reliable result, different statistical techniques are integrated with RS and GIS by several researchers (Ali et al. 2019). Commonly used statistical techniques are Analytical Hierarchy Process (AHP) (Ali et al. 2019; Elkhrachy 2015; Gazi et al. 2019; Hammami et al. 2019; Hoque et al. 2019; Jabbar et al. 2019; Lawal 2012; Matori et al. 2014; Souissi et al. 2018; Mishra and Sinha 2020; Phrakonkham et al. 2019; Rahman et al. 2019; Vojtek and Vojteková 2019), Frequency Ratio (FR) (Ali et al. 2019; Khosravi et al. 2019; Lee et al. 2018; Liuzzo et al. 2019; Rahman et al. 2019; Chen et al. 2020; Sahana et al. 2020), Logistic Regression (LR) (Lee et al. 2018; Liuzzo et al. 2019; Pradhan 2010; Rahman et al. 2019; Tehrany and Jones 2017), Evidential Belief Function (EBF) (Chowdhuri et al. 2020; Tehrany et al. 2019). In the current research, AHP and FR models have been employed for flood vulnerability analysis. Those models used to use widely because of their clear and strong practical applications for flood vulnerability assessment (Khosravi et al. 2016; Chen et al. 2020).

In eastern India, floods are frequent in the West Bengal state and are caused by the overflow of different rivers. The Brahmaputra, Damodar, Teesta, Torsha, Raidak, Sankosh, Mahananda, Ganga, Rupnarayan, Dwarkeswar, Subarnarekha River and its tributaries flood almost every year in West Bengal causing interruption to the daily life of the people living there. Around 55.80% area of West Bengal has been facing floods hazard (Nath et al. 2008). The eastern Himalayas controlled the physiographic setting and climate condition of the northern parts of West Bengal. The Teesta, Torsha, Raidak, Jaldhaka, Sankosh river and its tributaries come down from the eastern Himalayas foothills, which finally empty into the Brahmaputra river. These rivers during

the monsoon season overflow on their banks and cause floods every year. It harasses the livelihoods of the floodplain people. To solve this recurrence occurrence of flood, first, we need to map the susceptible areas where flood used to occur. The next step should be to establish the factors responsible for a flood to occur. Keeping these things in mind, the main objectives of this research are: (i) to prepare the flood susceptibility map of the study area and (ii) to identify the responsible factors based on spatial technique. The output of this present research can be useful to government agencies to take necessary steps in those regions that are susceptible to floods and have very high possibility for runoff harvesting.

6.2 Study Area

For this research, the Torsa-Raidak River integrated basin has been selected that is located in the north-eastern part of West Bengal (Fig. 6.1). The geographical extension of the river basin is 26°08'6.46"N to 27°55'1.43"N and 88°36'18.26" E to 90°08'9.34"E with a catchment area of 12,316 km². The basin covers parts of Bhutan and two districts of West Bengal, namely Alipurduar and Coochbehar. The basin was demarcated followed by the Annual Flood Report 2016, West Bengal, India. Chumbi Valley (7,065 m) in southern Tibet is the origin of the Torsa River and Mt. Akungphu in Bhutan (6,400 m) is the origin of the Raidak River. The Raidak River joined the Torsa River at Hasi-marabridge on NH-31 of India and after that, the combined river falls into the Brahmaputra near Nageswari at Rangpur in Bangladesh (Hasanuzzaman and Mandal 2020). The study area experiences subtropical monsoon climatic conditions, and receives more than 250 cm of rainfall annually. Most of the rainfall (80%) occurs in the monsoon period (June to September). Almost every year, the lower reach of the basin encounters floods owing to physiographic characteristics and excessive rainfall over a short time

span. Among the various hazards, floods are regular and highly influencing hazards during the monsoon season in the study area. The duration of the flood is one week and occurs every year (Hasanuzzaman et al. 2021). The river basin is funnel shaped, and thus prolonging the stagnation of surface runoff (Jana 1997). From 1950 to 2017, around 67 flood events occurred but not all floods were widespread and disastrous, while some flood events were very dangerous (Chakraborty and Mukhopadhyay 2019). The Torsa-Raidak River integrated basin morphological setting; especially the lower part is demarcated by the formation of the moribund river channel. This area is made of newly alluvium sediments deposition and the regional slope is from south to the southeast (Saha and Pal 2019). Two major flood hazards that occurred in the recent past (1993 and 2017) in the Torsa- Raidak River integrated basin caused huge damages. In 2017, a flood was occurred due to 3 days (10.07.2017–12.07.2017) of heavy intensive rainfall (Chakraborty and Mukhopadhyay 2019).

6.3 Materials and Methods

6.3.1 Data Source

For the flood risk mapping of Torsa- Raidak River integrated basin, various types of multi-source geospatial data were used: (a) Digital Elevation Model (DEM) of Shuttle Radar Topography Mission (SRTM) with 30 m spatial resolution (2014) downloaded from USGS Earth Explorer (<https://earthexplorer.usgs.gov>), (b) Landsat 8 Operational Land Image (OLI) (Path and Row Id-138/41, 138/42, 139/41) of 30 m spatial resolution (March 1, 2021) obtained from <https://earthexplorer.usgs.gov>, (c) The annual rainfall data, collected from <http://worldclim.org>. All spatial data was corrected radiometrically and geometrically and also corrected for the projection coordinate system. The work has been carried out as per the following framework (Fig. 6.2).

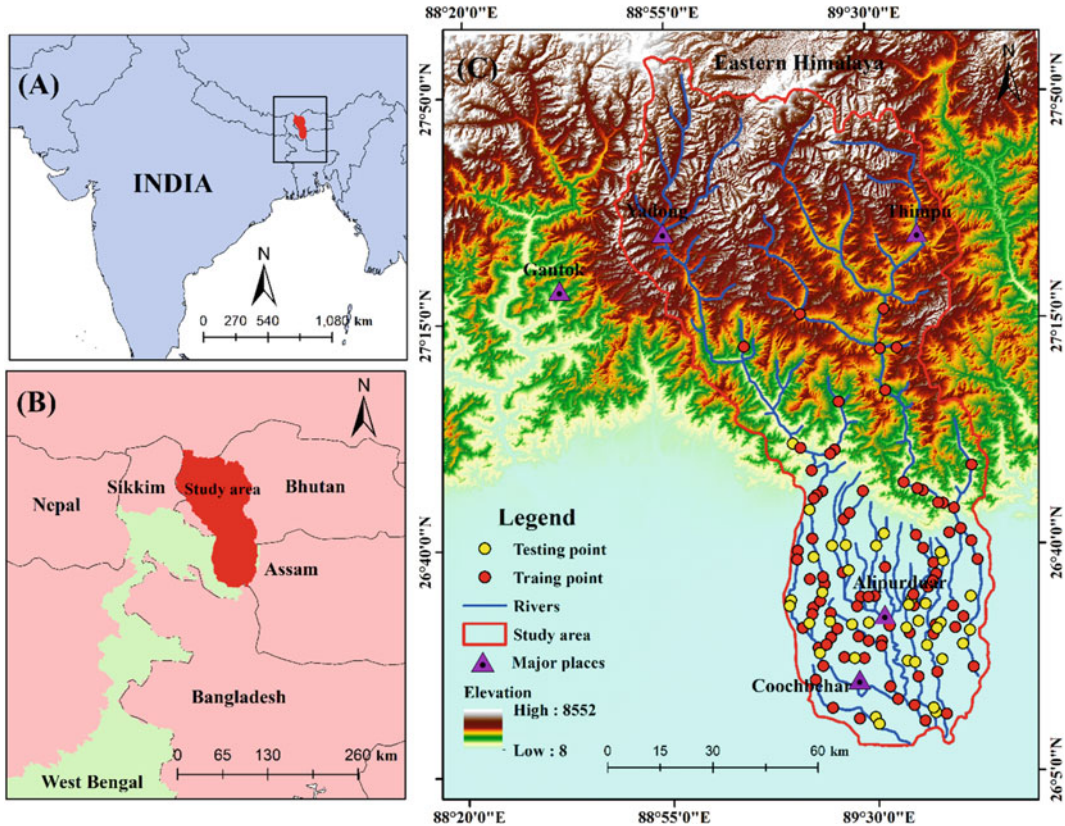


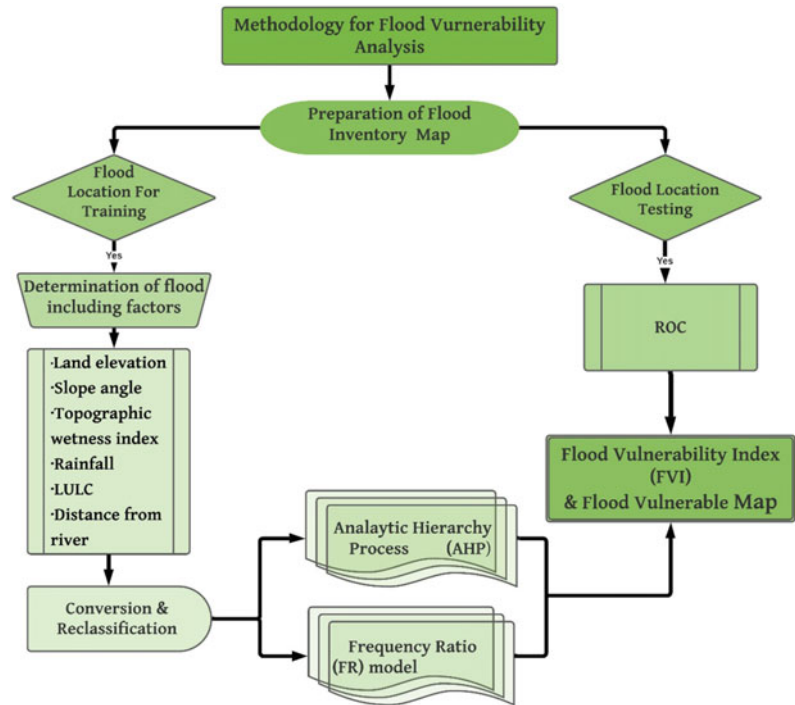
Fig. 6.1 Location map of the study area showing the training and testing points of the used models

6.3.2 Selection of Indicators of Flood Hazard

Selecting the causative factors influencing flood incidence of an area is important for flood susceptibility analysis and modeling (Tehrany et al. 2014). In this current research, six influential factors including elevation, slope angle, topographic wetness index, rainfall, land use land cover, and distance from the river were taken into consideration to perceive the nature of the flood event. All the adopted factors were processed using different RS and GIS software (ArcGIS 10.8 and ERDAS Imagine 2014). First of all, the Torsa-Raidak River integrated basin was delineated followed by the Annual Flood Report 2016, West Bengal, India and prepared all thematic layers. Flood is a very important hydrologic hazard and rainfall is the most important factor. In this basin, rainfall is one of the main controlling

factors due to location and climate conditions. The average annual rainfall data from 1970 to 2000 was used for preparing rainfall maps. Elevation is the prime factor for determining areas susceptible to flood occurrence (Das 2018, 2019; Janizadeh et al. 2019). Flat, low-land area tends to have a higher potentiality to be flooded than the area located at higher elevation (Ali et al. 2019; Liuzzo et al. 2019; Rahman et al. 2019; Vojtek and Vojteková 2019). Slope refers to the amount of inclination of surface in respect to the horizontal plane. This factor plays a crucial role in controlling surface runoff, infiltration process, and sub-surface flow (Ali et al. 2019; Das 2018; Hammami et al. 2019). An area with a gentle slope makes itself more vulnerable during a flood as flat terrains are more susceptible to water stagnation compared to the area under a steep slope (Hammami et al. 2019; Periyasamy et al. 2018). Topographic wetness index is commonly

Fig. 6.2 Conceptual framework of the methods used to map the flood vulnerability



used to evaluate the influence of topography in the accumulation of flow or generation of runoff at any point of the basin area (Ali et al. 2019; Moore et al. 1991; Sørensen et al. 2006). It is expressed as $TWI = \ln(As/\tan\beta)$, where “ TWI ” refers to topographic wetness index, “ As ” is the specific basin area, and “ β ” is the local slope (Das 2018, 2019; Sørensen et al. 2006; Tien Bui et al. 2019). The area with a higher TWI value indicates the high potentiality of the flood event (Das 2018; Tien Bui et al. 2019). Distance of an area from an active channel is very significant in the field of flood risk mapping (Das 2018). Areas near the active channels are more vulnerable to flood (Ali et al. 2019; Gazi et al. 2019). Land use/land cover has a significant role in determining surface runoff, which is directly related to a flood event in the catchment area (Phrakonkham et al. 2019). An area covered with vegetation reduces the intensity of surface runoff, and enhances the proliferation of the infiltration process; whereas a buildup area impedes strongly water percolation into the ground and hastens the surface flow (Hammami et al. 2019; Roslee et al. 2018). To

perceive the nature of land use in the study area, a supervised classification is done by adopting the maximum likelihood method in ERDAS Imagine software (Sarkar and Mondal 2020).

6.3.2.1 Assigning Weights of Indicators Using AHP

The AHP model was applied to assign different weights to the selected factors considered in this study. Basically, the AHP introduced by Saaty in 1980 is a semi-quantitative multi-criteria decision-making approach, in which decisions are made through pair-wise comparison between different factors without inconsistency (Das 2019). In this research, the AHP consisted of two major parts such as evaluating the main causative factors, and assessing the sub-classes of causative factors. Therefore, each part comprises the same steps including preparation of hierarchical order of factors, assignment of a score of each factor on the basis of their relative importance, creation of a pair-wise comparison matrix, computation of weight of each individual factor and finally measurement of consistency.

The hierarchical arrangement of factors was made based on their priority. The Saaty’s 1–9 scale (i.e., 1—equally significant, 3—slightly significant, 5—strongly significant, 7—very strongly significant, 9—extremely significant; while 2, 4, 6, and 8 are intermediate values) was used to assign a score to the factors based on their relative influence and importance. Thereafter, a pair-wise comparison matrix (Table 6.1) was developed, where diagonal elements were equal to 1, and the inverse value of each and every factor was complied by column, and signifies with other factors.

After relative rank is found out for the six factors, the factor weight values have to be measured for divided sub-factors to judge the consistency in taking the scale of significance into consideration. Hence, the eigenvector was calculated by considering the following equation (Ali et al. 2019):

$$Ex = \lambda_{max}x \tag{6.1}$$

where E is the comparison matrix of n number of criteria, x is the eigenvector of n size of criteria and λ is the eigenvalue.

The eigenvalues help in measuring consistency in a set of pairwise rankings. For a consistent reciprocal matrix, the largest eigenvalue (λ_{max}) is equal to the number of comparisons n . Hence, the Consistency Ratio (CR) is compulsory to calculate for the same. Saaty suggested that if the CR exceeds ‘0.1’, the set of decisions is considered as ‘inconsistent’ and has to repeat again. Concomitantly, if CR is equal to ‘0’, it means the decision is perfectly consistent but the value between 0 and 0.1 is also

considered as consistent (Saaty 1990). To ensure the efficiency of given scores, consistency ratio (CR) was calculated adopting Eqs. (6.2) and (6.3).

$$CR = \left(\frac{CI}{RI} \right) \tag{6.2}$$

$$CI = \left(\frac{\lambda_{max} - N}{N - 1} \right) \tag{6.3}$$

where “ CI ” refers to consistency index, “ RI ” indicates the random index, ‘ λ_{max} ’ is the principal eigenvalue of the matrix, and “ n ” stands for the number of parameters in the comparison matrix. The value “ RI ” depends on the number of parameters taken into account (Saaty 1980).

6.3.2.2 Frequency Ratio Model and Flood Vulnerable Index

Frequency ratio is a significant quantitative method of bivariate statistical and for the development of flood risk map, this model is very popular and widely accepted (Lee and Talib 2005; Pourghasemi et al. 2013; Khosravi et al. 2016; Samanta et al. 2018). A bivariate probability is calculated based on the spatial correlation between independent and dependent variables. In this current research, the spatial correlation has been measured between flood-inducing determinants as independent variables and flood training points as a dependent factor. This model has been employed for flood susceptibility mapping by Ali et al. (2019).

Therefore, Eq. (6.4) has been used to measure the frequency ratio for each class of six factors.

Table 6.1 Flood-inducing factors and their selected factor weight value (SFWV)

Factors	Elevation	Slope	TWI	Rainfall	LULC	DR	SFWV
Elevation	1	0.33	0.33	0.16	0.25	0.16	0.0381
Slope	3	1	0.33	0.2	0.25	0.25	0.0564
TWI	3	3	1	0.33	2	0.33	0.0858
Rainfall	6	5	3	1	1	0.33	0.324
LULC	4	3	3	0.5	1	0.33	0.146
DR	6	4	4	3	3	1	0.265

Consistency ratio (CR) = 0.0571, consistency index (CI) = 0.0753, random consistency index (RI) = 1.31.

$$FR = (P_{pixE}/P_{pixT}) / \left(\sum pixE / \sum P_{pixT} \right) \quad (6.4)$$

where P_{pixE} is the number of pixels containing flood points in class p , P_{pixT} is the total number of pixels having in class p in the study area, $\sum pixE$ is the total number of pixels containing flood points in class p and $\sum P_{pixT}$ is the total number of pixels in the in the study area.

The relationship between the definite class of the particular factor and flood training points can be considered strong or positive when the frequency ratio value is more > 1.0 . It means high flood risk. If the frequency ratio value is less $<.0$, it means the relationship is negative and has minimum flood risk (Pradhan 2010; Lee et al. 2012; Rahmati et al. 2016). In the present study, each class RF value was considered as a particular class weight value. AHP and FR method was employed to estimate the flood vulnerable index (FVI) map. The weight value of a particular class of six parameters was employed to calculate the flood vulnerable index (FVI) using the following Eq. (6.5):

$$FVI = \sum_{n=1}^n (w_i * FR) \quad (6.5)$$

where n is the total number of selected factors ($n = 6$ in the present study), w_i is the weight of factors, and FR is the frequency ratio value of each class.

6.4 Results and Discussion

For pre-floods hazard management, the flood vulnerability index is a very important and useful approach. Current work successfully employed the AHP and RF method (decision-making approach) to get the correlation between the six selected parameters (rainfall, elevation, slope angle, TWI, distance from rivers, and LULC) and floods risk area and to create a floods prediction map. For the flood as a hydrological hazard, rainfall is always considered a direct controlling

factor. In the study area, 90% of annual rainfall occurs during the monsoon and at that time flood events occurred. It was found that the rainfall varied between < 7.5 and > 29.41 cm. Here, the study result depicted that high rainfall areas were coinciding with high flood vulnerable areas. The highest elevation was found in the northern part of the basin, and continuously decreases towards the southern direction.

The elevation of the study area varies between < 06 and > 432 m but the area where the elevation was less < 70 as a strong relation with the flood. It is observed from the slope map that the slope ranges from 0° to 81.57° in the study area (Fig. 6.3). The area where the slope angle varies from 0° to 8.83° indicated the flood risk areas. The area with a higher topographic wetness index value indicates the high potentiality of flood event. It is evident that the higher topographic wetness index value was found in the active flood plain region of the Torsa- Raidak River integrated basin because of the lower elevated area (Fig. 6.3). In the study area, six LULC such as water bodies, agriculture land, vegetation, built-up area, sandbar, and others were observed. Among these classifications, sandbar and agricultural land are positively correlated with flood vulnerability. Distance from the river is a significant factor for flood risk. The output of the study depicted that the area where the distance from the river was < 1 km and very positive correlation with the flood risk was observed.

6.4.1 Flood Vulnerability Mapping

The final vulnerability map was generated based on the integration of factor weight and class weight value from AHP and FR investigations using a raster calculator in ArcGIS software (Figs. 6.4 and 6.5). The derived map was categorized into five distinctive classes. The classes are very high, high, moderate, low, and very low susceptibility to flood and their respective areas were 576.9 km^2 , 2867.04 km^2 , 3239.5 km^2 , 5281.4 km^2 , and 538.6 km^2 of the total basin area (Table 6.2). The lower segment (Alipurduar and

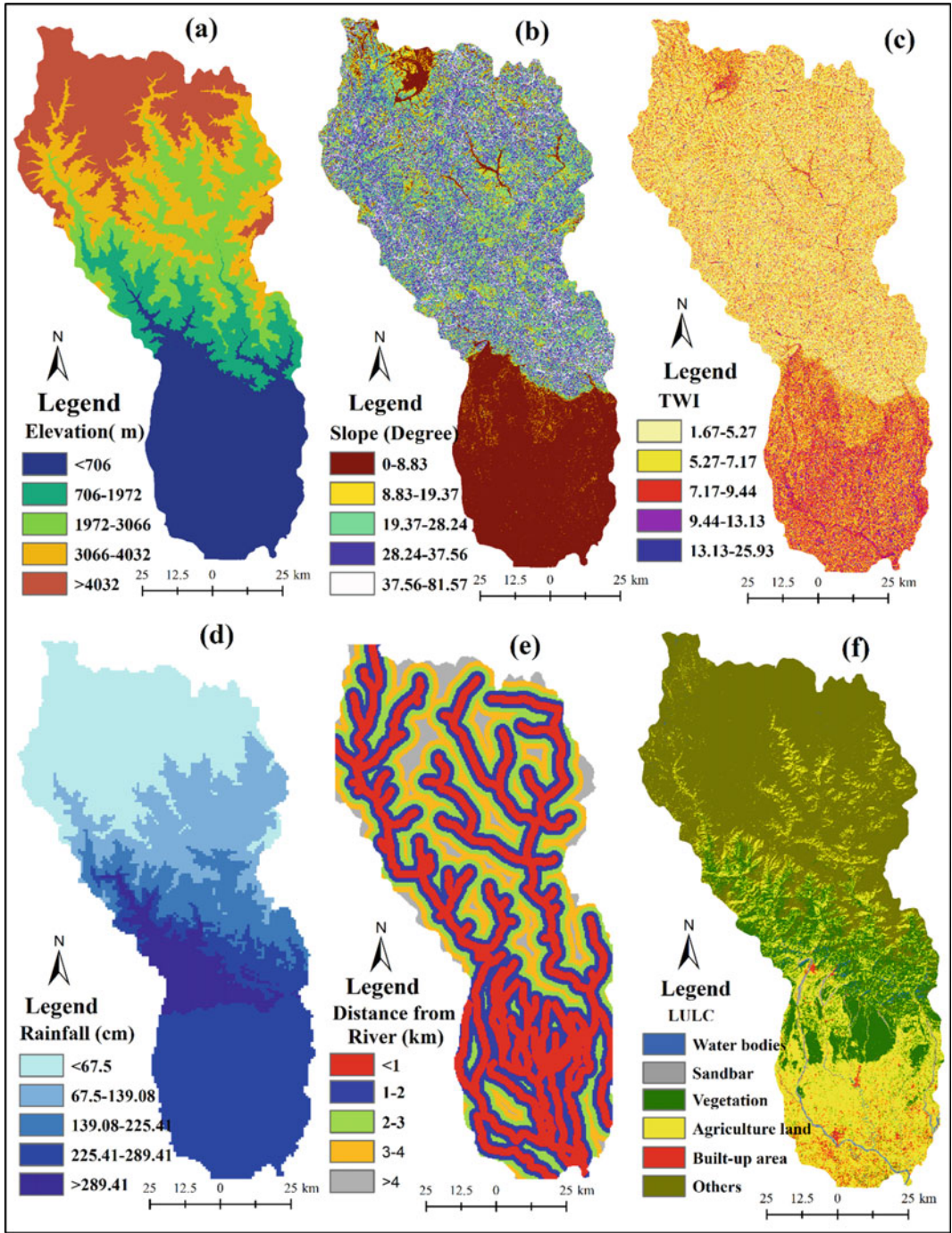
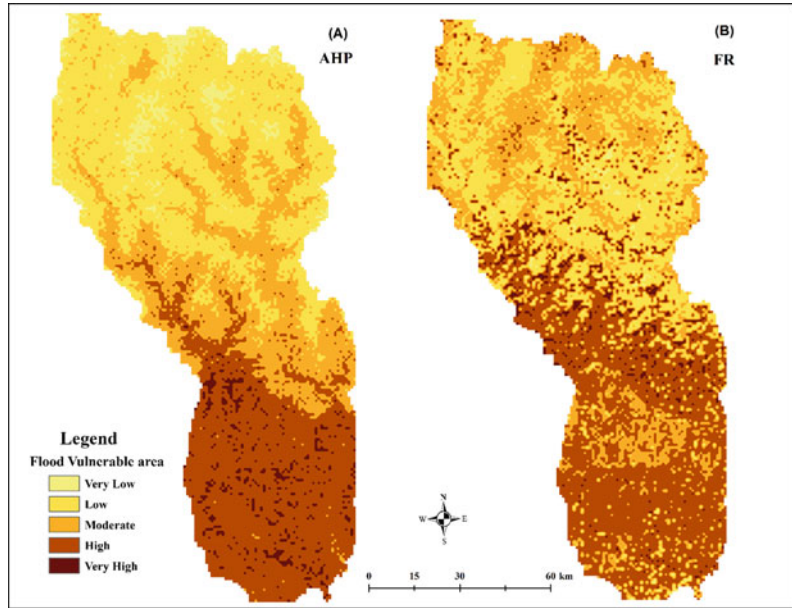


Fig. 6.3 Distribution of six causative factors used in this study: (a) elevation, (b) slope, (c) TWI, (d) rainfall, (e) distance from river, and (f) LULC

Fig. 6.4 Map showing the flood vulnerable area of the study area estimated by (A) AHP and (B) frequency ratio (RF)



Cooch Behar district, West Bengal) of the river basin is observed to be in a vulnerable condition, since it belongs to the very high to high flood susceptible category. It is because the area has low elevation and low slope. This portion is distinguished by flat alluvial plain and well-developed flood plain. The degree of flood vulnerability is greatly influenced by the social and economic factors of this area. The northern part of the basin comes to the very low to low flood susceptibility zone as the elevation is observed to be high, and the slope is seen very high. In this section, the Torsa-Raidak River integrated basin, flowing through the undulating high topography of Himalaya, is characterized by narrow restricted valley, lower width-depth ratio, lacking of flood plain development, rough bed configuration, and fewer number of bars; whereas the middle reach of the basin with moderate elevation shows moderate vulnerability to flooding. It is observed that flood susceptibility varies from higher in the southern to lower in the northern direction (Fig. 6.5). Thus, the susceptibility of flood decreases as the elevation increases toward north–west direction. The geospatial modeling provided an effective way of flood management in the study area. The various spatial components

of a flood are identified and extend of the potential flooded area is quantified as well. It will facilitate the implementation of evacuation strategy, rehabilitation plan, and damage assessment during a critical flood situation. It may also be effective in the development of policy, guidelines, and recommendation of land use planning.

6.4.2 Result Validation

In the present context, accurate validation of flood susceptibility maps is a very crucial and difficult task. The present study used success and prediction rate methods to validate the model by comparing predicted hazard areas to existing hazard locations (Zare et al. 2013). To do this, a total number of 156 known flood sites were demarcated from a historical flood map (Fig. 6.1) published by National Remote Sensing Centre (bhuvan.nrsc.gov.in). Out of the total sample points, 75% ($n = 117$) were generated randomly as training data and others used as testing data. Therefore, an Area Under Curve (AUC) method evaluated the prediction capabilities of validation of the model (Swets 1988; Hong et al. 2015). In

Fig. 6.5 Flood vulnerable map of the study area

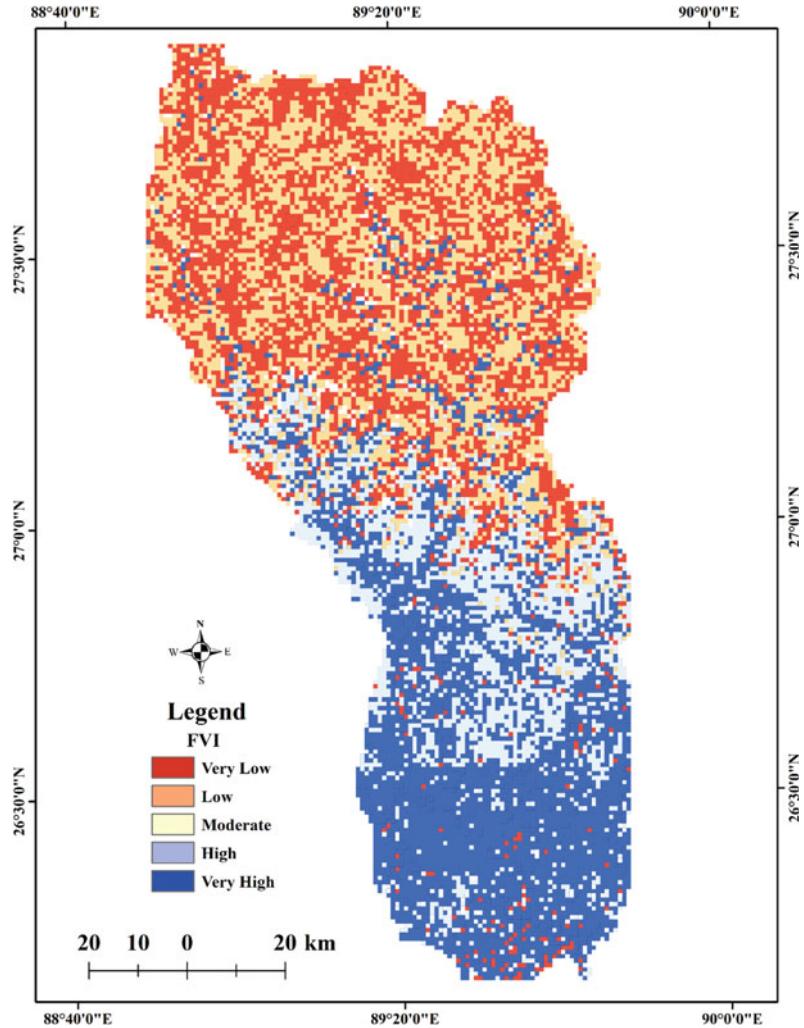


Table 6.2 Result of the various classes of different models for the flood vulnerable area

Flood vulnerable classes	AHP (km ²)	FR (km ²)	FVI (km ²)
Very low	548.5	519.3	538.6
Low	5094.8	5118.9	5281.4
Moderate	3375.67	3271.4	3239.5
High	2874.58	2957.8	2867.04
Very high	469.07	598.8	576.9

this work, the AUC has been considered to evaluate the performance and efficiency of the AHP, FR, and FVI methods. The training data and the testing data both were employed for the success and prediction rate percentage of each model by the AUC calculation. Figure 6.6

depicted the accuracy rates of 81.2%, 85.7%, and 86.6% for the Flood Vulnerability Index (FVI), Frequency Ratio (FR), and Analytical Hierarchy Process (AHP) classification methods, respectively. These results show that all models are good and acceptable for floods prediction.

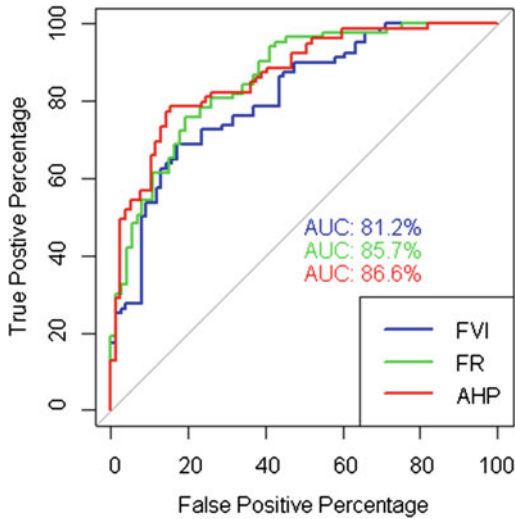


Fig. 6.6 Receiver Operating Curves (ROC) for flood vulnerable index, Frequency Ratio (FR), and Analytic Hierarchy Process (AHP)

6.5 Conclusion

The absence of long-term accurate data of historical floods is the main obstacle for developing an appropriate flood risk map but in the present day, those are possible with the use of scientific geospatial techniques. In the current study, Analytical Hierarchy Process (AHP) and Frequency Ratio (FR) model has been used to prepare a flood susceptibility map. According to the contributions of selected factors (elevation, rainfall, topographic wetness index, slope angle, distance from rivers, and land use land cover), the weightage was given using the AHP method. Moreover, AHP and FR methods were used to find out the flood vulnerability index (FVI). To investigate and perceive the flood vulnerability of the Torsa- Raidak River integrated basin, three factors, such as rainfall, LULC, and distance from turnout was found to be the most dominating parameters out of the adopted six factors considered for the present study. It is found that an area of 27.84% of the total basin comes under a very high to high flood susceptibility zone, and most of this area lies in Alipurduar and Cooch Behar districts. As a result, a large number of

populations have been witnessing and suffering from floods almost every year for decades. Their misery is the consequence of losing shelter, crops, and life. In this work, the AUC is considered to evaluate the performance and efficiency of the Flood Vulnerability Index (FVI), Frequency Ratio (FR), and Analytical Hierarchy Process (AHP) methods with the accuracy rates of 81.2, 85.7, and 86.6%. This research work may help the policy-makers and implementing authorities to gather basic information related to the flood, including its vastness and areas under risk. It is suggested that regional assessment of flood susceptibility can give accurate flood potentiality at the local scale. Moreover, a flood simulation study can be helpful to quantify the depth, velocity and duration of a flood and to access the surface water and groundwater interaction during a flood.

References

- Ali SA, Khatun R, Ahmad A, Ahmad SN (2019) Application of GIS-based analytic hierarchy process and frequency ratio model to flood vulnerable mapping and risk area estimation at Sundarban region, India. *Model Earth Syst Environ* 5:1083–1102. <https://doi.org/10.1007/s40808-019-00593-z>
- Central Water Commission (CWC) (2010) Water and related statistics, water resource information system directorate, New Delhi. Central Water Commission (CWC), New Delhi
- Chakraborty S, Mukhopadhyay S (2019) Assessing flood risk using analytical hierarchy process (AHP) and geographical information system (GIS): application in Coochbehar district of West Bengal, India. *Nat Hazards* 99(1):247–274. <https://doi.org/10.1007/s11069-019-03737-7>
- Chen W, Li Y, Xue W, Shahabi H, Li S, Hong H, Wang X, Bian H, Zhang S, Pradhan B, Ahmad BB (2020) Modeling flood susceptibility using data-driven approaches of naïve bayes tree, alternating decision tree, and random forest methods. *Sci Total Environ* 701:134979
- Chowdhuri I, Pal SC, Chakraborty R (2020) Flood susceptibility mapping by ensemble evidential belief function and binomial logistic regression model on river basin of eastern India. *Adv Space Res* 65:1466–1489. <https://doi.org/10.1016/j.asr.2019.12.003>
- Dano U, Balogun A-L, Matori A-N et al (2019) Flood susceptibility mapping using GIS-based analytic network process: a case study of Perlis Malaysia. *Water* 11:615. <https://doi.org/10.3390/w11030615>

- Das S (2018) Geographic information system and AHP-based flood hazard zonation of Vaitarna basin, Maharashtra India. *Arab J Geosci* 11:576. <https://doi.org/10.1007/s12517-018-3933-4>
- Das S (2019) Geospatial mapping of flood susceptibility and hydro-geomorphic response to the floods in Ulhas Basin, India. *Remote Sens Appl Soc Environ* 14:60–74. <https://doi.org/10.1016/j.rsase.2019.02.006>
- Elkhrachy I (2015) Flash flood hazard mapping using satellite images and GIS tools: a case study of Najran City, Kingdom of Saudi Arabia (KSA). *Egypt J Remote Sens Space Sci* 18:261–278. <https://doi.org/10.1016/j.ejrs.2015.06.007>
- Feloni E, Mousadis I, Baltas E (2020) Flood vulnerability assessment using a GIS-based multi-criteria approach—the case of Attica region. *J Flood Risk Manag* 13. <https://doi.org/10.1111/jfr3.12563>
- Gazi MY, Islam MA, Hossain S (2019) Flood-hazard mapping in a regional scale—way forward to the future hazard Atlas in Bangladesh. *Malays J Geosci (MJG)* 3:1–11
- Gupta S, Javed A, Datt D (2003) Economics of flood protection in India. *Nat Hazards* 28:199–210. <https://doi.org/10.1023/A:1021142404009>
- Hammami S, Zouhri L, Souissi D et al (2019) Application of the GIS based multi-criteria decision analysis and analytical hierarchy process (AHP) in the flood susceptibility mapping (Tunisia). *Arab J Geosci* 12:653. <https://doi.org/10.1007/s12517-019-4754-9>
- Hoque M, Tasfia S, Ahmed N, Pradhan B (2019) Assessing spatial flood vulnerability at Kalapara-Upazila in Bangladesh using an analytic hierarchy process. *Sensors* 19:1302. <https://doi.org/10.3390/s19061302>
- Hasanuzzaman M, Mandal S (2020) A morphology-independent methodology to assess erosion, accretion and lateral migration of an alluvial channel using geospatial tools: a study on the Raidak-I river of Himalayan foothills. *Sustain Water Resour Manag* 6:35. <https://doi.org/10.1007/s40899-020-00393-9>
- Hasanuzzaman M, Gayen A, Shit P (2021) Channel dynamics and geomorphological adjustments of Kaljani River in Himalayan foothills. *Geocarto Int* 1–28. <https://doi.org/10.1080/10106049.2021.1882008>
- Hong H, Pradhan B, Xu C, Bui DT (2015) Spatial prediction of landslide hazard at the Yihuang area (China) using two-class kernel logistic regression, alternating decision tree and support vector machines. *CATENA* 133:266–281
- Jabbar FK, Grote K, Tucker RE (2019) A novel approach for assessing watershed susceptibility using weighted overlay and analytical hierarchy process (AHP) methodology: a case study in Eagle Creek Watershed, USA. *Environ Sci Pollut Res* 26:31981–31997. <https://doi.org/10.1007/s11356-019-06355-9>
- Jana MM (1997) Management and development of River Basins in North Bengal using remote sensing techniques. *J Indian Soc Remote Sens* 25(2):105–111
- Janizadeh S, Avand M, Jaafari A et al (2019) Prediction success of machine learning methods for flash flood susceptibility mapping in the Tafresh Watershe Iran. *Sustainability* 11:5426. <https://doi.org/10.3390/su11195426>
- Khosravi K, Nohani E, Maroufinia E, Pourghasemi HR (2016) A GIS-based flood susceptibility assessment and its mapping in Iran: a comparison between frequency ratio and weights-of-evidence bivariate statistical models with multi-criteria decision-making technique. *Nat Hazards* 83:947–987. <https://doi.org/10.1007/s11069-016-2357-2>
- Khosravi K, Shahabi H, Pham BT, Adamowski J, Shirzadi A, Pradhan B, Dou J, Ly H-B, Gr'of G, Ho H.L, Hong H, Chapi K, Prakash I (2019) A comparative assessment of flood susceptibility modeling using multi-criteria decision-making analysis and machine learning methods. *J Hydrol* 573:311–323
- Lawal DU (2012) Detecting flood susceptible areas using GIS-based analytic hierarchy process. 2012 International conference on future environment and energy. IACSIT press, Singapore, pp 1–5
- Leskens JG, Brugnach M, Hoekstra AY, Schuurmans W (2014) Why are decisions in flood disaster management so poorly supported by information from flood models? *Environ Model Softw* 53(53):61. <https://doi.org/10.1016/j.envsoft.2013.11.003>
- Lee S, Lee S, Lee M-J, Jung H-S (2018) Spatial assessment of urban flood susceptibility using data mining and geographic information system (GIS) tools. *Sustainability* 10:648. <https://doi.org/10.3390/su10030648>
- Lee S, Talib JA (2005) Probabilistic landslide susceptibility and factor effect analysis. *Environ Geol* 47:982–990
- Lee MJ, Kang JE, Jeon S (2012) Application of frequency ratio model and validation for predictive flooded area susceptibility mapping using GIS, pp 895–898. *Geoscience and Remote Sensing Symposium (IGARSS)*, Munich
- Liuzzo L, Sammartano V, Freni G (2019) Comparison between different distributed methods for flood susceptibility mapping. *Water Resour Manage* 33:3155–3173. <https://doi.org/10.1007/s11269-019-02293-w>
- Matori AN, Lawal DU, Yusof KW, et al (2014) Spatial analytic hierarchy process model for flood forecasting: an integrated approach. *IOP Conf Ser Earth Environ Sci* 20:012029. <https://doi.org/10.1088/1755-1315/20/1/012029>
- Majumder R, Bhunia GS, Patra P, Mandal AC, Ghosh D, Shit PK (2019) Assessment of flood hotspot at a village level using GIS-based spatial statistical techniques. *Arab J Geosci* 12(13):1–12. <https://doi.org/10.1007/s12517-019-4558-y>
- Mishra K, Sinha R (2020) Flood risk assessment in the Kosimegafan using multi-criteria decision analysis: a hydro-geomorphic approach. *Geomorphology* 350:106861. <https://doi.org/10.1016/j.geomorph.2019.106861>
- Nath SK, Roy D, Singh Thingbaijam KK (2008) Disaster mitigation and management for West Bengal, India—an appraisal. *Curr Sci* 94(7):858–866

- Moore ID, Grayson RB, Ladson AR (1991) Digital terrain modelling: a review of hydrological, geomorphological, and biological applications. *Hydrol Process* 5:3–30. <https://doi.org/10.1002/hyp.3360050103>
- Periyasamy P, Yagoub MM, Sudalaimuthu M (2018) Flood vulnerable zones in the rural blocks of Thiruvallur district South India. *Geoenviron Disasters* 5:21. <https://doi.org/10.1186/s40677-018-0113-5>
- Phrakonkham S, Kazama S, Komori D, Sopha S (2019) Distributed hydrological model for assessing flood hazards in Laos. *JWARP* 11:937–958. <https://doi.org/10.4236/jwarp.2019.118056>
- Pradhan B (2010) Flood susceptible mapping and risk area delineation using logistic regression, GIS and remote sensing. *J Spat Hydrol* 9(2):1–18
- Pourghasemi HR, Pradhan B, Gokceoglu C, Deylami Moezzi K (2013) A comparative assessment of prediction capabilities of Dempster-Shafer and weights-of-evidence models in landslide susceptibility mapping using GIS. *Geomat Nat Hazards Risk* 4:93–118
- Rahman M, Ningsheng C, Islam MM et al (2019) Flood susceptibility assessment in Bangladesh using machine learning and multi-criteria decision analysis. *Earth Syst Environ* 3:585–601. <https://doi.org/10.1007/s41748-019-00123-y>
- Rahmati O, Pourghasemi HR, Zeinivand H (2016) Flood susceptibility mapping using frequency ratio and weights-of-evidence models in the Golastan Province Iran. *Geocarto Int* 31:42–70. <https://doi.org/10.1080/10106049.2015.1041559>
- Roslee R, Tongkul F, Mariappan S, Simon N (2018) Flood hazard analysis (FHAn) using multi-criteria evaluation (MCE) in Penampang Area, Sabah Malaysia. *ASM Sci J* 11(3):104–122
- Saaty TL (1980) *The analytic hierarchy process: planning, priority setting, resource allocation*. McGraw-Hill International Book Co., New York, London
- Saaty TL (1990) How to make a decision: the analytic hierarchy process. *Eur J Oper Res* 48:9–26
- Sarkar D, Mondal P (2020) Flood vulnerability mapping using frequency ratio (FR) model: a case study on Kulik river basin Indo-Bangladesh Barind Region. *Appl Water Sci* 10:17. <https://doi.org/10.1007/s13201-019-1102-x>
- Sahana M, Rehman S, Sajjad H, Hong H (2020) Exploring effectiveness of frequency ratio and support vector machine models in storm surge flood susceptibility assessment: a study of Sundarban Biosphere Reserve, India. *Catena* 189:104450
- Samanta RK, Bhunia GS, Shit PK, Pourghasemi HR (2018) Flood susceptibility mapping using geospatial frequency ratio technique: a case study of Subarnarekha River Basin, India. *Model Earth Syst Environ* 4:395–408. <https://doi.org/10.1007/s40808-018-0427-z>
- Saha TK, Pal S (2019) Emerging conflict between agriculture extension and physical existence of wetland in post-dam period in Atreyee River Basin of Indo-Bangladesh. *Environ Dev Sustain* 21(3):1485–1505
- Şen Z (2018) *Flood modelling, prediction and mitigation*. Springer International Publishing, Cham
- Swets JA (1988) Measuring the accuracy of diagnostic systems. *Science* 240:1285–1293
- Singh O, Kumar M (2017) Flood occurrences, damages, and management challenges in India: a geographical perspective. *Arab J Geosci* 10:102. <https://doi.org/10.1007/s12517-017-2895-2>
- Souissi D, Msaddek MM, Zouhri L, Chenini I, El May M, Dlala M (2018) Mapping groundwater recharge potential zones in arid region using GIS and Landsat approaches, SE Tunisia. *Hydrol Sci J*. <https://doi.org/10.1080/02626667.2017.1414383>
- Sørensen R, Zinko U, Seibert J (2006) On the calculation of the topographic wetness index: evaluation of different methods based on field observations. *Hydrol Earth Syst Sci* 10:101–112. <https://doi.org/10.5194/hess-10-101-2006>
- Subbarayan S, Sivaranjani S (2020) Modelling of flood susceptibility based on GIS and analytical hierarchy process—A Case study of Adayar River Basin, Tamilnadu, India. In: Pal I, von Meding J, Shrestha S, Ahmed I, Gajendran T (eds) *An Interdisciplinary Approach for Disaster Resilience and Sustainability*, pp 91–110. Springer, Singapore
- Tehrany MS, Jones S (2017) Evaluating the variations in the flood susceptibility maps accuracies due to the alterations in the type and extent of the flood inventory. *Int Arch Photogramm Remote Sens Spatial Inf Sci XLII-4/W5:209–214*. <https://doi.org/10.5194/isprs-archives-XLII-4-W5-209-2017>
- Tehrany MS, Lee MJ, Pradhan B, Jebur MN, Lee S (2014) Flood susceptibility mapping using integrated bivariate and multivariate statistical models. *Environ Earth Sci* 72:4001–4015
- Tehrany MS, Kumar L, NeamahJebur M, Shabani F (2019) Evaluating the application of the statistical index method in flood susceptibility mapping and its comparison with frequency ratio and logistic regression methods. *Geomat Nat Haz Risk* 10:79–101. <https://doi.org/10.1080/19475705.2018.1506509>
- Tien Bui D, Khosravi K, Shahabi H et al (2019) Flood spatial modeling in Northern Iran using remote sensing and GIS: a comparison between evidential belief functions and its ensemble with a multivariate logistic regression model. *Remote Sens* 11:1589. <https://doi.org/10.3390/rs11131589>
- Toduse NC, Ungurean C, Davidescu S, Cliniciu I, Marin M, Nita MD, Davidescu A (2020) Torrential flood risk assessment and environmentally friendly

- solutions for small catchments located in the Romania Natura 2000 sites Ciucas, Postavaru and Mare. *Sci Total Environ* 698:134271. <https://doi.org/10.1016/j.scitotenv.2019.134271>
- Vojtek M, Vojteková J (2019) Flood susceptibility mapping on a national scale in Slovakia using the analytical hierarchy process. *Water* 11:364. <https://doi.org/10.3390/w11020364>
- Yousefi S, Mirzaee S, Keesstra S, Surian N, Pourghasemi HR, Zakizadeh HR, Tabibian S (2018) Effects of an extreme flood on river morphology (case study: Karoon River, Iran). *Geomorphology* 304:30–39
- Zare M, Pourghasemi HR, Vafakhah M, Pradhan B (2013) Landslide susceptibility mapping at vaz watershed (Iran) using an artificial neural network model: a comparison between multilayer perceptron (mlp) and radial basic function (rbf) algorithms. *Arab J Geosci* 6:2873–2888



Application of Hybrid Machine Learning Algorithms for Flood Susceptibility Modeling

7

Swapan Talukdar, Sujit Kumar Roy,
Showmitra Kumar Sarkar, Susanta Mahato,
Swades Pal, Atiqur Rahman, Bushra Praveen, and
Tanmoy Das

Abstract

This study combines machine learning (ML) algorithms with statistical models to generate new hybrid models for flood susceptibility mapping (FSM) in the Teesta River basin of Bangladesh (LR). Two-hybrid ML algorithms,

such as ANN-LR and RF-LR models for FSM, have been created by combining two ML techniques, such as artificial neural network (ANN) and random forest (RF), with one statistical approach, such as logistic regression. The FSMs were then validated using parametric and non-parametric receiver operating characteristic curves (ROC), such as empirical and binormal ROC. We evaluated the impact of the parameters on FSM using a Random forest-based sensitivity analysis. The extremely high (1023–1120 km²) and high flood vulnerability zones were estimated using three methods and two hybrid models (521–674 km²). Based on the ROC's area under the curve, the ANN-LR model (ROCe-AUC: 0.883; ROCb-AUC: 0.936) outperformed other models (AUC). According to the validation results, two hybrid models outperformed three machine learning and statistical models. The findings of this research will aid FSMs in building long-term flood control strategies by increasing their efficiency.

S. Talukdar · A. Rahman · T. Das
Faculty of Natural Science, Department of
Geography, Jamia Millia Islamia, New Delhi
110025, India
e-mail: arahman2@jmi.ac.in

T. Das
e-mail: tanmoy2008953@st.jmi.ac.in

S. K. Roy
Institute of Water and Flood Management (IWFM),
Bangladesh University of Engineering and
Technology (BUET), Dhaka, Bangladesh

S. K. Sarkar
Department of Urban and Regional Planning,
Khulna University of Engineering and Technology,
Khulna, Bangladesh

S. Mahato (✉)
Special Centre for Disaster Research, Jawaharlal
Nehru University, New Delhi 110067, India
e-mail: susantamahato@jnu.ac.in

S. Pal
Department of Geography, University of Gour
Banga, Malda, India

B. Praveen
School of Humanities and Social Science, Indian
Institute of Technology Indore, Madhya Pradesh,
India

Keywords

Flood susceptibility · Machine learning ·
Statistical technique · ROC curve · Artificial
neural network · Sensitivity analysis · Remote
sensing

7.1 Introduction

Natural catastrophes have emerged as one of society's most critical global issues (Kabir and Hossain 2021). Flooding is one of the most prevalent, well-known, and everyday occurrences among all-natural catastrophes (Ahmed et al. 2021). Floods create a devastating situation and often occur during the monsoon, especially in the Indian subcontinent (Zhang et al. 2021), which receives nearly 80% of the annual rainfall in the monsoon. Flooding occurs in the surrounding land area because of heavy rainfall and massive river runoff (Yousefi et al. 2018). A flood becomes a catastrophe when it causes significant damage to people and their livelihood and habitat (De Silva and Kawasaki 2018). Floods hit Bangladesh every year in the Ganges–Brahmaputra–Meghna (GBM) basin (Uhe et al. 2019). Riverine, rainfall-induced, flash, tidal, and cyclonic/storm surgical floods have all been recorded (Uhe et al. 2019; Islam et al. 2021a). Being the GBM's outflow, Bangladesh has to deal with a lot of stream-flow during the rainy season (which begins in June and lasts till the end of October). Floods are more common and conspicuous in flatlands (which account for 79.1% of the geographical area) and hence get the most significant study and planning focus. Approximately 20–25% of the area is affected by flooding on an annual basis. Sixty percent of the region had been impacted by floods in 1987, 1988, and 1998 (Lin et al. 2019). The socioeconomic repercussions of these regular floods are enormous. Between 2009 and 2014, floods of various magnitudes affected 57.01% of Bangladeshi houses on average. In economic terms, the cost of damage was estimated to be 0.85 billion USD (De Silva and Kawasaki 2018; Rahman et al. 2020).

Despite the enormous financial and development costs, flood losses were unavoidable because of a lack of comprehensive flood assessment tools for improved preparation. The flood risk may be defined and assessed in a variety of ways. The mathematical modeling of flood susceptibility has been considered the most complicated process. It is possible to expect

the geographical distribution of floods that have happened or are expected to occur in a particular location quantitatively and qualitatively. As a consequence, flood susceptibility mapping may help policymakers and other stakeholders establish disaster preparedness plans. While flood dangers cannot be eliminated, flood damages may be circumvented or considerably declined if flood inundated areas are correctly predicted (Shafizadeh-Moghadam et al. 2018).

As a consequence, determining flood susceptibility is crucial for disaster assistance. Researchers have presented a variety of flood risk assessment models. The bulk of recent models in geographic information systems (GIS) integrate hydrological, multi-criteria decision analysis, hydrodynamic, statistical models (SM), and ML algorithms (Jamali et al. 2020). GIS and remote sensing are one of the most significant databases and tools that have been extensively employed in hazard analysis (Pourghasemi and Rossi 2019).

The Frequency Ratio (FR) (Aditian et al. 2018), the Analytical Hierarchical Process (AHP) (Mukherjee and Singh 2020), the Analytical Network Process (ANP) (Abedi Gheshlaghi et al. 2020), Support Vector Machines (SVM) (Fan et al. 2020), and Random Forest (RF) (Probst et al. 2019) have all been used to study flood (Adnan et al. 2020). Every modeling approach has benefits and drawbacks. The accuracy, structure, and data of each model affect its performance. Consequently, a wide range of ensemble techniques to geohazard susceptibility and potentiality mapping has gained popularity quickly (Elmahdy et al. 2020).

Experimental hybrid techniques for FS modeling research have been researched in recent years since there is a necessity to evaluate existing prediction methods and procedures to get a better scientific basis and, as a result, more accurate conclusions (Eyoh et al. 2018). ANN-fuzzy logic, rough set-SVM, and other hybrid approaches created by combining SM with ML algorithms have been successfully employed in FS modeling (Chen et al. 2018; Jahangir et al. 2019). However, experts have emphasized that no model is ideal for modeling and that results

might differ from area to region and data. Thus, a new model should be designed and evaluated to get reliable results. As a result, in order to achieve the research gaps as mentioned earlier, the primary objectives are:

1. Construct a hybrid ensemble machine learning based FSM by merging LR with ML algorithms.
2. Conduct sensitivity modeling employing RF.
3. Verify the FS models using ROC curves.

The present study will aid decision-makers and governments in effectively regulating flood management.

7.2 Materials and Methods

7.2.1 Study Area

The Teesta sub-catchment is in northern Bangladesh and includes the districts of Nilphamary, Lalmanirhat, Rangpur, Kurigram, and Gaibandha (Fig. 7.1). Its drainage basin comprises several minor rivers with heights varying from 5 to 110 m, making it Bangladesh's most significant geomorphic unit. During floods, the river's usual gradient is between 0.46 and 0.56 m per kilometer, reflecting a very level area (Rahman et al. 2011). The research area's hydrological characteristics are complicated, and the region has a dense river network. This basin has a subtropical monsoonal climate. Monsoon (June–September) and dry (October–November) are the two major seasons in the basin (October–December). This basin gets around 1900 mm of precipitation per year on average (Islam et al. 2021b), with the monsoon season accounting for 80% of total annual precipitation.

7.2.2 Materials

In the present study, a variety of datasets have been obtained and used for flood susceptibility modeling. The details of datasets used for generating FSM were tabulated in Table 7.1.

7.2.3 Flood Inventory

For the creation of FSM maps, several researchers have started with the locations of previously flooded areas. It was determined that FSM was based on historical flooding regions. Two hundred ten flood points have been collected from different sources and a comprehensive site assessment for the inventory map. There must be a need to acquire non-flood data analogous to the flood data utilized in FSM (Islam et al. 2021a). The choice was based on the field survey, which included an identical amount of non-flood locations (210 points). Using a random separation to all flood and non-flood datasets, 80 (336):20 (84) training and testing datasets have been generated (Fig. 7.1). Training data has been employed to calibrate the model, while testing data has been employed to measure the accuracy of the models (Mallick et al. 2021). In the same way, inventory maps for other locations have been generated.

7.2.4 Methods for Preparing FS Conditioning Factors

Flood-influencing variables must be included as independent variables when creating a flood susceptibility map (El-Haddad et al. 2021; Azareh et al. 2019). According to Dodangeh et al. (2020), contributing factors utilized in one research area may have no effect in another, hence parameter identification must be event based. Among the highly significant and often utilized variables are elevation, aspect, TWI, SPI, STI, LULC, TRI, distance to the river (dR), curvature, soil condition, slope, and rainfall. The contributing variables have been translated into 30 m spatial resolution using resampling technique.

The topography and its derivative variables serve a vital part in determining FSM (Falah et al. 2019) (Fig. 7.2). Topography has a direct impact on runoff speed (Abdel-Fattah et al. 2017), and high slopes increase the speed of runoff and reduce infiltration rates (Abdel-Fattah et al. 2017). Furthermore, the dR has a significant

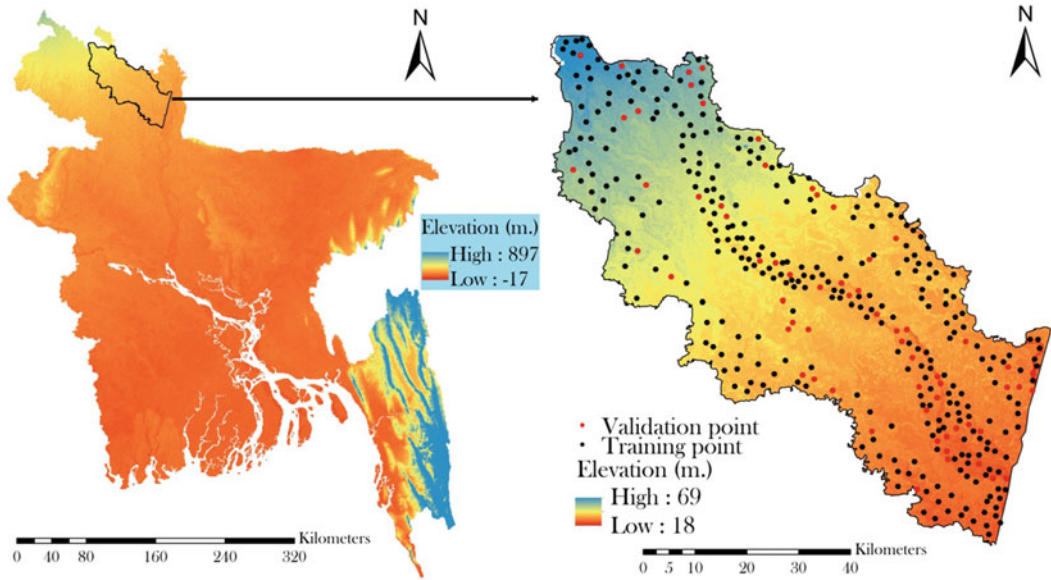


Fig. 7.1 The location of the study area

Table 7.1 Materials used for preparing FSM

Data types	Purpose	Resolution/scale	Source
ASTER DEM	For deriving different topographic and hydrologic parameters like slope, aspect, curvature, TPI, STI, TWI	Version 2, spatial resolution: 30 m	https://asterweb.jpl.nasa.gov/gdem.asp
Landsat 8 OLI	For generating LULC	Path/Row: 138/42, Spatial resolution: 30 m., date: 19/03/2019	https://earthexplorer.usgs.gov/
Rainfall	For generating rainfall map	–	Meteorological Department (BMC), Dhaka
Soil map	For preparing soil types map	1:50,000	Natural Resources Conservation Service of United States Department of Agriculture (USDA)

impact on flood magnitude. High drainage density causes a reduced capture rate and hence flow accumulation, which is one of the variables that substantially influences flood occurrence (Ogato et al. 2020; Bogale 2021).

Rainfall is recognized as the vital variable in determining FS levels (Wasko and Nathan 2019). Because heavy rain in a short period of time can create flash flooding (Wasko and Nathan 2019).

In the ArcGIS 10.3 environment, acquired precipitation data from four Bangladeshi meteorological stations was utilized to create rainfall using the kriging interpolation procedure. Because the amount of data is so small, this approach is highly recommended (Islam et al. 2021b). The research area's annual rainfall, on the other hand, ranges from 361 to 550 mm (Fig. 7.3c).

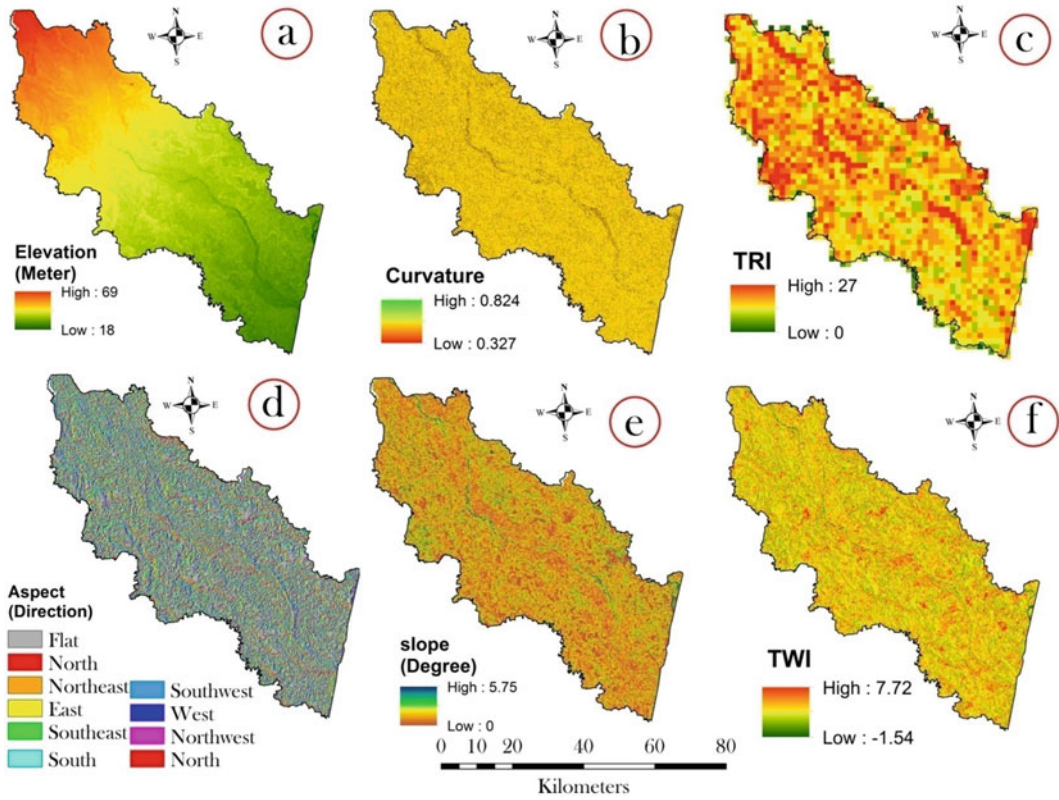


Fig. 7.2 Data layers for FS conditioning factors such as **a** elevation, **b** curvature, **c** TRI and **d** aspect, **e** slope, and **f** TWI

Soil property is the most critical factor for generating overflow (Yin et al. 2019). Flügel (1995) contends that soil quality regulates water penetration, affecting rainfall-runoff generation while indigenous climatic forms and erosion procedures also play a role. When the degree of penetration is high, susceptibility events are more likely to occur. According to USDA soil classification, the research area comprises 12 different types of soil (Fig. 7.3d).

LULC affects surface runoff, which in turn affects sediment flow, and hence has a substantial impact on the incidence of FS (Islam et al. 2021a). FS is relatively high in built-up areas because the LULC totally regulates surface flow generation and infiltration. Because different land use features preclude or help water for penetrating and generating surface water. The forest environment, on the other hand, increases water infiltration, resulting in lower FS (Islam et al. 2021b). The association between FS occurrences and plant density is

adverse while comparing hydrological reactions at different temporal conditions. A LULC map has been created using the ANN model in ENVI software (version 5.3) (Talukdar et al. 2020) and classified into six classes (Fig. 7.3e).

7.2.5 Multicollinearity Analysis

The 12 conditioning variables were examined to see whether there was any association between them using the VIF and tolerance approach. If the variables are multicollinear, they are interrelated, and one of them could be predicted by other factors. Hence, it must be eliminated from the model. Among various models, such as Pearson's correlation coefficients, variance decomposition proportions, the VIF, and tolerance are the most frequent and extensively utilized. Multicollinearity is present if the VIF is more than ten or the tolerance is less than 0.1 (Talukdar et al. 2021).

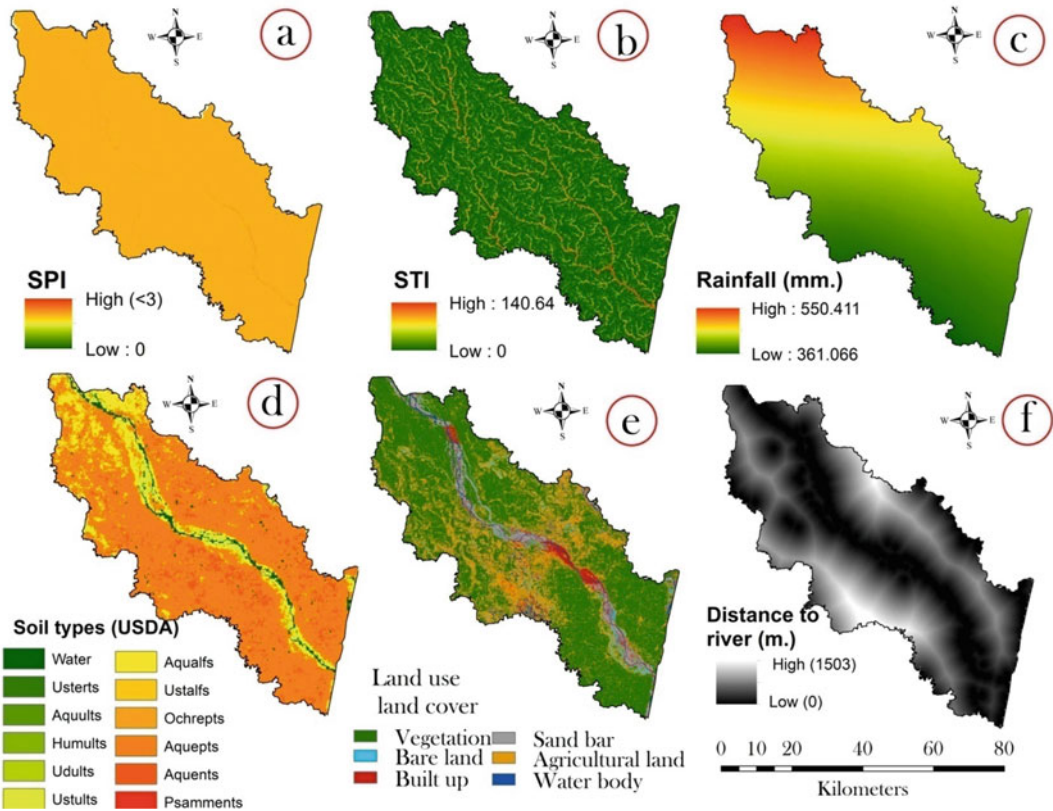


Fig. 7.3 Data layers for FS conditioning factors such as **a** SPI, **b** STI, **c** rainfall **d** soil types, **e** LULC, and **f** distance to river

7.2.6 Method for FS Modeling

7.2.6.1 Artificial Neural Network (ANN)

Artificial Neural Networks (ANNs) mimic the human nervous system and are able to acquire and simplify from instances to provide expressive solutions even while the input data includes errors or is inadequate (Jahangir et al. 2019; Khoirunisa et al. 2021). Many problems have been solved with ANNs (Kia et al. 2012). Reconstruction of the strange association between a set of input variables, such as rainfall and output variables, such as streamflow or groundwater level using ANN has been carried out (Fang et al. 2021) (Kia et al. 2012). This means that artificial neural networks can be used for flood predictions.

7.2.6.2 Random Forest (RF)

Random forest (Breiman 2001) could be summarized as a decision tree ensemble approach. It generates decision trees by randomly picking data from the training set. The decision trees were assessed independently during the training stage, with the best score being the average of the trees' outcomes. When generating decision trees, RF seeks to identify the most essential characteristics, hence feature selection is crucial. For RF, there are a few key factors to consider. The first is the forest's number of trees, which determines how many decision trees are formed during training. A large number of trees help in generalizing the model better, according to the general approach to setting this parameter. The number of features is another parameter that

refers to the depth of the decision trees. Accuracy can be improved by using a higher number of characteristics. It should be noted that bigger numbers take longer to compute, therefore time should be taken into account while parameterizing.

7.2.6.3 Logistic Regression

The LR method has been regarded as highly applied model in predicting natural hazards like flood, landslide, and drought susceptibility by many scholars throughout the world (Ali et al. 2020). In this work, the logistic regression model was chosen as one of the multivariate analytic methods to quantitatively measure flood susceptibility. The use of logistic regression to create a multivariate regression connection between a target variable and certain conditioning variables is effective for forecasting the presence or absence of the events like flood and landslide. By adding an appropriate link function to the conventional linear regression model, logistic regression allows the variables to be either continuous or discrete, or any mix of both, and they do not have to have normal distributions (Cao et al. 2020). The dependent variable in this study is a binary variable (0 or 1), with 1 indicating the existence of a flood and 0 indicating the absence of a flood.

7.2.7 Validation of the Models

The Receiver Operating Characteristic (ROC) curve is a common means of visually illustrating a marker's discriminating accuracy for differentiating between two populations. It has been utilized in radiology, psychology, epidemiology, factory inspection systems, and biomedical informatics, among other fields. The application of the ROC curve for natural hazards prediction has expanded recently, with researchers assessing the efficiency of models in discriminating between positive and negative functions of natural hazards (Tehrany et al. 2014). A depiction of the false positive rates versus the true positive rates for different diagnostic test cutoff settings is known as a ROC

curve. The area under the ROC curve is the most often used metric for describing accuracy (AUC). The AUC may have a value of 0–1, with higher AUC values showing better accuracy (Yesilnacar and Topal 2005).

The nonparametric ROC techniques do not make assumptions about the distributions of diagnostic test results and do not produce a smooth ROC curve. On the other hand, parametric techniques presume that some function of the diagnostic test measures is normally distributed in both the positive and negative events, but with different means in each case. The parametric ROC approaches may create a smooth ROC curve. For the nonparametric ROC analysis in our work, we employed the empirical technique. We performed the parametric ROC analysis using the binormal approach.

7.3 Sensitivity Analysis

Mean decrease accuracy (MDA) and mean decrease Gini (MDG) coefficient are two significant measures for ranking variables and selecting variables in Random Forest. MDA analyzes the change in prediction accuracy when the values of a variable are randomly permuted compared to the original data, which determines the relevance of a variable. When a variable is used to produce a Random Forest split, MDG is the total of all Gini impurity reductions generated by that variable, normalized by the number of trees in the Random Forest (For details of RF, see method section).

7.4 Results and Discussion

7.4.1 Computation of the Multicollinearity Analysis and Importance of the Parameters

Findings of the multicollinearity test show the VIF and tolerance values of the variables are less than ten and greater than 0.2, respectively. Therefore, there is no requirement to concern

about multicollinearity between independent variables. Since all twelve flood-conditioning factors were included in this present research, FS maps included them all. The multicollinearity analysis findings for this research are as follows:

Elevation (VIF: 2.71, TOL: 0.635), slope (1.34, 0.805), curvature (1.08, 0.794), TWI (1.19, 0.653), SPI (1.56, 0.629), distance to river (1.3, 0.9), rainfall (2.76, 0.846), soil types (1.32, 0.804), and LULC (1.1, 0.803), aspect (1.08, 0.725), TRI (1.2, 0.821), STI (1.62, 0.87).

7.4.2 Description of the Parameters

The FS of an area may be affected by various factors (Bhattacharya et al. 2021). Influencing factors in this study were presented in Figs. 7.2 and 7.3. Low-lying locations, particularly those in the floodplain, retain higher soil moisture due to the continuous depressions, increasing the flooding probability. The elevation of the study area varied from 18 to 69 m above sea level (Fig. 7.2). In general, the capacity to recharge water is highest while the curvature has the feature of a concave surface. On the other hand, the water recharge capacity is less on the plain surface (Mishra et al. 2019). The DEM was used to create a curvature map with a range of 0.32–0.82 degrees of curvature (Fig. 7.2). The DEM has been employed to generate a curvature map with a range of 0.32–0.82 (See Fig. 7.2b.) A total of nine classifications were established: zero to twenty-five, twenty-five to sixty-five, seventy-five to ninety-five, and one hundred and fifty to three hundred and sixty-five (Fig. 7.2). The presence of a flat or mild slope is also advantageous since it helps to slow down water flow and enhance the sensitivity to recharge (Mahato and Pal 2019). The slopes that were employed in this study varied from 0 to 5.75°. TRI helps to determine how water flow was affected by competing for underlying surfaces (Fig. 7.2d) (Straatsma and Baptist 2008). Due to the rapid water flow created by the high hills around the Teesta River, it has lower TRI because of the rapid water flow, which suggests a greater likelihood of flooding (Mahato et al. 2021). According to the findings of this study, the

highest TRI score was 27. (See Fig. 7.2 for an example.) A high TWI also guarantees that a person's susceptibility to infection is regenerated, which is beneficial. Between TWI levels and FS, there is a significant inverse relationship. Figure 7.3 depicts TWI value ranges from -1.54 to -7.72 linearly. Therefore, regions with higher SPI and STI values are more vulnerable to floods because of the greater water level represented by higher SPI and STI values (Bui et al. 2019). According to the findings of this investigation, the highest STI level measured was 140.64. Figure 7.3 depicts the distance between this location and the river, which was 1503 m in this case. It was possible to account for extra rainfall and water penetration by analyzing soil data (Johnson 2000). The 12 soil types were identified in this study area (Fig. 7.3).

7.4.3 FS Models and Their Validation

Figure 7.4 depicts the FS models built using hybrid machine learning techniques such as ANN, RF, LR, and combined ANN-LR and RF-LR. In the present study, we first applied standalone ML algorithms, and then we applied semi-machine learning algorithms, like logistic regression, for predicting flood susceptibility zones. Then, we developed hybrid models by integrating ML algorithms with the LR model. The LR model has been employed to define the weights for each parameter. The parameters are then allocated weights and turned into weighted parameters. We then used machine learning methods like ANN and RF to create hybrid models. In this way, ANN-LR and RF-LR hybrid models have been created. The weights derived using the LR model is as follows:

$$FSM = 18.30 + (\text{Aspect} * 0.0012) + (\text{Curvature} * 0.0325) + (\text{Elevation} * 0.0825) + (\text{LULC} * 0.3694) + (\text{Rainfall} * 0.156) + (\text{Distance to river} * 0.0884) + (\text{Slope} * 0.3029) + (\text{Soil types} * 0.0027) + (\text{SPI} * 0.0007) + (\text{STI} * 0.0032) + (\text{TWI} * 0.1975) + (\text{TRI} * 0.0761).$$

There are five categories in Jenkin's natural break method: very high, high, moderate, low, and very low flood susceptible zones. This

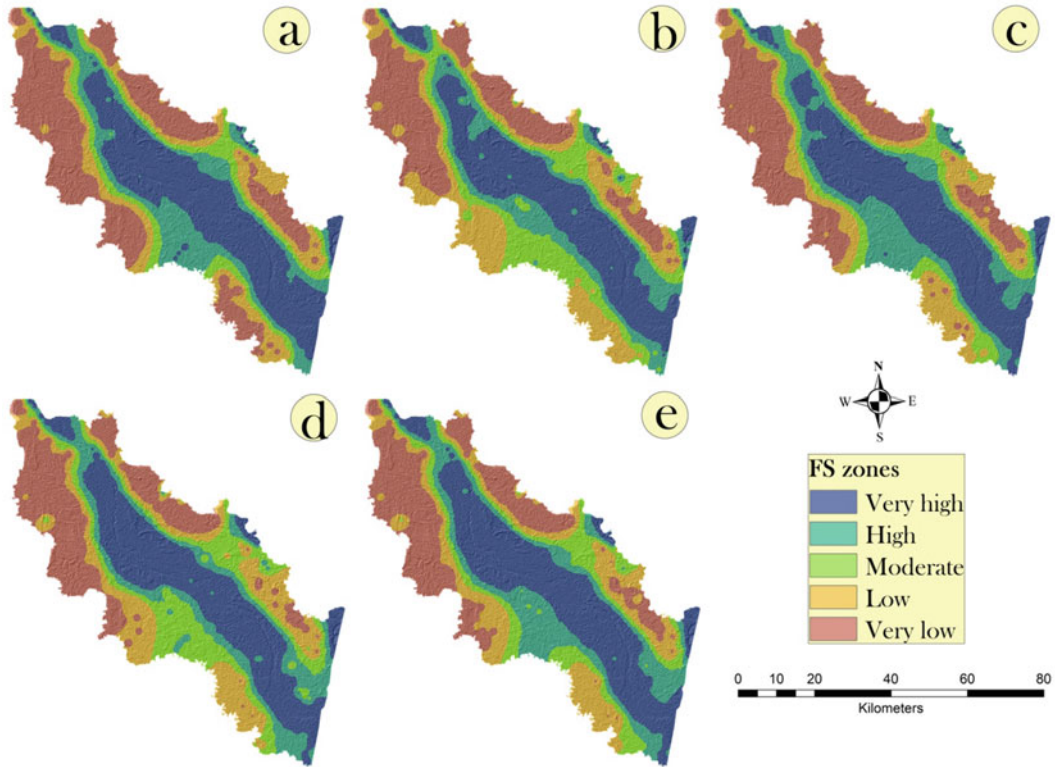


Fig. 7.4 FS models using **a** ANN, **b** RF, **c** LR, **d** ANN-LR, and **e** RF-LR

algorithm was used to classify the produced flood susceptible models (Fig. 4.4). Parallel to the drainage path of the watershed, the flood vulnerability zone runs northwest-southeast. Places with high susceptibility zones are concentrated in the south and southeast, whereas areas with low susceptibility zones are concentrated in the north and northwest of the country.

For ANN model, 2.26 and 36.69% of the entire basin area observed very “high” and “high” flood susceptibility, respectively (Table 7.2). However, all models anticipated 1023.99 km²–1120.58 km² regions to be very susceptible to flooding. All models projected that 800.01 km²–1103.01 km² regions were very low flood susceptible zone (Table 7.2). According to the models, most river catchment areas were classified as having high to very high FS zones. However, since the region’s size varies, it is vital to choose the most accurate model.

The AUC of empirical and binormal ROC curves has been utilized to test the FS models based on the GPS locations that have been collected (Meten et al. 2015; Nahayo et al. 2019). The AUC under each ROC (empirical and binormal) for ANN, it is 0.874 and 0.912; for RF, it is 0.88 and 0.93; for LR, it is 0.861 and 0.873; for ANN-LR, it is 0.883 and 0.936; and for the RF-LR model, it is 0.89 and 0.92 (Fig. 7.5a–e). Results of ROC curves show that the ANN-LR model was the most effective, followed by the RF-LR model, the RF model, the ANN model, and the LR model. According to the binormal ROC curve, the best model was ANN-LR (AUCb: 0.936), followed by RF (AUCb: 0.93), RF-LR (AUCb: 0.92), ANN (AUCb: 0.912), and LR (AUCb: 0.912). Overall, all of the models performed well, with hybrid machine learning methods beating all of them in terms of overall performance.

Table 7.2 Calculation of area for five FS zones

FS zones	Area (km ²)				
	ANN	RF	LR	ANN-LR	RF-LR
Very high	1102.21	1023.99	1071.70	1045.91	1120.58
High	584.87	546.11	674.62	521.65	627.35
Moderate	361.61	592.62	395.50	596.45	444.38
Low	507.79	722.03	584.31	668.68	642.29
Very low	1103.01	800.01	956.86	806.01	848.96

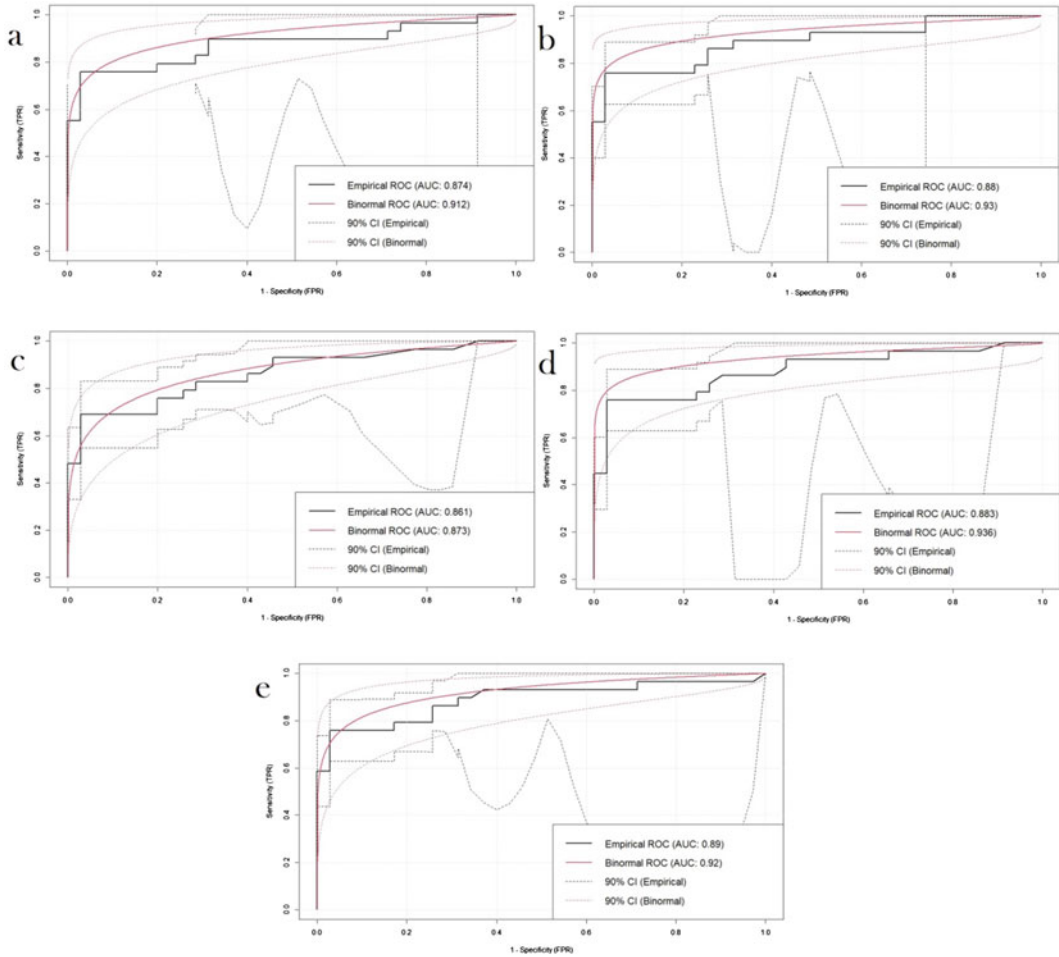


Fig. 7.5 Application of empirical and binormal ROC curve for validating the FS models based on **a** ANN, **b** RF, **c** LR, **d** ANN-LR, and **e** RF-LR

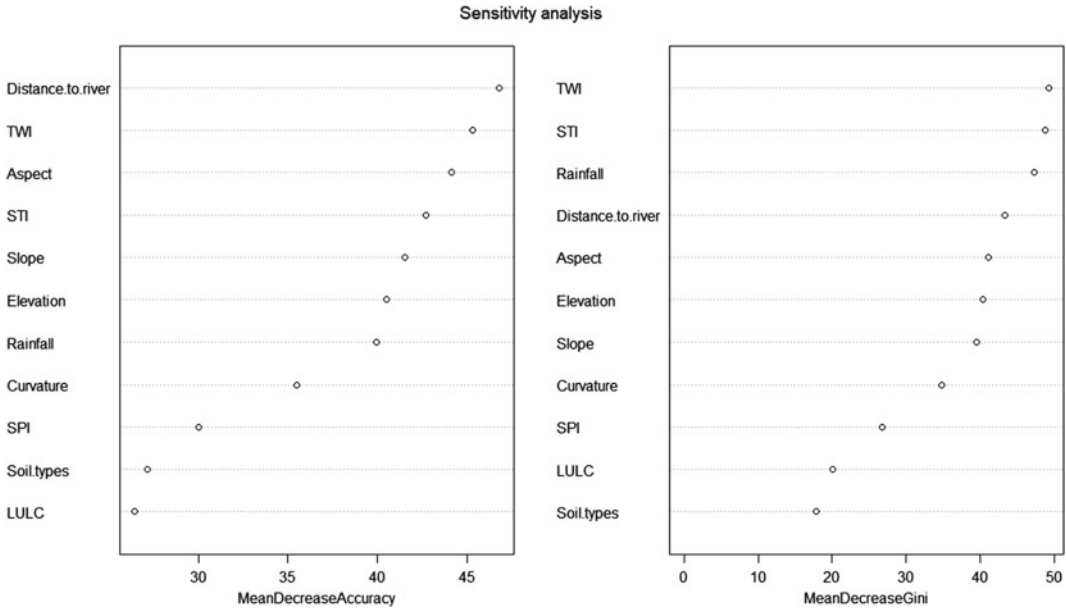


Fig. 7.6 Sensitivity analyses of susceptibility conditioning factors in terms of best FS models using **a** MDG, and **b** MDA

7.4.4 Sensitivity Analysis Using Machine Learning Algorithms

Advanced ensemble machine learning methods must be developed in order to map robust flood susceptibility zones. Dependent on the intricate mathematical association between historical floods and their conditioning factors, these algorithms can only depict the likely area around the future occurrence of a considerable and quantifiable amount of flooding. On the other hand, these models do not address the role that variables play in a given region during a flood event. Since several variables impact the possibility of flooding, the issue arises on how flood control strategies could be designed and implemented without this knowledge.

If the variables' influence on FS is uncertain, how management plans will be established and implemented. Floods may be less damaging if the variables of a particular area are identified that are associated with susceptibility zones. Consequently, it is essential to identify which factors have the most considerable impact. The

significance of each triggering variable was determined using matrices from RF-based sensitivity models, such as MDG and MDA. Both the MDG and the MDA are significant metrics (Hollister et al. 2016). Results show that all the variables of the FSM model were taken into consideration, with dR, TWI, and aspect being the most important (Fig. 7.6). Among 12 variables, three of them were less influential than others in deciding the importance of the variables.

7.5 Conclusion

The present research focuses on creating hybrid models that use machine learning and statistical approaches to forecast flood susceptibility models. Three algorithms and two hybrid models were used to estimate the very high (1023–1120 km²) and high flood susceptibility zones (521–674 km²) flood susceptibility zones. The ANN-LR-based FSM (ROCe-AUC: 0.883; ROCb-AUC: 0.936) beat all FS models as per the AUC value. Results show that two hybrid models beat three ML and statistical models in terms of

performance. On the other hand, an RF-dependent sensitivity analysis was devised to assess the importance of the input factors for FSM. The distance to the river was the most dominating and sensitive variable for FSM, followed by slope, curvature, elevation, LULC, and SPI.

Hybrid models beat three ML and statistical models when it came to FS modeling. These findings lead the researchers to recommend adopting hybrid and ensemble algorithms for predicting natural hazards based on various factors in the future. Additionally, this study recommends that a few other hydrological, geological, and climatic variables be incorporated into the models for enhancing the robustness of the model findings. The Teesta River basin is acknowledged for flooding because of irregular rainfall, dams' construction, and other artificial issues. Therefore, these findings might be helpful in the creation of long-term flood control and farming techniques. Specifically, the paper states that land cover and vegetation conditions appeared as significant conditioning variables for FSM. Deforestation, conversely, is incontrovertible realities. Consequently, the maintenance of forest cover will benefit flood control. Further research is required for the scientific evaluation of floods at distinct susceptible zones to provide more accurate advice on what management techniques should be implemented from each possible zone.

References

- Abdel-Fattah M, Saber M, Kantoush SA, Khalil MF, Sumi T, Sefelnasr AM (2017) A hydrological and geomorphometric approach to understanding the generation of wadi flash floods. *Water* 9(7):553
- Abedi Gheshlaghi H, Feizizadeh B, Blaschke T (2020) GIS-based forest fire risk mapping using the analytical network process and fuzzy logic. *J Environ Plan Manage* 63(3):481–499
- Aditian A, Kubota T, Shinohara Y (2018) Comparison of GIS-based landslide susceptibility models using frequency ratio, logistic regression, and artificial neural network in a tertiary region of Ambon, Indonesia. *Geomorphology* 318:101–111
- Adnan MSG, Abdullah AYM, Dewan A, Hall JW (2020) The effects of changing land use and flood hazard on poverty in coastal Bangladesh. *Land Use Policy* 99:104868
- Ahmed N, Hoque MAA, Howlader N, Pradhan B (2021) Flood risk assessment: role of mitigation capacity in spatial flood risk mapping. *Geocarto Int* 1–23
- Ali SA, Parvin F, Pham QB, Vojtek M, Vojteková J, Costache R, Linh NTT, Nguyen HQ, Ahmad A, Ghorbani MA (2020) GIS-based comparative assessment of flood susceptibility mapping using hybrid multi-criteria decision-making approach, naïve Bayes tree, bivariate statistics and logistic regression: a case of Topľa Basin, Slovakia. *Ecol Indic* 117:106620
- Azareh A, Rafiei Sardooi E, Choubin B, Barkhori S, Shahdadi A, Adamowski J, Shamshirband S (2019) Incorporating multi-criteria decision-making and fuzzy-value functions for flood susceptibility assessment. *Geocarto Int* 1–21
- Bogale A (2021) Morphometric analysis of a drainage basin using geographical information system in Gilgel Abay watershed, Lake Tana Basin, upper Blue Nile Basin Ethiopia. *Appl Water Sci* 11(7):1–7
- Breiman, 2001. Breiman L (2001) Random forests. *Machine Learn* 45(1):5–32
- Bui DT, Ngo PTT, Pham TD, Jaafari A, Minh NQ, Hoa PV, Samui P (2019) A novel hybrid approach based on a swarm intelligence optimized extreme learning machine for flash flood susceptibility mapping. *Catena* 179: pp 184–196
- Cao Y, Jia H, Xiong J, Cheng W, Li K, Pang Q, Yong Z (2020) Flash flood susceptibility assessment based on geodetector, certainty factor, and logistic regression analyses in Fujian Province China. *ISPRS Int J Geo-Inf* 9(12):748
- Chen W, Peng J, Hong H, Shahabi H, Pradhan B, Liu J, Zhu AX, Pei X, Duan Z (2018) Landslide susceptibility modelling using GIS-based machine learning techniques for Chongren County, Jiangxi Province, China. *Sci Total Environ* 626:1121–1135
- De Silva MGMT, Kawasaki A (2018) Socioeconomic vulnerability to disaster risk: a case study of flood and drought impact in a rural Sri Lankan community. *Ecol Econ* 152:131–140
- Dodangeh E, Choubin B, Eigdir AN, Nabipour N, Panahi M, Shamshirband S, Mosavi A (2020) Integrated machine learning methods with resampling algorithms for flood susceptibility prediction. *Sci Total Environ* 705:135983
- El-Haddad BA, Youssef AM, Pourghasemi HR, Pradhan B, El-Shater AH, El-Khashab MH (2021) Flood susceptibility prediction using four machine learning techniques and comparison of their performance at Wadi Qena Basin Egypt. *Nat Hazards* 105(1):83–114
- Elmahdy SI, Mohamed MM, Ali TA, Abdalla JED, Abouleish M (2020) Land subsidence and sinkholes susceptibility mapping and analysis using random forest and frequency ratio models in Al Ain, UAE. *Geocarto Int* 1–17
- Eyoh I, John R, De Maere G, Kayacan E (2018) Hybrid learning for interval type-2 intuitionistic fuzzy logic

- systems as applied to identification and prediction problems. *IEEE Trans Fuzzy Syst* 26(5):2672–2685
- Falah F, Rahmati O, Rostami M, Ahmadisharaf E, Daliakopoulos IN, Pourghasemi HR (2019) Artificial neural networks for flood susceptibility mapping in data-scarce urban areas. In: *Spatial modeling in GIS and R for earth and environmental sciences*, pp 323–336. Elsevier
- Fan J, Wu L, Ma X, Zhou H, Zhang F (2020) Hybrid support vector machines with heuristic algorithms for prediction of daily diffuse solar radiation in air-polluted regions. *Renew Energy* 145:2034–2045
- Fang Z, Wang Y, Peng L, Hong H (2021) Predicting flood susceptibility using LSTM neural networks. *J Hydrol* 594:125734
- Flügel WA (1995) Delineating hydrological response units by geographical information system analyses for regional hydrological modelling using PRMS/MMS in the drainage basin of the River Bröl Germany. *Hydrol Process* 9(3–4):423–436
- Hollister JW, Milstead WB, Kreakie BJ (2016) Modeling lake trophic state: a random forest approach. *Ecosphere* 7(3): p e01321
- Islam ARMT, Talukdar S, Mahato S, Kundu S, Eibek KU, Pham QB, Kuriqi A, Linh NTT (2021a) Flood susceptibility modelling using advanced ensemble machine learning models. *Geosci Front* 12(3):101075
- Islam M, Tamanna S, Amstel AV, Noman M, Ali M, Saadat S, Aparajita DM, Roy P, Tanha SR, Sarkar N, Ashiquzzaman M (2021b) Climate change impact and comprehensive disaster management approach in Bangladesh: a review. In: *Bangladesh II: climate change impacts, mitigation and adaptation in developing countries*, pp1–39
- Jahangir MH, Reineh SMM, Abolghasemi M (2019) Spatial prediction of flood zonation mapping in Kan River Basin, Iran, using artificial neural network algorithm. *Weather Clim Extrem* 25:100215
- Jamali B, Bach PM, Deletic A (2020) Rainwater harvesting for urban flood management—an integrated modelling framework. *Water Res* 171:115372
- Johnson RA, (2000) Habitat segregation based on soil texture and body size in the seed-harvester ants *Pogonomyrmex rugosus* and *P. barbatus*. *Ecol Entomology* 25(4): pp 403–412
- Kabir MH, Hossain T (2021) Assessment on social vulnerability and response towards natural disaster in a disaster-prone coastal village: an example from Bangladesh. *Int J Disaster Manag* 4(1):39–60
- Khoirunisa N, Ku CY, Liu CY (2021) A GIS-based artificial neural network model for flood susceptibility assessment. *Int J Environ Res Public Health* 18(3):1072
- Kia MB, Pirasteh S, Pradhan B, Mahmud AR, Sulaiman WNA, Moradi A (2012) An artificial neural network model for flood simulation using GIS: Johor River Basin Malaysia. *Environ Earth Sci* 67(1):251–264
- Lin L, Di L, Tang J, Yu E, Zhang C, Rahman M, Shrestha R, Kang L (2019) Improvement and validation of NASA/MODIS NRT global flood mapping. *Remote Sens* 11(2):205
- Mallick J, Talukdar S, Alsubih M, Ahmed M, Islam MT, Shahfahad AR, Thanh NV (2021) Proposing receiver operating characteristic-based sensitivity analysis with introducing swarm optimized ensemble learning algorithms for groundwater potentiality modelling in Asir region, Saudi Arabia. *Geocarto Int* 1–28
- Mahato S, Pal S (2019) Groundwater potential mapping in a rural river basin by union (OR) and intersection (AND) of four multi-criteria decision-making models. *Natural Resources Research* 28(2): pp 523–545
- Mahato S, Pal S, Talukdar S, Saha TK, Mandal P (2021) Field based index of flood vulnerability (IFV): a new validation technique for flood susceptible models. *Geoscience Frontiers* 12(5): p 101175
- Mukherjee I, Singh UK (2020) Delineation of groundwater potential zones in a drought-prone semi-arid region of east India using GIS and analytical hierarchical process techniques. *Catena* 194:104681
- Ogato GS, Bantider A, Abebe K, Geneletti D (2020) Geographic information system (GIS)-Based multicriteria analysis of flooding hazard and risk in Ambo Town and its watershed, West shoa zone, oromia regional State, Ethiopia. *J Hydrol RegNal Stud* 27:100659
- Pourghasemi HR, Rossi M (eds) (2019) *Natural hazards GIS-based spatial modeling using data mining techniques*. Springer
- Probst P, Wright MN, Boulesteix AL (2019) Hyperparameters and tuning strategies for random forest. *Wiley Interdiscip Rev Data Min Knowl Discov* 9(3):e1301
- Rahman M, Rani L, Hossain S (2020) Factors Affecting Workers Performance
- Rahman MM, Arya DS, Goel NK, Dhamy AP (2011) Design flow and stage computations in the Teesta River, Bangladesh, using frequency analysis and MIKE 11 modeling. *J Hydrol Eng* 16(2):176–186
- Shafizadeh-Moghadam H, Valavi R, Shahabi H, Chapi K, Shirzadi A (2018) Novel forecasting approaches using combination of machine learning and statistical models for flood susceptibility mapping. *J Environ Manage* 217:1–11
- Talukdar S, Singha P, Mahato S, Pal S, Liou YA, Rahman A (2020) Land-use land-cover classification by machine learning classifiers for satellite observations—a review. *Remote Sens* 12(7):1135
- Straatsma MW, Baptist MJ (2008) Floodplain roughness parameterization using airborne laser scanning and spectral remote sensing. *Remote Sensing of Environ* 112(3): pp 1062–1080
- Talukdar S, Eibek KU, Akhter S, Ziaul S, Islam ARMT, Mallick J (2021) Modeling fragmentation probability of land-use and land-cover using the bagging.random forest and random subspace in the Teesta River Basin, Bangladesh. *Ecol Indicators* 126: p 107612

- Tehrany MS, Lee MJ, Pradhan B, Jebur MN, Lee S (2014) Flood susceptibility mapping using integrated bivariate and multivariate statistical models. *Environ Earth Sci* 72(10):4001–4015
- Uhe PF, Mitchell DM, Bates PD, Sampson CC, Smith AM, Islam AS (2019) Enhanced flood risk with 1.5° C global warming in the Ganges–Brahmaputra–Meghna basin. *Environ Res Lett* 14(7):074031
- Wasko C, Nathan R (2019) Influence of changes in rainfall and soil moisture on trends in flooding. *J Hydrol* 575:432–441
- Yesilnacar E, Topal TAMER (2005) Landslide susceptibility mapping: a comparison of logistic regression and neural networks methods in a medium scale study, Hendek region (Turkey). *Eng Geol* 79(3–4):251–266
- Yin S, Bai J, Wang W, Zhang G, Jia J, Cui B, Liu X (2019) Effects of soil moisture on carbon mineralization in floodplain wetlands with different flooding frequencies. *J Hydrol* 574:1074–1084
- Yousefi S, Mirzaee S, Keesstra S, Surian N, Pourghasemi HR, Zakizadeh HR, Tabibian S (2018) Effects of an extreme flood on river morphology (case study: Karoon River, Iran). *Geomorphology* 304:30–39
- Zhang Z, Yao Q, Liu KB, Li L, Yin R, Wang G, Sun J (2021) Historical flooding regime along the Amur River and its links to East Asia summer monsoon circulation. *Geomorphology* 388:107782



Flash Flood Susceptibility Mapping Using GIS-Based AHP Method

8

Subhasish Choudhury, Amiya Basak,
Sankar Biswas, and Jayanta Das

Abstract

Proper identification of urban flash flood susceptible areas is a crucial and essential task in developing a comprehensive plan to address the adverse effects of this natural hazard. Therefore, the present study aimed to identify flood susceptible areas in Cooch Behar urban agglomeration region (CBUAR) using the simple Analytic Hierarchy Process (AHP) method. A total of twelve flash flood influencing factors were initially selected. After that, a multicollinearity test was performed prior to assigning these flood conditioning factors' weight to determine the intercorrelation of these factors. Afterward, the importance of each factor contributing to the identification of flash flood-prone areas was evaluated by assigning weightage using the AHP method. The result showed that the most important flash flood influencing factors

were LULC (26.20%), distance to river (19.00%), NDVI (14.20%), and distance to road (11.00%). Following that, a flood susceptibility map was created, which depicted 12.23%, 15.42%, 19.14%, 37.51%, and 15.70% of study areas as very high, high, medium, low, and very low susceptible flash flood susceptible areas, respectively. Finally, the flash flood susceptibility mapping was validated using receiver operating characteristic (ROC) and Area Under Curve (AUC) analysis. The validation results showed a higher AUC value (0.85), indicating this AHP method's reliability. The findings of this study will aid hydrologists, planners, and water resource managers in managing highly flash flood-prone areas and reducing potential damages.

Keywords

Flash flood · Susceptibility mapping · AHP · Validation · Cooch Behar

S. Choudhury

Centre for Himalayan Studies, University of North Bengal, PO- North Bengal University, Darjeeling 734013, India

A. Basak · S. Biswas

Department of Geography and Applied Geography, University of North Bengal, PO- North Bengal University, Darjeeling 734013, India

J. Das (✉)

Department of Geography, Rampurhat College, PO- Rampurhat, Birbhum 731224, India

8.1 Introduction

Flash flood is the most common devastating natural hazard (Tekeli and Fouli 2016; Diakakis et al. 2020) that happens on a very small spatial scale (Terti et al. 2015). It usually occurs as a result of the sudden rise in water level caused by

heavy torrential rainfall across a small region (Saharia et al. 2017; Pham et al. 2020; Lin et al. 2020; Papagiannaki et al. 2015). Besides, natural and man-made dam failures (Yang et al. 2020) or melting snow water also induce flash flood conditions. Flash flood has significant adverse effects on socioeconomic conditions, infrastructure, agriculture, ecosystems, and most importantly, a large number of human lives are lost due to this natural hazard. These adverse effects may become more widespread in the future due to constant climate change and unplanned anthropogenic activity (Bui et al. 2019). Hence, we must improve the prediction and mapping system to reduce or eliminate these effects. Because of the complexity of the flooding process, it is widely accepted that accurate and timely flood prediction is not possible (Pappenberger et al. 2006). Instead, more emphasis is placed on the spatial flood susceptibility analysis, since adverse flood consequences can effectively be reduced through proper flood susceptibility mapping. Therefore, scientists and governments have focused their efforts on developing accurate flood modeling (Tehrany et al. 2014).

Nowadays, a comprehensive assessment and proper management for flood events have attracted the widespread attention of hydrologists, planners, and water resource managers, who are usually looking for an effective and reliable technique to eliminate flood risk. In this context, developing a flood susceptibility map is considered the most fundamental and reliable technique. Flood susceptibility mapping usually applies various statistical methods to identify flood-prone areas. In order to properly manage flood, it is necessary to map the areas those are vulnerable to historical flood events. Therefore, a proper flood susceptibility mapping can also be adopted as a benchmark procedure for decision-makers to minimize flood damages (Wang et al. 2019a).

Flood susceptibility is typically associated with a variety of physical and anthropogenic factors, and spatial estimation of flood occurrence is conducted under the idea that future occurrence of flood events could happen under similar conditions that triggered previous floods

(Youssef et al. 2016). Therefore, it is crucial to identify flood conditioning factors to prevent and reduce flood damages. Moreover, these factors are conducive to understand the nature and extent of flood occurrences. In order to develop appropriate flood susceptibility mapping, we must consider a sufficient number of factors, including topographic, landcover, hydrologic, geological parameters, and their patterns (Kanani-Sadat et al. 2019). Besides, it is also important to note that effective flash flood mapping in urban environments is primarily reliant on selecting relevant flood influencing factors. Some factors contribute more, while others are less important in the occurrence of the flash flood event. Rainfall intensity, in particular, does not vary greatly across a small urban area. Consequently, in small urban areas, this factor is not considered in flash flood analysis. Besides, soil structure, texture, and nature in urban settings are not regarded as key factors in flash flood analysis. Man-made elements, on the other hand, are given remarkable importance in this analysis. Therefore, selecting relevant flood affecting factors is an essential step in designing flash flood mapping. In this study, we considered twelve flash flood conditioning factors for flash flood susceptibility mapping. The spatial map of elevation, aspect, curvature, slope, TPI, and TWI factors was made from DEM. It is pertinent to note that we created DEM file from Google Earth. During the creation of DEM, we selected more than 1,800,000 points on google earth for the study area. Afterward, we obtained a very high-quality DEM with a spatial resolution of 5 x 5 m.

In flood susceptibility mapping, choosing an appropriate method is considered a crucial step for researchers. Over time, different methods have been evolved for flood susceptibility, vulnerability and risk analysis. Souissi et al. (2019) have mentioned four broad categories of methods in flood susceptibility analysis. These methods are (1) Statistical and bivariate methods such as logistic regression (Al-Juaidi et al. 2018; Chowdhuri et al. 2020; ShafapourTehrany et al. 2019), Certainty Factor (C.F.) (Cao et al. 2020), frequency factor (F.R.) (Rahmati et al. 2016; Samanta et al. 2018; Ramesh and Iqbal 2020;

Siahkamari et al. 2018), weights-of-evidence (Rahmati et al. 2016; Khosravi et al. 2016a), Fuzzy logic (F.L.) (Sahana and Patel 2019; Bouamrane et al. 2020), (2) Expert knowledge-based methods or Multi-Criteria Decision-Making (MCDM) methods such as Technique for Order of Preference by Similarity to Ideal Solution (TOPSIS (RazaviTermeh et al. 2018) analytical hierarchy process (Das 2020; Dahri and Abida 2017; Das and Gupta 2021; Hammami et al. 2019), Vlse Kriterijumska Optimizacija I Kompromisno Resenje (VIKOR) (Akay, 2021), (3) hydrological methods such as Soil Water Assessment Tool (SWAT), Hydraulic Engineering Centre-River Analysis System (HEC-RAS) (Joshi and Shahapure 2020; Malik and Pal 2021), (4) Machine learning (ML) algorithms such as support vector machine (SVM) (Tehrany et al. 2015;), artificial neural network (ANN) (Falah et al. 2019), random forest (R.F.) (Lee et al. 2017; Chen et al. 2020), extreme gradient boosting (XGB) (Mirzaei et al. 2021; Abedi et al. 2021), Adaptive Neuro-Fuzz Inference System (ANFIS) (Vafakhah et al. 2020; Wang et al. 2019b), K-nearest neighbor (KNN) (Prasad et al. 2021). Each of these methods listed above has its own set of advantages and disadvantages. However, a considerable number of recent studies using ML-based models have noted promising outcomes compared to other methods (Khosravi et al. 2019; Nachappa et al. 2020). Generally, ML models are appropriate for areas where there is a historical dataset for the occurrence of flood events. However, these ML models are inapplicable in ungauged areas where a historical dataset of flood events is lacking (Azareh et al. 2019; Kanani-Sadat et al. 2019). In addition, ML-based models are complex and require a lot of time to get the output. Hence, scientists have been looking for a simple method to obtain reliable results for the past few decades using the limited information available. In this context, MCDM methods are the most suitable approach and these have been widely used in recent decades. These MCDM approaches, in particular, comprise a variety of mathematical models which serve a variety of purposes (Kiani

et al. 2019). As time progressed, various MCDM approaches have been developed. Among them, AHP is the most simple and usable MCDM technique. Remote sensing and GIS techniques combined with the AHP method provide a good platform for quickly and efficiently coupling, manipulating, and analyzing information to determine the potential flood susceptible areas. The spatial thematic layers of twelve flash flood influencing factors were prepared using remote sensing and GIS environment in this study. It is also worth mentioning that the most crucial aspect of using the AHP method is accurately assigning weightage to each factor. In this regard, two methods are primarily used; one is the subjective method and the other is the objective method. We applied the subjective method in this study to assign weightage to each factor and hence, each flash flood conditioning factor was given importance based on the Expert's opinion.

Cooch Behar urban agglomeration region (CBUAR) is considered as the most flash flood-prone area of West Bengal. Due to its unique topographic location, heavy rainfall, lack of proper drainage, and the presence of several perennial rivers, this region is subjected to flash floods every year. Thus, in light of the aspects mentioned earlier, the present study was conducted over the Cooch Behar urban agglomeration region. Therefore, the primary goal of this study was to identify flood susceptible areas in Cooch Behar urban agglomeration using the simple Analytic Hierarchy Process (AHP) method.

8.2 Study Area

The CBUAR is located in the mid-eastern part of Koch Bihar district, a part of the sub-Himalayan plain region (Chakraborty and Mukhopadhyay 2019). The area lies between the latitudes of 26° 17'14" N to 26°21'12" N and longitudes of 89° 25'15" E to 89°29'21" E. It comprises with Cooch Behar urban area along with some peri-urban areas, which are denoted as census town (Census of India 1971, 1981, 2001, 2011), i.e.,

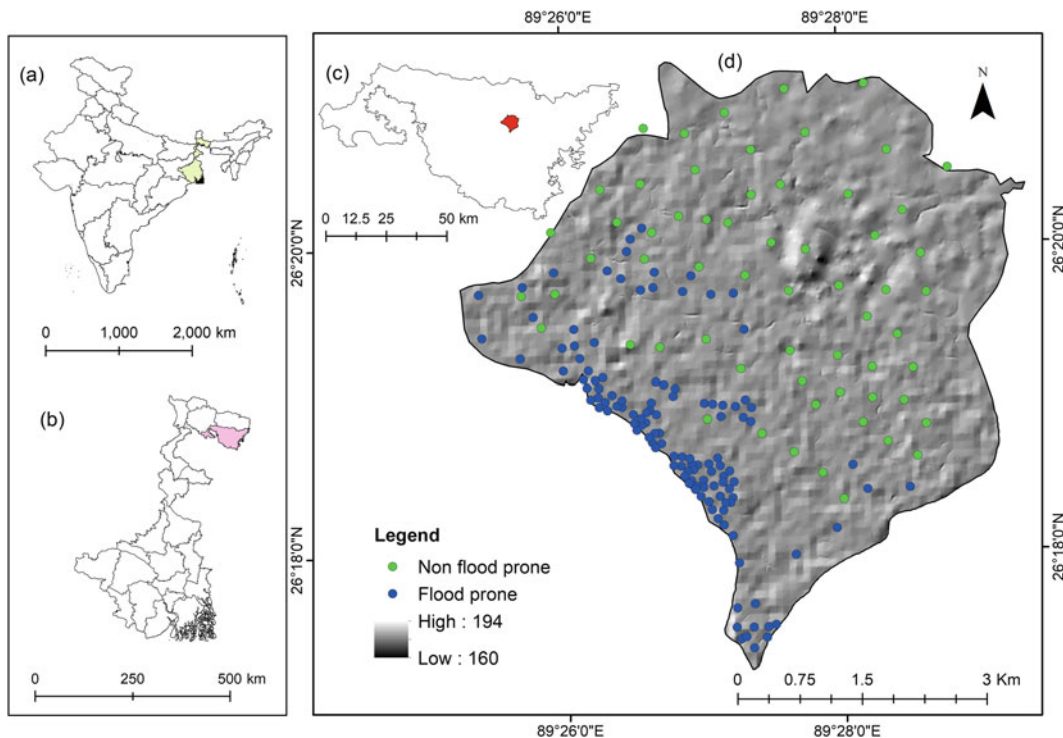


Fig. 8.1 Location map of the study area

Guriahati and Chakchaka in the east; Kharimala Khagrabari and Baisguri in the north-east; Kha-grabari in the north and Takagachh in the west and termed as Cooch Behar urban agglomeration (Fig. 8.1). The total area of the present study area is 26.15 km². Topographically, the study area is flat with a slight south-western slope and the elevation varying from 37.60 to 60.0 m. (Debnath 2007). The river Torsa and its tributaries are flowing across the study area. Most parts of the study area use for settlement and commercial purposes (Choudhury et al. 2011). The study area experiences a typical subtropical monsoon climate characterized by hot and humid summer and cold and dry winter with high annual rainfall and moderate temperature (Pradhan et al. 2020). The annual average rainfall is 3773 mm and the average summer temperature is about 24.68 °C and the winter temperature is about 17.30 °C (India Meteorological Department 2020). About

70% of the annual rainfall is received during June–September when the southwest monsoon season has prevailed in the study area (Gupta and Singh 2017). The main reasons behind the overwhelming occurrences of flash flooding include an extra precipitation runoff of rainwater; more sediment accumulates in the river bed, the unattainability of forest area and open space and the effect of tropical southwest monsoon.

8.3 Materials and Methods

8.3.1 Data Sources

In the present study, twelve flash flood influencing factors, namely, elevation, aspect, curvature, slope, LULC, NDVI, NDWI, distance to road, distance to the river, annual rainfall, TPI and TWI, were considered for the flash flood

Table 8.1 Data collection and preparation

Sl. no.	Data types	Data format	Spatial resolution/scale	Sources of data	Derived map
1	DEM	Raster	5 m	Google earth	Elevation, aspect, curvature, slope, distance to river, TPI, TWI
2	Sentinel—2	Raster	10 m	https://earthexplorer.usgs.gov	NDVI, NDWI, LULC
3	Open street map	Vector	1:8000	https://www.openstreetmap.org	Distance to road
4	Meteorological data	Point	–	www.imdpune.gov.in	Rainfall map

susceptibility mapping (Khosvari et al. 2016b; Khosvari et al. 2019; Kanani-sadat et al. 2019; Costache et al. 2019; Chakraborty and Mukhopadhyay 2019; Souissi et al. 2020; Arabameri et al. 2020; Pham et al. 2020; Haque et al. 2021). It is worth noting that we created the DEM file from Google Earth. When creating the DEM, we selected about two million points in Google Earth for the study area. After which, a very high-quality DEM with a spatial resolution of 5×5 m was obtained. A detailed data sources of these factors is given in Table 8.1.

8.3.2 Flood Inventory Map

The preparation of a flood inventory map is viewed as a crucial prerequisite step in flood susceptibility assessments. Generally, a historical flood record obtained from a flood inventory map can be used to analyze flood risks in a specific place (Khosravi et al. 2018). A flood inventory map of CBUAR was prepared using available 122 flood event points drawn from the data collected by a comprehensive field survey. The field survey was done to collect primary data by interviewing such residents and photographs of the various localities during June 2020 to September 2020 (monsoon period). We indicated two sorts of points (flash flood and non-flash flood point) in our study region based on the data collected from the respondents. Afterward, the flash flood points were processed and validated in Google Earth.

8.3.3 Selection of Flash Flood Influencing Factors

8.3.3.1 Elevation

Elevation is considered as a key factor in flash flood susceptibility mapping. (Nachappa et al. 2020). It is defined as the difference between highest and lowest point in a particular region. Generally, the surface water flows from higher to lower areas. As a consequence, the lower region is subjected to flash floods due to the constant flow of surface water (Pham et al. 2020). In this study, the elevation map was classified into five categories: very high (37.60–40), high (40.01–45), moderate (45.01–50), low (50.01–55), and very low (55.01–60 m) susceptible areas.

8.3.3.2 Aspect

The direction of slope in earth surface is known as slope aspect. It greatly controls the convergence and direction of surface water flow (Mohammadi et al. 2020). Hence, it can be identified as a key factor in developing the flood susceptibility map. In this study, we classified the slope aspect map into two categories: high (360) and low (0).

8.3.3.3 Curvature

Another important factor in determining the severity of a flash flood is curvature, representing the earth's shape. This component has an important role in regulating surface water flow and infiltration process. In this study, curvature was categorized into three groups: Positive

curvature (convex), negative curvature (concave), and zero curvature (flat) (Chapi et al. 2017). The region of concave curvature is more susceptible to flash floods compared to convex curvature.

8.3.3.4 Slope

In general, surface slope has a significant impact on a variety of hydrological processes, particularly on infiltration process and surface water flow (runoff) (Ngo et al. 2021). Therefore, it can be regarded as a significant factor in flash flood susceptibility mapping. Infiltration process is comparatively lower on steep gradient slopes, while speed of surface water (runoff) becomes greater on steeper slopes. This excessive surface water flow (runoff) on flat regions causes flash flood condition. As a consequence, flat regions nearer to higher slopes are frequently subjected to flash flood events. We classified the slope map into five classes: very low ($0-1.81^\circ$), low ($1.81-3.62^\circ$), moderate ($3.61-5.43^\circ$), high ($5.44-7.24^\circ$), and very high ($7.25-9.05^\circ$).

8.3.3.5 LULC

Landscapes in a particular location are mostly modified as a result of changing the LULC map (Vignesh et al. 2021). The LULC map is a key component in determining flood-prone areas since it has a significant role in numerous hydrological processes such as evaporation, runoff, evapotranspiration, and infiltration (Rahmati et al. 2016; Souissi et al. 2020). Thematic maps of LULC usually include buildings, roads, bare lands, vegetation cover, agricultural areas, and water bodies, etc. We created a LULC map for the present study, which contained five features: water bodies, plant cover, built-up area, agricultural land, and open areas.

8.3.3.6 NDVI

The Normalized Difference Vegetation Index (NDVI) is a useful graphical index that depicts the distribution of healthy vegetation in a particular region. Besides, infiltration capacity and surface water flow are also dependent on the vegetation cover. Hence, it can also be adopted

as a significant factor in determining flood susceptibility areas. This index was usually derived from satellite image. The NDVI is computed by the following equation:

$$\text{NDVI} = \frac{P_{\text{NIR}} - P_{\text{R}}}{P_{\text{NIR}} + P_{\text{R}}} \quad (8.1)$$

where, P_{NIR} represents reflectance in the form of infrared portion and P_{R} represents reflectance in the for red.

The NDVI value is ranged between -1 and $+1$. In this study, the obtained NDVI map was classified into five categories: very low ($-0.03 -0.00$), low ($0.00-0.28$), moderate ($0.29-0.35$), high ($0.36-0.43$), and very high ($0.44-0.61$) susceptible areas.

8.3.3.7 NDWI

NDWI is typically applied to identify the water bodies in a specific region (McFeeters 1996). In fact, this index is capable of properly collecting water-related data compared to another index. It is widely accepted that the locations with higher NDWI values are more vulnerable to flash flood events. NDWI is computed by the following equation:

$$\text{NDWI} = \frac{\text{NIR} - \text{SWIR}}{\text{NIR} + \text{SWIR}} \quad (8.2)$$

where, INR defines the near-infrared band and SWIR presents the Short-Wave infrared bands.

The NDWI value also ranges from -1 to $+1$. In this study, the NDWI was classified into five groups namely very high ($0.01-0.11$), high ($-0.24 -0.00$), moderate (-0.31 to -0.25), low (-0.37 to -0.32), and very low (-0.54 to -0.38) susceptible areas.

8.3.3.8 Distance to Road

The distance of any location from the road is another important factor in determining flash flood susceptible places. Roads, in fact, slow down the infiltration process by preventing water from entering the ground. As a result, areas with a high density of roadways are inundated by light rain and hence, creating a flash flood situation. Furthermore, regions closer to the road are more

prone to flash floods due to less infiltration and a faster runoff process. In this study, we divided the spatial map of distance to road into five classes: very high (0–36.31 m), high (36.32–86.74 m), moderate (86.75–155.33 m), low (155.34–215.15 m), and very low (250.16–514.42 m).

8.3.3.9 Distance to River

The severity and extent of a flood in a region are primarily determined by the distance from the river to that location. Generally, distance from the river is widely considered to be disproportionately connected with the flash flood occurrence. Hence, flash flood is a common phenomenon in areas that are close to rivers. Contrarily, places far away from river are less vulnerable in terms of flood damages (Souissi et al. 2020). We divided the spatial map of distance to river into five classes: very high (0–250 m), high (251–500 m), moderate (501–775 m), low (776–1000 m), and very low (1001–1617 m).

8.3.3.10 Rainfall

Rainfall has the greatest impact on the occurrence of flash flood events among the various climatic components of climate. It is considered as the principal source for surface runoff (Pham et al. 2020). Flash floods are usually caused by increased surface water flow as a result of intense torrential rainfall over a smaller area. Therefore, the flash flood events are proportionate to the amount of rainfall. In the “Arc GIS environment,” the inverse Distance Weighted (IDW) interpolation tool is used to prepare the rainfall distribution map. Afterward, the obtained map was classified in five categories. These categories are very high (5538–5556 mm), high (5527–5537 mm), moderate (5517–5526 mm), low (5510–5516 mm), and very low (5494–5509 mm) susceptible areas.

8.3.3.11 TPI

TPI is the most important morphometric factor defined by the difference between focused and

neighbor cells (Costache et al. 2019). This indicator is used as another factor for developing susceptibility mapping since it has a significant influence on runoff. It is often assumed that areas with lower TPI values are more susceptible to flash floods. For the present study, we classified the thematic TPI map into five groups. These groups are very high (–2.92 to –0.75), high (–0.74 to –0.25), moderate (–0.24–0.00), low (0.01–0.74), and very low (0.75–3.74) susceptible areas.

8.3.3.12 TWI

TWI is a prominent terrain-derived parameter that assesses topographic effects on some hydrological processes, especially flood events (Khosravi et al. 2018; Tehrani et al. 2015). In general, a higher TWI score implies a greater susceptibility of a specific region to flash flood events. For the present study, we developed a TWI map and classified it into five classes as very low (0.00–35), low (0.36–1.46), moderate (1.47–2.47), high (2.88–4.35), and very high (4.36–7.99) susceptible groups.

8.3.4 Multicollinearity Test

It is necessary to perform a multicollinearity test if we take many independent factors. In a regression model, multicollinearity is defined as the existence of a linear relationship between independent variables (Al-Juaidi et al. 2018). When a researcher evaluates the influence of each independent variable on the dependent variable, multicollinearity can lead to misleading results. It also examines if an input variable can be predicted linearly from other input variables, resulting in a result with a non-trivial degree of accuracy (Basak et al. 2021). Before using any regression model, it is necessary to validate multicollinearity among these input variables.

In this test, R is first determined and afterward, the value is again used to calculate tolerance and VIF (variance inflation factor) of input variable applying to Eqs. 8.3 and 8.4:

$$Tolerance\ of\ the\ i\ th\ predictor\ variable\ (T_i) = 1 - R_i^2 \tag{8.3}$$

$$VIF\ of\ the\ i\ th\ predictor\ variable\ (VIF_i) = 1/T_i \tag{8.4}$$

The processes have been performed for each independent factor, and VIF and tolerance have been calculated for individual input variables. Multicollinearity issues arise when the VIF value is ≥ 10 and the tolerance value is <0.10 . (Saha 2017). For this work, we performed multicollinearity test in ‘‘R’’ environment. Table 8.2 shows the results of the multicollinearity test. The tolerance value of >0.10 and VIF value of <10 for each flash flood influencing factor ($p < 0.01$, $p < 0.05$) revealed that there is no collinearity issue among the flood influencing factors.

8.3.5 Analytical Hierarchy Process (AHP)

AHP is a useful and widely used multicriteria decision method, which is first introduced by Saaty in 1980. It is typically used to rank factors in order to determine the most dominant factor based on Expert opinion (Das 2017). In this study, a total of twelve flash flood influencing factors were incorporated for developing the flash flood susceptible areas.

8.3.5.1 Pairwise Comparison Matrix

Based on the selected flash flood influencing factors, we created a pairwise comparison matrix table. Following that, each factor was assigned a specific weight based on the Expert’s opinion. As stated in Table 8.2, the relative importance or value was assigned using the scale relative importance. It is pertinent to mention that the length of the comparison matrix table is equivalent to the number of factors selected in the specific study. In the comparison matrix table, factors weight, class weight, and the CR value were computed, as shown in Table 8.6. For the computation of CR value following expression is used (Saaty 1980, 2000):

$$CR = \frac{CI}{RI} \tag{8.5}$$

8.3.5.2 Consistency Index (CI)

For testing the consistency of results, the rule of transitivity is commonly used. The value of λ_{max} is computed by the following expression:

$$\lambda_{max} = \sum_{j=1}^n a_{ij} \frac{w_j}{w_i} = n \tag{8.6}$$

The obtained CR value determines the consistency of the matrix. If $CR = 0$, the matrix will be consistent, however, a value of >0 indicates that the matrix is inconsistent. To eliminate type

Table 8.2 Saaty’s 9 intensity scale

Degree of importance	Linguistic scale	Description
Equally	1	Two exercises contribute equally to the target
Intermediate	2	Intensity between 1 and 3
Moderately	3	The judgment moderately favors one action over another
Intermediate	4	Intensity between 1 and 5
Strongly	5	The judgment essentially or strongly favors one action over another
Intermediate	6	The intensity between 1 and 7
Very strongly	7	Very strong importance and viewed as better than another
Intermediate	8	The intensity between 1 and 9
Extremely	9	Proof that favors one exercise over another

II error, Saaty (1980) proposed the consistency of the matrix (CR.10). In the present study, the computed CR value was 0.089.

In most cases, max does not equal to n. As a result, we evaluated CI to see if the transitivity criteria were violated or not. The following equation was used to calculate CI:

$$CI = \frac{\lambda_{\max} - n}{n - 1} \quad (8.7)$$

8.3.6 AUC and ROC Analysis

ROC and AUC curve is one of the most acceptable performance metrics methods for the validation of the AHP model. ROC curve is a graph of the interrelationship between sensitivity and 1-specificity, which recognizes an area under itself called AUC. AUC is very suitable for assessing the accuracy of flash flood modeling. The AUC ranges between 0 and 1. A higher AUC value represents the excellent quality of the model; contrarily, a lower value indicates unsatisfactory adaptation of the model. The AUC value of the present study was 0.85 (very good model: 0.8–0.9, Grozavu et al. 2017), which showed that the AHP model is suited for recognizing flash flood susceptibility zonation for the current research.

8.4 Results and Discussion

8.4.1 Development of Flash Flood Influencing Thematic Layers

The elevation is a critical factor in determining the flash flood susceptibility mapping in any region. The lowest value of the elevation was 37.60 m and the highest elevation value was 60.00 m in the study area (Fig. 8.2a). The light blue color area of the map indicates low elevation, which was found sporadically in the marginal eastern part. The red portion of the map indicates high elevation, particularly in the most

central part of the study area. Although, the maximum area belonged to very low and moderate classes. The very low elevation was found in the eastern, north-eastern, and western part of the study area. On the other hand, moderate elevation was found mainly in the southern and south-western portions of the study area.

Aspect is a crucial topographic factor for flash flooding. It is indirectly affecting the directions of water flow in the flooded area. It also affects the humidity of soil with extreme runoff. The green portion of the study area indicates a lower aspect value and the red portion indicates the high aspect value at a range between 0 and 360 (Fig. 8.2b). The aspect value was distributed sporadically throughout the study area.

The curvature affects the flooding water budget directly in the study area. The curvature of the study area was categorized into three sub-groups, which were convex, flat, and concave. The blue portion of the map shows the concave curvature in the study area, which is greatly susceptible to flash flooding in the rainy season. On the other hand, the yellow portion of the study area indicates convex curvature, which is less susceptible to flash flooding (Fig. 8.2c). Except for the north-eastern parts, the whole study area belonged under a concave slope.

The slope map of study area was categorized into five different classes. The highest slope value ranged between 7.25 and 9.05°, while the lowest slope value was ranged between 0 and 1.81° (Fig. 8.2d). The light blue portion shows the lower slope occupying most of the study area. In contrast, a comparatively higher slope value was noticed in some dispersed and nominal parts of the study area. LULC is another key factor in determining flood susceptibility mapping. LULC of the study area was divided into five categories: vegetation cover, build-up area, agriculture area, water bodies, and open space. The build-up area occupied the maximum area, 30.51% and the water body occupied the minimum area of about 2.36% (Fig. 8.3a). The build-up area of the study area directly affects the surface runoff and infiltration. Thus, the build-up area is more susceptible to flash flood. In contrast, vegetation cover

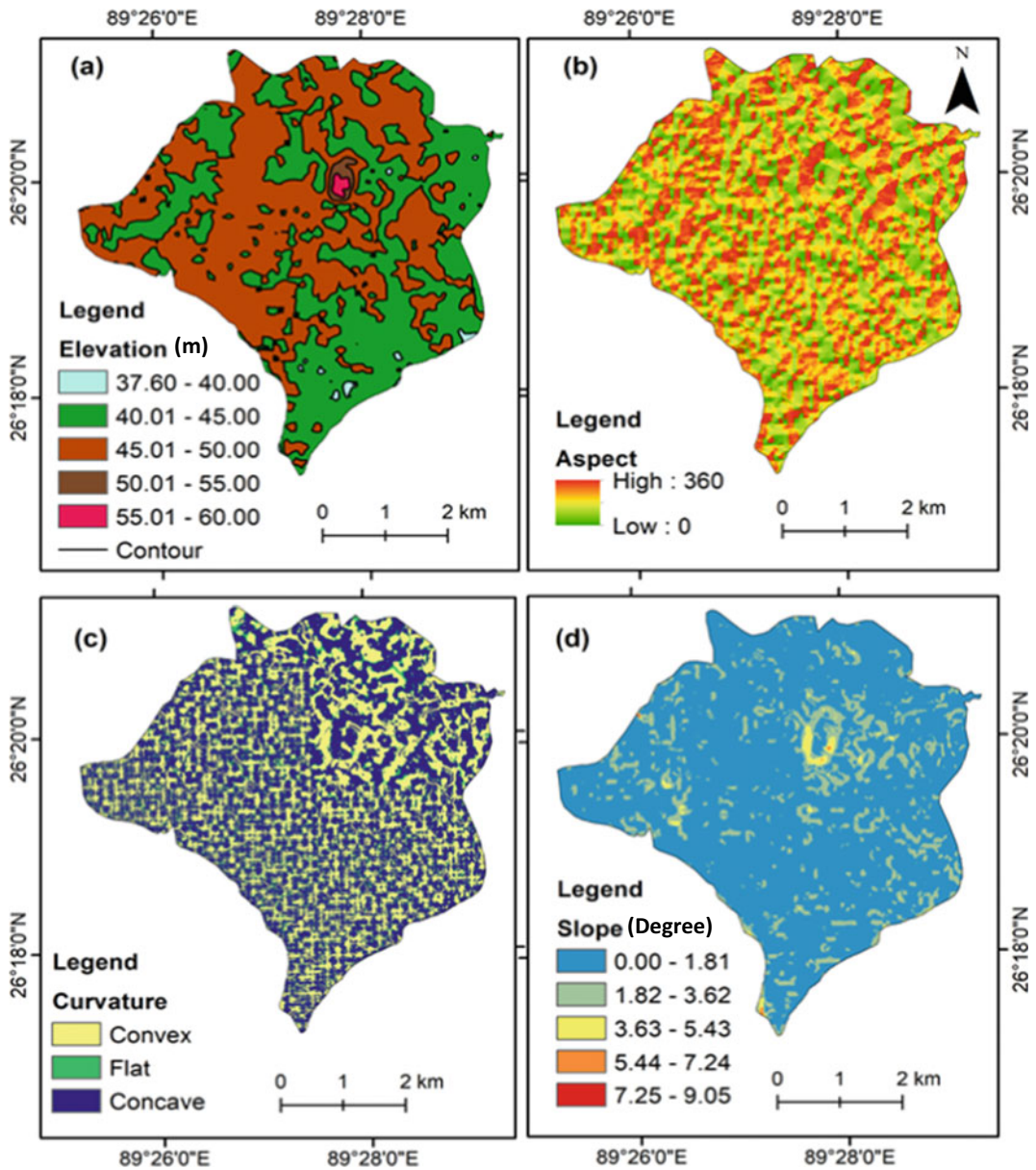


Fig. 8.2 Thematic layer of **a** Elevation, **b** Aspect, **c** curvature, and **d** Slope factor

permits infiltrating flooded water and open space allows surface runoff and hence, the areas with vegetation cover are less susceptible to flood.

NDVI is one of the crucial factors for flash flood susceptibility mapping. The NDVI of the study area was categorized into five classes that ranging from -0.03 to 0.61 (Fig. 8.3b). The red areas are indicating less vegetation and the green

portion indicating dense vegetal cover. From western, south-western to the central part of the study area is experienced to be less vegetation cover obtaining the value range between 0.01 and 0.28 compared to the other parts of the study area. Thus, the area frequently experienced flood occurrences as less vegetal cover fails to infiltrated rainwater. On the other hand, marginal

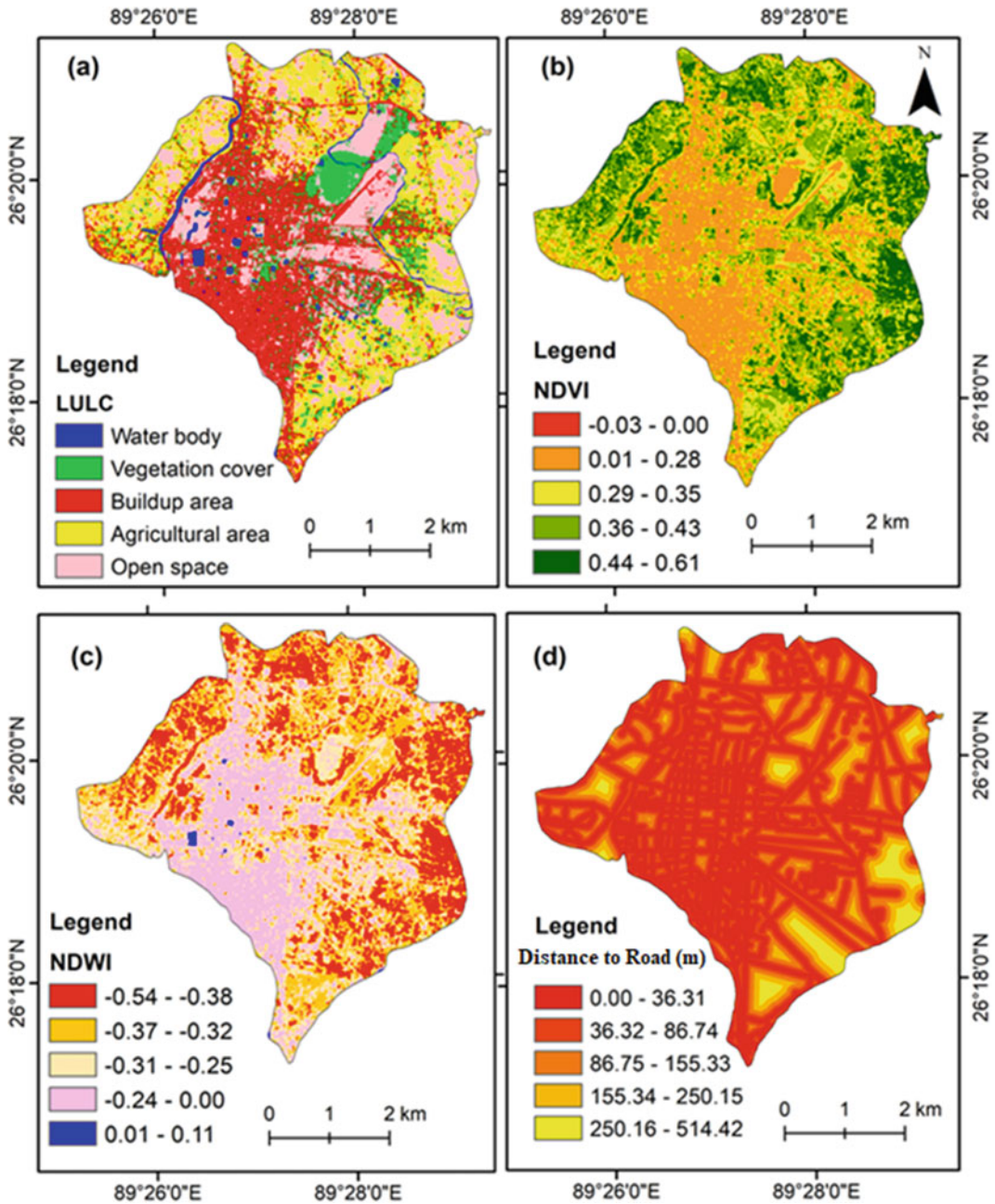


Fig. 8.3 Thematic Layer of **a** Land use/Land cover (LULC), **b** Normalized Difference Vegetation Index (NDVI), **c** Normalized Difference Water Index (NDWI), and **d** Distance to Road

eastern, north-eastern, and northern parts having the highest value ranging between 0.44 and 0.61, representing thick vegetal cover. NDWI was categorized into five classes which was ranged from -0.54 to 0.11 (Fig. 8.3c). The red portion

shows the lowest value of NDWI observed in the north-western, northern, north-eastern, and eastern parts of the study area; thus, this area is generally experienced with low flash flood susceptibility. On the other hand, the pink and blue

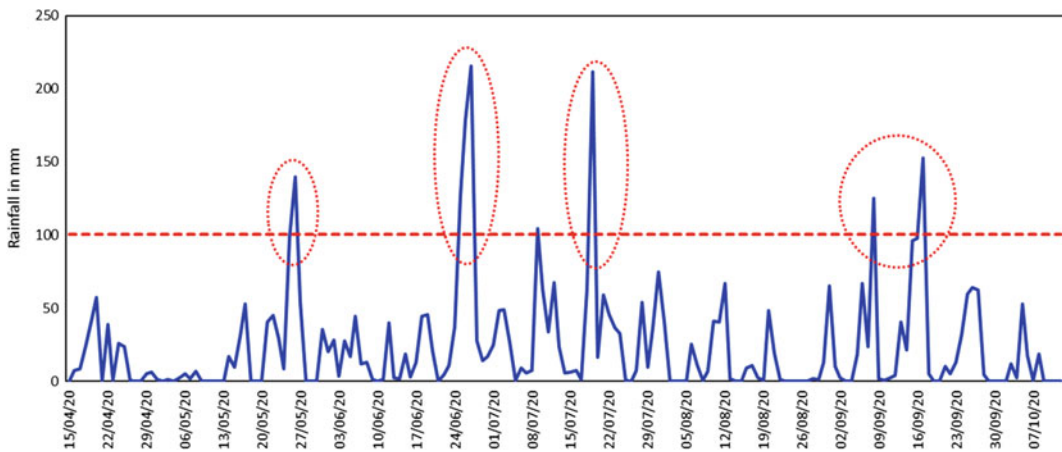


Fig. 8.4 Annual rainfall graph with threshold point

portion indicates the higher value of NDWI, which experienced more flash flood susceptibility. It was observed in the western, south-western to central parts of study area.

Distance to the road is a crucial factor for flash flood susceptibility mapping in the study area, which obstructs the infiltration process of rain-water that causes a devastating flash flood. Distance to road was classified into five classes that ranged from 0.00 to 514.42 (Fig. 8.3d). It was observed from the study that the flash flood inundation areas are usually located near to road of the study area with the lowest value and indicated by the red color. On the other hand, the higher of this factor usually less susceptible to flash flood.

Distance of any area from the river is an essential conditioning factor for the flash flood vulnerability in the study area. The value of distance to the river was ranged between 0 and 1617 m (Fig. 8.5a). Places with lower value usually experience higher occurrence of flash flood. Contrarily, places with higher value indicates a less flood-prone area. North-eastern, south-western, and western parts are far away from the river.

Annual rainfall is another essential factor to flash flood susceptibility in the study area. The map shows that the study area was classified into five annual rainfall classes, ranging between 5494 and 5556 mm (Fig. 8.5b). The annual

amount of rainfall consecutively increased from the western parts to the eastern parts of the study area. Eastern parts of the study area experienced less annual rainfall. In contrast, the western parts of the study area experienced less annual rainfall due to the increasing nature of the build-up area. Figure 8.4 also shows the threshold value graphically in annual rainfall (15/04/2020–07/10/2020). In this figure, the threshold value of 100 mm rainfall was exceeded five times during this period.

A positive TPI indicates a higher altitudinal position of the central point compared to the adjacent area. On the contrary, a negative value of TPI illustrates a lower altitude at the central point relative to the neighboring areas. The TPI value of the study area was ranged between -2.92 and 3.74 (Fig. 8.5c).

The value of TWI ranged between 0 and 7.99 (Fig. 8.5d). The higher value of TWI indicates lower possibility of flash floods. On the contrary, the lower value of TWI represents the decreasing rate of moisture which accelerates the flooding possibility in the study area.

8.4.2 Multicollinearity Test

The results of the Multicollinearity test (Table 8.3) revealed that the NDWI had the highest VIF (7.285), followed by NDVI,

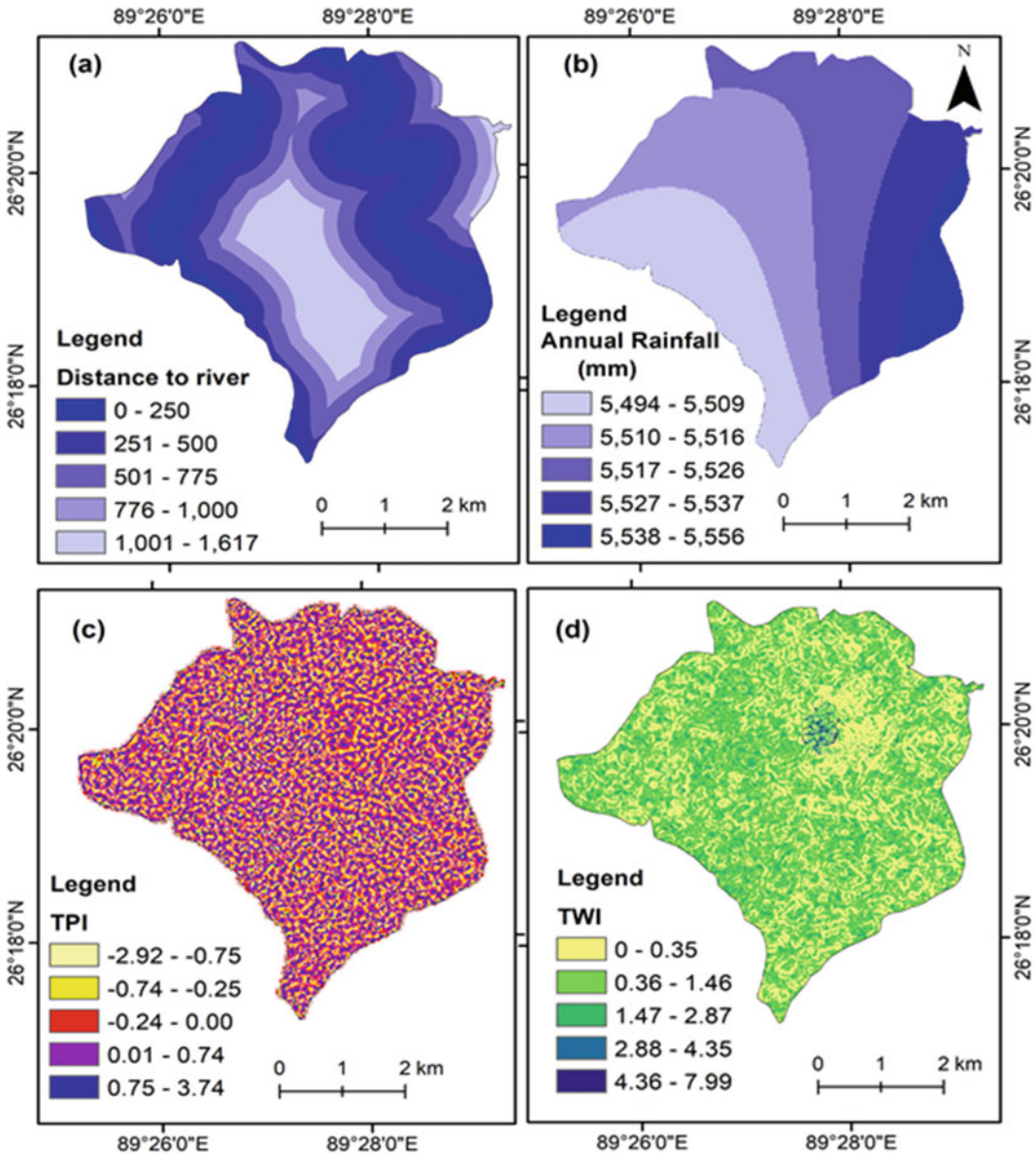


Fig. 8.5 Thematic layer of **a** Distance to River, **b** Annual Rainfall, **c** Topographic Position Index (TPI), **d** Topographic Wetness Index (TWI)

elevation, distance to the road, distance to the river, curvature, TPI, slope, aspect, annual rainfall, LULC, and TWI respective. The results also portrayed no collinearity issue among the twelve selected parameters adopted for the study. Additionally, the statistical R^2 value between flash flooding and its factors can be seen in Table 8.3. Douglas et al., 2000 in their study

mentioned that a higher R^2 value intensifies flash flood events. In this study area, the occurrence of flash flood events had been noticed where the elevation is <50 m, aspect is flat, the curvature is concave, the slope is $<1.81^\circ$, land use and land cover occupied by build-up area, NDVI is <0.28 , NDWI is >-0.24 , distance to the road is minimum (<155.33 m), distance to the river

Table 8.3 Multicollinearity Statistics of selected flash flood influencing factors

Sl no.	Factors	R ²	Tolerance	VIF
1	Elevation	0.313	0.687	1.456
2	Aspect	0.079	0.921	1.085
3	Curvature	0.114	0.886	1.129
4	Slope	0.085	0.915	1.093
5	LULC	0.031	0.969	1.032
6	NDVI	0.859	0.141	7.107
7	NDWI	0.863	0.137	7.285
8	Distance to road	0.230	0.770	1.299
9	Distance to river	0.137	0.863	1.159
10	Rainfall	0.070	0.930	1.075
11	TPI	0.105	0.895	1.117
12	TWI	0.017	0.983	1.017

is <1000 m, annual rainfall is about 5500 mm, TPI belonging negative value, and the value of TWI is <2.87.

8.4.3 Assessment of Flash Flood Influencing Factors for Developing Susceptibility Map

The present study considered twelve major flood influencing factors (elevation, aspect, curvature, slope, LULC, NDVI, NDWI, distance to road, distance to river, annual rainfall, TPI, and TWI) in developing the flood susceptibility map. For this study, a comparison matrix table (Table 8.4) was created for comparing these factors and subfactors. In this regard, we also calculated the randomness index among the factor and subfactors (Table 8.4). Thereafter, the CR value was then computed, and the obtained CR value was 0.089. Hence, it is appropriate to claim that such factors and subfactors can reasonably be taken into consideration for AHP analysis.

Table 8.7 represents the relative importance of each factor and its subfactors in the study. It is evident from Table 8.7 that the LULC (26.20%) was the most important factor in determining the flash flood susceptible zones. Among the

subfactors of LULC thematic layer, the built-up area was the most important subfactor in identifying the flash flood susceptible areas. The built-up regions cover the majority of the study area, and these built-up areas, particularly roads and buildings, have a considerable impact on some hydrological processes. More importantly, the built-up regions have a significant impact on infiltration capacity and surface runoff. The infiltration capacity is generally substantially reduced by these built-up areas, and hence, surface runoff water flourished into the study area. Thus, the LULC factor may be regarded as the most essential factor in determining flash flood-prone areas. After the LULC, NDVI (14.20%) and distance to river (19.00%) were the next most important factors (11.00% that have a substantial role in determining the flash flood susceptible areas. Ngo et al. (2021) in their study identified LULC, slope, curvature, and TWI factors as the most important factor in developing flash flood susceptibility map. However, in the study, curvature (1.20%), slope aspect (1.20%), TPI (1.90%), and TWI (2.60%) were identified as the least affected factors. All of these factors had little influence in developing flood susceptibility map of study area. This is probably due to the fact that all of these elements occupy less surface area in urban areas.

Table 8.4 Pairwise comparison matrix table

Parameter	EL	AS	CR	SL	LULC	NDVI	NDWI	DR	DRI	RF	TPI	TWI
EL	1	5	6	2	1/7	1/3	1/2	1/3	1/4	3	4	3
AS	1/5	1	2	1/5	1/9	1/7	1/6	1/7	1/8	1/4	1/2	1/3
CR	1/6	1/2	1	1/5	1/9	1/9	1/8	1/8	1/9	1/5	1/3	1/4
SL	1/2	5	5	1	1/7	1/5	1/3	1/4	1/6	2	4	3
LULC	7	9	9	7	1	3	5	4	2	8	9	9
NDVI	3	7	9	5	1/3	1	3	2	1/2	6	8	7
NDWI	2	6	8	3	1/5	1/3	1	1/2	1/4	4	6	7
DR	3	7	8	4	1/4	1/2	2	1	1/3	5	7	6
DRI	4	8	9	6	1/2	2	4	3	1	7	9	8
RF	1/3	4	5	1/2	1/8	1/6	1/4	1/5	1/7	1	3	2
TPI	1/4	2	3	1/4	1/9	1/8	1/6	1/7	1/9	1/3	1	1/2
TWI	1/3	3	4	1/3	1/9	1/7	1/5	1/6	1/8	1/2	2	1

Table 8.5 Randomness Index (R.I.) for different number factors (N) used to calculate consistency (Saaty and Vargas 1991)

N	3	4	5	6	7	8	9	10	11	12	13	14	15
RI	0.58	0.9	1.12	1.24	1.32	1.41	1.45	1.51	1.52	1.54	1.56	1.58	1.59

Table 8.6 Results for checking the consistency of AHP model

λ_{max}	N	RI	CI	CR	Consistency check
13.51	12	1.54	0.137	0.089	CR < 0.1(yes)

8.4.4 Flash Flood Susceptibility Mapping

The most important aspect in developing flash flood susceptibility map is to precisely identify the areas that will be flooded in the future. And in this regard, another important thing is to validate the obtained susceptibility map. In this study, a flash flood susceptibility map was prepared by incorporating the twelve flood influencing layers. Based on the natural breaking slope method in the “ArcGIS 10.4 environment,” the obtained susceptibility was classified into five

groups: very high, high, moderate, low, and very low susceptible areas. According to Fig. 8.6, the major portions of northwestern, southwestern, and some parts of north-eastern areas were classified as more susceptible areas to flash floods. This finding was also accorded with the observations of flood inventory maps, which showed that the northwestern and southwestern areas of the study area were more vulnerable to flash floods. A variety of administrative centres, residential areas, road, financial institutes, educational institutes, health centres, recreation centers (such as parks and cinema halls) have

Table 8.7 Weightage of each factor and subfactors in developing flood susceptible map of CBUAR

Sl no.	Factors	AHP foe each factor	Sub factors	Descriptive level (flood hazard)	Area in km ²	Area in %	AHP weight for subfactor
1	Elevation	0.059	37.60–40.00	Very high	0.13	0.49	0.446
			40.01–45.00	High	11.96	45.60	0.301
			45.01–50.00	Moderate	13.88	52.93	0.142
			50.01–55.00	Low	0.18	0.67	0.075
			55.01–60.00	Very low	0.08	0.30	0.036
2	Aspect	0.015	North (0–22.5°)	Very low	4.84	18.45	0.052
			North (337.5–360°)				
			Northeast (22.5–67.5°)	Medium	7.12	27.15	0.164
			East (67.5–112.5°)	Low	6.45	24.61	0.1
			Southeast (112.5–157.5°)				
			South (157.5–202.5°)	Very high	6.22	23.73	0.404
			Southwest (202.5–247.5°)				
			West (247.5–292.5°)	High	1.59	6.06	0.28
Northwest (292.5–337.5°)	1.59	6.06					
3	Curvature	0.012	Convex	Very low	10.10	38.51	0.164
			Flat	High	2.40	9.16	0.297
			Concave	Very high	13.72	52.33	0.539
4	Slope	0.046	0.00–1.81	Very high	22.01	83.94	0.446
			1.82–3.62	High	3.97	15.14	0.301
			3.63–5.43	Moderate	0.23	0.86	0.142
			5.44–7.24	Low	0.02	0.06	0.075
			7.25–9.05	Very low	0.00	0.00	0.036
5	LULC	0.262	Water body	Moderate	0.62	2.36	0.131
			Vegetation cover	Very low	3.23	12.30	0.035
			Buildup area	Very high	8.00	30.51	0.506
			Agricultural area	High	7.12	27.17	0.265
			Open space	Low	7.25	27.65	0.063
6	NDVI	0.142	–0.03–0.00	Very high	0.00	0.01	0.446
			0.01–0.28	High	8.83	33.67	0.301
			0.29–0.35	Moderate	6.08	23.17	0.142
			0.36–0.43	Low	7.11	27.11	0.075
			0.44–0.61	Very low	4.20	16.04	0.036

(continued)

Table 8.7 (continued)

Sl no.	Factors	AHP foe each factor	Sub factors	Descriptive level (flood hazard)	Area in km ²	Area in %	AHP weight for subfactor
7	NDWI	0.083	-0.54 to -0.38	Low	5.45	20.80	0.075
			-0.37 to -0.31	High	7.82	29.82	0.036
			0.31 to -0.25	Very low	6.30	24.04	0.301
			-0.24-0.00	Very high	6.59	25.14	0.446
			0.01-0.11	Moderate	0.05	0.19	0.142
8	Distance to road	0.11	0.00-36.31	Very high	12.03	45.87	0.446
			36.32-86.74	High	7.64	29.15	0.301
			86.75-155.33	Moderate	3.86	14.73	0.142
			155.34-250.15	Low	1.84	7.02	0.075
			250.16-514.42	Very low	0.85	3.23	0.036
9	Distance to river	0.19	0-250	Very high	6.77	25.81	0.503
			251-500	High	6.53	24.89	0.26
			501-775	Moderate	6.27	23.92	0.134
			776-1000	Low	2.98	11.37	0.068
			1001-1617	Very low	3.67	14.00	0.035
10	Rainfall	0.035	5494-5509	Very high	6.25	23.84	0.416
			5510-5516	High	7.57	28.85	0.262
			5517-5526	Moderate	6.92	26.38	0.161
			5527-5537	Low	3.71	14.13	0.099
			5538-5556	Very low	1.78	6.80	0.062
11	TPI	0.019	-2.92 to -0.75	Very high	2.95	11.13	0.415
			-0.74 to -0.25	High	5.98	22.60	0.306
			-0.24-0.00	Moderate	4.85	18.32	0.164
			0.01-0.74	Low	9.66	36.51	0.071
			0.75-3.74	Very low	3.03	11.44	0.044
12	TWI	0.026	0-0.35	Very low	7.99	32.84	0.044
			0.36-1.46	Low	10.78	44.32	0.071
			1.47-2.87	Moderate	5.44	22.37	0.164
			2.88-4.35	High	0.08	0.32	0.306
			4.36-7.99	Very high	0.04	0.16	0.415

been developed in these areas. Hence, a dense built-up area and dense road network (Fig. 8.3) have been grown-up in these areas which reduce infiltration capacity and increase surface runoff. Furthermore, as compared to other areas, the values of some parameters such as distance to river (<250 m), elevation (<45 m), and slope (<1.82°) were lower in these south-western and northwestern regions (Figs. 8.2 and 8.5). These

are the most probable reasons why the north-western and southwestern areas were depicted as highly susceptible areas to flash flood.

Another notable finding is that places that received more rainfall were not considered as high susceptible areas. This suggests that rainfall in smaller urban regions may not play a significant role in flash flood occurrence. Conversely, Anthropogenic factors (Built-up area, high road

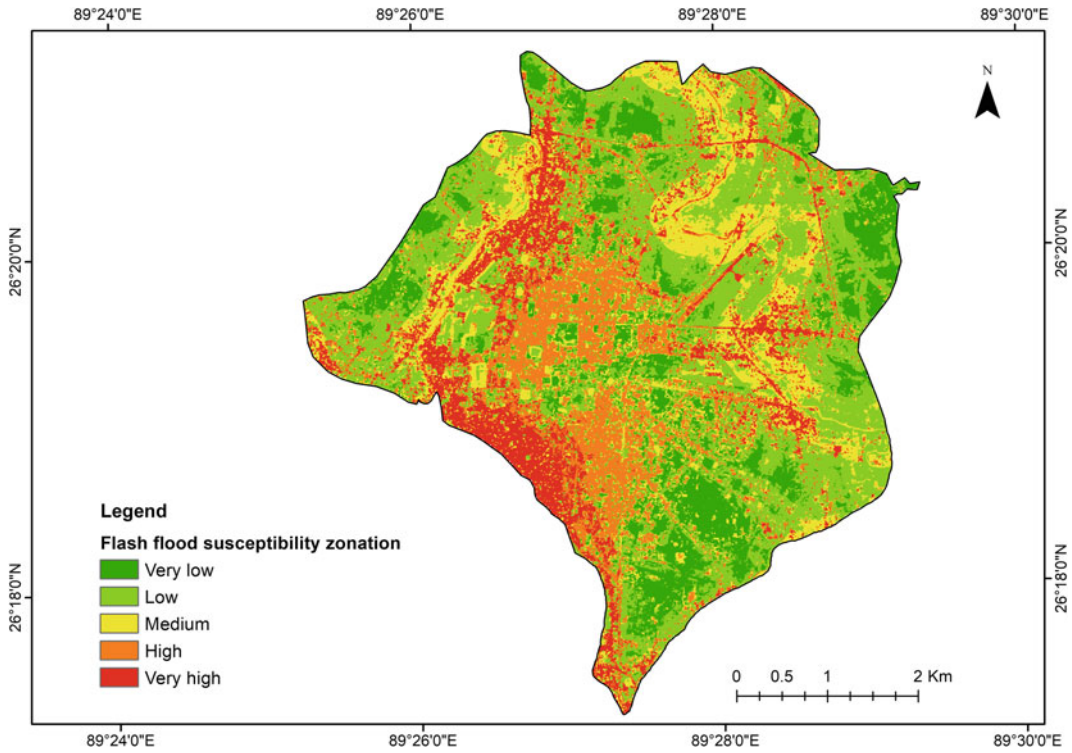


Fig. 8.6 Flash flood susceptibility map of CBUAR

density) may be the staple factor for developing flash flood condition. Moderate susceptible areas, on the other hand, were prevalent in the northern and northern-eastern regions of the study area (Fig. 8.6). Similarly, very low and low flash flood zones were prominent in the south-eastern parts of the map, while some areas of western, eastern, and northern regions

were also classified as very low and low flash flood susceptible zones. The spatial map also revealed that places far from built-up areas were less susceptible to flash flood occurrences. Table 8.8 depicts how much area is covered by each flood susceptible area. It is evident from Table 8.8 that 53.21% were classified as very low–low prone to flash flooding, 27.65% as high

Table 8.8 Area covered by each flash flood susceptibility zonation in CBUAR

Sl no.	Class	Area in km ²	Area in %
1	Very low	4.09	15.70
2	Low	9.77	37.51
3	Medium	4.99	19.14
4	High	4.02	15.42
5	Very high	3.19	12.23

Fig. 8.7 Distribution of flash flood susceptible areas in CBUAR

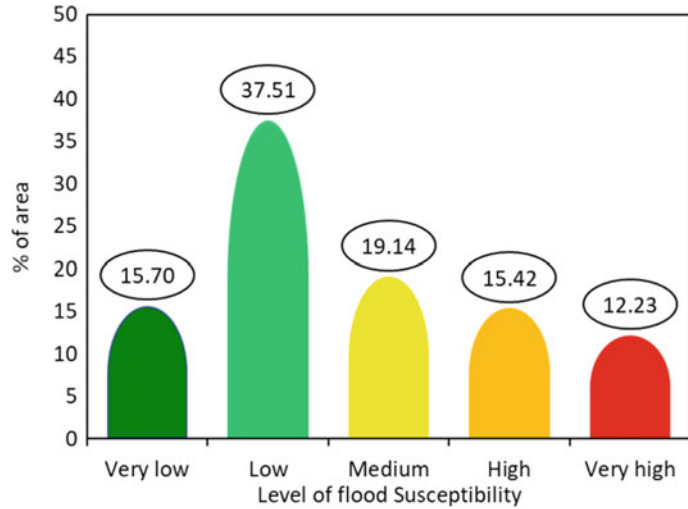


Table 8.9 Results of AUC analysis

Area	Std. Error ^a	Asymptotic Sig. ^b	Asymptotic 95% confidence interval	
			Lower bound	Upper bound
0.850	0.038	0.000	0.0776	0.924

a. Under the non-parametric assumption

b. Null hypothesis: true area = 0.5

to very high-risk flash flooding zones, and 19.14% as moderate flash flood risk zones (Fig. 8.7). The spatial flood susceptibility map (Fig. 8.6) also revealed that the north-western, south-western parts of the study area were more susceptible to flash floods. This result is a matter of concern, since almost every year the north-eastern and south-western parts are affected by flash floods. As a result of this finding, the local government should establish and improve an early warning system in order to reduce the flash flood damages.

8.4.5 Justification of Model Performance

The area justifies the quality of the AHP model for flash flood susceptibility under the ROC curve, which is shown in Fig. 8.8. The AUC value of 0.038 is the standard error value shown in Table 8.9, which is statistically significant at 95% confidence interval (0.00). So, according to the outcome of the validation study, AHP-based model is suitably applicable, which is used in the present study to determine the flash flood susceptibility zonation.

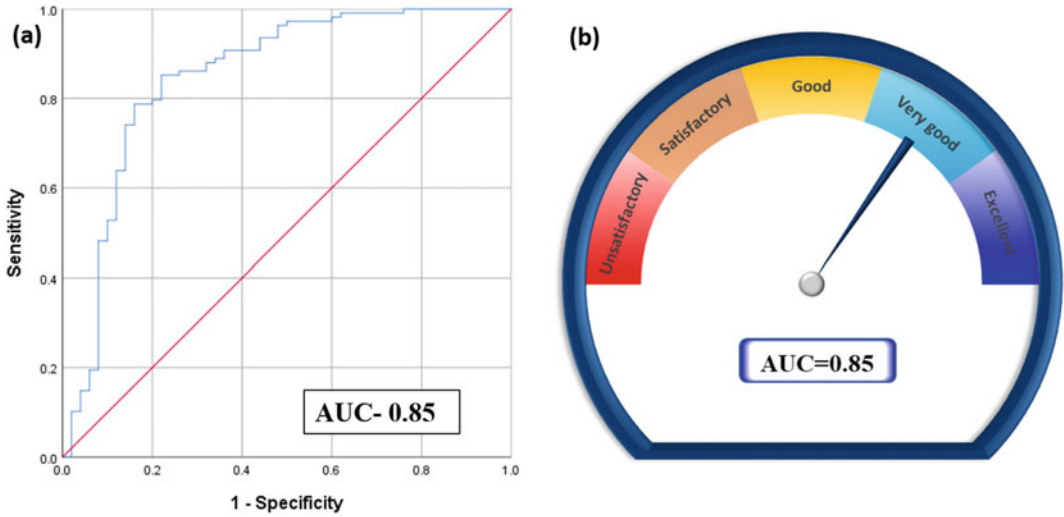


Fig. 8.8 Diagram for AUC and ROC analysis

Figure 8.8 represents the photographs of different particular flash flood areas of CBUAR taken from June to September 2020 when the area experienced a devastating flash flood. Interaction with residents and emphasize the

comprehensive field survey to validate the data was done during this period. We collected comprehensive ideas and information about flash flood vulnerability zones in different locations in the research area (Fig. 8.9).



Fig. 8.9 Flash flood occurrences in the study area

8.5 Conclusions

The identification of flash flood-prone areas has gained widespread attention from water resource managers, planners, and hydrologists due to their continuous outbreaks and damages in various parts of the world. In this context, developing an accurate flash flood susceptibility map is an essential task for decision-makers to minimize flood-related damages infrequent flash flood-affected areas. Hence, we applied a simple AHP method to produce a flash flood susceptibility map in Cooch Behar urban agglomeration region (CBUAR) in this study. For this, twelve flash flood influencing factors were selected to incorporate layers in the AHP method. Afterward, each factor was given a specific weightage based on the Expert's opinion. In this context, LULC (26.20%), distance to the river (19.00%), NDVI (14.20%), and distance to the road (11.00%) were the most prominent factors to determine the flood susceptible areas.

On the contrary, aspect (01.20%), curvature (01.50%), and TWI (02.60%) were shown to be the least affected factors. After incorporating all the thematic layers of flood influencing factors, a flash food susceptible map was created, which was divided into five distinct classes to depict the severity of flash flood in terms of susceptibility zone. The developed map identified 12.23%, 15.42%, 19.14%, 37.51%, and 15.70% of study areas as very high, high, medium, low, and very low susceptible flash flood susceptible areas, respectively. This spatial flash flood susceptibility map portrayed that the south-western and northwestern regions of the study area were highly susceptible to flash floods. In contrast, the majority of south-eastern and northwestern areas were classified as low or very low susceptible areas. Therefore, the spatial flash flood susceptibility map developed in this study might be useful in providing advance warning in areas that are particularly prone to flash floods. Nonetheless, using the ROC and AUC curves to validate the results revealed that the applied model achieved a very higher accuracy (AUC = 0.85). However, it is also recommended that a

similar study using subjective and objective MCDM methods be conducted to compare the results and determine the most reliable method for flood susceptibility mapping. We further recommend developing a flood susceptibility map in gauge station areas, where the feature selection method should be used in selecting flood influencing factors.

References

- Abedi R, Costache R, Shafizadeh-Moghadam H, Pham QB (2021) Flash-flood susceptibility mapping based on XGBoost, random forest and boosted regression trees. *Geocarto Int* 1–18
- Akay H (2021) Flood hazards susceptibility mapping using statistical, fuzzy logic, and MCDM methods. *Soft Comput* 1–22
- Al-Juaidi AE, Nassar AM, Al-Juaidi OE (2018) Evaluation of flood susceptibility mapping using logistic regression and GIS conditioning factors. *Arab J Geosci* 11(24):1–10
- Arabameri A, Saha S, Chen W, Roy J, Pradhan B, Bui DT (2020) Flash flood susceptibility modelling using functional tree and hybrid ensemble techniques. *J Hydrol* 587:125007
- Azareh A, RafieiSardooi E, Choubin B, Barkhori S, Shahdadi A, Adamowski J, Shamshirband S (2019) Incorporating multi-criteria decision-making and fuzzy-value functions for flood susceptibility assessment. *Geocarto Int* 1–21
- Basak A, Das J, Rahman ATMS, Pham QB (2021) An integrated approach for delineating and characterizing groundwater depletion hotspots in a coastal state of india. *J Geol Soc India*. 97:1429–1440. <https://doi.org/10.1007/s12594-021-1883-z>
- Bouamrane A, Derdous O, Dahri N, Tachi SE, Boutebba K, Bouziane MT (2020) A comparison of the analytical hierarchy process and the fuzzy logic approach for flood susceptibility mapping in a semi-arid ungauged basin (Biskra basin: Algeria). *Int J River Basin Manag* 1–11
- Bui DT, Ngo PTT, Pham TD, Jaafari A, Minh NQ, Hoa PV, Samui P (2019) A novel hybrid approach based on a swarm intelligence optimized extreme learning machine for flash flood susceptibility mapping. *CATENA* 179:184–196
- Cao Y, Jia H, Xiong J, Cheng W, Li K, Pang Q, Yong Z (2020) Flash flood susceptibility assessment based on geodetector, certainty factor, and logistic regression analyses in Fujian Province China. *ISPRS Int J Geo-Inf* 9(12):748
- Census of India (1971) District Census Handbook. Director of Census operation, Koch Bihar, West Bengal. Ministry of Home Affairs, Government of India.

- Census of India (1981) District Census Handbook. Director of Census operation, Koch Bihar, West Bengal. Ministry of Home Affairs, Government of India.
- Census of India (2001) District Census Handbook. Director of Census operation, Koch Bihar, West Bengal. Ministry of Home Affairs, Government of India.
- Census of India (2011) District Census Handbook. Director of Census operation, Koch Bihar, West Bengal. Ministry of Home Affairs, Government of India.
- Chakraborty S, Mukhopadhyay S (2019) Assessing flood risk using analytical hierarchy process (AHP) and geographical information system (GIS): application in Cooch Behar district of West Bengal India. *Nat Hazards* 99(1):247–274
- Chapi K, Singh VP, Shirzadi A, Shahabi H, Bui DT, Pham BT, Khosravi K (2017) A novel hybrid artificial intelligence approach for flood susceptibility assessment. *Environ Model Softw* 95:229–245
- Chen W, Li Y, Xue W, Shahabi H, Li S, Hong H, Ahmad BB (2020) Modeling flood susceptibility using data-driven approaches of naïve bayes tree, alternating decision tree, and random forest methods. *Sci Total Environ* 701:134979
- Choudhury S, Biswas S, Biswas A (2011) Urban infrastructural scenario of Cooch Behar town with special reference to public amenities and facilities. *Geo Analyst* 1(2):95–99
- Chowdhuri I, Pal SC, Chakraborty R (2020) Flood susceptibility mapping by ensemble evidential belief function and binomial logistic regression model on river basin of eastern India. *Adv Space Res* 65(5):1466–1489
- Costache R, Pham QB, Sharifi E, Linh NTT, Abba SI, Vojtek M, Khoi DN (2019) Flash-flood susceptibility assessment using multi-criteria decision making and machine learning supported by remote sensing and gis techniques. *Remote Sens* 12(1):106
- Costache R, Pham QB, Sharifi E, Linh NTT, Abba SI, Vojtek M, Khoi DN (2020) Flash-flood susceptibility assessment using multi-criteria decision making and machine learning supported by remote sensing and gis techniques. *Remote Sens* 12(1):106
- Dahri N, Abida H (2017) Monte Carlo simulation-aided analytical hierarchy process (AHP) for flood susceptibility mapping in Gabes Basin (south-eastern Tunisia). *Environ Earth Sci* 76(7):302
- Das S (2020) Flood susceptibility mapping of the Western Ghat coastal belt using multi-source geospatial data and analytical hierarchy process (AHP). *Remote Sens Appl Soc Environ* 20:100379
- Das S, Gupta A (2021) Multi-criteria decision based geospatial mapping of flood susceptibility and temporal hydro-geomorphic changes in the Subarnarekha basin, India. *Geosci Front* 12(5):101206
- Das J, Gayen A, Saha S, Bhattacharya SK (2017) Modelling of alternative crops suitability to tobacco based on Analytical hierarchy process in Dinhat subdivision of Koch Bihar district, West Bengal. *Model Earth Syst Environ* 3(4):1571–1587. <https://doi.org/10.1007/s40808-017-0392-y>
- Debnath M (2007) Sahar Cooch Behar-er Tinsha Bacchar (in Bengali). Lakhapara Press, Cooch Behar, pp 10–16
- Diakakis M, Deligiannakis G, Antoniadis Z, Melaki M, Katsesiadou NK, Andreadakis E, Gogou M (2020) Proposal of a flash flood impact severity scale for the classification and mapping of flash flood impacts. *J Hydrol* 590:125452
- Douglas EM, Vogel RM, Kroll CN (2000) Trends in floods and low flows in the United States: impact of spatial correlation. *J Hydrol* 240(1–2):90–105
- Falah F, Rahmati O, Rostami M, Ahmadisharaf E, Daliakopoulos IN, Pourghasemi HR (2019) Artificial neural networks for flood susceptibility mapping in data-scarce urban areas. In: *Spatial modeling in GIS and R for earth and environmental sciences*, pp 323–336. Elsevier
- Grozavu A, Valeriu Patriche C, Mihai F (2017). Application of AHP method for mapping slope geomorphic phenomena. *Proc 17th Int Multidiscip Sci Geoconferrence* 17(23):377–384
- Gupta A, Singh S (2017) Spatial analysis of rainfall variability and rainfed rice crop using GIS technique in West Bengal (India). *Mausam* 68(2):288–298
- Hammami S, Zouhri L, Souissi D, Souei A, Zghibi A, Marzougui A, Dlala M (2019) Application of the GIS based multi-criteria decision analysis and analytical hierarchy process (AHP) in the flood susceptibility mapping (Tunisia). *Arab J Geosci* 12(21):1–16
- Haque MN, Siddika S, Sresto MA, Saroar MM, Shabab KR (2021) Geo-spatial analysis for flash flood susceptibility mapping in the North-East Haor (Wetland) Region in Bangladesh. *Earth Syst Environ* 1–20
- India Meteorological Department (2020) Gridded data. Retrieved from https://www.imdpune.gov.in/Clim_Pred_LRF_New/Grided_Data_Download.html
- Joshi MM, Shahapure SS (2020) Flood susceptibility mapping for part of Bhima River basin using two-dimensional HEC-RAS model. In: *Techno-societal 2018*, pp 595–605. Springer, Cham
- Kanani-Sadat Y, Arabsheibani R, Karimipour F, Nasserri M (2019) A new approach to flood susceptibility assessment in data-scarce and ungauged regions based on GIS-based hybrid multi criteria decision-making method. *J Hydrol* 572:17–31
- Khosravi K, Nohani E, Maroufinia E, Pourghasemi HR (2016a) A GIS-based flood susceptibility assessment and its mapping in Iran: a comparison between frequency ratio and weights-of-evidence bivariate statistical models with multi-criteria decision-making technique. *Nat Hazards* 83(2):947–987
- Khosravi K, Pourghasemi HR, Chapi K, Bahri M (2016b) Flash flood susceptibility analysis and its mapping using different bivariate models in Iran: a comparison between Shannon's entropy, statistical index, and weighting factor models. *Environ Monit Assess* 188(12):1–21
- Khosravi K, Pham BT, Chapi K, Shirzadi A, Shahabi H, Revhaug I, Bui DT (2018) A comparative assessment

- of decision trees algorithms for flash flood susceptibility modeling at Haraz watershed, northern Iran. *Sci Total Environ* 627:744–755
- Khosravi K, Shahabi H, Pham BT, Adamowski J, Shirzadi A, Pradhan B, Prakash I (2019) A comparative assessment of flood susceptibility modeling using multi-criteria decision-making analysis and machine learning methods. *J Hydrol* 573:311–323
- Kiani M, Bagheri M, Ebrahimi A, Alimohammadlou M (2019) A model for prioritizing outsourceable activities in universities through an integrated fuzzy-MCDM method. *Int J Constr Manag* 1–17
- Lee S, Kim JC, Jung HS, Lee MJ, Lee S (2017) Spatial prediction of flood susceptibility using random-forest and boosted-tree models in Seoul metropolitan city, Korea. *Geomat Nat Hazards Risk* 8(2):1185–1203
- Lin K, Chen H, Xu CY, Yan P, Lan T, Liu Z, Dong C (2020) Assessment of flash flood risk based on improved analytic hierarchy process method and integrated maximum likelihood clustering algorithm. *J Hydrol* 584:124696
- Malik S, Pal SC (2021) Potential flood frequency analysis and susceptibility mapping using CMIP5 of MIROC5 and HEC-RAS model: a case study of lower Dwarakeswar River, Eastern India, S.N. *App Sci* 3(1):1–22
- McFeeters SK (1996) The use of the Normalized Difference Water Index (NDWI) in the delineation of open water features. *Int J Remote Sens* 17(7):1425–1432. <https://doi.org/10.1080/01431169608948714>
- Mirzaei S, Vafakhah M, Pradhan B, Alavi SJ (2021) Flood susceptibility assessment using extreme gradient boosting (EGB) Iran. *Earth Sci Inform* 14(1):51–67
- Mohammadi A, Kamran KV, Karimzadeh S, Shahabi H, Al-Ansari N (2020) Flood detection and susceptibility mapping using sentinel-1 time series, alternating decision trees, and Bag-ADTree models. *Complexity* 2020
- Nachappa TG, Piralilou ST, Gholamnia K, Ghorbanzadeh O, Rahmati O, Blaschke T (2020) Flood susceptibility mapping with machine learning, multi-criteria decision analysis and ensemble using Dempster Shafer theory. *J Hydrol* 125275
- Ngo PTT, Pham TD, Nhu VH, Le TT, Tran DA, Phan DC, Bui DT (2021) A novel hybrid quantum-PSO and credal decision tree ensemble for tropical cyclone induced flash flood susceptibility mapping with geospatial data. *J Hydrol* 596:125682
- Papagiannaki K, Lagouvardos K, Kotroni V, Bezes A (2015) Flash flood occurrence and relation to the rainfall hazard in a highly urbanized area. *Nat Hazard* 15(8):1859–1871
- Pappenberger F, Matgen P, Beven KJ, Henry JB, Pfister L (2006) Influence of uncertain boundary conditions and model structure on flood inundation predictions. *Adv Water Resour* 29(10):1430–1449
- Pham BT, Avand M, Janizadeh S, Phong TV, Al-Ansari N, Ho LS, Prakash I (2020) GIS based hybrid computational approaches for flash flood susceptibility assessment. *Water* 12(3):683
- Pradhan R, Manohar A, Sarkar BC, Bhat JA, Shukla G, Chakravarty S (2020) Ecosystem services of urban green sites-A case study from Eastern Himalayan foothills. *Trees For People* 2:100029
- Prasad P, Loveson VJ, Das B, Kotha M (2021) Novel ensemble machine learning models in flood susceptibility mapping. *Geocarto Int* 1–23
- Rahmati O, Pourghasemi HR, Zeinivand H (2016) Flood susceptibility mapping using frequency ratio and weights-of-evidence models in the Golastan Province Iran. *Geocarto Int* 31(1):42–70
- Ramesh V, Iqbal SS (2020) Urban flood susceptibility zonation mapping using evidential belief function, frequency ratio and fuzzy gamma operator models in GIS: a case study of Greater Mumbai, Maharashtra, India. *Geocarto Int* 1–26
- RazaviTermeh SV, Pourghasemi HR, Alidadganfard F (2018) Flood inundation susceptibility mapping using analytical hierarchy process (AHP) and TOPSIS decision making methods and weight of evidence statistical model (case study: jahrom township, fars province). *J Watershed Manag Res* 9(17):67–81
- Saaty TL (1980) *The analytic hierarchy process: planning, priority setting, resource allocation*. McGraw, New York, p 281
- Saaty TL (2000) *Fundamentals of decision making and priority theory with the analytic hierarchy process*, vol 6. RWS Publications
- Saha S (2017) Groundwater potential mapping using analytical hierarchical process: a study on Md. Bazar Block of Birbhun district, West Bengal. *Spat Inf Res* 25(4):615–626
- Sahana M, Patel PP (2019) A comparison of frequency ratio and fuzzy logic models for flood susceptibility assessment of the lower Kosi River Basin in India. *Environ Earth Sci* 78(10):1–27
- Saharia M, Kirstetter PE, Vergara H, Gourley JJ, Hong Y, Giroud M (2017) Mapping flash flood severity in the United States. *J Hydrometeorol* 18(2):397–411
- Samanta RK, Bhunia GS, Shit PK, Pourghasemi HR (2018) Flood susceptibility mapping using geospatial frequency ratio technique: a case study of Subarnarekha River Basin India. *Model Earth Syst Environ* 4(1):395–408
- ShafapourTehrany M, Kumar L, NeamahJebur M, Shabani F (2019) Evaluating the application of the statistical index method in flood susceptibility mapping and its comparison with frequency ratio and logistic regression methods. *Geomat Nat Hazards Risk* 10(1):79–101
- Siahkamari S, Haghizadeh A, Zeinivand H, Tahmasebipour N, Rahmati O (2018) Spatial prediction of flood-susceptible areas using frequency ratio and maximum entropy models. *Geocarto Int* 33(9):927–941
- Souissi D, Zouhri L, Hammami S, Msaddek MH, Zghibi A, Dlala M (2020) GIS-based MCDM-AHP modeling for flood susceptibility mapping of arid areas, south-eastern Tunisia. *Geocarto Int* 35(9):991–1017

- Tehrany MS, Pradhan B, Jebur MN (2014) Flood susceptibility mapping using a novel ensemble weights-of-evidence and support vector machine models in GIS. *J Hydrol* 512:332–343
- Tehrany MS, Pradhan B, Mansor S, Ahmad N (2015) Flood susceptibility assessment using GIS-based support vector machine model with different kernel types. *CATENA* 125:91–101
- Tekeli AE, Fouli H (2016) Evaluation of TRMM satellite-based precipitation indexes for flood forecasting over Riyadh City, Saudi Arabia. *J Hydrol* 541:471–479
- Terti G, Ruin I, Anquetin S, Gourley JJ (2015) Dynamic vulnerability factors for impact-based flash flood prediction. *Nat Hazards* 79(3):1481–1497
- Vafakhah M, Mohammad Hasani Looor S, Pourghasemi H, Katebikord A (2020) Comparing performance of random forest and adaptive neuro-fuzzy inference system data mining models for flood susceptibility mapping Arab *J Geosci* 13:1–16
- Vignesh KS, Ananda kumar I, Ranjan R, Borah D (2021) Flood vulnerability assessment using an integrated approach of multi-criteria decision-making model and geospatial techniques. *Model Earth Syst Environ* 7(2):767–781
- Wang Y, Hong H, Chen W, Li S, Pamučar D, Gigović L, Duan H (2019a) A hybrid GIS multi-criteria decision-making method for flood susceptibility mapping at Shangyou China. *Remote Sens* 11(1):62
- Wang Y, Hong H, Chen W, Li S, Panahi M, Khosravi K, Costache R (2019b) Flood susceptibility mapping in Dingnan County (China) using adaptive neuro-fuzzy inference system with biogeography-based optimization and imperialistic competitive algorithm. *J Environ Manage* 247:712–729
- Yang Q, Guan M, Peng Y, Chen H (2020) Numerical investigation of flash flood dynamics due to cascading failures of natural landslide dams. *Eng Geol* 276:105765
- Youssef A, Pradhan B, Sefry S (2016) Flash flood susceptibility assessment in Jeddah city (Kingdom of Saudi Arabia) using bivariate and multivariate statistical models. *Environ Earth Sci* 75:1–16



GIS-Based Hydrological and Hydraulic Models to Forecast River Flood Risks and Proposition of Management Measures

Gisele Icyimpaye and Chérifa Abdelbaki

Abstract

Nyabugogo River is being flooded every year resulting in human and economic losses. For sustainable flood management, flood risk forecasting is a useful component to show the extent of floodplain for each event. Therefore, this chapter aims to forecast Nyabugogo River's flood risk and propose mitigation measures to reduce flood impacts by using GIS, HEC-HMS combined with HEC-GEOHMS and HEC-RAS integrated with HEC-GEORAS. Nyabugogo River floods are mainly due to high topography, rainfall, soil texture that is mainly composed of clay and informal settlement, and urbanization. The peak runoff was simulated for 10-, 30-, 50-, and 100-year return periods, and flood inundation area increased slightly from the lower event to the higher event. In addition, the water depth increased slightly with the return period where the high water depth of 3.24 m was obtained for a 100-year return period. For the events modelled, the more vulnerable land use included annual

cropland, open grassland, open shrubland, settlement, sparse forest, and wetland. Consequently, some proposed mitigation measures include the construction of storage reservoirs at the upstream location of the reach, relocation of infrastructures within the flood plain area, buffer zoning around Nyabugogo River, rainwater tanks for each house, and raising public awareness on flood risks. Thus, this study can provide a basic support for decision-making and can help in the planning and management of land use and future probable flood event within the catchment.

Keywords

Flood risk · GIS · Modelling · HEC-RAS · HEC-HMS · Nyabugogo River Basin

9.1 Introduction

Floods are among the most harmful of natural hazards which are likely to be more frequent, dominant, and serious in the future because of climate change and urbanization coupled with increase of population in flood prone area and other diverse factors related to watershed characteristics and human activities (Machtar 2010). Flood is a weather-related disaster in the type of hydrological events which occurs when the river water inundates or overflows the land which is

G. Icyimpaye · C. Abdelbaki (✉)
Pan-African University Institute for Water and
Energy Sciences (PAUWES), Tlemcen, Algeria

C. Abdelbaki
Laboratoire EOLE, Université de Tlemcen, Tlemcen,
Algeria

generally dry, and affects individual life and property causing economic and social impacts, and harm the natural environment in different countries of the world (Queensland Government 2011). Generally, the losses of flood are categorized into direct and indirect losses, where direct losses are physical damage of roads, buildings, cars, and death of people, and indirect losses are water quality deterioration, interruption of transport, and lowering of economic status of a region. (Queensland Government 2011).

Globally, 3062 flood disasters were recorded between 1995 and 2015, accounting 47% of all weather-related disasters' meteorological hazards like storm and climatological hazards like drought (UNISDR 2015). The flood disasters affected 2.3 billion people which represented 56% of all people affected by weather-related disasters where 157,000 people died, accompanied with the economic loss of USD 662 billion (UNISDR 2015).

Rwanda is experiencing floods in its different regions every year due to its geographical features of hilly slopes and abundant rain with an annual average of 1200 mm accentuated by an overexploitation of natural environment such as deforestation, inappropriate farming practices, and housing systems (MIDIMAR 2012). In addition, the resulting landslides are significant and the affected populations is often avoided to have mechanisms to manage natural hazards.

Historically, flood events have been observed in Rwanda since 1960 and their occurrence started to increase significantly since 2000 with impacts on people, environment, and human activity (Habonimana et al. 2015). In the year 2011, where north-western part of the country experienced flood after heavy rain and at least 10 people died, 354 houses were destroyed, and 3000 ha of farmland were damaged (MIDIMAR 2012). In the year 2012, some districts of north-western part of the country got flooded and as a result five deaths and strong damages to houses and other property of the indigenous population were recorded, where 2232 households with 11,160 people had been affected, 348 houses

were totally destroyed, 446 were partly damaged, and that flood had damaged water supplies networks along with almost 1000 ha of potatoes, maize, bananas, and tea were inundated (DREF 2012).

On 3 April 2015, Rubavu and Nyamasheke districts located in the western province of Rwanda experienced heavy rainfall that resulted in flooding and landslides. A total of 3425 people (685 households) had been affected; 206 ha of crops had been inundated, and household items had been washed away. On 7–8 May 2016, 49 people died due to floods caused by heavy rainfall where Gakenke district in north province, Muhanga district in south, Rubavu and Ngororero districts in western province were the worst affected districts; within the same period, the quality of water resources had been affected as former Energy Water and Sanitation (EWASA) Ltd. transformed into Water and Sanitation Cooperation (WASAC) temporally postponed water treatment at Nzonve treatment plants due to increase of turbidity (Floodlist 2016).

Kigali city which is the capital of the country in which Nyabugogo river passes through also experienced floods events. Heavy rainfall, urbanization which promotes the presence of impervious layer in different places coupled with increase of population and inadequate drainage cause flash floods in different areas of Kigali city leading to flooding in the downstream area (Habonimana et al. 2015). Generally, floods on Nyabugogo river cause effects which are classified as primary effects in which there is physical damage of any type of infrastructure such as bridges, cars, buildings, sewerage systems, roadways and canals and loss of people, and secondary effects which affect water supplies, crops, food supplies, trees, vegetation, transport, and cause disease then tertiary and long-term effects which affect economic status of a region or a place (Munyaneza et al. 2013). Nyabugogo river floods cause an estimated loss of 178 million francs Rwanda which is equal to 209,412 USD annually by Nyabugogo business (New times-Rwanda 2016) including social losses.

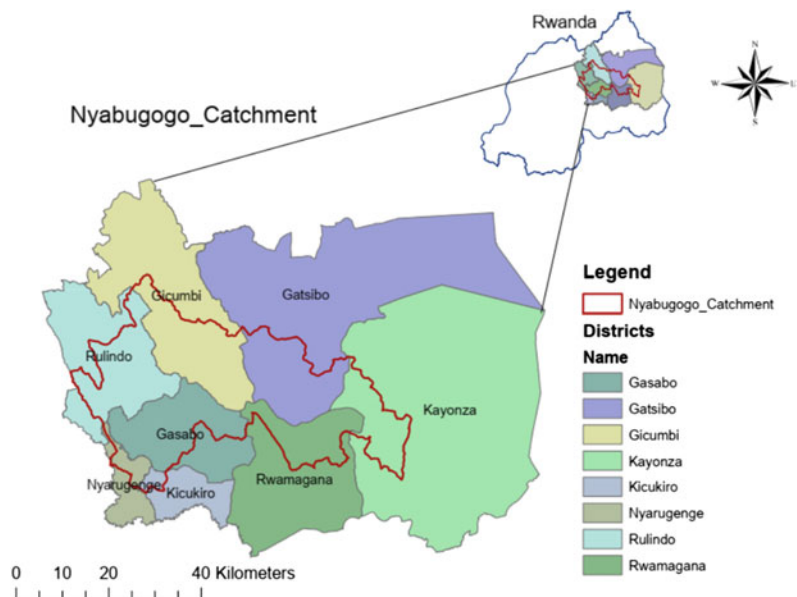
The government of Rwanda through its different institutions is trying to mitigate floods where there was a mapping of vulnerable area to flood and landslides at national level to know exactly in which area the management actions should focus to mitigate and adapt to both floods and landslides. However, flood events continue to cause losses not only in Nyabugogo catchment but also in other catchments of the country. Therefore, there is a need of forecasting flood risks using models so that decisions can be taken based on the results of those models to make people aware of the events and come up with mitigation measures to secure different useful aspects necessary to achieve sustainable development goals. Therefore, the main objective of this chapter is to forecast flood risks on Nyabugogo River and to propose different management measures which can reduce flood effects by (1) investigating the causes and impacts of flood in the catchment, (2) identifying the existing flood management measures, (3) describing the geospatial data characteristics of the catchment that are relevant to flood generation, and (4) generating inundation maps and water depths for different return periods.

9.2 Materials and methods

9.2.1 Study Area

The Nyabugogo catchment covers both rural and urban areas including Kigali city which is the capital city of Rwanda. It is between 1352 and 2288 m above sea level and extended between latitude: 01°51'46.06"–01°46'11.22" degrees south and longitude: 30°05'57.02"–30°04'07.41" degrees east. The drainage area is about 1661 km² representing 6.31% of the total surface area of the country (Water for Growth Rwanda 2017a, b). It is the most densely and populated catchment in Rwanda covering the major part of Kigali city and other districts in the north and eastern part of Rwanda. The catchment has temperate and equatorial climate with an annual average temperature lying between 16 and 23 °C, depending on the altitude of the area and the annual average rainfall of 1,200 mm. The main land use/cover activities are rain-fed agriculture, irrigation and small forests in the center and eastern part and a small part of natural open lands (Water for Growth Rwanda 2017a, b). Figure 9.1 shows the location of Nyabugogo catchment within the country.

Fig. 9.1 Location of Nyabugogo catchment in Rwanda (Niyonkuru 2019)



9.2.2 Causes and Impacts of Flooding in Nyabugogo River

a) Causes of Flooding in Nyabugogo River

The observed factors influencing flood in Nyabugogo River were meteorological factors, catchment characteristics, urbanization, and informal settlement.

The main meteorological factor contributing to flood is rainfall. It has been found that the average annual rainfall is between 1200 and 1400 mm and the high rainfall intensity is observed during the long period of rain starting from March and extending till May. Figure 9.2 shows the monthly rainfall from the year 2012 to 2017 where rainfall is unevenly distributed in a year with the high rainfall observed during the months of March till May and September till October representing the period of long rainy season and short rainy season, respectively, and those periods are similar to the period when the flood event that took place in Nyabugogo River during 23 March 2013.

Catchment characteristics influencing flood in Nyabugogo River are topography, land use, and soil texture. First, Nyabugogo catchment has a topography which varies between 1352 and 2288 m above mean sea level as shown in Fig. 9.3; based on this topography, Nyabugogo

River is located at lower elevations between 1352 and 1526 m, and the fact that Nyabugogo River is located at the downstream of the catchment makes all runoff from the hillside to flow towards it.

Secondary, soil characteristics are also another factor influencing runoff and hence flooding, as demonstrated in Fig. 9.4. Texture of Nyabugogo soil is composed of clay, clay loam, sand clay, and silt clay which have high runoff potential and very slow infiltration; it is also composed of silt loam and loam which have slow infiltration rate but also moderate high runoff potential when thoroughly wet.

Lastly, land use and land cover degradation is also another factor which is influencing flood in Nyabugogo catchment apart from topography and soil. From the land use map demonstrated in Fig. 9.5, particularly at the downstream of Nyabugogo catchment, there is a build-up area of Kigali city with high density housing; the fact that this area of high density is located in Kigali city produce the huge amount of runoff as it is an urbanized area then the produced runoff flow towards the Nyabugogo River which passes in Kigali. Also, land degradation in Nyabugogo catchment is influenced by over-grazing and collection of fuelwood leading to deforestation especially in the upland of the watershed (Water

Fig. 9.2 Monthly rainfall 2012–2017

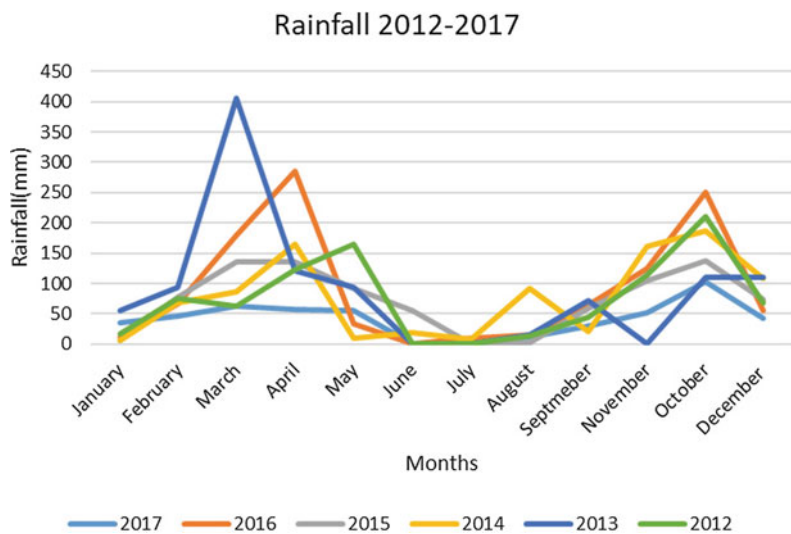


Fig. 9.3 Topography of the catchment

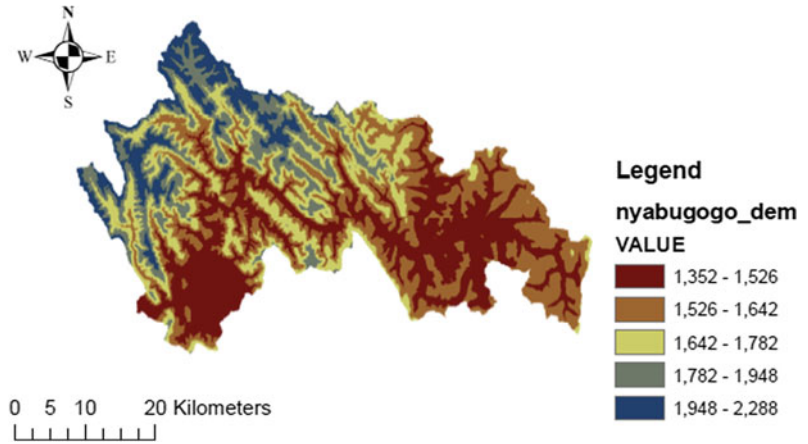
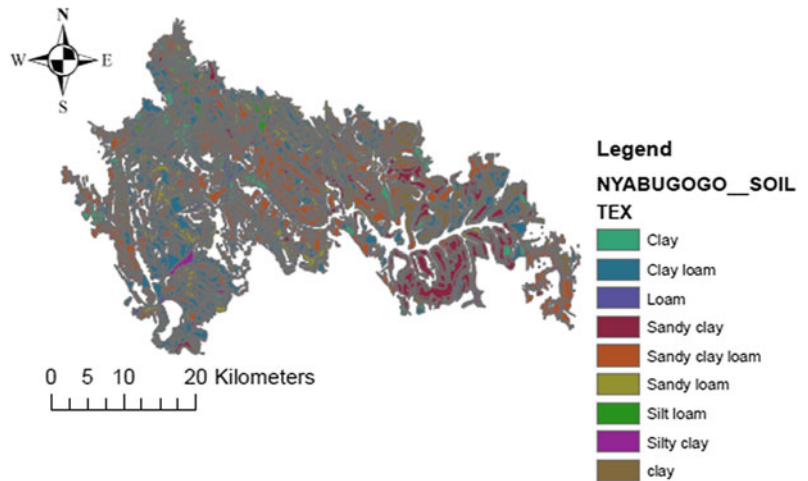


Fig. 9.4 Soil texture of Nyabugogo catchment



for Growth Rwanda 2017a, b) reducing the infiltration capacity of the soil and contributing to huge runoff generation.

The urbanization is also the factor which is influencing the huge amount of runoff and hence flooding, which is due to the increase of impervious surface as those impervious surfaces are composed of roads and houses that reduce infiltration capacity of the soil (Mukherjee 2016). Since Nyabugogo River passes through Kigali city which is classed among the fastest growing cities of Africa with annual growth rate of 4.0% of population (NISR 2012), this factor shows how Nyabugogo River is being flooded due to urbanization. Figure 9.6 shows the increase of

the build-up area (urbanization) from 1987 to 2014.

Informal settlement is also another factor influencing flooding and landslides in Nyabugogo River especially in Kigali City since they are located on the steeper slope without storm water management technology. In 2015, the Ministry of infrastructure declared that 79% of population lives in informal settlements in Kigali city (MINENFRA 2015).

b) Impacts of Flooding of Nyabugogo River

The impacts of Nyabugogo River flood have been categorized into primary, secondary, and

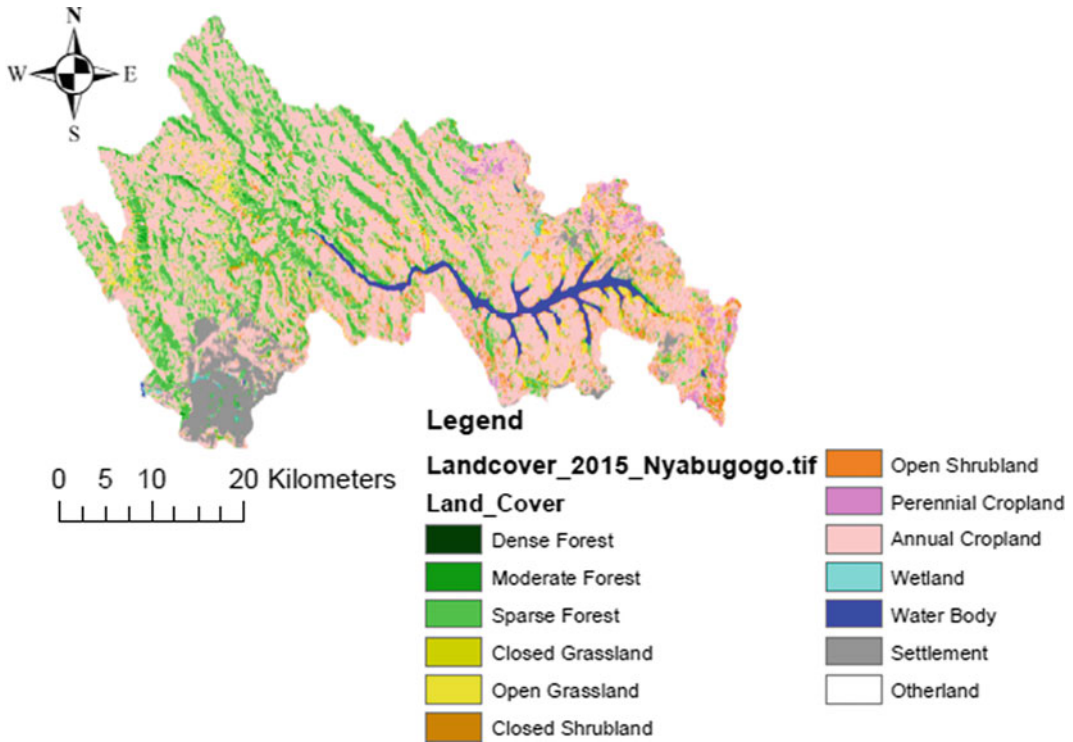


Fig. 9.5 Land cover of Nyabugogo catchment

tertiary impacts. The observed primary impacts were loss of people, loss of properties; the secondary impacts were transport interruption, water quality deterioration; and the tertiary impacts were disturbance of economic status. Some of the cases are as follows: In April 2006, a flood event damaged 40 houses and caused two deaths; Again Kiruhura market and RWANTEXICO factory both were located in Nyabugogo River Basin before their location got flooded as Nyabugogo River overflowed into the market shops and in different houses of factories reaching 1.5 m of height as shown in Fig. 9.7 (Bizimana and Shilling 2010).

Also, in February 2013, flood affected Nyabugogo River and caused loss of four people's life who were in a car drained away by water; it also affected different socio-economic activities such as business shops and it interrupted transport modes as shown in Fig. 9.8 (Munyaneza et al. 2013). Therefore, according to new times, about 178 million francs Rwanda

which is equal to 209,412 USD are lost annually by Nyabugogo business due to the effects of flooding (REMA 2009).

9.2.3 Existing Flood Management Measures

Currently the Rwanda Water and Forestry Authority through its Department of Integrated Water Resources Management has elaborated the program called Nyabugogo catchment plan 2017–2023. This program is intended to develop the catchment in order to meet water demand in terms of quantity and quality needed for socio-economic activities and minimize water-related disasters. It is in this line that different activities within the aim of land scape rehabilitation, land conservation, and disaster risk management are being implemented as shown in Table 9.1.

Some of those stated measures have been started being implemented like afforestation where

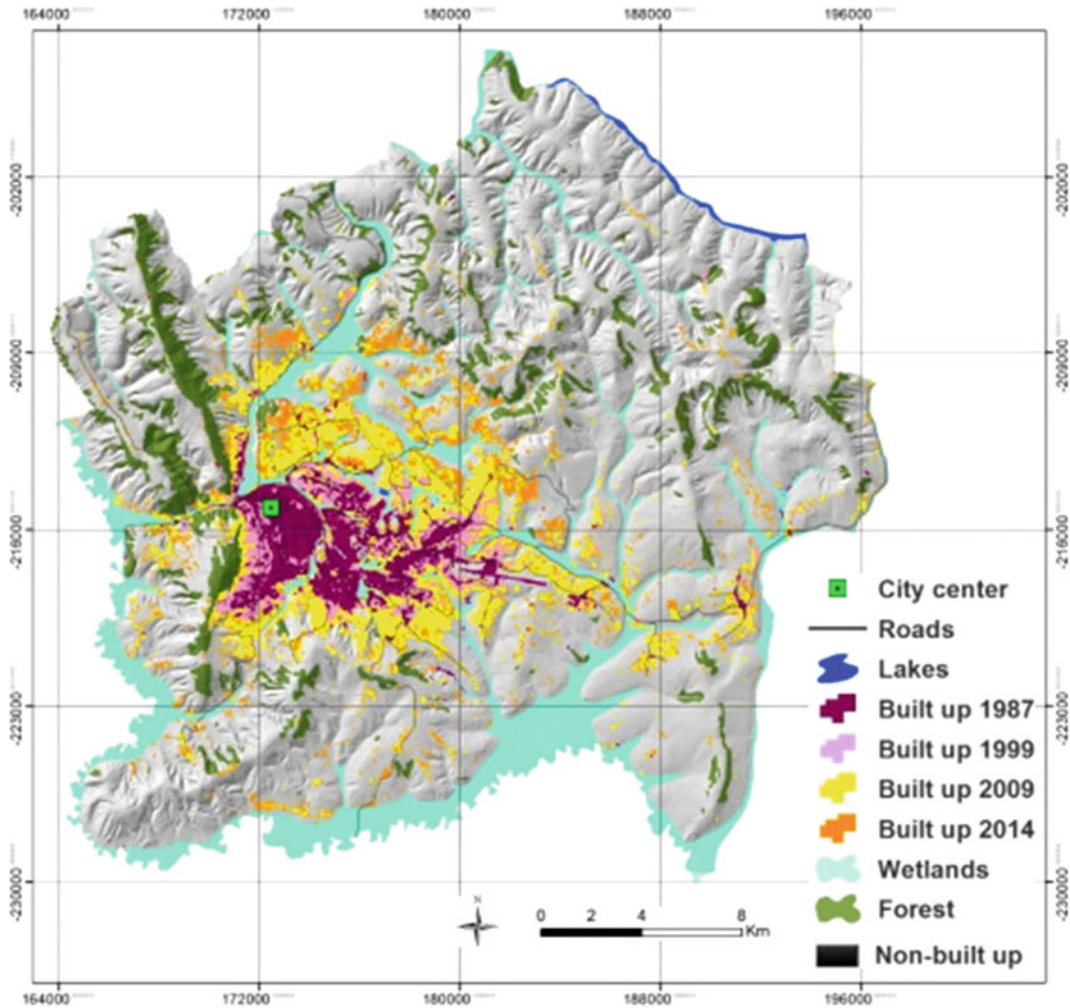


Fig. 9.6 Built-up area in Kigali city from 1987 to 2014 (Nduwayezu et al. 2017)

884.3 ha of Gicumbi district has been benefited with forest plantation; 1800 ha near the right side of the lake Muhazi dyke located at upstream of the catchment have been developed by agro forestry, construction of progressive bench and narrow cut terraces, re-afforestation, river and reservoir buffer zone protection and gully rehabilitation.

Rainwater harvesting technology is also being applied in Kigali city with 4% of household using rain water tanks, 27% of households using ditches included and 2.9% households using piped away (Water for Growth Rwanda 2017a, b); it is clearly shown that rain water tank technology is still at lower level which must be

increased as it is the one which is reliable compared to other used technologies.

Presently there are on-going projects like the construction of multipurpose dam in Nyabugogo catchment, specifically in its upstream which is intended to be used for irrigation, power generation, and flood control. The act of reallocating household living in high-risk zones of landslides and flooding is being applied in Nyabugogo catchment as well as in the other catchments of the country. Regular removal of sand and solid waste in the channel is normally done through the monthly community activity called Umuganda which used to happen at the last Saturday of each month.



Fig. 9.7 Flood water level observed in April 2006 (Bizimana and Shilling 2010)



Fig. 9.8 A man carrying a lady across the flood area and the car damaged by flooding water (Munyaneza et al. 2013)

9.2.4 Data Collection and Modelling Input

The data required were 30 years time series rainfall data from the year of 1987 to the year of 2017 which was collected from Rwanda Meteorological Agency at Gitega station situated at

−1.95 latitude and 30.06 longitude with 1516 m of elevation, and these data were applied to obtain extreme frequency rainfall events. The P_{\max} series are often represented by the Gumbel extreme value distribution method that will be used to determine the return period of precipitation required for planning studies. Gumbel

Table 9.1 Existing flood management measures in Nyabugogo catchment (Water for Growth Rwanda 2017a, b)

Target	Measures	Location
Land rehabilitation and land conservation	Afforestation and landscape restoration	Gicumbi, Rulindo, Gatsibo, Rwamagana and Kayonza
	Water ponds to collect water from road drainage and settlement sites	Rulindo
	Regular removal of sand and solid waste in water channel specifically in Nyabugogo channel	Nyarugenge and Kicukiro
	Buffer zone protection alongside lakes and rivers	Rwamagana, Kayonza, Rulindo and Gicumbi
Control of the hazard risk to public infrastructure, communities, and property	Construction of appropriate structure works to increase flow capacity of Nyabugogo River	Nyarugenge, Kicukiro, Gasabo
	Construction of multipurpose dam on Muhazi (flood control, irrigation, and domestic water supply) which is still a project waiting to be implemented	Gicumbi and Gasabo
	Rainwater harvesting for households and public institutions	All districts within the catchment
	Reallocation of household living in high-risk zones of landslides and flooding	Rulindo, Kigali City, and Gicumbi

extreme value distribution method and the given return period precipitation are determined as described in the step 2.

For rainfall runoff modelling methods, there are a number of hydrological models used to simulate runoff taking into consideration all the processes of how rainfall is transformed into runoff. In this chapter, HEC- HMS 4.2.01 model was used. It works in conjunction with HEC-GEOHMS which is a GIS extension used to prepare the basin input model needed for HEC-HMS to transform rainfall into runoff based on basin geomorphological characteristics. To obtain runoff from rainfall in HEC-HMS Model the Soil Conservation Service (SCS) Curve Number model was applied.

The major data used for developing Nyabugogo HEC-HMS model were collected from Rwanda Water and Forestry Authority especially in its department of Integrated Water Resources Management and consist of topography with 10 m resolution, basin land use/cover and basin soil data.

To perform the hydraulic modelling of Nyabugogo River, HEC_RAS software combined with the GIS extension named HEC-GEORAS have been used in this study.

Basically, the methods used to forecast Nyabugogo floods risks and to propose management measures are grouped into five steps as explained below:

1. The first step was to investigate the causes and impacts of flood in the catchment and identifying the existing flood management measures in the catchment through the literature review made by different researches including field observation and interview made to understand deeply and see them clearly.
2. Determine frequencies of extreme rainfall events using Gumbel extreme value distribution method. Under this method following formulas have been applied.
 - Sort the maximum daily rainfall of each year (P_{max})

- Determine the mean and standard variation of the sorted maximum rainfall data

$$2. \quad P_{\text{mean}} = \frac{1}{n} \sum_{i=1}^n P_{\text{max}} \quad (9.1)$$

$$2. \quad S = \sqrt{\frac{1}{n-1} \sum_{i=1}^n (P_i - P_{\text{mean}})^2} \quad (9.2)$$

- Determine the reduced variate Y,

$$Y = 1.282 \frac{P_i - P_{\text{mean}}}{S} + 0.577 \quad (9.3)$$

- Calculate the probability P,

$$P = 1 - e^{-e^{\Lambda - Y}} \quad (9.4)$$

- Determine the return period T,

$$T = 1/P \quad (9.5)$$

- Determine frequency rainfall P_T (mm) corresponding to each return period T (years)

$$2. \quad P_T = P_{\text{mean}} + K_T S \quad (9.6)$$

$$2. \quad K_T = \frac{-\sqrt{6}}{\pi} \left(0.5772 + \ln \left(\ln \left(\frac{T}{T-1} \right) \right) \right) \quad (9.7)$$

T is the return period (year)

K_T know as Gumbel frequency factor.

n is the number of years used for the

3. Rainfall runoff modelling methods

HEC-HMS 4.2.01 model together with GIS and its extension ARC-hydro and HEC-GEOHMS helped to obtain catchment runoff event for different return periods through those processes. Figure 9.9 summarizes the steps of the study.

4. Hydraulic modelling methods

The river flow analysis applied to this study was one-dimensional steady flow computations with subcritical flow regime. Following are the steps adopted to come up with flood inundating maps and flood stages (Fig. 9.10).

The forecast of flood risk was done through the analysis of flood delineation area and flood depth or stage of each event, and the intersection of flood delineation area with the land use/cover produced the vulnerable maps demonstrating the vulnerable land use type of each event modelled and the intersection of flood delineation with flood depth resulted into flood hazard map showing the inundation area corresponding to each flood stage.

5. The last step was to propose flood management measures based on the results of model analysis and the available existing flood management measures.

9.3 Results and Discussions

9.3.1 HEC-HMS and HEC-RAS Model Simulation and Discussion Results

The results of 10, 30, 50, and 100 years return period of frequency precipitation using Gumbel's extreme value probability distribution are shown in Table 9.2.

After calibration, the frequency precipitation depths based on the specific return period were introduced in the model to simulate hydrograph and peak discharge. The introduced frequency precipitation depth was the one of 10, 30, 50, and 100 year return period. From the above obtained simulated hydrographs of different return period, the peak discharged increased from the low return period to the high return period but the date and time to peak were similar. Table 9.3 summarizes the peak discharged for each event modelled.

The result obtained from hydraulic modelling is represented in Fig. 9.11. It involves the

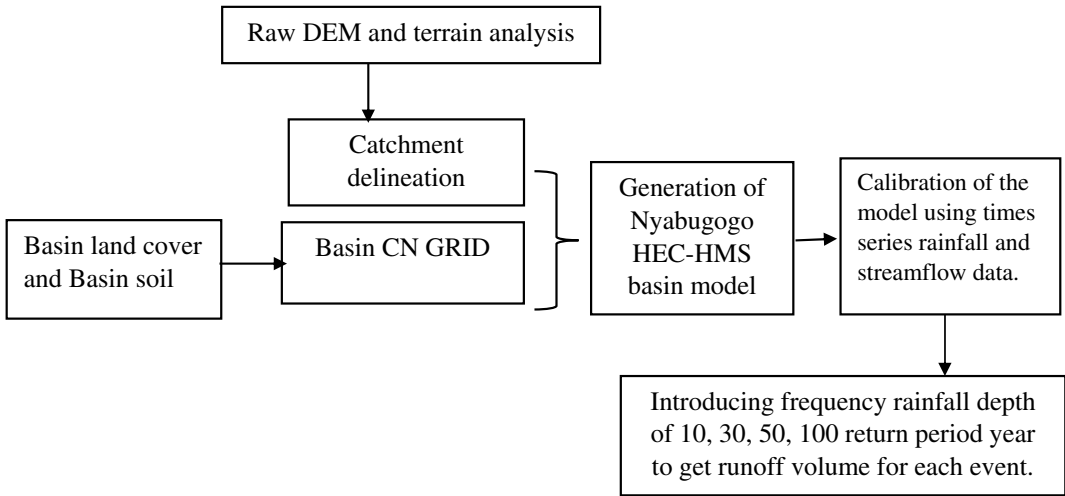


Fig. 9.9 Flowchart of rainfall-runoff modelling

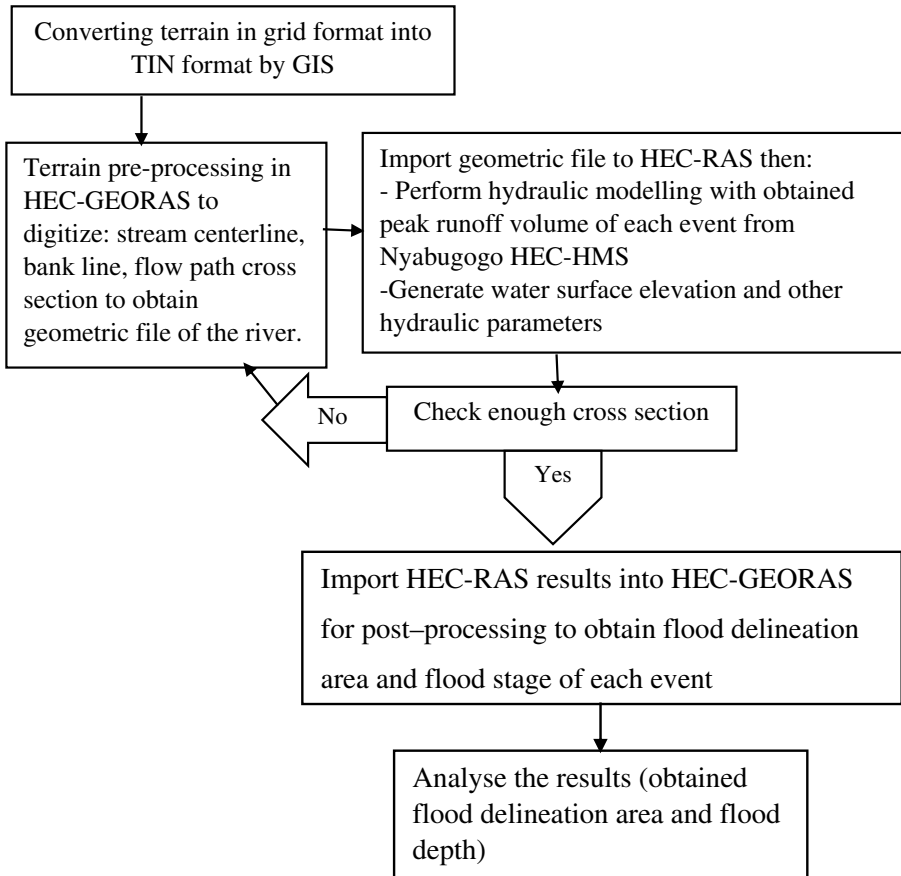


Fig. 9.10 Flowchart of hydraulic modelling

Table 9.2 Frequency rainfall corresponding to each event

Return period T (year)	Gumbel frequency factor within each return period K_T	Frequency precipitation P_T (mm)
10	1.305	52.310
30	2.190	66.136
50	2.594	72.564
100	3.138	81.288

Table 9.3 HEC-HMS simulated peak discharge of each event

Return period year	Peak discharge (m ³ /sec)
10	515.7
30	680.2
50	761.5
100	875.8

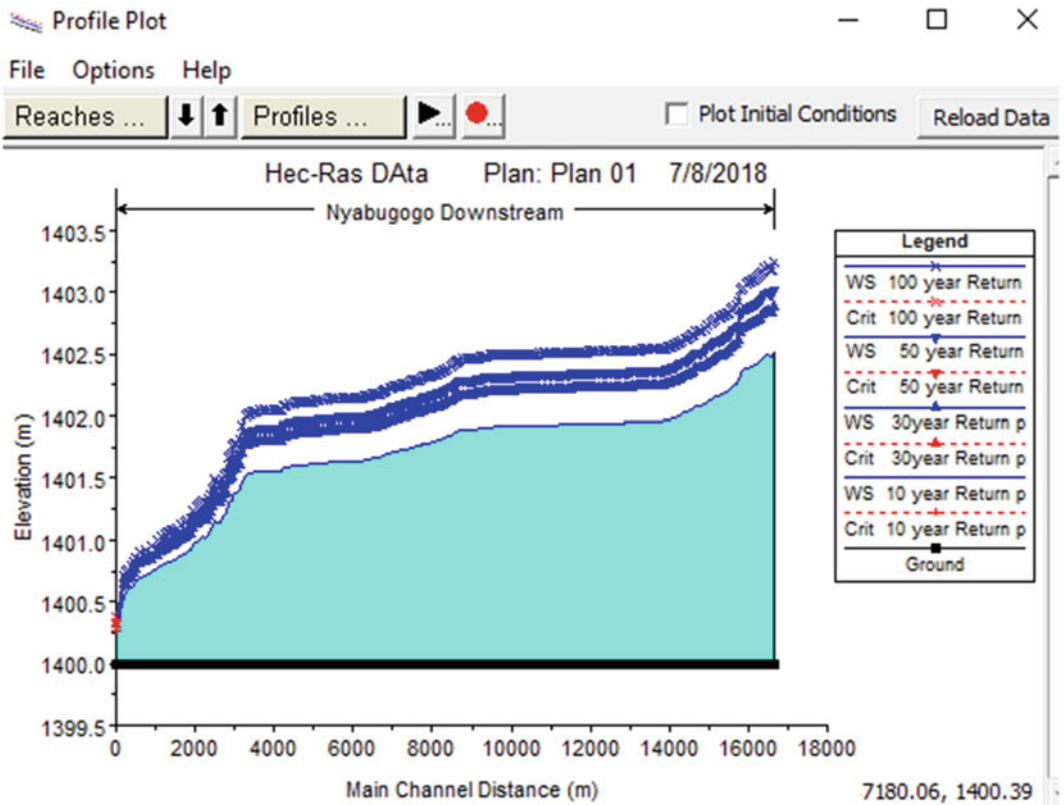


Fig. 9.11 Profile plot for Nyabugogo River

profiles plot and cross-sectional output parameters (hydraulic parameters) for 10, 30, 50, and 100 return period years, respectively.

Water surface elevation increase slightly from upstream to downstream and from lower return period to the high return period year. Critical depth also increase slightly as the return period year increase. In addition, HEC-RAS displayed hydraulic parameters for any station of the cross section of the reach with respect to each event modelled. Figure 9.12 shows the hydraulic parameters for 100 years return period.

9.3.2 Floodplain Inundation Area and Flood Depth Analysis

Basically two maps for each event modelled were generated: one map shows floodplain area or inundation coverage which indicates the extents of flooding and the other map shows depths of inundation like how deep it would be for different return period events. Figures 9.13 and 9.14 show the inundation area and water depth for 100 years return period, respectively.

The intersection of the land use map with the flood inundation area polygon was done to obtain the vulnerable land use for each flood event modelled which resulted into the vulnerable map. Table 9.4 demonstrates the summary of 100 years return period vulnerability map.

From Table 9.4, it is shown that the most vulnerable land uses consist of annual cropland, open grassland, open shrubland, settlement, sparse forest, and wetland. By considering the high event modelled of 100 years, the inundation area is 54.804, 53.672, 53.238, 54.804, 139.359, 50.106 ha corresponding to the annual cropland, open grassland, open shrubland, settlement, sparse forest, and wetland, respectively, which represent the most vulnerable land use as shown in Fig. 9.15.

Flood depths were divided into 5 classes ranging from the lower depth to the high depth where each class represents a range of flood depths or water surface elevation for each event modelled.

Generally, from all the event modelled, the total inundation area coverage increases as the return period increases or flow magnitude

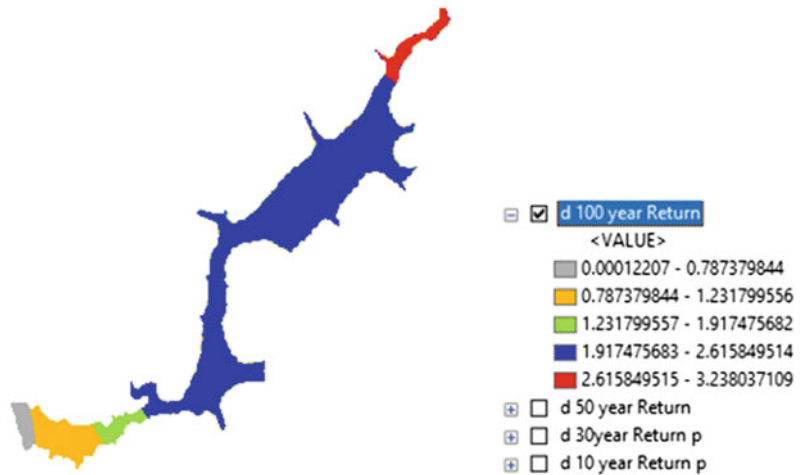
Plan: Plan 01 Nyabugogo Downstream RS: 215.4895 Profile: 100 year Return					
Element	Left OB	Channel	Right OB		
E.G. Elev (m)	1400.78				
Vel Head (m)	0.06				
W.S. Elev (m)	1400.72				
Crit W.S. (m)					
E.G. Slope (m/m)	0.000434				
Q Total (m3/s)	875.80				
Top Width (m)	1158.67				
Vel Total (m/s)	1.05				
Max Chl Dpth (m)	0.72				
Conv. Total (m3/s)	42037.9				
Length Wtd. (m)	206.43				
Min Ch El (m)	1400.00				
Alpha	1.00				
Frctn Loss (m)	0.19				
C & E Loss (m)	0.01				
Wt. n-Val.	0.015	0.016	0.016		
Reach Len. (m)	182.65	209.19	216.05		
Flow Area (m2)	96.00	559.33	176.26		
Area (m2)	96.00	559.33	176.26		
Flow (m3/s)	106.41	584.11	185.28		
Top Width (m)	134.52	778.75	245.40		
Avg. Vel. (m/s)	1.11	1.04	1.05		
Hydr. Depth (m)	0.71	0.72	0.72		
Conv. (m3/s)	5107.4	28037.1	8893.4		
Wetted Per. (m)	134.67	778.75	246.12		
Shear (N/m2)	3.03	3.06	3.05		
Stream Power (N/m s)	3.36	3.19	3.20		
Cum Volume (1000 m3)	16.49	87.06	29.37		
Cum SA (1000 m2)	32.91	157.48	54.00		

Fig. 9.12 Hydraulic parameter for 100 years return period



Fig. 9.13 Floodplain inundation map for 100 years return period

Fig. 9.14 Flood depth map for 100 years return period



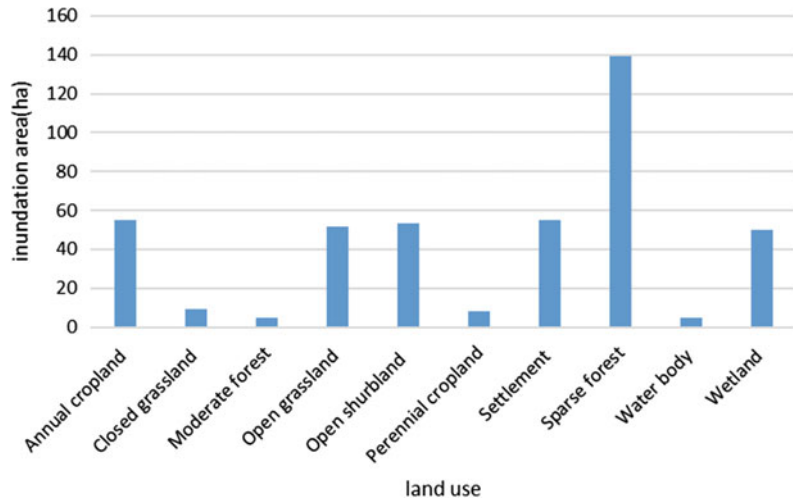
increases and the water depth range increases as the return period increases or flow magnitude increases. The big inundation area covered for 10 years comprises 33.5% of the total area (370.92 ha) inundated and its depth ranges between (0.61–0.95) m; for 30 years comprise 33.52% of the total area (371.66 ha) inundated and its depth ranges between (0.69–1.10) m; for

50 years comprises 33.43% of the total area (372.94 ha) inundated and its depth ranges between (0.74–1.15) m, and finally for 100 years comprises 33.442% of the total area (375.24 ha) and its depth ranges between (0.79–1.23) m. The lower water depth was 0.69 m and the high water depth of 3.2 was observed for 100 year return period.

Table 9.4 Inundation area with respect to the land use vulnerability

Land use type	Total vulnerable area (ha)	
	100 years	
	Area(ha)	%
Annual cropland	54.80	12.72
Closed grassland	9.39	2.18
Moderate forest	4.69	1.09
Open grassland	51.67	12
Open shrubland	53.23	12.36
Perennial cropland	7.82	1.81
Settlement	54.80	12.72
Sparse forest	139.35	32.36
Water body	4.69	1.09
Wetland	50.10	11.63
Total	430.60	100

Fig. 9.15 Inundation area for each vulnerable land use for 100 year return period



9.3.3 Flood Mitigation Measures

Flood mitigation refers to the measures adopted to reduce potential impacts of flood on people, environment, and economy of the region. Basically, flood mitigation measures are grouped into engineering such as construction of reservoir, dyke, and diversion of water to side channels, levees along floodways and non-engineering such relocation and zoning flood-prone areas.

In the case of Nyabugogo River, where annual cropland, open grassland, open shrubland, settlement, sparse forest, and wetland, are the most

observed land use to be affected, following mitigation were proposed:

- Flood proofing measures
These measures can be applied to the building within the flood delineation area in two ways which are elevating of building so that flood waters can pass under it or constructing a wall to avoid flood water from reaching a building.
- Construction of storage reservoir at the upstream location of the reach.
Since there are agriculture activities within the flood delineation area, the storage

reservoir can be used both for flood protection and irrigation purpose.

- Relocation of infrastructures within the flood delineation area.
- Buffer zoning around Nyabugogo River
- Rainwater Harvesting Strategies
Rain water harvesting techniques especially rain water tank for each house within the catchment can reduce the amount of runoff and also serve as a source of water supply.
- Raising public awareness on flood risks

Flood risks assessment as a vital component of flood management which elaborates hazards maps and provides information to the city planners, policy decision-makers and also to other risks managers within different governmental institutions. This information should not be limited to them, but it has to be disseminated to the local people as well, especially to the ones who are expected to be affected in order to raise their awareness in a sense of being responsible to manage flood.

9.4 Conclusion

The use of HEC-HMS and HEC-RAS models contributed to the forecasting of Nyabugogo River flood risks by identifying the flood plain area, the expected water depth, and showing the vulnerability in terms of land use types affected for different return period. Flooding in Nyabugogo River were found to be caused by high rainfall intensity, topography varying between 1352 and 2888 m, soil texture mainly composed of clay mixed with other texture, urbanization, informal settlement, and inappropriate agriculture practices. Frequency analysis of daily annual maximum rainfall data has been performed to obtain frequency rainfall depth for different return periods. Then HEC-HMS model was used to transform rainfall depth into runoff to obtain peak discharges. HEC-RAS combined with HEC-GEORAS was used to obtain the flood delineation area and water depth corresponding to each event. The analysis obtained from floodplain area and water depth showed that there is a slight increase in floodplain area from

the lower event to high event modelled due to the high topography of the area; the high water depth obtained of 3.2 m occurred during the 100- year event and the more vulnerable land use types affected mostly for all the events consisted of annual cropland, open grassland, open shrubland, settlement, sparse forest, and wetland. Although the increase in floodplain area were small, there is a need of protecting the affected area, therefore different flood mitigation measures have been proposed; however, their cost benefit analysis need to be considered before implementation.

Acknowledgements This research is supported by the African Union through the Pan African University, Institute for Water and Energy Sciences (PAUWES). The authors would like to thank the Rwanda Water and Forestry Authority (RWFA) especially the Integrated Water Resources Management Department officers for their support during the data collection.

References

- Bizimana JP, Shilling M (2010) Geo-information technology for infrastructural flood risk analysis in unplanned settlements: a case study of informal settlement flood risk in the Nyabugogo flood plain, Kigali city, Rwanda. In *Geospatial techniques in urban hazard and disaster analysis*, pp 99–124. https://doi.org/10.1007/978-90-481-2238-7_6
- Disaster Relief Emergency Find (DREF), Rwanda (2012) Floods. <https://reliefweb.int/report/rwanda/rwanda-floods-dref-final-report-mdrrw08>. Accessed 25 February, 2018
- Feldman DA (2000) Hydrological modelling system HEC-HMS, technical reference manual, 148 p
- Floodlist (2016) At least 49 killed in Floods and Landslides, 5000 homes destroyed. <http://floodlist.com/Africa/Rwanda-floods-landslides-Gakenke-Muhanga>. Accessed on 25 February, 2017
- Habonimana H, Bizimana V, Uwayezu E, Uyishimire J, Mugisha J (2015) Integrated flood modelling for flood hazard assessment in Kigali city, Rwanda. *GeoTechRwanda 2015–Kigali*, 18–20 November, 2015
- Machtar A (2010) Using geographical information system to estimate vulnerable settlement for flood hazard and risk assessment. Malaysia: University of Malaysia Kelantan. <http://umkeprints.umk.edu.my/26.1/conferencepaper6.pdf>
- Ministry of Disaster and Refugee Affairs (MIDIMAR), Rwanda (2012) Disaster high risks zones on floods and landslides. Kigali, Rwanda
- Ministry of infrastructure (MININFRA), Rwanda (2015) National informal settlement. Kigali, Rwanda

- Mukherjee D (2016) Effect of urbanization on flood—a review with recent flood in Chennai, India. *Int J Eng Sci Res Technol* 5(7):451–455
- Munyaneza O, Nzeyimana YK, Wali GU (2013) Hydraulic structures design for flood control in Nyabugogo wetland, Rwanda. *Nile Basin Water Sci Eng J* 6(2):26–37
- National Institute of statistics of Rwanda (NISR), Ministry of finance and economic planning (MINICOFIN), Rwanda (2012) Fourth Rwanda population and housing census. Thematic report: population projections. Kigali, Rwanda
- Nduwayezu G, Sliuzas RV, Kuffer M (2017) Modeling urban growth in Kigali city Rwanda. *Rwanda J Ser D Life Nat Sci* 1(1):1–32. [III]. <https://doi.org/10.4314/rj.v1i1S.7D>
- New times–Rwanda (2016) Nyabugogo businesses lose rwf178 m to flooding annually. Available on <http://www.newtimes.co.rw/section/read/198071>. Accessed on 23 February, 2017
- Niyonkuru P (2019) Calibration and validation of EPA SWMM for stormwater runoff modelling in Nyabugogo catchment, Rwanda. *J Sustain Res Eng [S. l.]*, 4(4): 152–159. ISSN 2409-1243
- Queensland Government (2011) Understanding floods: questions answers. www.chiefscientist.qld.gov.au
- Rwanda environmental management authority (REMA), Rwanda (2009) Rwanda state of environmental and outlook report. Kigali, Rwanda
- United Nations Office for disaster risk reduction (UNISDR) (2015) The human coast of weather related disaster (1995–2015) report. <https://www.unisdr.org/we/inform/publicatins/46796>. Accessed on 24 February, 2018
- Water for Growth Rwanda (2017a) IWRM programme Rwanda TR24-catchment plan Nyabugogo 2017–2013
- Water for Growth Rwanda (2017b). TR31-Rainwater harvesting strategy–IWRM programme Rwanda. Kigali, Rwanda



Large-Scale Human Intervention and Estimation of Flood Susceptibility Applying Frequency Ratio Model

Meelan Chamling, Biswajit Bera,
and Sudipa Sarkar

Abstract

Extreme weather events induced by rapid climatic change owing to irrational anthropogenic actions in recent times have dramatically increased the frequency and severity of floods across the world. Modeling the flood susceptible zones provide the much-needed requisite sustainable tool to prevent and mitigate the flood occurrence and its possible adversity on human society. The fundamental objective of the present study is to investigate the application of Frequency Ratio (FR) model in estimating the flood susceptibility areas of Torsa river basin located at the eastern Himalayan Foreland Basin. Flood inventory data of 100 flooding locations for 2017–2019 is collected from National Disaster Management Plan and processed in ArcGIS 10.3 platform to prepare the flood inventory map with 70% training and 30% validation. Eleven major flood causative factors such as altitude, geology, slope angle, slope aspect, rainfall, drainage density, plan curvature,

distance from river, soil type, topographic wetness index, and land use and land cover are extracted from SRTM DEM with 30 m spatial resolution. Each individual causative parameter is processed in ArcGIS 10.3 software to prepare individual causative maps for acquiring the essential values of fluvio-hydrological and spatiotemporal features of flooding parameters mandatory for the calculation of F.R model. The flood susceptibility map computed on the basis F.R model is finally validated using Receiver Operating Characteristics (ROC) curve method to measure its scientific temperaments such as accuracy and efficiency. The estimated ROC curve value for Frequency Ratio (F.R) model is 0.92 which is considerably good and reliable for flood susceptibility determination. The model depicts that around 12 blocks are susceptible to flooding events in the district of Alipurduar and Cooch Behar district of Terai-dooars region. In Alipurduar district nearly 11.01% of people are vulnerable to flood while in Cooch Behar district it is about 3.79%. Most of these blocks and their people are highly exposed to flood and other fluvio-hydrological hazards.

Keywords

Torsa river system · Himalayan foreland basin · Frequency ratio (F.R) model · ROC

M. Chamling · B. Bera (✉) · S. Sarkar
Department of Geography, Sidho-Kanho-Birsha
University, Ranchi Road, Purulia, India

10.1 Introduction

Flood is a natural persuasive phenomenon defined by the inundation and overflow of water from the surrounding streams, rivers, lakes, aquifers, estuaries, and reservoirs to the contiguous areas that usually remain unsubmerged (Fattorelli et al. 1999). Flood is generally the outcome of a complex geological and hydrogeomorphological environment and often epitomizes the most intimidating and outrageous natural disaster of global scale owing to its rampant adversity in terms of destruction to life and property (Gashaw and Legesse 2011). Though the flood occurrence and its decimating impact are inevitable, yet the rational scientific evaluation and management of flooding events along with its causes and repercussion can be dealt with the adaptation of radically relevant analysis and forecasting methods (Cloke and Pappenberger 2009; Tehrany et al. 2015). Ascertaining the flood hazard zone and computing flood susceptibility maps will certainly become an imperious tool in preventing, managing, and mitigating the flooding prevalence and its prospective hostile imprints on the human society.

Generally, flood management methods are broadly divided into three segments viz. pre-flood measures, flood event forecast, and post-flood response (Kourgialas and Karatzas 2011). Flood management can usually be accomplished by integrating the anticipation, preparation, prevention, and evaluation of destruction (Konadu and Fosu 2009). Such critically acclaimed flood management programs can be conceivable only through the effective determination of flood susceptibility areas (Tehrany et al. 2013). The accurate and consistent identification of flood-prone areas and preparation of flood susceptibility maps enables the prompt response, diminishes the probable adversity of flood hazard, and thereby present a scientific means of early warning or caution (Kia et al. 2012).

Effective neutralization of flooding adversity through rational and scientific flood modeling is the paramount attribute of the formulation of

comprehensive watershed management (Rahmati et al. 2016). Forecasting of flood events by determining the flood susceptible areas are relatively challenging owing to the lack of availability of specific and reliable hydrological data due to the dearth of sophisticated hydrological observation stations (Khosravi et al. 2016). In the recent time, hydrologists across the world have designed and enunciated different types of flood risk and susceptibility models formulated on the basis of the natural properties or parameters of watershed. These models are found to be reasonably successful in resolving the flood induce hazards in different parts of the world (Jayakrishnan et al. 2005; Bahremand et al. 2007). In case of traditional hydrological model, the adopted methodology is simple and mostly based on linear assumption mechanism which is relatively inappropriate and irrational for the holistic studies of watershed management (Liu and De Smedt 2004). Thus, these conventional and traditional hydrological methods are somewhat incompetent and have failed to provide a comprehensive assessment of flood susceptibility (Li et al. 2012; Tehrany et al. 2014). The advent of Remote Sensing and GIS techniques in the field of Hydrological science has greatly helped the researcher and administrator to streamline various fluvio-hydrological mitigation plans to deal with the pre-hazard, during hazard, and post-hazard environmental circumstances. Frequency Ratio (F.R) model based on robust Remote Sensing and GIS manoeuvre is considered significantly competitive and highly precise in contrast to any other nonlinear multivariate models to accurately evaluate the flood susceptibility area for any regional studies (Liu and De Smedt, 2004; Pourghasemi et al. 2012; Youssef et al. 2014). Several studies carried out across the world in recent contemporary period that unveils the satisfactory result of Frequency Ratio model. For example, Naghibi et al. (2015) while using Frequency Ratio model in Moghan watershed concluded that the model is highly accurate with nearly 91.21% in flood susceptibility determination. Similarly, Jaafari et al. (2014) used Frequency Ratio (F.R) model to

demarcate and prepare the landslide susceptibility map of Caspian forest. The model yields around 89.12% of precision. In another instance, Rajsekhar et al. (2013) achieved remarkable higher accomplishment of exactitude in measuring the drought categorization, drought duration identification, and drought severity studies.

Unscientific and unreasonable practices of land use and land cover (LULC) like indiscriminate deforestation, unplanned expansion of cropland, overgrazing, uncontrolled and irrational growth of human settlement, unscientific method of mining, extension of linear infrastructure such as roadway and railway, etc., are gradually degrading the spatiotemporal homeostatic equilibrium mechanism of the watershed (Bishaw 2001; Tiwari and Chatterjee 2010). The evidence of such jeopardizing adversity is apparent in recent times manifested in the form of frequent flood events along with the longer duration of water inundation within the flood plain areas. The Torsa river basin/watershed situated in the Himalayan Foreland Basin in the Eastern Himalaya is no exception in such cases. The intense increase in channel bed elevation owing to excessive sedimentation as a result of radical LULC transformation experienced by the region in recent decades have massively caused the obstruction of active channel path and frequent change in cross valley slope (Jain and Sinha 2004; Mukhopadhyay 2014). As a result, the high rate and magnitude of river channel sedimentation along with the substantial channel migration has induced severe flood events and related repercussions (Chakraborty and Ghosh 2010). The densely populated blocks under the district of Alipurduar and Cooch Behar located in the northern edge of the state of West Bengal, India are continuously exposed to the vulnerability of recurring flood hazards particular from the adverse impact of the Torsa river and its tributaries. Every year, tens and thousands of people along with the huge natural resources are utterly devastated by the dreadful and catastrophic hydro-geomorphic hazards like floods triggered by the mighty Torsa river and its tributaries in its basin areas. Therefore, an attempt has been undertaken to make a scientific

study of the Torsa river basin and determine the potential flood susceptibility areas by applying the Frequency Ratio (F.R) model.

10.2 Study Area

The study area includes the Torsa river basin located at the Eastern Himalayas foredeep basin and extents between 25°55'46" N to 26°51' 35"N and 89°15' 22" E to 89°47' 22" E (Fig. 10.1). It covers an area of about 3340.99 km² and predominantly lies in the district of Alipurduar and Cooch Behar of West Bengal, India. The Torsa river is a transboundary river originating from Tibet and flows through Tibet, India, and Bangladesh. The entire course of Torsa river extends to around 295 km, out of which 75 km is in Tibet, 80 km in Bhutan, 99 km in West Bengal, India, and 45 km in Bangladesh. The important tributaries of Torsa rivers are Holong, Chhoto Torsa, Kaljani, Napania, Gadadhar, etc. The south-easterly dipping, fast-changing dynamic landscape at the foredeep basin of Himalayas controls the entire physical units or more clearly the drainage system in this area. The basin comprises alluvial soil of recent geological formation (Holocene period) and it is characterized by the presence of numerous hydro-fluvial features like swamps, natural levees, oxbow lakes, palaeo-channels, flood plains, etc. The entire designated area which lies in the Terai-dooars belt experiences tropical monsoonal climate with temperature ranging between 23 °C in summer and 10 °C in winter. Moderate and heavy rainfall encourages extensive agricultural activities.

10.3 Methods and Materials

10.3.1 Earth Observation Data

Remotely sensed multispectral band satellite data has emerged as a cost-effective, time-saving, and highly accurate tool to inspect flood hazards (Mouat et al. 1993; Coppin and Bauer 1996; Kaiser 2009; Chamling and Bera 2020). Landsat 8 Operational Land Imager (OLI) with 30 m

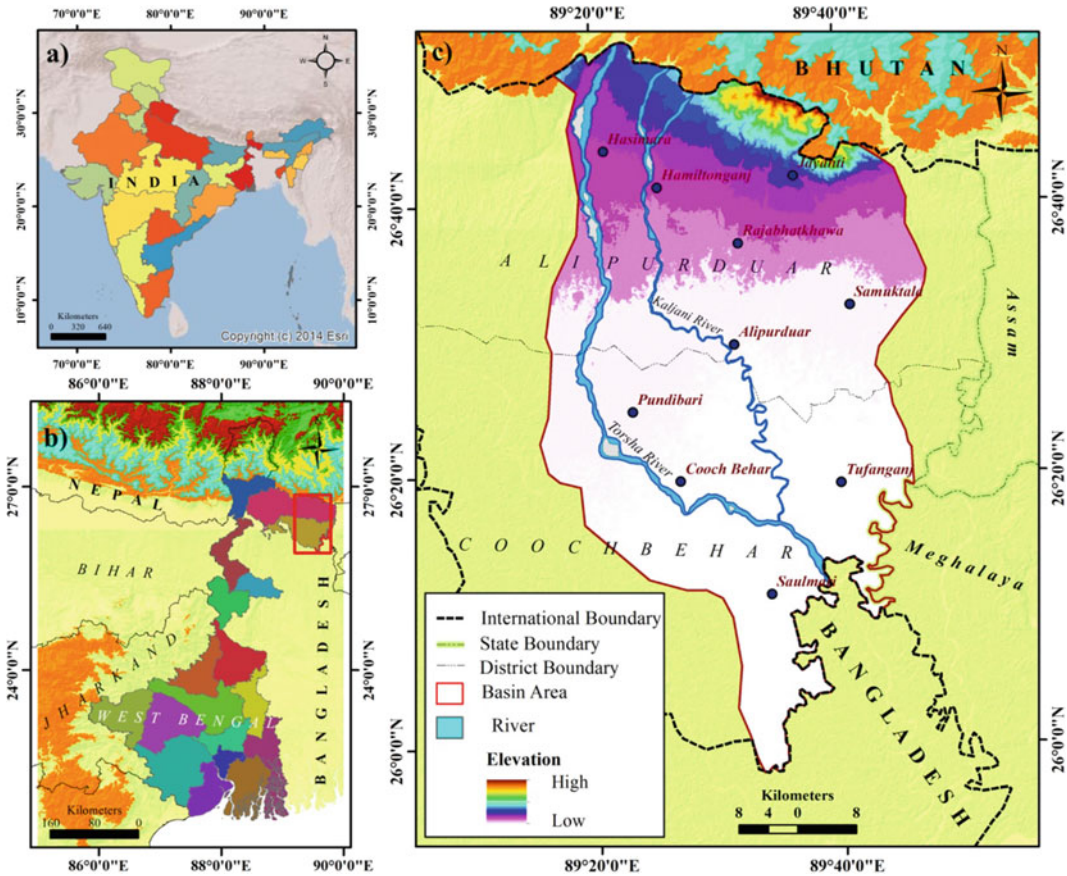


Fig. 10.1 Location of the study area

compatible spatial resolution satellite imageries are downloaded from US Geological Earth Explorer Landsat data archive (<http://earthexplorer.usgs.gov/>). It comprises of multi-spectral band of green ($0.5 \mu\text{m}$), red ($0.6\text{--}0.7 \mu\text{m}$), and near Infrared ($1.1 \mu\text{m}$) which is then registered in Universal Transverse Mercator (UTM) projection to prepare hybrid composite land use and land cover (LULC) classification map of study area in the ERDAS IMAGINE 2014, a raster-based geospatial software version: 16.5 (v16.5.0.852). For delineation of Torsa river watershed along with extraction of important flood causative parameters, Shuttle Radar Topography Mission (SRTM) digital elevation model (DEM) with 90 m resolution is obtained from US Geological Earth Explorer (<http://earthexplorer.usgs.gov/>)

(Table 10.1). All the prerequisite computations of hydrological outputs are processed and executed in the ArcGIS 10.3, ESRIgeospatial software.

10.3.2 Delineation of Watershed and Extraction of Flood Causative Parameters

Torsa river basin is delineated using ArcHydro tool by exercising SRTM DEM and topographical map in ArcGIS 10.3 software following WGS 1984, UTM zone 45N projected coordinate system. Principal watershed area, drainage basin, length of river, drainage density, and drainage network with 20 m contour interval are computed and extracted employing hydrological toolset

Table 10.1 Specifications of standard data set

Sl. no.	Data type	Path/row Index/map no	Acquisition period/publication	Spatial coverage	Resolution	Source
1	SRTM DEM		2017	Alipurduar and Cooch Behar district	30 m	USGS earth explorer
2	Landsat OLI 8	139/42 139/41	2019	Alipurduar and Cooch Behar district	30 m	USGS earth explorer
3	Geological quadrangle map	78/F	2002	Alipurduar and Cooch Behar district	1:500,000	Geological survey of India
4	Topographical map	78F/7, 78F/11	1970–71	Alipurduar and Cooch Behar district	1:500,000	Survey of India
5	Soil map	Sheet no. 3	1991	Alipurduar and Cooch Behar district	1:500,000	National bureau of soil survey and land use planning
6	Meteorological	Rainfall data of 2017 is retrieved from Hasimara, Cooch Behar, Alipurduar, TufanganjNagrakata, and Banarhat submeteorological stations		Alipurduar and Cooch Behar district	–	Indian meteorological department

performed in ArcGIS 10.3 platform (Bera et al. 2019). The watershed SRTM DEM with 3,650,694 pixels having 30 m spatial resolution is analyzed in ArcGIS spatial analyst surface tool to extract slope angle and slope aspect. For identification of the major soil composition of the study area, soil map derived from National Bureau of Soil Survey (NBSS) and for demarcating the prominent lithology and geology of the region, geological map of Geological Survey of India are processed and digitized in ArcGIS 10.3 software using geographical coordinate system (WGS 1984; WKID 4326). The rainfall data is retrieved from Indian Metrological Department (IMD) local metrological substations (Table 10.1). The land use classifications are computed from multispatial band raster imageries, image interpretation, and classification process. Maximum Likelihood Classification (MLC) supervised method; a commonly used algorithm geospatial quantitative appraisal technique is used to prepare the land use categorization by performing in

ERDAS IMAGINE, a raster-based geospatial software version: 16.5 (v16.5.0.852).

10.3.3 Flood Causative Conditioning Factors

To develop a strong methodology (Fig. 10.2) and to identify and evaluate the flood susceptibility, it is perquisite exercise to determine the potential causative parameters or factors and establish their relationship with flood occurrence (Liu and De Smedt 2005; Pradhan 2009). Flood susceptibility determination of any watershed relies on a large set of data as the independent variables which are effective enough to cause flooding. The processing and analyzing of such large set of causative factors in modeling process demand sufficient time and technology which often delays the quick and prompt response to flood mitigation (Campolo et al. 2003; Sanyal and Lu 2004). Considering some important parameters

and their subsequent critical analysis are required to evaluate the flood susceptibility for any region (Pradhan and Lee 2010; Skilodimou et al. 2003; Erena and Worku 2018). Therefore, eleven major flood causative factors of the Torsa river basin are considered to identify the flood susceptibility areas. These are altitude, geology, soil type, slope angle, rainfall, slope aspects, land use, drainage density, plan curvature, and topographic wetness index (TWI). The quantile method is applied to classify the each and every independent variable as each class contains similar number of features and found to be highly

efficient in classification (Tehrany et al. 2013; Kia et al. 2012; Rahmati et al. 2016).

Altitude

Elevation differences always fabricate alteration in the climatic features, vegetation composition, and soil conditions (Aniya et al. 1985). Hence, altitude is one of the decisive factors in flood susceptibility mapping. The elevation map is for the designated basin using SRTM DEM with five important elevation (m) categories viz. <100, 100–200, 200–300, 300–400, and >400 (Fig. 10.3a).

Fig. 10.2 Schematic presentation of methodology

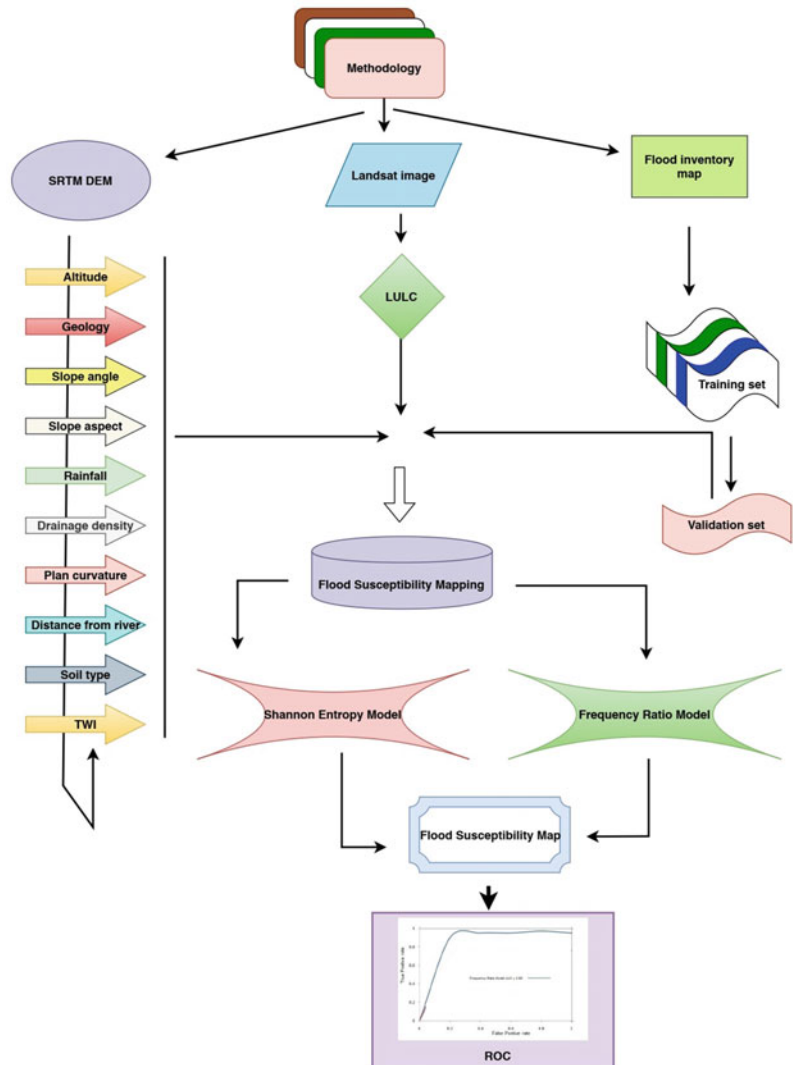
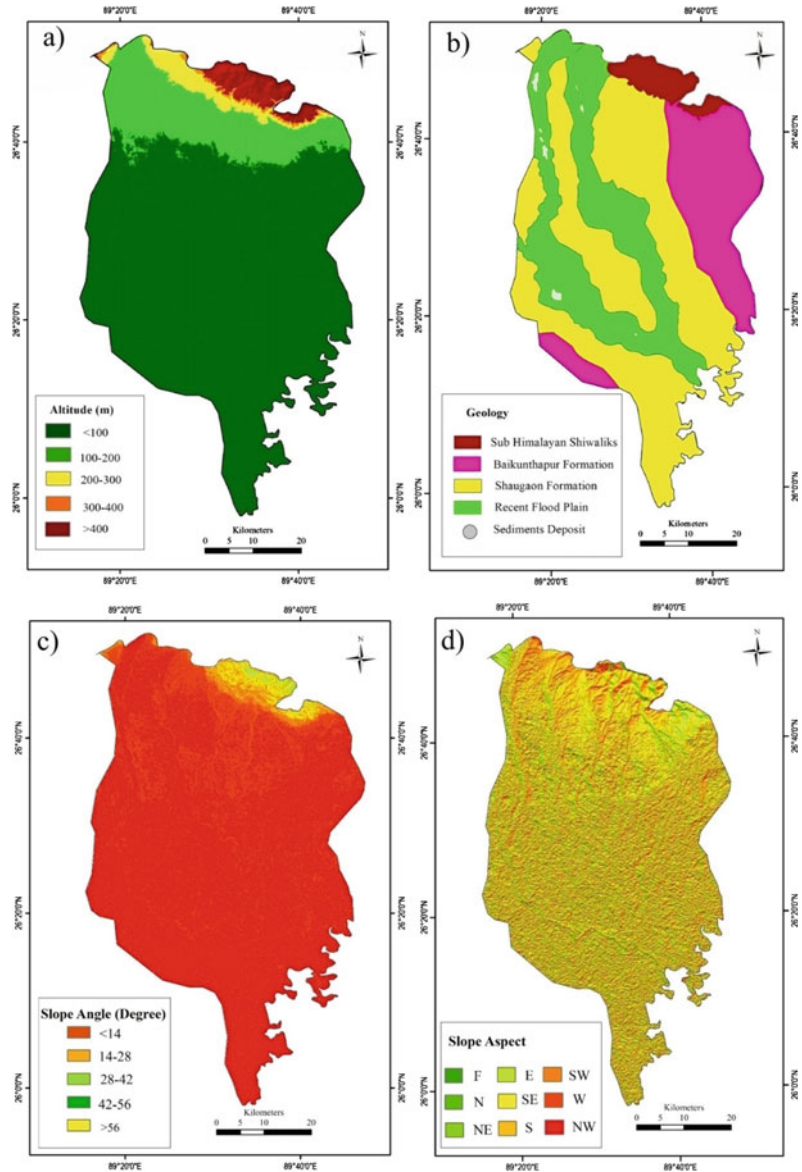


Fig. 10.3 Flood causative factors **a** Altitude **b** Geology **c** Slope angle **d** Slope aspects



Geology

Among the dominant parameters in driving the hydrological response like flood events, geology is often considered as the prominent one. The geology directly governs the flow path of surface and subsurface flow and its spatial distribution within the catchment, bedrock permeability, layers thickness, outcrop size, nature of interface between bedrocks and soil horizons, watershed water storage, etc. Drainage network, drainage

density runoff, permeability power, etc., which are vital in manoeuvring the flood and it is immediately controlled by the underlying geological arrangement. Therefore, the knowledge of geological structures and their characteristic is essential in predicting flood susceptibility. The prepared geological map of selected basin area shows four major geological formations. It includes Sub Himalayan Shivalik, Baikunthapur formation, Shaogaon formation, and recent flood plain (Fig. 10.3b).

Slope Angle

Considered as one of the important factors in flood occurrence due to its direct control over surface runoff and percolation, slope angle is extracted from the SRTM DEM, and the entire study area is classified into five slope angle ($^{\circ}$) zone viz. <2.42, 2.42–9.98, 9.98–22.39, 22.39–35.08, and >35.08 (Fig. 10.3c).

Slope Aspect

Slope aspect is a crucial parameter in evaluating the geomorphological stability by influencing the intensity of precipitation and soil moisture. To determine the water flow direction is perhaps the most important application of slope aspect computation. It is prepared in ArcGIS 10.3 software using Arc hydrological tool and classified slope into nine major direction classes. They are flat, north, south, east, west, northeast, northwest, southeast, and southwest (Fig. 10.3d).

Rainfall

The most widespread meteorological factor which leads to flooding is the amount, intensity, and duration of rainfall. The magnitude of flood is often portrayed by analyzing the peak water level during the flood by considering the various aspects of rainfall. During the monsoon season due to heavy rainfall, the rivers and lakes are frequently overburdened with additional water which results in inundation and overflow into surrounding areas. The chosen study area is divided into five rainfall zone viz. <2650, 2650–2900, 2900–3150, 3150–3400, and >3400. The computed rainfall map shows the basin receive relatively higher rainfall (Fig. 10.4a).

Drainage Density

The ratio of total length of watershed channels to the basin area is considered as drainage density. The watershed with high drainage density often triggers flashy flood hydrograph and frequent flood susceptibility. It is expressed as

$$Dd = \frac{\sum_1^n L}{A} \quad (10.1)$$

where, Dd means drainage density, L stands for length of stream, and A denotes stream basin. The selected basin is divided into six drainage density classes, namely, <0.39, 0.39–0.78, 0.78–1.17, 1.17–1.56, and >1.56 (Fig. 10.4b).

Plan Curvature

Plan curvature is an important parameter on flood probability of watershed. The curvature map processed and computed in ArcGIS 10.3. The whole areas of basin have three important curvature plans. They are concave, flat, and convex. The Plan curvature value ranges between <2.02, 2.02–0.033, 0.33–0.45, 0.45–0.56, and >0.56 (Fig. 10.4c).

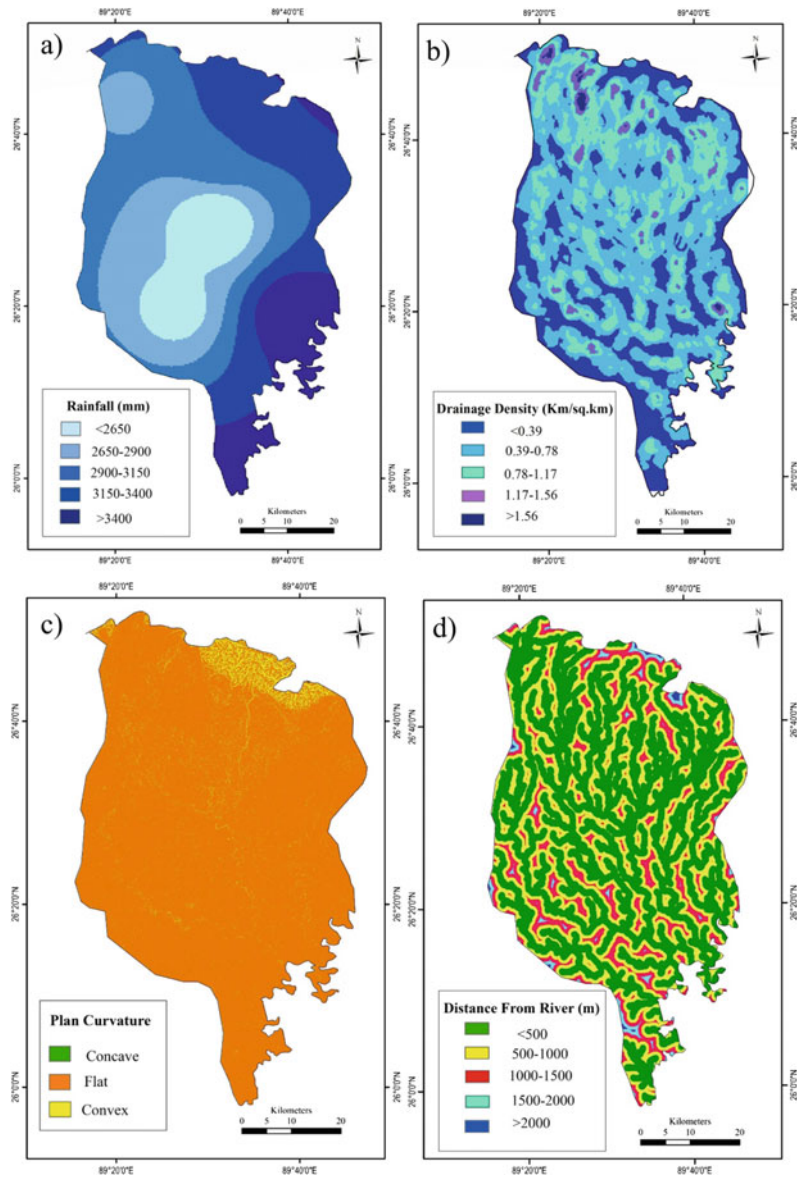
Distance from the River

Generally, flood occurs adjacent to river banks and inundates the low-lying areas of flood plains. Flood magnitude and its spatial distribution usually depend on the distance from the river. Being one of the important causative factors, distance from the river is produced based on digital layer of flow network of proximity analysis on ArcGIS software. Six flood potential classes were obtained on the basis of distance from the river. They are >500, 500–1000, 1000–1500, 1500–2000, and >2000 (Fig. 10.4d).

Soil Type

Soil plays a crucial role in influencing the runoff and subsurface characteristics in watershed and acts as a potential factor in causing flood in the downstream of the watershed. Pedological factors like soil types, characteristics, and compositions strongly determine the hydrological response to rainfall, water storage capacity, infiltration rate, and eventually the flood recurring condition. On the basis of the National Bureau of Soil Survey and Land Use Planning (NBSS& LUP), the major soil type which is

Fig. 10.4 Flood causative factor **a** Rainfall **b** Drainage density **c** Plan curvature **d** Distance from river



found in the study area and includes very fine loamy (W007) and coarse loamy soil (W008) of piedmont plain soils (Ap) and coarse loamy (W010), fine (W026) and fine silty (W028) belonging to Active alluvial plain or flood plain soils (AaA) (Fig. 10.5a).

Topographic Wetness Index (TWI)

Topographic Wetness Index (TWI) is also commonly known as compound topographic index (CTI) which is widely used to quantify the topographic or spatial scale control on

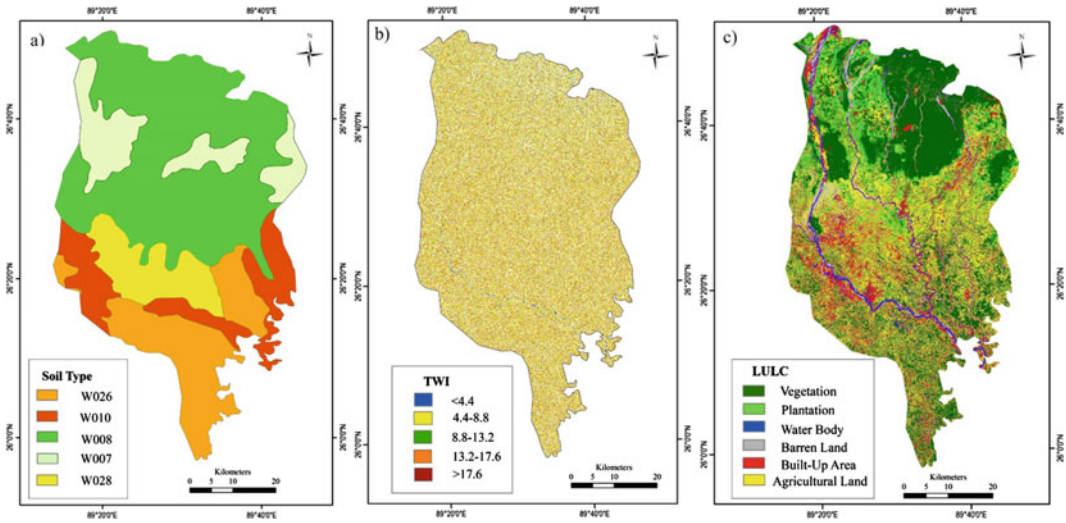


Fig. 10.5 Flood causative factor **a** Soil type **b** TWI **c** LULC

hydrological processes. It is based on the slope and upstream area which helps to identify the surface runoff flow paths and thus regarded as a significant index in examining the flood potential of any watershed. It is expressed as

$$TWI = \ln\left(\frac{As}{\tan\beta}\right) \quad (10.2)$$

where, TWI means Topographic Wetness Index, *As* stands for specific watershed area and β denotes curvature slope (in degree). The high TWI with the value of >17.6 is randomly distributed over the basin area while the low TWI value of <4.4 lies in the extreme northern parts of the study area (Fig. 10.5b).

Land Use and Land Cover (LULC)

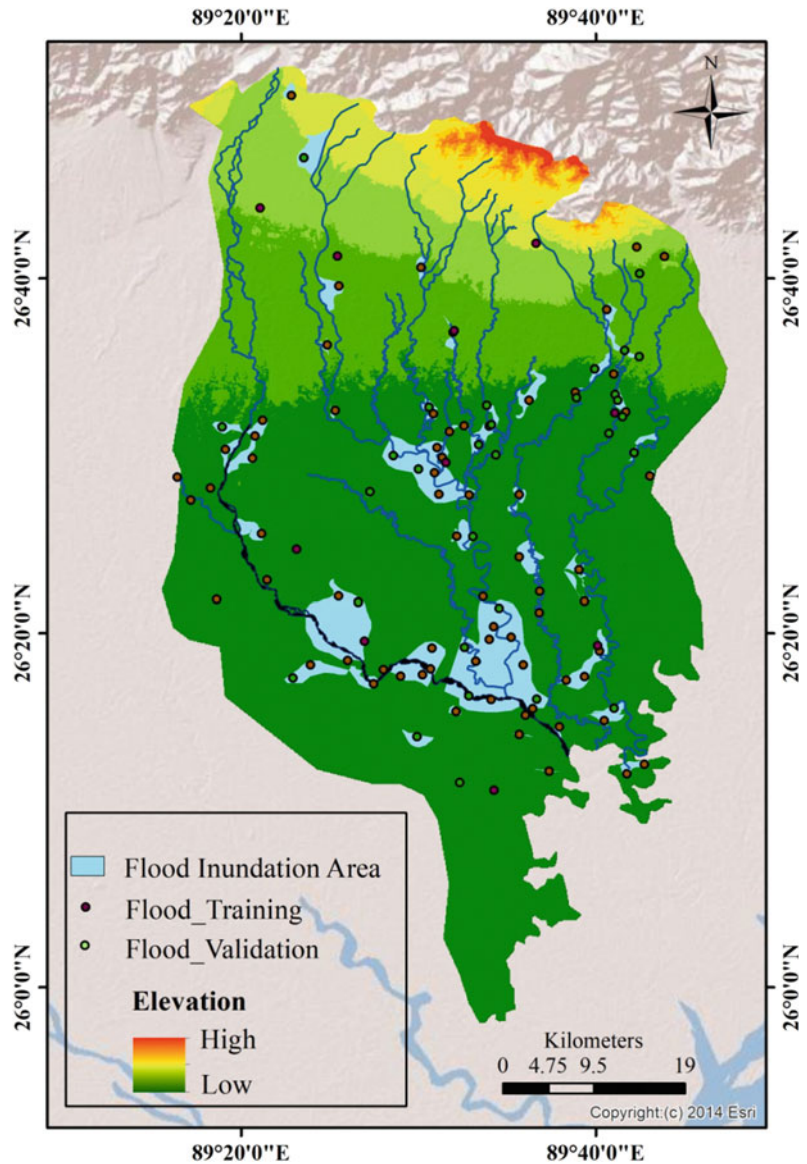
Land use and land cover (LULC) is an important factor in determining the hydrological condition of watershed along with topography and geology. With increasing anthropogenic activities and far and wide development and alteration of catchment area land use/cover, the incidence of flood frequency has increased many folds over the year. The land use and land cover transformation is found to be highly capable to trigger alteration of river basin hydrograph and increase

the annual mean discharge, flood frequency, and overall damage. In total six LULC classes are identified in the study area namely agricultural land, built-up area, current fallow land, barren land, vegetation, and water body. The northern part of the basin area is covered with dense vegetation while the middle portion of the study area shows moderately high built-up scenario. Overall the study basin area is dominated by agricultural land with sporadic barren land (Fig. 10.5c).

10.3.4 Statistics and Mapping of Past Flood Location

In order to examine the flood potentiality, the flood inventory maps are prerequisite for the study of relationship between flood occurrence and their causative factors (Manandhar et al. 2010). The highly accurate and appropriate data of past historical flooding is obtained to create the spatial database and prepare the flood susceptibility map of the Torsa river basin. Around 100 flood location statistics that were occurred in the past from 2017 to 2019. These were collected from Disaster Management Plan of Alipurduar and Cooch Behar district and verified with intensive field survey. The specific flood events

Fig. 10.6 Flood inventory map of Torsa river basin



location is used as raster network (30×30 m) applicable in Frequency (FR) model. Thereafter, flood inventory map is prepared using “create fishnet” technique of PNRIS field survey, satellite dataset, disaster management database, and aftermath flooding events. 70% of total flood location points (i.e., 70 points) were randomly designated as the training data for flood modeling while the remaining 30%, i.e., 30 points were used as non-flood points for validation group on

the scale of 1:25,000 (Rahmati et al. 2016) and are shown in Fig. 10.6.

10.3.5 Flood Susceptibility Modelling

10.3.5.1 Frequency Ratio (FR) Model

Frequency Ratio (F.R) model is a bivariate statistical analysis (BSA) method which facilitates the computation of probabilistic relationship

between the independent and dependent variable along with multiclassified map. It is a simple method that predicts the possibility of occurrence of certain attributes and the results can be understood with an ease (Bonham-Carter 1994; Yilmaz 2010). Past flooding events and their condition factors forms the basis for FR model. The relationship between the flood events occurrence area and the flood causative factors can be inferred from the association among the areas where the flood has not occurred and the flood causative factors. To identify the closeness of such relationship, frequency ratio approach is the highly suitable statistical technique. Frequency Ratio (F.R) model is found to be significantly effective in ranking the preferred causative factors on the basis of their capacity to influence the flood events (Kannan et al. 2013). It is expressed as

$$FSI = \sum FR \tag{10.3}$$

where, FSI indicates Flood Susceptibility Index while FR means frequency ratio. To compute frequency ratio, the empirical equation is used.

$$FR = \frac{N_{pix}(SX_i) / \sum_{i=1}^m SX_i}{N_{pix}(X_j) / \sum_{j=1}^n (X_j)} \tag{10.4}$$

where, FR stands for Frequency Ratio, $N_{pix}(SX_i)$ indicates the number of pixels of floods within the class i of parameter variable X , $N_{pix}(X_j)$ denotes the number of pixels of parameter variable X_j , m means number of classes in parameter variable X_i , and n is the number of parameters in the area of interest (study area).

The frequency ratio (FR) is calculated for all the layers which are used in this investigation and the frequency ratio (FR) is acquired on the basis of these values (Table 10.2). Using the spatial analysis tool of ArcGIS 10.3 software, the thematic maps are reclassified and prepared.

Frequency ratio (F.R) is a reliable method which is used globally for mapping flood susceptibility and analyses the relationship of ratio between the area where the flood event occurred to the whole area of interest (Yilmaz 2009; Shafapour et al. 2019). If the FR value is found to be higher than 1, it indicates that the parameters or factors are strong enough in influencing the

Table 10.2 Determining the relationship between the flood locations and flood causative factors applying Frequency Ratio (F.R)

Factors	Class	No. of pixels in sub-basin	No. of floods	Frequency ratio (F.R)
Altitude	<100	288,963	70	1.03
	100–200	62,818	10	0.00
	200–300	29,315	0	0.00
	300–400	12,563	0	0.00
	>400	25,128	0	0.00
Geology	Sub Himalayan	117,260	29	3.02
	Shivaliks	150,763	22	0.75
	Baikunthapur	8375	10	0.06
	Formation	20,941	19	0.24
	Shaugaon Formation Recent Flood Plain			
Slope angle (°)	<14	409,037	75	1.10
	14–28	8905	5	0.04
	28–42	804	0	0.00
	42–56	34	0	0.00
	>56	7	0	0.00
Slope aspect	F	39,416	3	0.55
	N	40,816	9	1.10

(continued)

Table 10.2 (continued)

Factors	Class	No. of pixels in sub-basin	No. of floods	Frequency ratio (F. R)
	NE	44,350	12	1.09
	E	53,782	10	1.06
	SE	64,797	9	1.01
	S	57,327	10	1.09
	SW	47,926	14	1.40
	W	41,376	9	1.01
	NW	28,997	4	0.61
Rainfall (mm)	<2650	123,570	5	1.01
	2650–2900	140,654	17	1.59
	2900–3150	78,504	8	0.89
	3150–3400	56,000	19	1.72
	>3400	16,019	31	2.00
Drainage density	<0.39	113,072	10	0.56
	0.39–0.78	159,139	29	1.09
	0.78–1.17	102,556	27	1.69
	1.17–1.56	37,691	8	0.90
	>1.56	6329	6	0.73
Plan curvature	Concave	142,387	0	0.00
	Flat	201,019	80	1.00
	Convex	75,381	0	0.00
Distance from river	<500	240,510	25	2.92
	500–1000	131,020	18	2.03
	1000–1500	41,212	16	1.90
	1500–2000	5385	11	0.87
	>2000	660	10	0.63
Soil type	W007	54,442	12	1.60
	W008	58,630	35	3.75
	W010	117,262	14	1.70
	W026	83,757	10	1.20
	W028	104,696	9	1.06
TWI	<4.4	203,212	30	0.80
	4.4–8.8	87,055	35	1.20
	8.8–13.2	78,321	5	1.85
	13.2–17.6	19,697	5	0.85
	>17.6	30,502	0	0.00
LULC	Vegetation	115,166	25	3.42
	Plantation	52,348	16	2.00
	Waterbody	16,751	10	1.90
	Barren land	25,127	8	1.84
	Built-up	41,880	14	1.98
	Agricultural land	167,512	7	1.00

flooding. On the other hand, if the FR is less than 1, it denotes the existence of a negative relationship between the flood event and operational variables (Lee and Talib 2005; Sujatha et al.

2013). The ratio is applied to determine the susceptibility index of the flooded area and finally, it prepares the flood susceptibility map based on frequency ratio model using empirical equation.

$$\begin{aligned}
 FSI = & (Altitude_{FR}) + (Lithology_{FR}) + (Slopeangle_{FR}) \\
 & + (Slopeaspect_{FR}) + (Drainagedensity_{FR}) \\
 & + (Distancefromriver_{FR}) \\
 & + (Plancurvature_{FR}) + (Soiltype_{FR}) \\
 & + (TWI_{FR}) + (Landuse_{FR})
 \end{aligned}
 \tag{10.5}$$

where, *FSI* means flood susceptibility index and *FR* is frequency ratio. The acquired pixel values are thereafter classified on the basis of natural break classification scheme (Regmi et al. 2014; Ozdemir 2011; Pourghasemi et al. 2012; Zare et al. 2013; Moghaddam et al. 2015).

10.3.5.2 Flood Susceptibility Map Validation

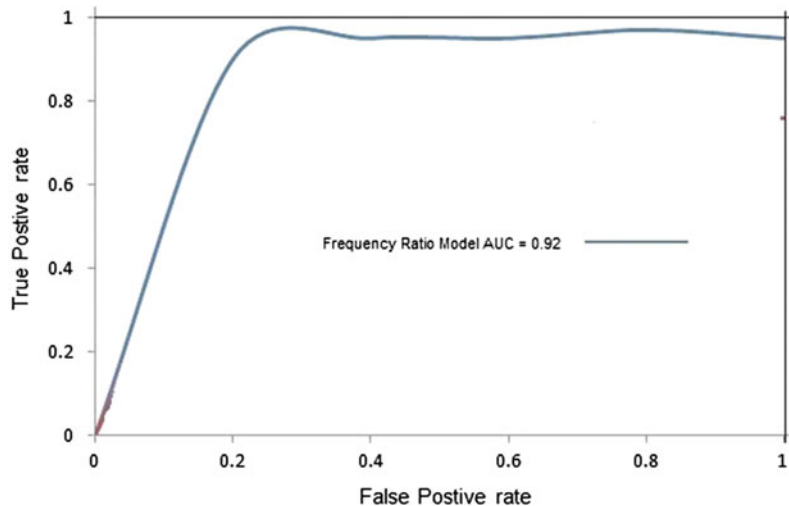
The application of any model depends on its accuracy and reliability which need to be validated scientifically (Akgun et al. 2008; Pradhan et al. 2009). For the present flood susceptibility map validation, the receiver operating characteristics (ROC) curve is applied to assess its suitability. The ROC curve is a simple, useful, and efficient universal method to determine the feature, identify and predict the system (Swets 1988; Hong and Cho 2015). In ROC curve, true positive (correctly predicted pixels) rates are plotted along Y-axis while false positive (incorrectly predicted pixels) rates are shown along X-axis. To substantiate the model, area under curve

(AUC) is considered. If the AUC value is 1, it indicates that the model is perfectly suitable for estimating flood susceptibility. The value of 0.5 or less means the model is inappropriate while the value greater than 0.75 denotes flood predictability is reasonably suitable (Egan 1975; Ozdemir and Altural 2013; Heagerty and Saha-Chaudhuri 2017). As per Rahmati et al. (2016), the quantitative relationship between AUC and model prediction accuracy is classified into five categories viz. poor (0.5–0.6), good (0.7–0.8), very good (0.8–0.9), and excellent (0.9–1.0). The result of ROC curve as in Fig. 10.7 reveals that AUC value of the Torsa river basin is found to be 0.92. Therefore, on the basis of computation and validation of AUC, it can be concluded that the flood susceptibility mapping of Torsa river basin is considerably accurate with FR model being a more suitable technique for identifying and mapping the flood susceptibility area.

10.4 Results and Discussion

The flood susceptibility zones or areas of Torsa river basin is determined by calculating the ten flood causative parameters or conditioning factors in Frequency Ratio model (Table 10.2). Each factor of flooding conditions is critically investigated and meticulously analyzed as flood occurrence is generally the outcome of one or

Fig. 10.7 ROC of flood susceptibility map of Torsa basin based on F.R model



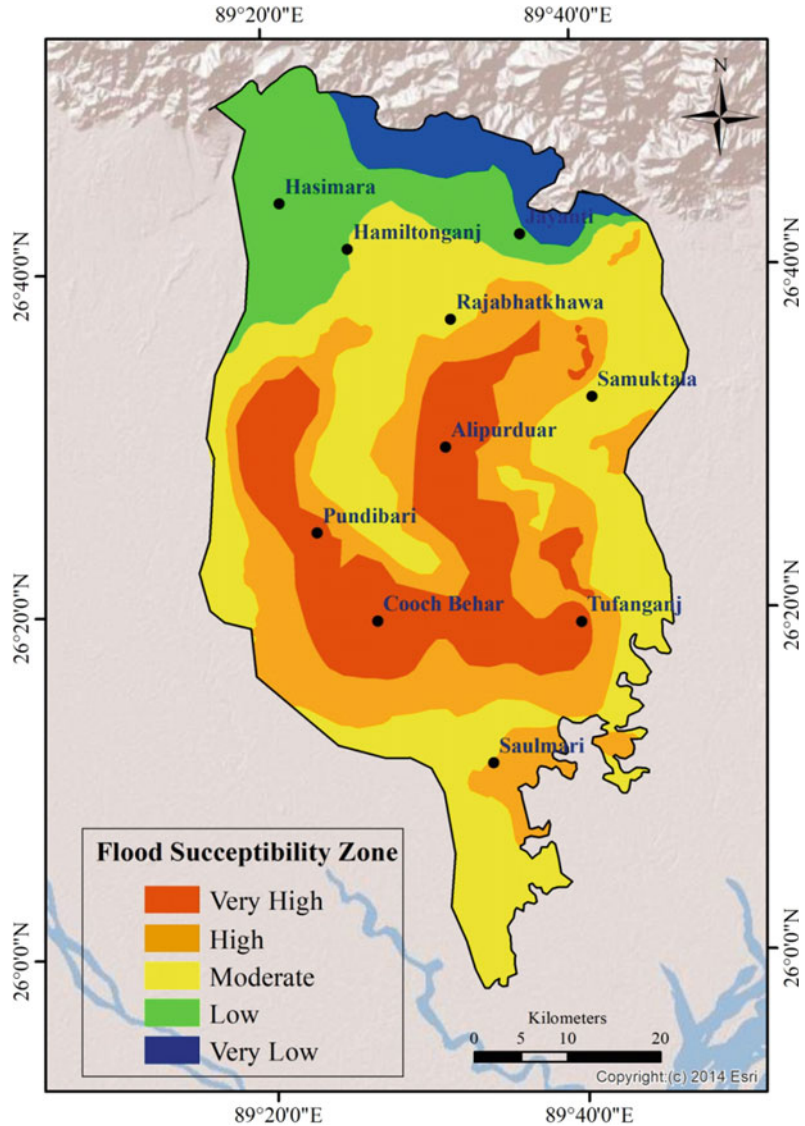
more causative parameters. The scrutiny of elevation map of the basin reveals that the area with less the 100 m altitude is highly prone to flood events. These high flood susceptibility areas are spread over the entire region except in the northern parts where higher altitude is found (Fig. 10.3a). With respect to geology, recent flood plain geological formation adjacent to river banks is liable to higher flooding incidents (Fig. 10.3b). Similarly, Shaogaon formation geological sites covering the larger part of the basin is also under moderately higher vulnerable to flood (Table 10.2). The whole basin except for a small portion in the northern part lies within a low slope angle of $<2.42^\circ$ which portrays very high flood frequency (Fig. 10.3c). While investigating Torsa river basin, it is observed that the areas with east, south-west, west, and south-east are under high flooding events zone (Fig. 10.3d). On the other hand, land with no aspect reveals low flood (Table 10.2). In terms of rainfall, the entire basin area receives sufficiently high rainfall. Higher rainfall of more than 3150 mm and above which mostly occurs in the northern and eastern portion of the upper catchment of river Torsa provides ample discharge to cause flooding in the southern part of the basin (Fig. 10.4a). In the study area, the Plan curvature index depicts that the entire region is a flat surface which can easily lead to flooding during heavy monsoonal rainfall season (Fig. 10.4c). The computed drainage density reveals that the basin has a dense network of streams. Very high drainage density of $>1.56 \text{ km}^2$ is randomly scattered all over the basin area which makes the southern part highly susceptible to flood (Fig. 10.4b). Distance from the river map indicates that the flood events are expected up to 2000 m away from the river. In other words, areas lying within this distance are more prone to flood than away from the 2000 m (Fig. 10.4d). The highest flood events are found within the 500–1000 m and 1000–1500 m distance away from the rivers (Table 10.2). The examination of soil type is found in the basin and it denotes that the coarse loamy soil (W008) of piedmont plain (Ap) is found in the northern and central part while at the south, fine loamy soil (W026) belonging to Active alluvial plain or

flood plain soils (Aa) spreads extensively. Fine silty soil (W028) of AaA lies near the river bank. On the other hand, very fine loamy soil (W007) of Ap is scattered away near northwest and northeast of the basin. In general, the pedological factors of soils reveal that the entire basin is highly susceptible to flood (Fig. 10.5a). Topographic Wetness Index (WTI) calculation indicates that the areas with 4.4–8.8 TWI value and less than 4.4 are under high flood incidents while TWI value of 13.2–17.6 and greater than 17.6 shows no flood events (Table 10.2). Land use and land cover (LULC) map depicts high flood events in agricultural land located at the central and southern areas of the Torsa river basin (Fig. 10.5c). Most of the flooding has taken place within the flood plains which are situated close to the rivers (water body) (Table 10.2).

The Frequency Ratio model susceptibility unveils that the areas lying near the river banks are under very high flood susceptibility zones in the river Torsa basin (Fig. 10.7). High flood susceptibility areas lie just at the margin of very high flood vulnerable zones. Low and very low flood-prone areas are scattered particularly at the outer parts. Flooding events with moderate magnitude are spatially found over the whole of the basin at the periphery areas of high flooding zones (Fig. 10.8).

Around six blocks each in the district of Alipurduar and Cooch Behar of Tera-dooars region of Himalayan foredeep basin is situated within the Torsa river basin (Fig. 10.9). In case of Alipurduar district, the six blocks/municipalities are Alipurduar-I, Alipurduar-II, Kalchini, Kumargram, Madarrihat-Birpara, and Alipurduar municipality. Alipurduar municipality with six wards is highly vulnerable as 31.37% of its populations are affected by the flooding events. Similarly, Kumargram and Alipurduar-II blocks are also under threat to high frequency of flood occurrence as nearly 22.42% and 22.165% of the populations are susceptible to flood, respectively (Table 10.3). Alipurduar-I (10.54%), Kalchini (9.91%), and Madarrihat-Birpara (8.23%) blocks are relatively less susceptible. Alipurduar-II block has the highest number of affected villages ($n = 41$) followed by

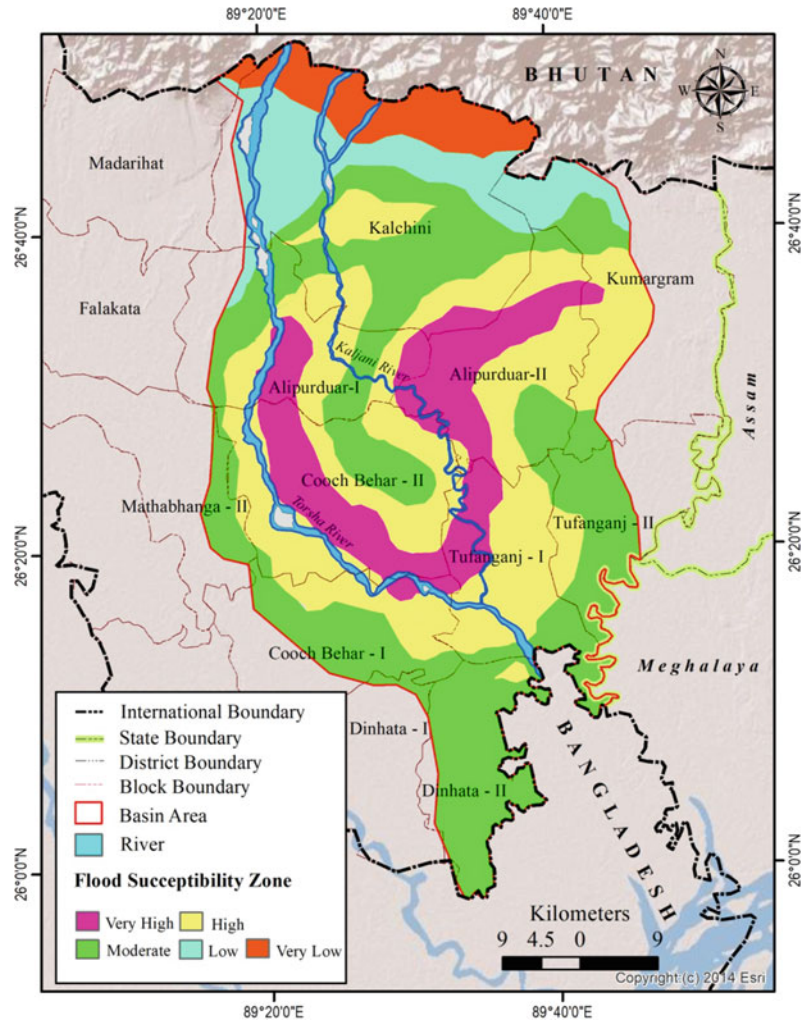
Fig. 10.8 Flood susceptibility map based on Frequency Ratio Model



Alipurduar-II ($n = 28$), Madarihat-Birpara ($n = 28$), Kumargram ($n = 24$), and Kalchini ($n = 18$). In general, 11.01% of the populations of Alipurduar district is susceptible to flood occurrence and associated events caused by river Torsa and its tributaries (Table 10.3). On the other hand, in case of Cooch Behar district, nearly 3.79% of people are exposed to havoc of floods arising from river Torsa and its associated tributaries. The people settled in six blocks of Cooch Behar-I, Cooch Behar-II, Mathabhanga-II, Tufanganj-I, Tufangaj-II, and Dinhat-II are

directly affected by the flood and inundation phenomena every year during the monsoonal season. Tufanganj-I shows that largest number of vulnerable people i.e. 22.71% followed by Mathabhanga-II with 17.86%. Blocks like Tufangaj-II (4.83%), Dinhat-II (3.65%), Cooch Behar-II (3.39%), and Cooch Behar-I (1.90%) were found to be less affected by fluvio-hydrological hazards like flood. Tufanganj-I block has the highest number of villages prone to flood, i.e., $n = 37$. Similarly, Cooch Behar-II ($n = 23$) and Mathabhanga-II ($n = 20$) blocks

Fig. 10.9 Flood susceptible blocks and districts of Torsa river basin of Himalayan foredeep basin



also have considerably higher number of villages vulnerable to flooding. Cooch Behar-I ($n = 12$), Dinhat-II ($n = 12$), and Tufanganj-II (11) are relatively under low susceptible belts (Table 10.3).

The very high or severely affected blocks are situated along the proximity of river Torsa, Sil Torsa Kaljani, Dima, Poro, Jayanti, and Raydak-I, etc. Sil Torsa and Buri Torsa are completely detached from the main Torsa due to nodal points (off-take) avulsion. Abovementioned rivers are the tributaries of river main Torsa. Basically, Sil Torsa and Buri Torsa are the spill channels of river Torsa. Different types of avulsion took place within the Torsa river basin due to natural

siltation on the channel courses and anthropogenic activities or stress on the river channels or within the river basin. River bed mining and channel bed thalweg shifting are very common fluvio-hydrological events in this fast-changing landscape. The Himalayan rivers are debouched in front of the Himalayan frontal thrust or specifically within the Himalayan foredeep basin. When Himalayan rivers enter in the foothill of the Himalayas, channel or geomorphic gradient drops suddenly. As a result, rivers become wide, sluggish, and braided in nature. National highways with railway corridors create this foredeep basin as interlacing drainage system. River Torsa and its tributaries are no exception. To mitigate

Table 10.3 Flood vulnerable statistics of Torsa river basin

District	No. of blocks	Blocks	No. of gram panchayat	Gram panchayat (GP)	Gram panchayat wise total no. of affected villages	Total no. of people affected	Blockwise % of people vulnerable to flood (Torsa river basin)	Total % of people vulnerable to flood in the district (Torsa river basin)
Alipurduar	6	Alipurduar-I	6	Pararpara Vivekananda-I Vivekananda-II PurbaKathalbari Tapshikatha Banchukumari	3 1 1 11 5 7 <i>n</i> = 28	20,800	10.54	11.01
		Alipurduar-II	5	Majherdabri Kohinoor Parokata Samuktala Mahakalguri	12 2 7 10 10 <i>n</i> = 41	43,654	22.16	
		Kalchini	6	Jaigaon Rajabathkhawa Dalsingpara Garopara Kachini Latabari	4 3 1 5 2 3 <i>n</i> = 18	25,035	9.91	
		Kumargram	5	Kumargram- Sankosh Barobisha Kamakhyaguri- I Kamakhyaguri- II Turtutikhanda	4 7 4 2 7 <i>n</i> = 24	39,921	22.42	
		Madarihat- Birpara	7	Birpara-I Birpara-II Bandapani Totopara Lankapara Hantapara Rangalibazna	1 3 6 3 3 3 9 <i>n</i> = 28	15,270	8.23	
		Alipurduar Municipality	6	Alipurduar Municipality ward no.5 Alipurduar Municipality ward no.8 Alipurduar Municipality ward no.13 Alipurduar Municipality ward no.16	<i>n</i> = 6	20,664	31.67	

(continued)

Table 10.3 (continued)

District	No. of blocks	Blocks	No. of gram panchayat	Gram panchayat (GP)	Gram panchayat wise total no. of affected villages	Total no. of people affected	Blockwise % of people vulnerable to flood (Torsa river basin)	Total % of people vulnerable to flood in the district (Torsa river basin)
				Alipurduar Municipality ward no.18 Alipurduar Municipality ward no.20				
Cooch Behar	6	Cooch Behar-I	5	Moamari Falimari Ghughumari Dawaguri Panisala	2 1 3 4 2 <i>n</i> = 12	5425	1.90	3.79
		Cooch Behar-II	8	Patlakhawa Madhupur Pundibari Khapaidanga Takagach Marichbari Baneswar Khagrabar	2 7 2 3 6 1 1 1 <i>n</i> = 23	10,112	3.39	
		Mathabhanga-II	12	Fulbari A Fulbari B Barasoulmar Ruidanga Latapata Putimari Ghoksadanga Premerdanga A.K. Paradubi Nishiganj-I Nishiganj-II Unishbisha	1 2 1 1 1 1 3 1 2 2 2 3 <i>n</i> = 20	35,072	17.86	
		Tufanganj-I	9	Natabari-I Maruganj Dhalpal-II Balabhut Chilakhana-I Chilakhana-II Deocharai Balarampur-I Balarampur-II	3 2 3 4 9 2 8 4 2 <i>n</i> = 37	50,685	22.71	
		Tufanganj-II	2	Baxirhat (Barokodali-II) Shalbari-I	3 4 4 <i>n</i> = 11	8090	4.83	
		Dinhata-II	2	Nazirhat-I Nazirhat-II	2 3 <i>n</i> = 12	7506	3.65	

the flood hazard, British ruler (since colonial period) along with Bengal landlord wanted to construct vertical concrete structures along both sides of the natural rivers. This unscientific and unrealistic approach has been practicing till today. Long stretch concrete high embankments have been built almost all the rivers within the Torsa river basin with the help of West Bengal Irrigation Department. Not only concrete high elevation embankments along with culverts, sluice gate, bridges etc. have also been constructed across the natural course of rivers. Due to unexpected population explosion along with forest land conversion, channel bed siltation is accelerating during monsoon seasons. In case of piedmont zone or Sub-Himalayan region of Bhutan–Bengal foothill zone produces a huge amount of dolomite dust and supplies to mainstream like river Torsa through its tributaries. So, flood hazard is very common recurring phenomenon in this region. Not only the above-mentioned blocks of Alipurduar and Cooch Behar districts of West Bengal almost all foothill blocks are suffering due to such fluvio-hydrological hazard or disaster. During monsoon, due to shallow depth of rivers, the channel beds are cannot accommodate the huge amount of precipitated water within the channel beds and results catastrophic or devastating flood.

10.5 Conclusion

Systematic computation and scientifically sound flood susceptibility mapping of any region provide the comprehensive knowledge of prominent factors that are responsible for triggering flood events, its spatial distribution, and formulation of preventive and risk management planning. In total, eleven flood causative factors viz. altitude, geology, slope angle, slope aspect, rainfall, drainage density, plan curvature, distance from river, soil type, topographic wetness index, and land use and land cover are taken into consideration. These flood causative parameters are processed to extract the necessary fluvio-hydrological and spatiotemporal features to identify the flood sus-

ceptibility areas of Torsa river basin processed by Frequency Ratio (FR) Model in Remote Sensing environment. The Frequency Ratio (FR) Model indicates very high flood susceptibility areas located at the south and southeastern part with high vulnerable zone at the margin of very high flooding susceptible zone. Moderate flood zones are randomly distributed over the basin while low, very low flood occurrence is found in the northern and central part. In general, Frequency Ratio (FR) model identifies the Torsa river basin susceptible to frequent flooding events. The model advocates that the entire basin is prone to flood every year with more severity in the southern and southeastern areas except in the north due to the presence of higher elevation. While validating the model with receiver operating characteristics (ROC), it is found that the Frequency Ratio model is highly reliable and accurate and can be significantly used to identify and predict the flood susceptibility zones of any areas. Therefore, the model can be effectively utilized by the policymakers and planners across the world to prevent and mitigate the flooding events and their adverse damage to human society. From the colonial era, we tried to borrow the western philosophy and models to combat such devastating fluvio-hydrological hazard or disaster without getting the similarities of the hydro-geomorphological setup of the region. The anthropogenic stresses on these rivers and within this river basin indirectly invite such recurring flood hazard. The model with field validation proves the realistic situation as well as the necessity of implementation of real-time management procedures.

Acknowledgements We are grateful to the various competent authorities for providing valuable fluvio-hydrological and remote sensing data. We also express our sincere gratitude to anonymous reviewers of the journal for lending their inclusive and befitting suggestion to enhance and refurbish the standard of the research article.

Conflict of Interest The authors declared that there is no potential conflict of interest.

Ethical Statement Authors state that the research was conducted according to ethical standards.

References

- Akgun A, Dag S, Bulut F (2008) Landslide susceptibility mapping for a landslide-prone area (Findikli, NE of Turkey) by likelihood-frequency ratio and weighted linear combination models. *Environ Geol* 54(6):1127–43. <https://doi.org/10.1007/s00254-007-0882-8>
- Aniya M, Etaya M, Shimoda H (1985) Evaluation of Landsat data for landslide identification as a means for watershed management. *J Jpn Soc Photogramm Remote Sens* 24(4):17–21. https://www.jstage.jst.go.jp/article/jsprs1975/24/4/24_4_17/_pdf/-char/ja
- Bahremand A, De Smedt F, Corluy J, Liu YB, Poorova J, Velcicka L, Kunikova E (2007) WetSpa model application for assessing reforestation impacts on floods in Margecany–Hornad Watershed, Slovakia. *Water Resour Manag* 21(8):1373–91. <https://doi.org/10.1007/s11269-006-9089-0>
- Bera B, Bhattacharjee S, Ghosh A, Ghosh S, Chamling M (2019) Dynamic of channel potholes on Precambrian geological sites of Chhota Nagpur plateau, Indian peninsula: applying fluvio-hydrological and geospatial techniques. *SN Appl Sci* 21(5):1–4. <https://doi.org/10.1007/s42452-019-0516-2>
- Bishaw B (2001) Deforestation and land degradation in the Ethiopian highlands: a strategy for physical recovery. *Northeast Afr Stud* 1:7–25. https://scholarworks.wmich.edu/cgi/viewcontent.cgi?article=1002&context=africancenter_icad_archive
- Bonham-Carter GF (1994) Geographic information systems for geoscientists-modeling with GIS. *Computer methods in the geosciences* 13:398. NII Article ID (NAID) 10016876159
- Campolo M, Soldati A, Andreussi P (2003) Artificial neural network approach to flood forecasting in the River Arno. *Hydrol Sci J* 48(3):381–98. <https://doi.org/10.1623/hysj.48.3.381.45286>
- Chakraborty T, Ghosh P (2010) The geomorphology and sedimentology of the Tista megafan, Darjeeling Himalaya: implications for megafan building processes. *Geomorphology* 115(3–4):252–6. <https://doi.org/10.1016/j.geomorph.2009.06.035>
- Chamling M, Bera B (2020) Spatio-temporal patterns of land use/land cover change in the Bhutan–Bengal foothill region between 1987 and 2019: study towards geospatial applications and policy making. *Earth Syst Environ* 12:1–4. <https://doi.org/10.1007/s41748-020-00150-0>
- Cloke HL, Pappenberger F (2009) Ensemble flood forecasting: a review. *J Hydrol* 375(3–4):613–26. <https://doi.org/10.1016/j.jhydrol.2009.06.005>
- Coppin PR, Bauer ME (1996) Digital change detection in forest ecosystems with remote sensing imagery. *Remote Sens Rev* 13(3–4):207–34. <https://doi.org/10.1080/02757259609532305>
- Egan JP (1975) Signal detection theory and ROC-analysis. Academic Press. ISBN-13: 978-0122328503; ISBN-10: 0122328507
- Erena SH, Worku H (2018) Flood risk analysis: causes and landscape based mitigation strategies in Dire Dawa city, Ethiopia. *Geoenviron Disasters* 5(1):1–9. <https://doi.org/10.1186/s40677-018-0110-8>
- Fattorelli S, Dalla Fontana G, Da Ros D (1999) Flood hazard assessment and mitigation. In *Floods and landslides: integrated risk assessment*. Springer, Berlin, Heidelberg, pp 19–38. https://doi.org/10.1007/978-3-642-58609-5_2
- Gashaw W, Legesse D (2011) Flood hazard and risk assessment using GIS and remote sensing in Fogera Woreda, Northwest Ethiopia. In *Nile River Basin*. Springer, Dordrecht, pp 179–206. https://doi.org/10.1007/978-94-007-0689-7_9
- Heagerty P, Saha-Chaudhuri P (2017) Time-dependent ROC curve estimation from censored survival data. 2013. R package version, 1(3).
- Hong CS, Cho MH (2015) Test statistics for volume under the ROC surface and hypervolume under the ROC manifold. *Commun Stat Appl Methods* 22(4):377–87. <https://doi.org/10.5351/CSAM.2015.22.4.377>
- Jaafari A, Najafi A, Pourghasemi HR, Rezaeian J, Sattarian A (2014) GIS-based frequency ratio and index of entropy models for landslide susceptibility assessment in the Caspian forest, northern Iran. *Int J Environ Sci Technol* 11(4):909–926. <https://doi.org/10.1007/s13762-013-0464-0>
- Jain V, Sinha R (2004) Fluvial dynamics of an anabranching river system in Himalayan foreland basin, Baghmata river, north Bihar plains, India 60 (1–2):147–70. <https://doi.org/10.1016/j.geomorph.2003.07.008>
- Jayakrishnan RS, Srinivasan R, Santhi C, Arnold JG (2005) Advances in the application of the SWAT model for water resources management. *Hydrol Proc Int J* 19(3):749–62. <https://doi.org/10.1002/hyp.5624>
- Kaiser MF (2009) Environmental changes, remote sensing, and infrastructure development: The case of Egypt's East Port Said harbour. *Appl Geogr* 29(2):280–8. <https://doi.org/10.1016/j.apgeog.2008.09.008>
- Kannan M, Saranathan E, Anabalagan R (2013) Landslide vulnerability mapping using frequency ratio model: a geospatial approach in Bodi-Bodimettu Ghat section, Theni district, Tamil Nadu, India. *Arab J Geosci* 6(8):2901–13. <https://doi.org/10.1007/s12517-012-0587-5>
- Khosravi K, Nohani E, Maroufinia E, Pourghasemi HR (2016) A GIS-based flood susceptibility assessment and its mapping in Iran: a comparison between frequency ratio and weights-of-evidence bivariate statistical models with multi-criteria decision-making technique. *Nat Hazards* 83(2):947–987. <https://doi.org/10.1007/s11069-016-2357-2>
- Kia MB, Pirasteh S, Pradhan B, Mahmud AR, Sulaiman WN, Moradi A (2012) An artificial neural network model for flood simulation using GIS: Johor River Basin, Malaysia. *Environ Earth Sci* 67(1):251–64. <https://doi.org/10.1007/s12665-011-1504-z>

- Konadu DD, Fosu C (2009). Digital elevation models and GIS for watershed modelling and flood prediction—a case study of Accra Ghana. In *Appropriate technologies for environmental protection in the developing world*. Springer, Dordrecht, pp 325–332. https://doi.org/10.1007/978-1-4020-9139-1_31
- Kourgialas NN, Karatzas GP (2011). Flood management and a GIS modelling method to assess flood-hazard areas—a case study. *Hydrol Sci J—Journal des Sciences Hydrologiques* 56(2):212–25. <https://doi.org/10.1080/02626667.2011.555836>
- Lee S, Talib JA (2005) Probabilistic landslide susceptibility and factor effect analysis. *Environ Geol* 47(7):982–90. <https://doi.org/10.1007/s00254-005-1228-z>
- Li C, Singh VP, Mishra AK (2012) Entropy theory-based criterion for hydrometric network evaluation and design: Maximum information minimum redundancy. *Water Resour Res* 48(5). <https://doi.org/10.1029/2011WR011251>
- Liu YB, De Smedt F (2004) WetSpa extension, a GIS-based hydrologic model for flood prediction and watershed management. Vrije Universiteit Brussel, Belgium 1:e108. https://www.vub.be/WetSpa/downloads/WetSpa_manual.pdf
- Liu YB, De Smedt F (2005) Flood modeling for complex terrain using GIS and remote sensed information. *Water Resour Manag* 19(5):605–24. <https://doi.org/10.1007/s11269-005-6808-x>
- Manandhar B, Balla MK, Awal R, Pradhan BM (2010) Floodplain analysis and risk assessment of lothar khola (stream). In *Proceedings of the 11th ESRI India user conference*, Noida, India, pp 21–22
- Moghaddam DD, Rezaei M, Pourghasemi HR, Pourtaghie ZS, Pradhan B (2015) Groundwater spring potential mapping using bivariate statistical model and GIS in the Taleghan watershed, Iran. *Arab J Geosci* 8(2):913–29. <https://doi.org/10.1007/s12517-013-11-561>
- Mouat DA, Mahin GG, Lancaster J (1993). Remote sensing techniques in the analysis of change detection. *Geocarto Int* 8(2):39–50. <https://doi.org/10.1080/10106049309354407>
- Mukhopadhyay SC (2014) Aspects of hydrogeomorphology of north Bengal drainage, India and surroundings with emphasis on the Torsa basin. *Indian J Landsc Syst Ecol Stud* 37(2):163–176
- Naghibi SA, Pourghasemi HR, Pourtaghi ZS, Rezaei A (2015) Groundwater qanat potential mapping using frequency ratio and Shannon's entropy models in the Moghan watershed, Iran. *Earth Sci Inf* 8(1):171–186. <https://doi.org/10.1007/s12145-014-0145-7>
- Ozdemir A (2011). GIS-based groundwater spring potential mapping in the Sultan Mountains (Konya, Turkey) using frequency ratio, weights of evidence and logistic regression methods and their comparison. *J Hydrol* 411(3–4):290–308. <https://doi.org/10.1016/j.jhydrol.2011.10.010>
- Ozdemir A, Altural T (2013) A comparative study of frequency ratio, weights of evidence and logistic regression methods for landslide susceptibility mapping: Sultan Mountains, SW Turkey. *J As Earth Sci* 64:180–97. <https://doi.org/10.1016/j.jseae.2012.12.014>
- Pourghasemi HR, Mohammady M, Pradhan B (2012) Landslide susceptibility mapping using index of entropy and conditional probability models in GIS: Safarood Basin, Iran. *Catena* 97:71–84. <https://doi.org/10.1016/j.catena.2012.05.005>
- Pradhan B (2009) Groundwater potential zonation for basaltic watersheds using satellite remote sensing data and GIS techniques. *Central Eur J Geosci* 1(1):120–9. <https://doi.org/10.2478/v10085-009-0008-5>
- Pradhan B, Lee S (2010) Landslide susceptibility assessment and factor effect analysis: backpropagation artificial neural networks and their comparison with frequency ratio and bivariate logistic regression modelling. *Environ Modell Softw* 25(6):747–59. <https://doi.org/10.1016/j.envsoft.2009.10.016>
- Pradhan B, Shafiee M, Pirasteh S (2009) Maximum flood prone area mapping using RADARSAT images and GIS: Kelantan river basin. *Int J Geoinf* 5(2).
- Rahmati O, Pourghasemi HR, Zeinivand H (2016) Flood susceptibility mapping using frequency ratio and weights-of-evidence models in the Golastan Province, Iran. *Geocarto Int* 31(1):42–70. <https://doi.org/10.1080/10106049.2015.1041559>
- Rajsekhar D, Mishra AK, Singh VP (2013) Regionalization of drought characteristics using an entropy approach. *J Hydrol Eng* 18(7):870–87. [https://doi.org/10.1061/\(ASCE\)HE.1943-5584.0000683](https://doi.org/10.1061/(ASCE)HE.1943-5584.0000683)
- Regmi AD, Devkota KC, Yoshida K, Pradhan B, Pourghasemi HR, Kumamoto T, Akgun A (2014) Application of frequency ratio, statistical index, and weights-of-evidence models and their comparison in landslide susceptibility mapping in Central Nepal Himalaya. *Arab J Geosci* 7(2):725–742. <https://doi.org/10.1007/s12517-012-0807-z>
- Sanyal J, Lu XX (2004) Application of remote sensing in flood management with special reference to monsoon Asia: a review. *Nat Hazards* 33(2):283–301. <https://doi.org/10.1023/B:NHAZ.0000037035.65105.95>
- Shafapour Tehrani M, Kumar L, Neamah Jebur M, Shabani F (2019) Evaluating the application of the statistical index method in flood susceptibility mapping and its comparison with frequency ratio and logistic regression methods. *Geomatics Nat Hazards Risk* 10(1):79–101. <https://doi.org/10.1080/19475705.2018.1506509>
- Skilodimou H, Livaditis G, Bathrellos G, Verikiou-Papaspirdakou E (2003) Investigating the flooding events of the urban regions of Glyfada and Voula, Attica, Greece: a contribution to Urban Geomorphology. *Geografiska Annaler Ser A Phys Geogr* 85(2):197–204. <https://doi.org/10.1111/1468-0459.00198>

- Sujatha ER, Rajamanickam V, Kumaravel P, Saranathan E (2013) Landslide susceptibility analysis using probabilistic likelihood ratio model—a geospatial-based study. *Arab J Geosci* 6(2):429–40. <https://doi.org/10.1007/s12517-011-0356-x>
- Swets JA (1988) Measuring the accuracy of diagnostic systems. *Science* 240(4857):1285–1293. <https://doi.org/10.1126/science.3287615>
- Tehrany MS, Lee MJ, Pradhan B, Jebur MN, Lee S (2014) Flood susceptibility mapping using integrated bivariate and multivariate statistical models. *Environ Earth Sci* 72(10):4001–15. <https://doi.org/10.1007/s12665-014-3289-3>
- Tehrany MS, Pradhan B, Jebur MN (2013) Remote sensing data reveals eco-environmental changes in urban areas of Klang Valley, Malaysia: contribution from object based analysis. *J Indian Soc Remote Sens* 41(4):981–91. <https://doi.org/10.1007/s12524-013-0289-9>
- Tehrany MS, Pradhan B, Jebur MN (2015). Flood susceptibility analysis and its verification using a novel ensemble support vector machine and frequency ratio method. *Stoch Environ Res Risk Assess* 29(4):1149–65. <https://doi.org/10.1007/s00477-015-1021-9>
- Tiwari MK, Chatterjee C (2010). Uncertainty assessment and ensemble flood forecasting using bootstrap based artificial neural networks (BANNs). *J Hydrol* 382(1–4):20–33. <https://doi.org/10.1016/j.jhydrol.2009.12.013>
- Yilmaz I (2009) Landslide susceptibility mapping using frequency ratio, logistic regression, artificial neural networks and their comparison: a case study from Kat landslides (Tokat—Turkey). *Comput Geosci* 35(6):1125–38. <https://doi.org/10.1016/j.cageo.2008.08.007>
- Yilmaz I (2010) Comparison of landslide susceptibility mapping methodologies for Koyulhisar, Turkey: conditional probability, logistic regression, artificial neural networks, and support vector machine. *Environ Earth Sci* 61(4):821–36. <https://doi.org/10.1007/s12665-009-0394-9>
- Youssef S, Rosenberg E, Deschamps H, Oughanem R, Maire E, Mokso R (2014) Oil ganglia dynamics in natural porous media during surfactant flooding captured by ultra-fast x-ray microtomography. In Symposium of the society of core analysts. <http://www.jgmaas.com/SCA/2014/SCA2014-023.pdf>
- Zare M, Pourghasemi HR, Vafakhah M, Pradhan B (2013) Landslide susceptibility mapping at Vaz Watershed (Iran) using an artificial neural network model: a comparison between multilayer perceptron (MLP) and radial basic function (RBF) algorithms. *Arab J Geosci* (8):2873–88. <https://doi.org/10.1007/s12517-012-0610-x>



Flood-Induced Transport Infrastructural Losses in India: Regional Assessments

Suvendu Roy

Abstract

Flood-induced damage in transport infrastructure (TI) is very prominent and growing rapidly with the increased establishment of human amenities within the flood-prone region of India. The estimation of actual damage of TI for flooding is now an essential task for sustainable planning in future development by reducing financial losses. The Government of India has significantly increased the share of the total GDP from 0.30 to 0.98% in the last ten years (2007–2017) for the development of the transport sector. The regional level statistical investigation has been done to show the temporal development of road networks for the past 60 years. After normalising with the Wholesale Price Index (WPI), the financial damages by flood events have been also presented here for the same period. The result shows that the flooding area of the country has been reduced by ~40% in comparison with the severe phase of the Indian Flood (1970–1980s), whereas the damage of public utility or primarily transport infrastructure loss has been significantly increased by ~240%. Maps are

also showing a positive association between higher flood-affected areas and maximum losses of public utility mainly in the states of Lower Gangetic Basin and Eastern Coast of India.

Keywords

Transport infrastructure · Flood · Public utility · Bridge failure · Road network

11.1 Introduction

Damages in the transport network and corresponding infrastructural loss due to flood events are becoming a serious problem for all countries. A global-level assessment by Koks et al. (2019) shows about 27% of assets of global roads and railways that are exposed to at least one regional geo-hazard, where river and surface flooding generates maximum (73%) global Expected Annual Damage (EAD) followed by the coastal flood (15.5%), earthquake (7.3%), and tropical cyclone (3.8%), as per their global-level vulnerability and risk assessment. The study has also estimated that India comes under the top ten countries in terms of the highest multi-hazard EAD of transport network. Over the period, economic and reinsurance losses due to floods have been gradually increased in corresponding with the increasing flood events (Mills 2005;

S. Roy (✉)
Department of Geography, Kalipada Ghosh Tarai
Mahavidyalaya, Bagdogra, Darjeeling, WB 734014,
India

Kundzewicz et al. 2013; Munich Re 2015; Swiss Re 2015). Najibi and Devineni (2017) have also noticed globally a significant fourfold increase in the long duration flood frequency since the beginning of the twenty-first century. Consequently, flooding becomes a severe threat for the transport networks by damaging roads, railway lines, and other infrastructural failures, e.g., bridge collapse, massive obstruction of traffic, and such events are leading to increase the repairing cost and significantly affect the regional economy and livelihood by reducing serviceability and accessibility (World Bank 2016; Taylor 2017). Jongman et al. (2012) has projected that the global exposure to river and coastal flooding is 46 trillion USD in 2010, which might be increased by 158 trillion USD by 2050, due to systematic and unplanned socio-economic development within the flood-prone areas. Recent researched data from the World Resource Institute (WRI) shows that by 2030 the number of people affected by the flood will be doubled from 65 to 132 million due to riverine floods and the loss of urban property will increase by threefold from 157 million USD to 535 million USD (Ward et al. 2020). Therefore, special consideration to figure out the transport infrastructural losses due to flood events is an essential task as an input in decision-making and planning of such infrastructures at the regional level.

The transport network in India is one of the largest as well as busiest public amenities in the World. In terms of the total length of transport networks, India is the second (after USA) and fourth largest country with more than 5.90 million km of roadways (MoRTH 2019a) and 67,415 km of total railways route length with 7321 railway stations, respectively (MoR 2019). The statistics on freight and passenger transportation are showing that Indian road network is transporting about 8.225 billion passengers and 980 million tonnes of cargo annually as of 2015 (World Bank 2016) and the Indian railway network is transporting about 8.44 billion passengers and 1.23 billion tonnes of freight annually as of 2019 (MoR 2019). Nevertheless, the flood statistic of India reveals that it becomes more

severe, unpredictable, and frequent than earlier. In 2018, the country has faced total damage of about 960 billion INR (₹), which cumulatively becomes about 4700 billion INR since 1953 (CWC 2019). In the last 66 years (1953–2018), the average annual flood-affected area of India is 7.14 million hectares (Mha) where about 33 million populations have been affected every year (CWC 2019). In 1980, Rashtriya Barh Ayog (RBA) had estimated that the total flood-prone area of the country was about 40 Mha, which has been raised by 49.815 Mha after being revised by the Working Group on Flood Management set up by the Planning Commission during 12th Five-Year Plan (2012–2017) through the available information furnished by the State Governments (cwc.gov.in/fm-projects).

In such circumstances, an effective assessment of the damages of transport infrastructure by flooding in India is crucial research for sustainable development and planning to mitigate the impact on transport network facility of the country. Such findings could reduce the financial losses and optimum use of the resource as the Government of India is spending about 0.94% of its total GDP during the 2020–21 financial year and has planned to invest about 1.4 trillion USD on overall infrastructural development by 2019–2023 (www.ibef.org). The prime objective of this work is to assess the losses of transport infrastructure due to frequent flooding over India with special attention on the flood-prone states (Bihar and West Bengal) of the Lower Gangetic Basin (LGB).

11.2 Impacts of Flood on Transportation System

Since being a natural phenomenon, the occurrence of flood is unpredictable but the flood-induced damages could be reduced with effective plans and coordination among the components of the society. Flood and concurrence phenomena like torrential rainfall, high water levels have significantly affected the performance and lifespan of affected transport infrastructure through the processes of landslide, landslips, washed away of road and railways, submerged and inundated bridge

support, and road closure (Pedrozo-Acuña et al. 2017; Bizikova et al. 2008). The impact of flooding on transport systems could be classified based on the level of exposure of any transportation elements to the floods. The consequences or damages through the physical contact of floodwater with the transport infrastructure are categorised as *direct impact*, whereas, the *indirect impact* designates by the problems arising through the obstruction in traffic flow, business interruption, increasing emission, which is affecting a large area and lasting for a long period (Pyatkova et al. 2019; Brown and Dawson 2016; Hammond et al. 2015; Walsh et al. 2012; Pregolato et al. 2017) (Table 11.1). The consequences are also having different dimensions like immediate/long-term, tangible/intangible effects depending upon the land use of flood-prone regions (Nicholls et al. 2015).

11.3 Date Used and Methods of Analysis

The states and union territory level data of the entire country (India) has been used for the present investigation with a special focus on the scenarios in Bihar and West Bengal states (Fig. 11.1). The main data that has been used for current work are annual flood damage data and transport infrastructure data for the last 60 years. The data relating to damage of flood has been

extracted from the different reports like Water and Related Statistics—2019 of Central Water Commission (CWC), Govt. of India; Annual Flood Reports of Govt. of West Bengal (2013–2019); Flood Hazard Atlas—Bihar: A geospatial approach (2020), prepared by National Remote Sensing Centre, Govt. of India; Report from National Disaster Management Authority, Govt. of India. The annual reports on ‘Basic Road Statistics of India’ published by Ministry of Road Transport and Highways, Govt. of India and ‘Indian Railway Year Book 2018–19’ by Ministry of Railway, Govt. of India have been used for the information regarding the development of Indian transport infrastructures.

Initially, the data related to financial damage due to flood events and any other old financial values have been normalised to eliminate the effect of temporal inflation on the country. Though, the Consumer Price Index (CPI) values are used for this practice worldwide, due to the unavailability of long-term consistent yearly CPI values of India, the Wholesale Price Index (WPI) (2010 = 100) has been used to adjust the effect of inflation on the value of money. The yearly WPI values of India since 1960 have been collected from the World Bank’s website <https://data.worldbank.org/indicator/FP.WPI.TOTL?locations=IN> accessed on 15 March 2021, which are compiled by the International Monetary Fund (IMF) and International Financial Statistics

Table 11.1 Multi-dimensional effects of flooding on transportation system

Direct impacts	Indirect impacts
Physical damages of infrastructures	Problem in traffic
– Bridge and Culvert Collapse	– Delay of traffic due to congestion
– Road and railway washed away	– Increasing transport cost for taking detour path
– Erosion of embankments for transport networks, e.g., approach road for bridge	– Larger carbon emission
– Damage of different vehicles	– Reducing reliability and network performance
	– Overall disturbances in regional economy and livelihood

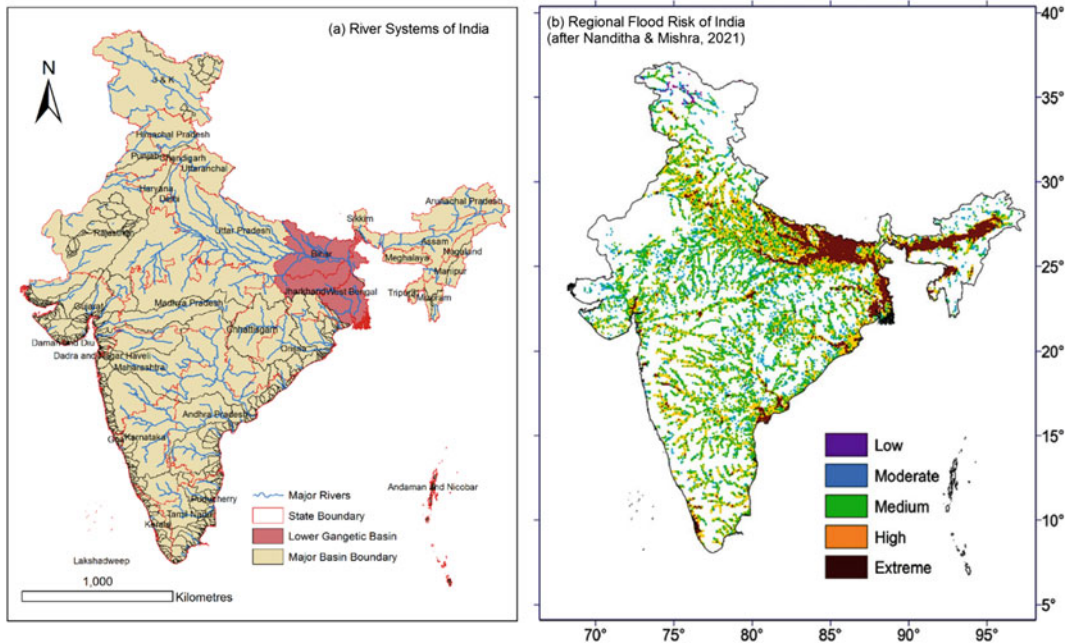


Fig. 11.1 a Distribution of major river systems in different states of India; b Regional flood risk map of India (after Nanditha and Mishra 2021)

(IFS). The widely used equation has been followed for this exercise:

$$\begin{aligned} \text{Normalised Value of Money} \\ &= \text{Past Money Value} \times \text{Ending WPI} \\ &\quad \div \text{Past WPI} \end{aligned}$$

Where ‘past money value’ indicates the amount of money spent in the past years, i.e., 1960 onwards and ‘ending WPI’ is the value of price index in 2018 (132.593), ‘past WPI’ means price index of the year 1960 and onwards.

The problem of autocorrelation, where applicable as per Durbin–Watson test, has been also removed from the normalised temporal data. The normality test shows that all data are negatively skewed; therefore, non-parametric tests have been followed for choosing any statistical techniques. For example, to analyse the temporal trends and magnitude of changes Mann–Kendall’s Test and Theil–Sen’s Slope techniques have been used, respectively. In the case of correlation analysis, Spearman’s correlation technique has been applied. To draw and run all

such statistical techniques and diagrams, software like IBM SPSS v. 20 and XLSTAT 2020 in combination with Microsoft Excel have been used. To show the state-level variation of different parameters during the last six decades chorochromatic map has been used using Arc-Map 10.4.

11.4 Result and Discussion

11.4.1 Scenario of Flood Damage in India (1960–2018)

In the last six decades, a steady-state condition ($\sigma = 3.50$) has been observed in the area affected by annual floods in India with a mean area of 7.22 Mha (Fig. 11.2 and Table 11.2). The most devastating flooding year was 1978 with a spatial coverage of 17.50 Mha followed by the years 1988 (16.29 Mha), 1971 (13.25 Mha), 2014 (12.78 Mha), 2005 (12.56 Mha), and 1976 (11.91 Mha). The decadal statistic shows that the 1970 and 1980s were the most flood-affected periods

of India with an average flooding area of 9.53 and 9.66 Mha, respectively. In recent decades (2000, 2010s), the area has been decreased to 5.82 and 5.52 Mha, respectively, and it might be due to the effective flood control measures by dams, barrages, embankments, etc. across the country with a possible effect of changing river regimes.

No significant change but a slightly negative trend has been observed in Mann–Kendall’s temporal trend analysis ($MK = -0.134$) of the country’s flood-affected area ($p = 0.272$). However, significant ($p < 0.05$) positive trend and/or changes have been observed in losses of human life, damages in the normalised values of house damage, public utility, and total damage with higher magnitudes as per Theil–Sen’s Slope values (Table 11.2). In particular, the maximum positive trend ($MK = 0.593$) has been observed in the normalised value of public utility damage

with the magnitude of 210.074 followed by the total flood damage ($MK = 0.455$; Sen’s Slope = 333.96).

The decadal statistic of Indian flood damage shows an important variation in the last six decades (Table 11.3). In comparison with the most devastating decade of Indian flood history (1980s), recently (2010s) negative changes have been observed in the total flood-affected area (-41.92%), the population affected by flood (-37.93%), human life loss (-14.29%), area of crops damage (-5.08) and its normalised losses in value (-6.91%), and losses of cattle (-53.15%). These values are indicating an improvement in the flood management system and awareness of the population in the flood-prone area. However, a significant increase has been observed in total damage (101.10%), in particular the damage of public utilities (240.64%) and value house damage (12.31%).

Fig. 11.2 Effect of flood hazard on different socio-economic aspects of India during last six decades (1960–2018) (Data Source FFM Directorate, CWC 2019)

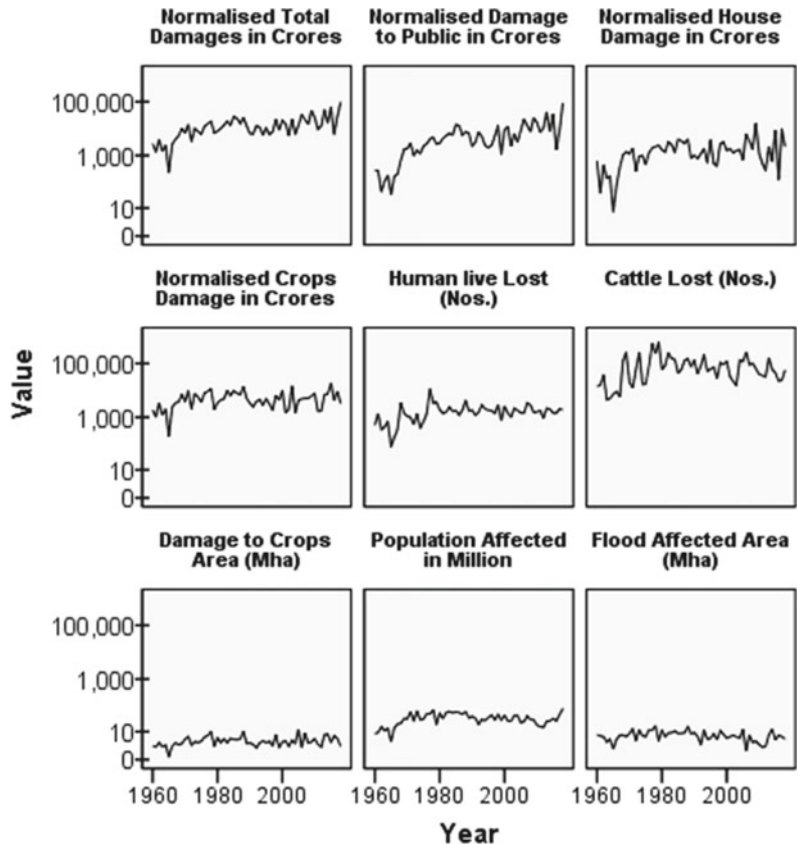


Table 11.2 Descriptive statistics and non-parametric (Mann–Kendall & Theil–Sen’s Slope) trend analysis of the flood hazard in India for 59 years (1960–2018)

Variable	Flood-affected area (Mha)	Population affected in million	Damage to crops area (Mha)	Cattle lost (nos.)	Human live lost (nos.)	Normalised crops damage in crores	Normalised house damage in crores	Normalised damage to public in crores	Normalised total damages in crores
Minimum	1.10	3.61	0.27	4572.00	79.00	193.09	6.58	35.20	234.86
Maximum	17.50	79.74	12.30	618248.00	11316.00	18372.23	15703.25	91430.20	96806.75
Mean	7.22	34.88	4.15	99120.90	1803.54	5332.23	2019.89	8049.66	15401.80
SD	3.50	16.94	2.34	116877.69	1545.94	3629.87	2597.33	13658.79	16100.29
Mann–Kendall (MK)	-0.134	0.053	0.133	0.082	0.282	0.153	0.280	0.593	0.455
Sig. (2-tailed)	0.272	0.765	0.138	0.494	0.005 ^a	0.068	0.002 ^a	<0.0001 ^a	<0.0001 ^a
Theil–Sen’s Slope	-0.038	0.112	0.021	337.551	18.538	39.795	29.844	210.074	333.956

^aSignificant at 0.01 level (2-tailed)

The positive changes of these three indicators are revealing the expansion of human habitat and allied infrastructure in the flood-prone area. The statement could be supported by the findings of Roy and Sahu (2017), where the study shows that in the last five decades the road network comes close to the river systems of eastern India. About 153% growth of transport network has been observed within a catchment and, in particular, about 220% growth has been observed within the 30 m buffers of river network (Roy and Sahu 2017).

11.4.2 Development of Road Infrastructure in India (1951–2017)

The expansion of transport network helps to increase the connectivity all over the country, which is essential for rapid development of the economy and level of other services. The information published in ‘Basic Road Statistics of India: 2016–2017’ by the Ministry of Road Transport and Highways, Govt. of India (MoRTH 2019a, b) shows tremendous growth in all types of road networks since 1951. The maximum growth has been observed in the rural road network, which contains about 70% of the total road network in India (Fig. 11.3). Although the National Highway (NH) of the country carries only 1.94% of the total length of road network, however, internationally India holds the second rank after Australia as of 31 March 2017 (MoRTH 2019a, b). Annually, about 5% growth of NH has been noticed in the last fifteen years of this century, which is about 4% for total road development. Since the beginning of the twenty-first century, significant kick-off has been observed in the growth of the country’s road network (Fig. 11.3). The country is also transforming its road into surfaced/paved very first, at present about 63.24% of the total road is paved, although much lesser than developed countries like UK and France. The country is also increasing its share of total Gross Domestic Product (GDP) for the expenditure of road network development. In 2017–18, the Govt. of

India shares 0.98% of its total GDP on road infrastructure, which was only 0.30% in 2007–08 (Fig. 11.4).

The expansion of the Indian rail network was started in 1853 between Mumbai and Thane over a distance of 34 km. At the beginning of the nineteenth century, the total length of the Indian railway turns into about 40,000 km. During Independence (15 August 1947), it was about 65,217 km of which 10,523 km went to Pakistan due to the partition of the country and the total length of Indian rail network became 54,694 km. After seven decades it has become 67,415 km as of 31 March 2019, of which ~93.30% comes under broad gauge line (>1.4 m), ~4.2% in metre gauge (1 m), and ~2.5% in narrow gauge (<1 m) (MoR 2019).

11.4.3 Damage of Public Utilities, as a Proxy Data of Transport Infrastructure Loss

As per the Webster’s Dictionary (2010), a public utility (PU) refers to ‘*an organization supplying water, electricity, transportation, etc. to the public, operated, usually as a monopoly, by a private corporation under governmental regulation or by the government directly*’. In India, most of these services are provided by the government and/or directly controlled by private organisations, e.g., electricity. In the context of flood-induced damages in PU, the maximum share of damaged value is generated from the losses of transport infrastructures only because of their direct contact with the floodwater in comparison with the underground and aboveground public utilities like pipelines for water, gas, electricity, telecommunication, etc. The data provided in the flood report regarding PU are mainly concerned about the physical damages of the transport and other infrastructures, although, the indirect effect on the economy and other services due to lack of serviceability has not been considered yet. Therefore, the damage value of PU (after normalised through WPI value of respective year) in different governmental reports

Table 11.3 Decadal pattern of flood damage in India during 1960–2018

Year (s)	Flood-affected area (Mha)	Population affected in Million	Damage to crops area (Mha)	Cattle lost (nos.)	Human live lost (nos.)	Normalised crops damage in crores	Normalised house damage in crores	Normalised damage to public in crores	Normalised total damages in crores
1960	5.53	15.06	2.34	49980.20	887.30	2622.40	427.53	364.91	3414.89
1970	9.53	43.30	4.95	187931.20	2475.80	6301.87	1329.47	2496.49	10,127.84
1980	9.66	51.53	4.96	114084.80	1971.00	7244.45	2503.87	7200.96	16,949.28
1990	7.11	33.71	3.34	87920.80	1817.00	3780.27	1586.01	4373.93	9740.21
2000	5.82	33.37	4.66	96787.50	1969.40	5442.01	3539.49	10980.33	19,961.83
2010	5.52	31.99	4.71	53454.22	1689.33	6743.55	2812.17	24529.33	34085.06
Change (%) (1980–2010)	-42.91	-37.93	-5.08	-53.15	-14.29	-6.91	12.31	240.64	101.10

Data Source FFM Directorate, CWC (2019) (<http://www.indiaenvironmentportal.org.in/files/file/water-and-related-statistics-2019.pdf>, retrieved on March 13, 2021)

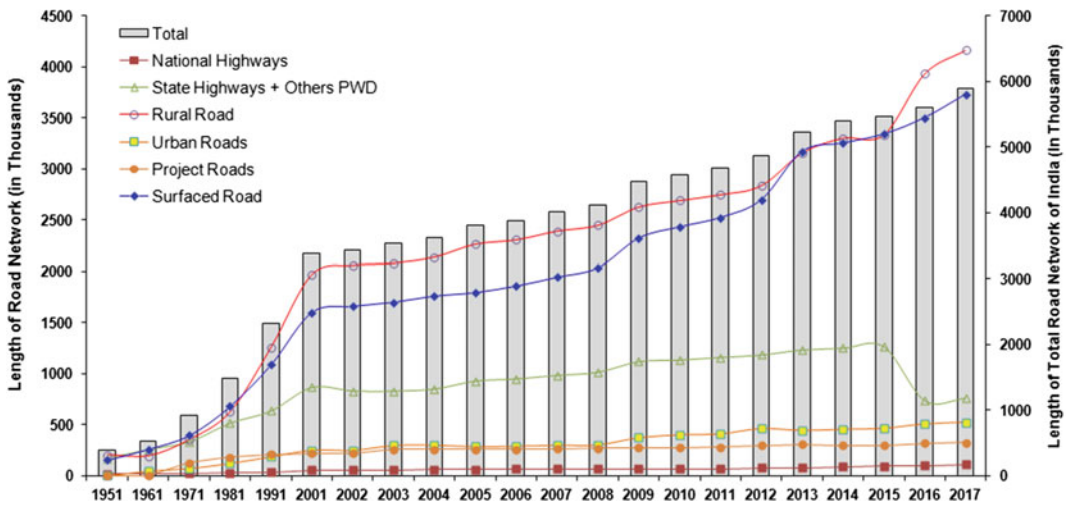
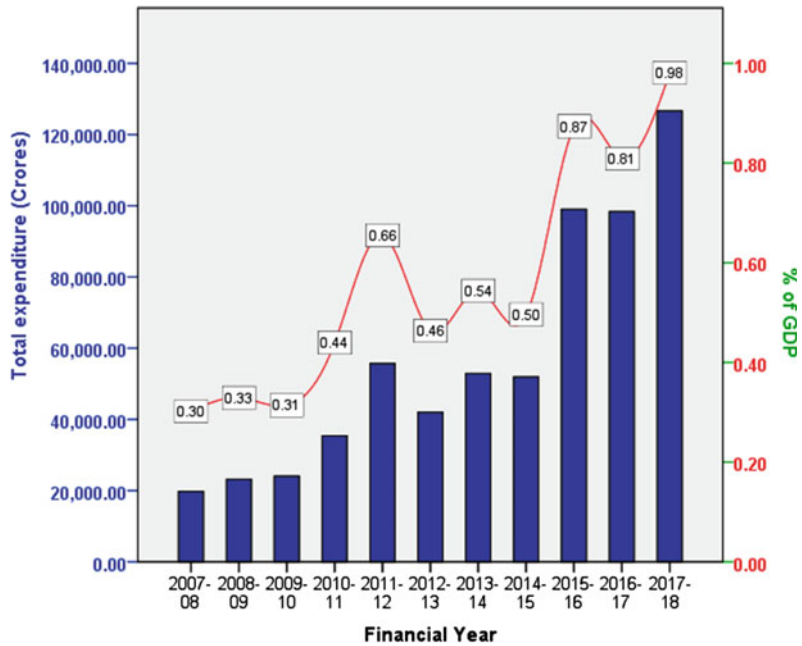


Fig. 11.3 Trend of Indian Road Network Development since 1951 (Data Source MoRTH 2019a)

Fig. 11.4 Temporal expenditure of Govt. of India on the Road Network Development (Data Source MoRTH 2019a)



has been considered here as a proxy data of transport infrastructure loss due to flood event.

The group scatters plot of temporal flood-affected area and normalised damage of public utility of the Bihar, West Bengal, and India shows over the period area affected by the flood are reducing with a negative trend or not significantly changed, whereas, the value of PU has

been increased significantly for India and non-significant but positively rise in Bihar and West Bengal (Fig. 11.5). Since 1960, the average damage value of PU in India is about 8049.66 crores and maximum loss (~91,430 crores) has been estimated in 2018 followed by the years 2013 (~41,960 crores), 2015 (~34,700 crores), 2009 (~25,435 crores), 2006 (~22,500 crores),

and 2010 (~16,900 crores) (CWC 2019). The result shows although in recent decades the flood-affected area has not significantly changed, the intensity of PU damage has been increased significantly since the beginning of the twenty-first century.

The correlation matrix (Spearman) between indicators of flood-induced damage in India shows very interesting facts about the country’s flooding scenario (Table 11.4). There is no correlation between flood-affected area and PU ($r = 0.002$), which reveals that the area of flooding over India has not been increased over time although the infrastructure of public utility significantly developed within the flood-prone area of the country. However, the significant ($p < 0.001$) positive correlations between flood-affected area and affected population (0.59), area and value of crop damage (0.655 & 0.465), and number of house damage (0.413) are indicating that the temporal expansion of flood inundation mainly happens over the new croplands and settlements area.

Although being the most flood vulnerable area of India, in the affected states (Bihar and WB) of the Lower Gangetic Basin (LGB), the correlation

values between the normalised cost of PU damage and the flood-affected area are showing opposite results in comparison with the whole country. Significant positive trends have been observed in Bihar ($r = 0.609$, $p < 0.001$) and WB ($r = 0.534$, $p < 0.001$) along with other parameters of flood damage. Recently Roy (2021) found that about 44% of total road networks (~3.23 lakh km) and about 26% of total railway lines (~4000 km) of WB are placed within the floodplain area of the state’s rivers, where about 13% roads are at risk of flood damage. Figures 11.6 and 11.7 are showing the state-level variation of flood-affected areas and damage of PU, respectively. The figures are also highlighting the presence of a very close association between the state-level most flood-affected area and the higher amount of PU damage for all six decades. Quartile-based classified range of values for the six different decades is indicating the state-wise flooding area that has been reduced over time, whereas the damages of PU have been increased significantly towards the recent decades. In the state-level analysis, Spearman’s correlation values between flood-affected areas and damages of PU are showing a

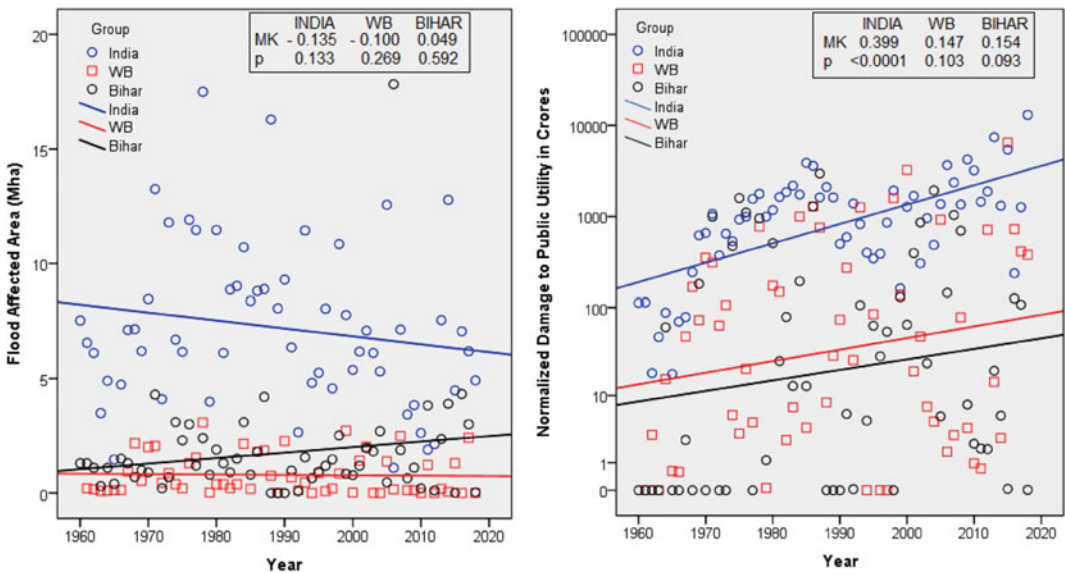


Fig. 11.5 Group scatter plots are showing the converse trend of flood-affected area and damages to the public utilities in India, West Bengal and Bihar

Table 11.4 Spearman's correlation matrix among the indicators of flood damage in India since 1960

	Flood-affected area (Mha)	Population affected in million	Damage to crops area (Mha)	Damage of houses (nos.)	Cattle lost (nos.)	Human live lost (nos.)	Normalised crops damage in crores	Normalised house damage in crores	Normalised damage to public utility in crores	Normalised total damages in crores
Flood-affected area (Mha)	1.000	0.590 ^b	0.655 ^b	0.413 ^b	0.348 ^b	0.272 ^a	0.465 ^b	0.228	0.002	0.173
Population affected in million		1.000	0.533 ^b	0.719 ^b	0.454 ^b	0.451 ^b	0.645 ^b	0.589 ^b	0.355 ^b	0.535 ^b
Damage to crops area (Mha)			1.000	0.424 ^b	0.240	0.426 ^b	0.638 ^b	0.346 ^b	0.364 ^b	0.487 ^b
Damage of houses (nos.)				1.000	0.535 ^b	0.471 ^b	0.583 ^b	0.754 ^b	0.347 ^b	0.486 ^b
Cattle lost (nos.)					1.000	0.640 ^b	0.400 ^b	0.539 ^b	0.339 ^b	0.419 ^b
Human live lost (nos.)						1.000	0.430 ^b	0.549 ^b	0.523 ^b	0.544 ^b
Normalised crops damage in crores							1.000	0.626 ^b	0.469 ^b	0.746 ^b
Normalised house damage in crores								1.000	0.631 ^b	0.784 ^b
Normalised damage to public utility in crores									1.000	0.905 ^b
Normalised total damages in crores										1.000

^aSignificant at 0.05 level (2-tailed)^bSignificant at 0.01 level (2-tailed)

significant positive relationship for all the decades (Table 11.5). The lower correlation value in the 1960s reveals the relatively minimal loss of PU due to lack of infrastructural development during the initial phase of independence.

11.4.4 Flood-Induced Major Bridge Failures in India

The details of bridge inventory and their performance data are still ignored in India, while such a database is essential for India as a riverine country to manage its transport infrastructures and for their continuous serviceability. Recently, Indian Bridge Management System (IBMS) of MoRTH (2019b) has prepared a database on the 172,517 bridges and/or crossing structure installed on NHs in India, which are structurally divided as 1,34,229 culverts (<6 m span), 32,806 minor bridges (6–60 m span), 3647 major (60–150 m span), and 1835 extra-long bridges (spanning >150 m). However, no convenient database is available on the structural losses due to floods or any other natural hazards. The developed countries are maintaining a comprehensive database of bridge infrastructure, e.g., National Bridge Inventory (NBI) of the USA. Worldwide comprehensive studies have been made on bridge failure and infrastructural performances (Sheer 2010; Farhey 2017; Proske 2019), and Indian researchers also have done some isolated works on the bridge failures (Aggarwal 2001; Datta et al. 2000; Basu and Gupta 2003; Birajdar et al. 2014).

Garg et al. (2020) have published a timely research on bridge failure of India in the last 40 years (1977–2017), which could be treated as an inventory of Indian bridge failures. Garg et al. (2020) have collected detailed information on more than 2130 cases of bridge failure due to different causes during various phases of construction in the last four decades. The study finds the average service life of Indian bridges that is 34.5 years which is very low than other countries. In ~80% of cases of bridge failure, the major causes are natural disasters like floods,

earthquakes, landslides, storms, avalanches, etc. In the USA also about 60% bridge failures have been caused by natural disasters (Cook and Barr 2017). In particular, about 52% of bridges have collapsed due to flood events only, which is a major cause in India (Garg et al. 2020). Cook and Barr (2017) also reported that in the USA about 55% of bridge failure cases are happened due to floods. In 2018, 38 cases of bridge and culvert failure have been reported by the Annual Flood Report: 2018 of Govt. of WB, and most of these cases happened in the rivers of North Bengal (IWB-GoWB 2019). The present study has also tabulated some major events of bridge failure in different parts of India during the monsoon season of 2020, and financial losses based on the report published in different sources (Table 11.6 and Fig. 11.8).

11.5 Conclusion

Flooding in Indian rivers is a major and worrying cause of transport infrastructural losses, which is primarily concentrated in the states of LGB and states of the Eastern Coast. The area affected by flood has been reduced by ~40% in comparison with the severe phase of the Indian Flood (1970–1980s), whereas, the damage of public utility or primarily transport infrastructure loss has been significantly increased by about 240%. Development of transportation system in India is noticeable, although the under-estimation and less attention on the effect of river flooding is the major cause of increasing damage of transport infrastructure in form of the number of bridge collapses, wash away of road and rail networks in every rainy season. Preparation of detailed bridge inventory and regular investigation of their performance is now essential for India, which is still neglected. The study only finds direct and/or tangible effect of flood on the transportation system that has been assessed largely in a quantitative way, although the indirect effect of flood on the transportation and related system has been less studied while having a long term and extended effect on the regional economy and human society.

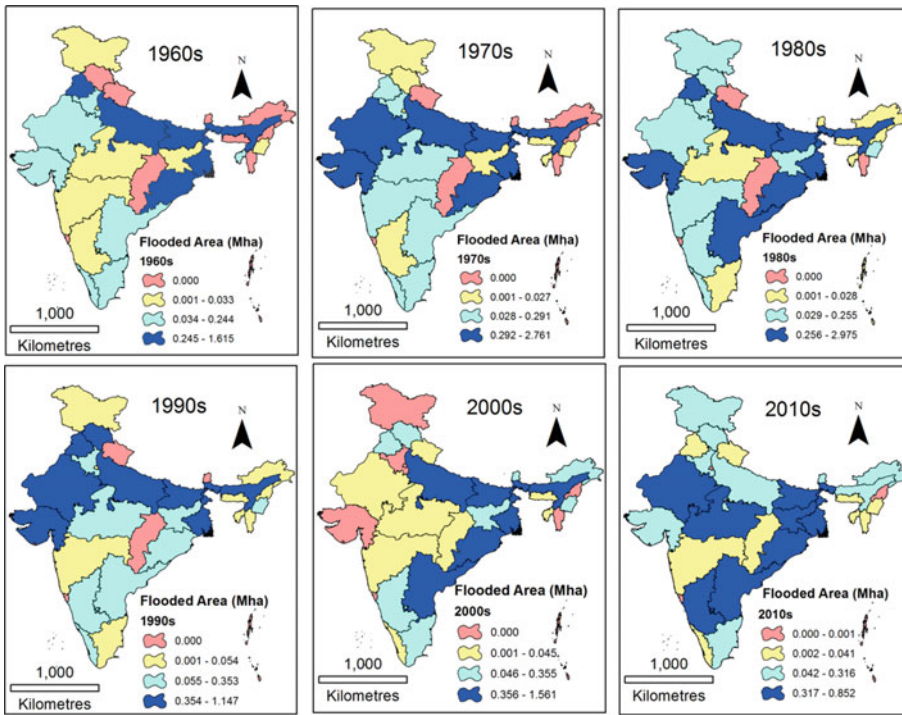


Fig. 11.6 State-level variation (quartile based) of average flooded area (Mha) in the respective decades

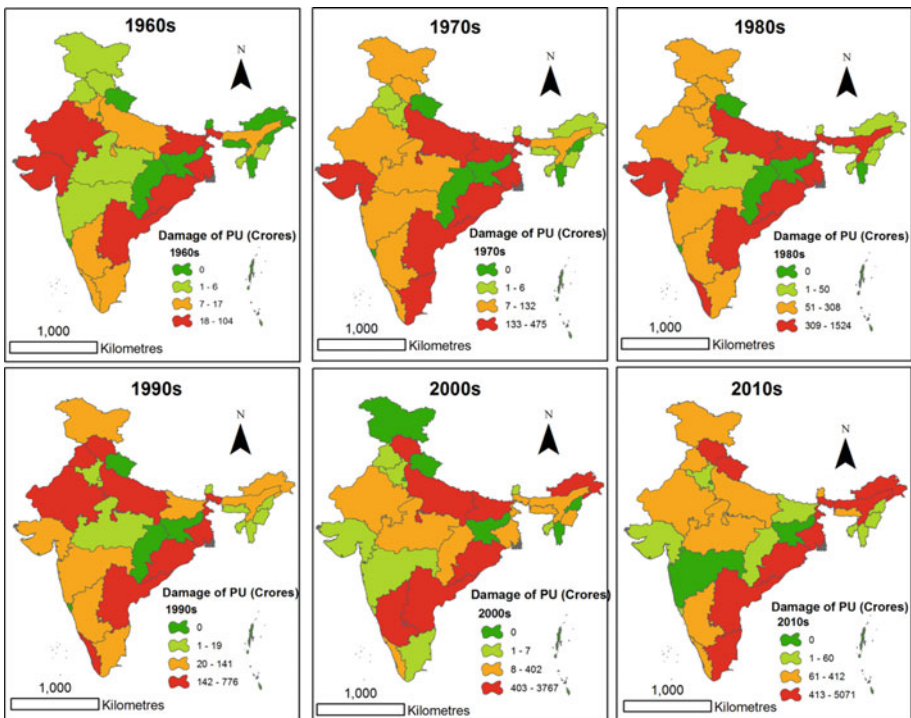


Fig. 11.7 State-level variation (quartile based) of mean damage of normalised value of PU (Crores) in the respective decades

Table 11.5 State-level correlation values between flooded area and PU damage of studied decades

Spearman's correlation	1960s	1970s	1980s	1990s	2000s	2010s
<i>r</i> -value	0.379 ^a	0.623 ^b	0.561 ^b	0.790 ^b	0.803 ^b	0.646 ^b
<i>p</i> -value	0.025	0.000	0.000	0.000	0.000	0.000

^aSignificant at 0.05 level (2-tailed)^bSignificant at 0.01 level (2-tailed)**Table 11.6** List of major events of bridge and structure failure during the rainy season of 2020 in different parts of India

Geomorphic events	Location/place/region	Date of occurrences	Nearest river	Details of transport network failure	Expected cost of losses	Source(s)
Landslide at Darjeeling Himalaya	Paglajhora, Darjeeling, WB	June 29, 2020	Panchai River	Disconnection of NH 110 (Hill Cart Road) from Siliguri to Darjeeling and Partly damage of Himalayan Railway Line to Drajeeling	N.A	Siliguri Times News Channel on Facebook (June 30, 2020)
Heavy rain and flood	Sattarghat Bridge, Gopalganj, Bihar	July 15, 2020	Across the Gandak River	260 Crore brand-new Bridge Collapses including two-kilometer road (approach road) also fully damaged. Eight years to take in its construction; Inaugurated on 16 June, 2020	260 crore	NDTV, INDIA (July 16, 2020)
Heavy rain and flood	Seoni district, Madhya Pradesh	August 30, 2020	Wainganga River	The bridge on Sunwara-Amanala road was built at a cost of ₹ 3.7 crore under the Prime Minister's rural road network scheme, PMGSY. The bridge was 150-m-long and 9.28 m high, DAM effect. Its construction started on September 1, 2018, and was scheduled to be completed before August 30, 2020	3.7 crore	NDTV, India Today, The INDIAN Express News (August 30, 2020)
Heavy rain and flood	Ramtek, Nagpur district, Maharashtra	August 30, 2020	N.A	The catchment area of the river in Madhya Pradesh received heavy rainfall; therefore, it released large amounts of water from the dam. The bridge was constructed between 2015 and 2018, and it used to connect many villages of the tribal communities	N.A	NDTV, INDIA (August 31, 2020)
Heavy rain and flood	Gadigarh area, Dharap near Jeevan Nagar, Jammu	August 26, 2020	N.A	The bridge that collapsed due to the flood water was an important link between Dharap and Bishnah Tehsil of Jammu District. This bridge was built just five years ago	N.A	NDTV, INDIA (August 31, 2020)

(continued)

Table 11.6 (continued)

Geomorphic events	Location/place/region	Date of occurrences	Nearest river	Details of transport network failure	Expected cost of losses	Source(s)
Heavy rain and flood	Araria, Bihar	August 25, 2020	Bakra river	According to a PTI report, a part of the 200-foot-long bridge, which is around 20 years old had collapsed on Tuesday afternoon. Reportedly, as the bridge collapsed, a tractor carrying several people as well as a motorcycle and several pedestrians fell into the river. It is unclear as to whether there were any casualties	N.A	Asian News International (ANI) Tweeter Page
Heavy rain and flood	Goabari village, Kishanganj, Bihar	September 17, 2020	Kankai river	A newly constructed bridge has washed away ahead of its inauguration in Bihar's Kishanganj following a rise in the water level of Kankai River. The bridge was built at a cost of Rs 1.42 crore	1.42 crore	timesnownews.com



Fig. 11.8 Examples of bridge failures during the monsoon of 2020 from different parts of India (*Source* Collected by author from various electronic media mentioned below in each photo)

References

- Aggarwal MK (2001) Case history of failure of the bridge due to natural calamity. *Indian Highways* 29(3):11–14
- Basu BK, Gupta AK (2003) Scour consideration for bridge foundation in Bouldery river bed—case study. *Indian Highways* 31(1):43–47
- Birajdar HS, Maiti PR, Singh PK (2014) Failure of Chauras bridge. *Eng Fail Anal* 45:339–346. <https://doi.org/10.1016/j.engfailanal.2014.06.015>
- Bizikova L, Neale T, Burton I (2008) Canadian communities' guide book for adaptation to climate change. Including an approach to generate mitigation co-benefits in the context of sustainable development, 1st edn. Environment Canada and University of British Columbia, Vancouver
- Brown S, Dawson RJ (2016) Building network-level resilience to resource disruption from flooding: case studies from the Shetland Islands and Hurricane Sandy. *Flood Risk*, Lyon, 17–21 October 2016. <https://doi.org/10.1051/e3sconf/20160704008>
- Cook W, Barr PJ (2017) Observations and trends among collapsed bridges in New York state. *J Perform Constr Facil* 31(4):04017011. [https://doi.org/10.1061/\(ASCE\)CF.1943-5509.0000996](https://doi.org/10.1061/(ASCE)CF.1943-5509.0000996)
- CWC: Central Water Commission (2019) Water related statistics. Water Planning & Project Wing, Government of India, New Delhi
- Datta SK, Datta S, Banerjee SN (2000) Repair and rehabilitation of Iswar Gupta Setu on river Ganges at Kalyani, West Bengal. *J Indian Roads Congr* 61(1):103–115
- Farhey DN (2017) Structural performances of bridge materials in the U.S. national bridge inventory 2013. *Struct Eng Int* 27(1):101–113. <https://doi.org/10.2749/101686617X14676303589039>
- Garg RK, Chandra S, Kumar A (2020) Analysis of bridge failures in India from 1977 to 2017. *Struct Infrastruct Eng*. <https://doi.org/10.1080/15732479.2020.1832539>
- Hammond MJ, Chen AS, Djordjević S, Butler D, Mark O (2015) Urban flood impact assessment: a state-of-the-art review. *Urban Water J* 12(1):14–29
- IWB-GoWB: Irrigation and Waterway Directorate-Government of West Bengal (2019) Annual Flood Report for the Year 2019. Advance planning, project evaluation, and monitoring cell, Jalsampad Bhavan, Salt Lake, Kolkata
- Jongman B, Ward PJ, Aerts JCJH (2012) Global exposure to river and coastal flooding: long term trends and changes. *Glob Environ Chang* 22:823–835. <https://doi.org/10.1016/j.gloenvcha.2012.07.004>
- Koks EE, Rozenberg J, Tariverdi M, Vousdoukas M, Fraser SA, Hall JW, Hallegatte S (2019) A global multi-hazard risk analysis of road and railway infrastructure assets. *Nat Commun* 10:2677
- Kundzewicz ZW et al (2013) Flood risk and climate change: global and regional perspectives. *Hydrol Sci J* 59(1):1–28. <https://doi.org/10.1080/02626667.2013.857411>
- Mills E (2005) Insurance in a climate of change. *Science* 309:1040+
- MoR: Ministry of Railway (2019) Indian Railways Year Book 2018–19. Rail Mantralay, Government of India, New Delhi
- MoRTH: Ministry of Road Transport and Highways (2019a) Basic Road Statistics of India (2016–2017). Transport Research Wing, Government of India, New Delhi
- MoRTH: Ministry of Road Transport and Highways (2019b) Indian bridge management system. Ministry of Road Transport & Highways, New Delhi. <https://pib.gov.in/newsite/PrintRelease.aspx?relid=187002>
- Munich Re (2015) NatCatSERVICE: Loss events worldwide 1980–2014 Munich Re, Munich
- Najibi N, Devineni N (2017) Recent trends in frequency and duration of global floods. *Earth Syst Dyn Discuss* <https://doi.org/10.5194/esd-2017-59>
- Nanditha JS, Mishra V (2021) On the need of ensemble flood forecast in India. *Water Secur* 12:100086. <https://doi.org/10.1016/j.wasec.2021.100086>
- Nicholls R, Zanuttigh B, Vanderlinden JP, Weisse R, Silva R, Hanson S, Narayan S, Hoggart S, Thompson RC, de Vries W, Koundouri P (2015) Developing a holistic approach to assessing and managing coastal flood risk. In: Zanuttigh B (ed) Coastal risk management in a changing climate, Butterworth-Heinemann, pp 9–53. <https://doi.org/10.1016/B978-0-12-397310-8.00002-6>
- Pedrozo-Acuña A, Moreno G, Mejía-Estrada P, Paredes-Victoria P, Breña-Naranjo JA, Meza C (2017) Integrated approach to determine highway flooding and critical points of drainage. *Transp Res Part D* 50:182–191
- Pregolato M, Ford A, Wilkinson SM, Dawson RJ (2017) The impact of flooding on road transport: a depth-disruption function. *Transp Res Part Transp Environ* 55:67–81. <https://doi.org/10.1016/j.trd.2017.06.020>
- Proske D (2019) Comparison of the collapse frequency and the probability of failure of bridges. *Proc Inst Civil Eng—Bridge Eng* 172(1):27–40. <https://doi.org/10.1680/jbren.18.00002>
- Pyatkova K, Chen AS, Butler D, Vojinović Z, Djordjević S (2019) Assessing the knock-on effects of flooding on road transportation. *J Environ Manage* 244:48–60
- Roy (2021) Impact of linear transport infrastructure on fluvial connectivity across the catchments of West Bengal, India. *Geocarto Int*. <https://doi.org/10.1080/10106049.2021.1903576>
- Roy S, Sahu AS (2017) Potential interaction between transport and stream networks over the lowland rivers in Eastern India. *J Environ Manag* 197:316–330. <https://doi.org/10.1016/j.jenvman.2017.04.012>
- Sheer J (2010) Failed bridges: case studies, causes and consequences. Ernst & Sohn-Wiley, Germany
- Swiss Re (2015). Natural catastrophes and man-made disaster in 2014, Swiss Reinsurance Company, Zurich, Switzerland, p 883
- Taylor MAP (2017) Vulnerability analysis for transportation networks. Elsevier, Amsterdam, Netherlands

- Walsh CL, Ford A, Barr S, Dawson RJ (2012) A spatio-temporal modelling framework for the integrate assessment of cities in Earth Systems Engineering 2012. In: A technical symposium on systems engineering for sustainable adaptation to global change. Centre for Earth Systems Engineering Research, Newcastle University, Newcastle upon Tyne (UK)
- Ward PJ, Winsemius HC, Kuzma S, Bierkens MFP, Bouwman A, de Moel H, Díaz Loaiza A et al (2020) Aqueduct floods methodology. Technical Note. World Resources Institute, Washington, DC. www.wri.org/publication/aqueduct-floods-methodology
- Webster Dictionary (2010) Webster's new world college dictionary, 4th edn. Houghton Mifflin Harcourt, Boston, USA
- World Bank (2016) Flood risk in road networks: technical notes. International Bank for Reconstruction and Development/The World Bank. Washington, DC. www.worldbank.org



Rural–Urban Differential in Flood Vulnerability and Community Preparedness for Flood Management Strategies

Aznarul Islam , Susmita Ghosh,
and Suman Deb Barman

Abstract

The present study examines the varying impact of flood hazards on selected rural and urban areas of the lower Mayurakshi River Basin. Flood hazard has been measured in terms of flood frequency, flood depth, and flood duration while flood vulnerability is measured in terms of selected physical, economic, demographic and social, and infrastructural indicators. An empirical survey was executed over 563 households across five severely affected villages and two municipal-ity wards. In the last 20 years, the study found no statistically significant difference between rural and urban areas regarding flood frequency and flood depth. However, flood duration varies as per the area of residence. Moreover, a statistically significant difference has been observed regarding some indicators of physical, demographic and social, and infrastructural vulnerability. However, economic vulnerability does not differ significantly between rural and urban areas. This is because, after the devastating flood of 2000,

the rural people opted for international migration especially in the Middle East countries that increased the per capita monthly income by remittance while the urban people received a fair share of the income from the non-agricultural occupation. Thus, this typical mechanism eliminates the socio-economic variation between the urban and rural communities. Though there are no such significant differences between rural and urban areas regarding flood hazard and flood vulnerability, a statistically significant difference has been observed regarding the majority of the flood preparedness activities.

Keywords

Riverine flood · Rural–urban gap · Flood hazard · Community preparedness · Barh plains

12.1 Introduction

Flood hazard is often naturally or quasi-naturally induced while flood vulnerability is mainly associated with community behaviour, and hence depends upon the exposure and coping capacities of a community (Wu et al. 2002). Community-wise flood vulnerability differs as per the variation of the demographic, societal, and economic traits of a community (Chakraborty et al. 2020). A lot of work have been done on community-

A. Islam (✉) · S. Ghosh
Department of Geography, Aliah University,
17 Gora Chand Road, Kolkata 700014, India

S. D. Barman
Department of Geography, The University of
Burdwan, Burdwan, West Bengal 713104, India

wise disaster risk management. The scholars give utmost priority to the community and include them in the management work as the first response to a disaster may come from them and then from the others (Surminski et al. 2015). Therefore, understanding the community behaviour and the needs of a community are vital in reducing flood vulnerability.

The nature of socio-economic characteristics differs drastically in terms of the rural and urban communities (Buciega et al. 2009). Flood negatively affects both the communities but in a different way. The backbone of the rural economy is agriculture and flood damages the crop which paralyzes the rural economy (Mahmood et al. 2019; Jahan et al. 2014). However, an urban community mainly depends upon the secondary and tertiary types of economic activities. Thus, the rural people are economically more fragile than that of the urban counterpart. In an urban area, people alter the landscape drastically. In the name of development, the whole urban area becomes concretized and the extent of land to encourage infiltration of the rainwater is negligible which increases the flood peak (Adebayo and Arohunsoro 2014; Suriya and Mudgal 2012). In the rural area, the exposed area is greater for groundwater recharge and lots of waterbodies are present for retaining the floodwater (McMinn et al. 2010). As with flood vulnerability, the nature of flood adaptation strategies also differs. The rural people emphasize strengthening their economy, i.e., giving emphasis on occupational diversification and increasing the per capita income, and they also believe in 'living with flood' (Mollah 2016). Moreover, Sahoo and Sreeja (2017) emphasized constructing the detention pond in Guwahati City to minimize the flood vulnerability. Suriya and Mudgal (2012) suggested quantifying the runoff amount of Thirusoolam sub watershed and also prepare an appropriate land use planning for development purposes. Moreover, Gupta (2020) studied that for urban areas proper development of sewage systems is important for minimizing the flood effect.

Twigger-Ross (2005) portrayed the differential impact of flooding in both rural and urban

communities in the UK from an empirical perspective to developing the rural and urban policy recommendation. A lot of work have been done regarding rural–urban linkages to face the flood (Jamshed et al. 2020, 2021; Satterthwaite and Tacoli 2002). In the Mayurakshi River Basin, a lot of work have been done regarding the flood hazard (Islam and Sarkar 2020; Islam and Deb Barman 2020; Ghosh and Mukhopadhyay 2015; Jha and Bairagya 2012; Pal 2015, 2016, 2017) and the anthropogenic control on flood (Islam et al. 2020). The majority of the scholars focus on the rural flood (Islam and Ghosh 2021; Mollah 2016) of the Mayurakshi River basin but there is no work till now regarding the urban flood or rural–urban differential in flood vulnerability and adaptation strategies. Thus, the present study would address the following objectives.

- (1) To unearth the differential impact of the flood on the rural and urban community of the lower Mayurakshi River Basin and
- (2) To find out the nature and spatial variation of different flood preparedness strategies taken by the rural and urban communities.

12.2 Study Area

Originating from the Trikut Hill, Deoghar, Jharkhand, the Mayurakshi River traverses 250 km, and then it debouches with the Bhagirathi River near Narayanpur. The latitudinal extension of the Mayurakshi Basin is from 23° 37' 43" N to 24° 37' 36" N and the longitudinal extension is from 86° 50' 16" E to 88° 15' 52" E, and it covers the total area of about 9596 km². The lower stretch of the Mayurakshi River is configured with the five C.D. blocks of Murshidabad Districts, i.e., Nabagram, Khargram, Kandi, Burwan, and Bharatpur-I. Among the five C.D. blocks, Kandi is the most flood-prone block (Mollah 2016; Islam and Ghosh 2021a). Almost every year, a flood visits Kandi. The present study deals with the urban and rural areas of C.D. Block Kandi. For the present study, two municipality wards (Wards No. 8 and 13) among

17 wards of Kandi Municipality and five villages (Hijal, Srikanthapur, Andulia, Sashpara, and Harinagar) among 84 villages have been selected using a purposive sampling aided by a pilot survey (Fig. 12.1). The population of C.D. Block Kandi is 220145 and the areal coverage is 227.48 km² while Kandi Municipality covers an area of 12.97 km² and contains a population of 55,632. The population density of C.D. Block Kandi and Kandi Municipality is 920 persons per km² and 4300 persons per km², respectively (District Census Handbook 2011).

The study area is a part of the *Rarh* plain of Murshidabad District and almost every year Mayurakshi-Dwarka and Kuea River system induce floods in this region. This area is a part of the lower Mayurakshi River Basin that exhibits drainage congestion and recurrent floods due to the gentle slope (Islam and Ghosh 2021b). The C.D. Block Kandi is drained by Mayurakshi, Dwarka, Brahmani, and Kuea. Moreover, lots of spill channels are spread over the region. The severity of the flood of this region is induced by the typical topographical configuration and outpouring of the rivers like Dwarka-Brahmani and the Kuea with the Mayurakshi River in a low-lying area of Hijal. And the peak flow Mayurakshi system in the monsoon season finds it difficult to pass through the north–south flowing mighty Bhagirathi River because the water level of the Bhagirathi also remains at a higher level (Islam and Sarkar 2021).

12.3 Database and Methodology

12.3.1 Collection of Data

The primary data concerning the nature of flood and its socio-economic aspects are collected taking a statistically significant sample size (n) for each village using simple random sampling as a particular area is homogeneous in terms of population. The sample size has been determined using the Eq. 12.1 following the United Nations Framework Convention on Climate Change (UNFCC 2020).

$$n \geq \frac{1.645^2 NV}{(1-N)x0.1^2 + 1.645^2 V} \quad \text{and} \quad (12.1)$$

$$V = \frac{p(1-p)}{p^2}$$

where n stands for sample size; N for the total number of households of the villages as per 2011 Census (Table 12.1); p for the proportion of the households having economic marginalization (loss of crops and building damage minus coping capacity) due to the flood of 2000 (Table 12.1) as derived through the pilot survey in the field; 1.645 for 90% confidence required; 0.1 for 10% relative precision.

Using this methodology, a total of 563 households were surveyed among which 396 rural households (Table 12.1) across five villages (Hijal, Srikanthapur, Andulia, Sashpara, and Harinagar) and 167 urban households across two municipality wards (Ward Nos. 8 and 13) of the Kandi Municipality.

12.3.2 Measuring Flood Hazard

Flood hazard has been assessed by using three parameters: flood frequency, flood depth, and flood duration. The C.D. Block Kandi experiences floods on an annual basis. Based on the last 20 years (1998–2017) data collected from the Kandi final report (2012), annual reports of Irrigation and Waterways Department, Govt. of West Bengal (2013–2016), a study carried out by Sanyal and Lu (2006), and field investigations (2017), the flood frequency, flood depth, and flood duration of the study area have been portrayed.

12.3.3 Measuring of Flood Vulnerability

Flood vulnerability has been measured in four categories, i.e., physical vulnerability, demographic vulnerability, economic vulnerability, and socio-infrastructural vulnerability. The physical vulnerability has been measured based

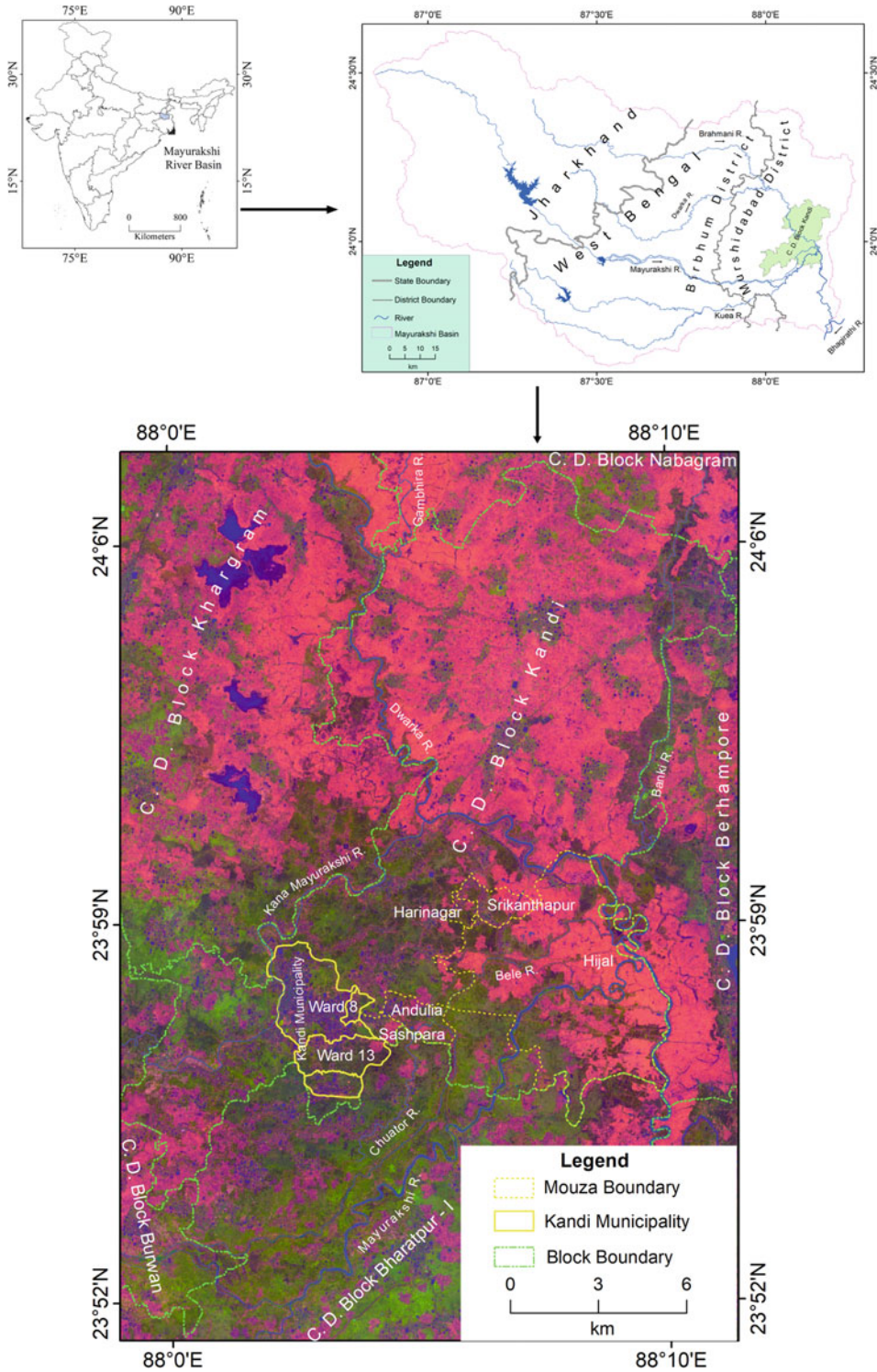


Fig. 12.1 Location of the study area

Table 12.1 Representative households of villages and wards

Village/wards	Total households (2011)	<i>p</i>	Sample			
			Households	Female	Male	Total
Srikanthapur	881	0.737	89	212	267	479
Hijal	2713	0.607	165	326	429	755
Andulia	521	0.865	40	94	106	200
Sashpara	1045	0.771	75	168	202	370
Harinagar	269	0.902	27	69	80	149
Ward No. 8	757	0.772	73	219	246	465
Ward No. 13	870	0.72	94	282	323	605
Total	7056		563	1370	1653	3023

on land use and land cover (areal percentages) extracted from Google earth imageries for 2019. Similarly, the demographic vulnerability parameters (population density, female–male ratio, and dependency ratio) are calculated following the District Census Handbook (2011). Moreover, the social and infrastructural vulnerability parameters such as the distance to flood shelter camp from home, distance to market from home, and distance to health center from home are derived through the intensive field investigation during 2017–2019. Furthermore, the location of the potential flood shelter is measured from the Google earth imageries for 2019. Furthermore, the economic vulnerability parameters (per capita income, percentage of the farming population, and diversification of occupation) have been calculated from the field data collected through extensive field surveys during 2017–2019.

12.3.4 Relative Importance Index

There is a block-wise variation on the perceptions of local people which is detected through the relative importance index (RII). The algorithm to compute RII is mentioned in Eq. 12.2.

$$RII = \frac{\sum W}{AN}$$

$$= \frac{1n_1 + 2n_2 + 3n_3 + 4n_4 + 5n_5 + 6n_6 + 7n_7 + 8n_8 + 9n_9 + 10n_{10}}{10N}$$

(12.2)

where ‘*W*’ stands for the weighting or rating given to each factor by the respondent which ranges from 1 to 10; *n*₁ for the number of respondents giving minimum rating (1) while *n*₁₀ for the number of respondents giving maximum rating (10). ‘*A*’ for the highest weight (i.e., 10 in the study) and ‘*N*’ for the total number of samples.

The RII ranges from 0 to 1 (Le and Tam 2007). The higher the value of RII the higher the intensity of the perceptual rating about the social-psychological parameters.

12.3.5 Occupational Diversification

Inverse Herfindahl-Hirshman Index (HHI) has been computed using Eq. 12.3 after Rhoades (1993) to identify occupational diversification.

$$HHI = \frac{1}{\sum_{i=1}^n (WS)^2}$$

(12.3)

where WS represents the share of the workforce under a certain occupation (*i*) to the total workforce under different occupational categories (*n*).

12.3.6 ANOVA

Analysis of variance (ANOVA), generally expressed by ‘F statistic’ compares the difference

between the groups to the difference within the group. For the present study, a one-way ANOVA has been carried out to detect the significant difference in hazard and vulnerability parameters across different religious and economic groups. It may be expressed using Eqs. 12.4–12.8.

$$F = \frac{MST}{MSE} \quad (12.4)$$

$$MST = \frac{SST}{p - 1} \quad (12.5)$$

$$SST = \sum n(x - \bar{x})^2 \quad (12.6)$$

$$MSE = \frac{SSE}{N - p} \quad (12.7)$$

$$SSE = \sum (n - 1)S^2 \quad (12.8)$$

where F stands for Anova Coefficient, MST for Mean sum of squares due to treatment, MSE for the mean sum of squares due to error, SST for sum of squares due to treatment, p for the total number of populations, n for the total number of samples in a population, SSE for sum of squares due to error, S for the standard deviation of the samples, N for the total number of observations.

12.3.7 Cluster Analysis

Cluster analysis is applied to classify the parameters/objects into meaningful clusters or groups which is different from the other group. Hierarchical clustering or dendrogram is a common approach to assembling similar pairs of objects and forming lower to higher clusters step by step. For cluster analysis between the group, the linkage method opted for similarity and squared Euclidean distance are taken into consideration. In this study, a dendrogram has been adopted for the grouping of flood preparedness activities of rural and urban areas.

12.4 Results and Discussion

12.4.1 Nature of Flood

The flood history of *Rarh* tract is well known, especially for the Mayurakshi, Ajay, and Damodar River Basin. The nature of the flood of the *Rarh* tract is quite different from that of the Bengal delta. The sudden monsoonal rain causes the flood in the peninsular rivers like the Ajay, Mayurakshi, and Damodar rivers and often goes beyond the coping capacity of the people. The C. D. Block Kandi is the most flood hazard-prone block of the *Rarh* tract of Murshidabad District (Mollah 2016). As per the historical records of the last 20 years (1998–2017), floods have been recorded a maximum of 15 times in the C.D. Block Kandi with at least 11 flood events. In the years 2006 and 2015, Kandi experienced floods two times a year, and in 2007 floods occurred three times. A huge rainfall in the Chottonagpur plateau and *Rarh* plain, and breaching of the embankment and sudden water release from Tilpara barrages are mainly responsible for the flood of Kandi area.

In the last 20 years (1998–2017), the average flood frequency of both rural and urban areas was 13. In rural areas, it ranges from 11 (Harinagar) to 15 (Hijal and Sashpara) while in the urban area the flood frequency was recorded 13 for Ward No. 13 and 12 for Ward No. 8 (Fig. 12.2a, b). The average agricultural flood depth in the rural area was 4.67 m; and in urban areas, it was 2.78 m (Fig. 12.3a). The highest agricultural flood depth recorded was 6.07 m in Hijal and the maximum floodwater stay was also 80 days (Fig. 12.3b). The floodwater stay on agricultural land of the urban area was found to range from 17 to 18 days, and the depth of flood also ranged from 2.74 to 2.81 m (Fig. 12.3b). An interesting observation was noted regarding floodwater depth in the settlement. The average depth of

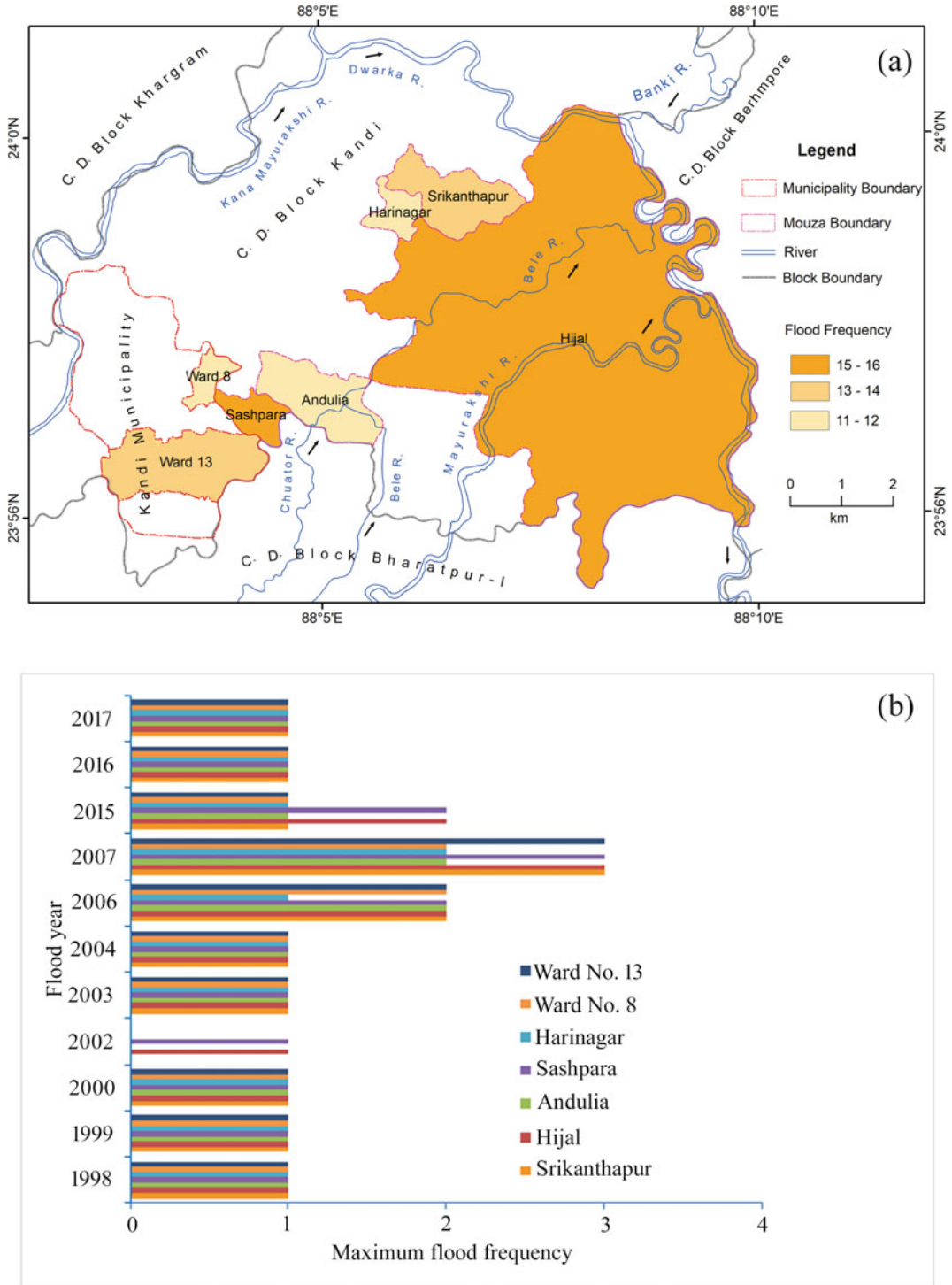


Fig. 12.2 Flood hazard of rural and urban area. **a** Spatiality of flood frequency. **b** Flood years

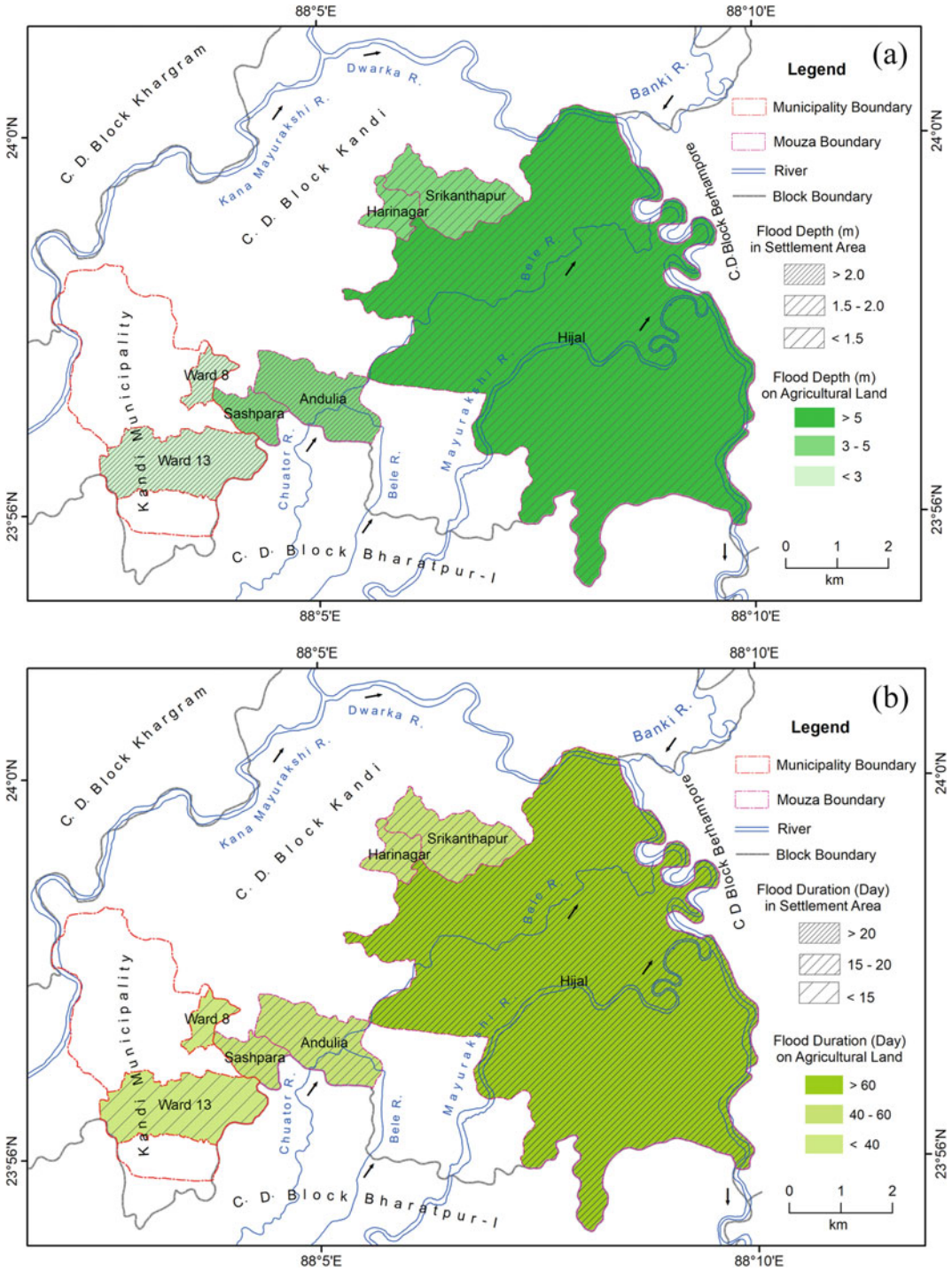


Fig. 12.3 Spatial variation of **a** flood depth, **b** flood duration

floodwater in rural and urban areas was 1.848 m and 2.362 m, respectively. The water depth of the urban area is higher than that of the rural area. This is due to the absence of a waterbody in the urban area and the percentages of agricultural land are lower in the urban area which fails to reserve the floodwater. Though the floodwater depth is comparatively higher in the settlement area of the urban land the floodwater stays comparatively for fewer days.

To find out the statistically significant difference between urban and rural areas regarding flood hazard, an ANOVA was applied to test at 1 degree of freedom and 0.05 significance level which depicts that the F critical value is lower than the computed value of F regarding agricultural depth, settlement, and agricultural duration. This signifies that there is a significant statistical difference between rural and urban areas (Table 12.2). However, regarding flood frequency and settlement depth, there is no statistically significant difference. The agricultural land of rural areas of C.D. Block Kandi is located at a lower elevation compared to the urban counterpart. Moreover, flood water stay in the settled area and on agricultural land is higher for the rural area than the urban counterpart. One interesting finding related to the flood depth and duration between the rural and urban areas is that though settlement depth is higher for the urban areas, settlement duration is higher for the rural area. This may be due to the paved surface in the municipal wards and agricultural land use in the rural area. This typical composition of land use allows fast movement of floodwater from the urban area compared to the rural area.

12.4.2 Flood Vulnerability

Vulnerability is closely related to the socio-economic structure of the society as it is related to the community characteristics (Mollah 2016). Kandi is a flood hazard-prone area but economically less vulnerable due to the recipient of higher remittances (Islam and Ghosh 2021a). The higher flood hazard proneness forced the people to migrate which brought remittances from the outside, and therefore flood appears as blessings to them.

Flood vulnerability has four components, i.e., physical vulnerability, demographic vulnerability, economic vulnerability, and socio-infrastructure vulnerability. Regarding physical vulnerability, percentages of agricultural land have an important role in the intensity of vulnerability. The higher the percentages of agricultural land the higher the exposure of it to flood vulnerability. In rural areas, the exposure is high in the monsoon season (Fig. 12.4a). For example, the village Hijal has the highest percentages of agricultural land (90%) and other villages also register about 75% of agricultural land. However, Ward Nos. 8 and 13 have registered 34 and 47% of agricultural land, respectively. Percentage coverage of settlement is also an indicator of higher vulnerability because the higher the percentages of households the higher the flood exposure. Higher coverage of settlement is observed in both Andulia and Sashpara (13%) while the lower percentage is recorded in Hijal (2%). However, Ward Nos. 8 and 13 have 46 and 37% of settlement coverage, respectively. Furthermore, strong connectivity reduces the level of

Table 12.2 ANOVA showing the variations of hazard between the rural and urban area

Parameters	F	P-value	F crit	Remarks
Flood frequency	0.26316	0.62981	6.60789	Null
Settlement depth	1.8215	0.23502	6.60789	Null
Agricultural depth	7.7454	0.03876	6.60789	Alternative
Settlement duration	13.7615	0.01386	6.60789	Alternative
Agricultural duration	16.1307	0.01016	6.60789	Alternative



Fig. 12.4 Flood vulnerability and preparedness. **a** Flood during the monsoon in Hijal. **b, c** Vulnerability of village roads to monsoon rain and flood. **d** Flood shelter camp at Kandi. **e** Concrete embankment under Kandi Master plan. **f** Flood-resilient building

vulnerability. The maximum road coverage is found in Ward No. 8 (7%) and the minimum is recorded in Hijal (1.5%). A statistically significant difference is found for the agricultural area, settlement, and road space (Table 12.3).

Population density is maximum for Ward No. 8 (about 57 persons/ha) and minimum for Hijal (3 persons/ha). The average population density for rural areas is 19 persons/ha while for urban areas it

is 37 persons/ha. The dependency ratio is recorded higher for urban areas (about 36) than rural areas (about 26). The maximum female–male ratio was noticed in Andulia (905) while the lowest was noticed in Hijal (712). There is a statistically significant difference between the rural and urban areas regarding only the dependency ratio.

The highest per capita income is recorded in village Hijal about Indian National Rupees

(INR) 2063 and the minimum in Andulia about INR 954. There is no significant difference regarding the economic vulnerability between urban and rural areas. Sashpara recorded the highest diversification of income, i.e., inverse HH index 2.67 while the lowest was recorded in Harinagar (2). Regarding urban areas, Ward No. 8 and 13 recorded 2.35 and 2.48, respectively. Harinagar and Hijal record more than 25% of the farming population. The minimum percentages of the farming population belong to the Andulia (18%). Ward Nos. 8 and 13 have about 19 and 20% of the farming population, respectively.

The socio-infrastructure vulnerability to flooding is comparatively higher in the rural areas, especially the rural roads (*kutchra*) often become vulnerable in the wake of the flood and heavy monsoon rain (Fig. 12.4b, c). Besides, the flood shelter camp, a concrete structure, helps to reduce the shock of the flood victims especially during and immediately after the flood events (Fig. 12.4 d). In the study area, it is nearer to the Srikanthapur (about 0.12 km) and the maximum from Hijal (1.58 km). Potential flood shelters are located at the elevation of 23.77 m and 24.76 m for ward Nos. 8 and 13 respectively. Regarding the rural zone, it is lowest for Hijal (about 18 m) and highest for Andulia (22.56 m). The average

market distance for rural areas is about 9 km while in urban areas it is only about 2.5 km. The distance from the health centre is recorded maximum for Hijal (3.42 km). The average distance to the health centre is recorded as 1.68 km for rural areas while it is 3.28 km for urban areas.

To find out the statistically significant difference between urban and rural areas regarding flood vulnerability, an ANOVA was applied to test at 1 degree of freedom and 0.05 significance level. The F critical is 6.607 for the 15 parameters of flood vulnerability (Table 12.3) out of which there are no significant differences regarding 10 parameters.

Regarding physical vulnerability, parameters such as waterbody and plantation exhibit no significant statistical difference in their areal coverage, although a higher percentage of the waterbody and plantation is observed in rural areas. However, regarding the coverage of the agricultural area, settlement, and road space, there is a statistically significant difference between the two major units. This is quite obvious because in rural areas agricultural land predominates while settlement and road space are predominant in an urban setup. Regarding the demographic vulnerability, parameters such as population density and female–male ratio exhibit

Table 12.3 ANOVA showing the variations of vulnerability between the rural and urban area

Parameters	F	P-value	F crit	Remarks
Agricultural area	34.1455	0.00208	6.60789	Alternative
Settlement	60.956	0.00055	6.60789	Alternative
Road space	14.4862	0.01255	6.60789	Alternative
Water body	0.23686	0.64706	6.60789	Null
Plantation	0.21568	0.66187	6.60789	Null
Population density	0.97478	0.36883	6.60789	Null
Dependency ratio	8.8928	0.03073	6.60789	Alternative
Female-male ratio	0.28945	0.61365	6.60789	Null
Per capita income	0.08041	0.78811	6.60789	Null
Inverse HHI	0.06829	0.80426	6.60789	Null
% farming population	0.37282	0.56816	6.60789	Null
Flood shelter camp	0.03941	0.85045	6.60789	Null
Potential flood shelter	7.9241	0.03733	6.60789	Alternative
Market distance	3.0026	0.14367	6.60789	Null
Health centre distance	3.405178	0.124296	6.607891	Null

significant rural–urban differences. This is because of the higher population density and female–male ratio in the urban area. However, the dependency ratio of rural areas portrays a significant departure from the urban area. This is due to the presence of the higher dependency ratio in an urban area as a consequence of the presence of aged people. Regarding economic vulnerability, the indicators such as per capita income, inverse HHI, percentages of the farming population show no significant rural–urban difference. This is due to the effect of balancing of per capita income between the rural and urban areas for a higher recipient of remittances from the middle east countries by the rural people and receipt of higher non-agricultural income by urban area. Furthermore, regarding the social-infrastructure vulnerability, location of flood shelter camp, market distance, health centre distance depicts no significant statistical difference between the rural–urban areas. Market distance and health centre distance is higher for rural area and the flood shelter camp is located nearer to the urban area. However, the potential flood shelter camp portrays a significant difference, and it has been observed that the potential flood shelter camps are located at the higher elevation in the urban area.

12.4.3 Differential Impact of the Flood on Rural and Urban Community

Urban flood mainly occurs due to heavy rainfall and insufficient or poor drainage condition (Tingsanchali 2012). However, in the study area, the urban flood occurs due to river overbank flow either triggered by higher rainfall and drainage basin characteristics or from the water release from reservoirs mainly from Tilpara barrages or for the breaching of embankments. The flood vulnerability depends upon the community traits (Cutter et al. 2008). The socio-economic characteristics of a rural and urban area differ significantly which is the main reason for higher deviation in flood vulnerability. In a rural area, a

flood devastates the crops and farmers face a huge loss. Rural houses and roads are mainly *kutchha* types which are easily broken by the floodwater while in urban areas stagnation of water and pollution is the main problem of the flood. The house and roads are less affected due to the concretization. In an urban area, the majority of the people depend on the non-agricultural income for their livelihood which is comparatively less affected by flood hazards. Urban people can fast recover because of their comparatively higher income; however, the rural people take a long time for recovery because of lower income and dependency upon agriculture. This is the general scenario of rural and urban floods but in the study area, the total scenario is quite different and interesting. The flood of 2000 was the most devastating in the history of Murshidabad. The flood occurred mainly due to the overflow of water from the Bhagirathi River and its tributaries and continuous heavy rainfall from 18 to 21 September and sudden discharge of water from the reservoir. The flood breached the embankment and washed away human lives, livestock, houses, and other properties, and 4,90,313 houses collapsed and 4,50,600 ha croplands were washed away. The loss of crops, livestock, and other properties was estimated to be exceeding Rs. 20,000 million. About 600 human lives were lost (Molla 2013).

The empirical survey of 563 households portrays a huge transformation in occupational structure from 1998 to 2018 and this transformation was noticed mainly in the rural areas (Fig. 12.5a). In 1998, 84.7% of the workforce was engaged in agriculture, and it is decreased to 60.13% in 2018, and the proportion of the population engaged in labour is increasing from 10.68 to 30.06% in that period. Similarly, for the other villages the people who engaged in agriculture also decreased, e.g., from 70.12 to 54.17% in Srikanthapur, 69.09 to 50.36% in Sashpara, 80.36 to 66.67% in Harinagar, and 58.06 to 52.94% in Andulia. In the urban area, the percentages of the farmers to the total workforce declined but it is negligible, e.g., from 57.59 to 55.35% in Ward No. 8 and from 56.64 to 54.42% in Ward No. 13.

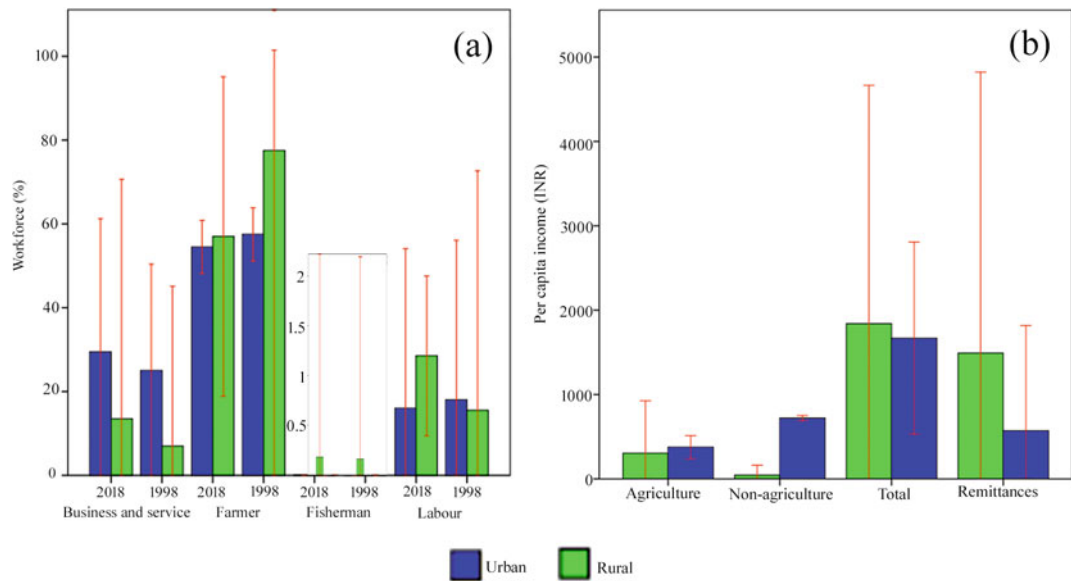


Fig. 12.5 Economic characteristics of rural and urban areas. **a** Occupational transformation. **b** Per capita income

After the 2000 flood, the severely affected villages become ‘proletariat’, and village people chose migration for their support of life and livelihood. Thus, the working population from Hijal, Srikanthapur, Sashpara, Harinagar, Andulia migrated to the middle east countries, e.g., Saudi Arabia. The migrated people received huge remittances which helped in fast recovery. Surprisingly, due to the receipt of remittances from foreign countries, the per capita monthly income of villages increased (e.g., INR 853 for Andulia to INR 2062 for Hijal) compared to the urban area (INR 1578 for Ward No. 8 and INR 1757 for Ward No. 13) (Fig. 12.5b).

Therefore, the devastating flood of 2000 comes as blessings to the rural community of the study area as it allowed them to become economically strong. The receipt of income can reduce the flood vulnerability and during the extensive field study, it was observed that the majority of the houses in the rural study area were *pakka*. So, regarding the socio-economic characteristics of the rural and urban areas, there are no such differences.

12.4.4 Flood Preparedness

Flood is a common phenomenon in both rural and urban study areas. All the study villages are flood-prone and the flood is recurrent throughout its history. From 1999 to 2018, some villages like Hijal, Srikanthapur, and Andulia faced floods more than 10 times and some villages have been inundated even for few months during the 2000 flood. Therefore, they are quite familiar with the flood and they consider flood as a natural hazard and they take some mitigation strategies for the flood. Therefore flood preparedness is essential for the proper planning of coping strategies. Besides, government, non-governmental strategies, and self-help strategies help to adapt to the situation. The field study portrays that different coping strategies are practised by rural and urban people like selling off assets, borrowing money, increasing awareness, savings, etc. Flood preparedness is divided into three broad categories—(1) self-help or preparedness by the community itself; (2) assistance from others including government, non-

government, relatives, and teachers; and (3) others preparedness by both community and others, especially government sometimes as a joint venture.

Therefore, among 27 flood preparedness parameters, eight are community preparedness and eight are in the form of assistance from others and the remaining 11 are taken by joint ventures of the community and others. The eight flood preparedness activities taken by the community are selling of assets, monetary savings for flood, indigenous knowledge about flood, local emergency plan, flood awareness programme, local emergency rescue team, training of rescue team members, and efficacy of rescue team members. However, the other eight activities taken are help from NGO, help from close relatives, help from local political leaders, flood awareness by the teachers', teachers help to the student, international help, flood forecasting, and loan for the reconstruction of broken house. Here international help signifies the help from different foreign organizations during the flood. Another eleven preparedness activities taken by both community and others include construction of embankment, maintenance of embankment, flood resilient building, maintaining of water bodies, land use planning in practices, crop insurance, house insurance, detection of flood prone areas, construction of shelter for environmental refugees, and association with the national disaster management organization at a regular interval. Construction of embankment and its maintenance at a regular interval keeps low-lying flood-prone areas safe (Wesselink et al. 2015). *Rarh* tract especially the lower part of the Mayurakshi River Basin gets inundated by the breaching of the embankment for long. Thus, creating and maintaining an embankment constitutes an integral part of the life and livelihood of the local people. Besides, the local community and government adopt different initiatives. For example, under the massive engineering project 'Kandi Master Plan', Government of West Bengal has started embanking along the middle and lower course of the Mayurakshi River (Fig. 12.4e). Flood resilient building means the special architecture that passes the water from the bottom of

the buildings and the building is located at a higher elevation than the ground so that the water does not easily enter into the houses. Though the people do not build up the flood-resilient building, the majority of the people have constructed *Pakka* buildings mostly with foreign remittances (Fig. 12.4f). However, many *pakka* buildings of the villages of Kandi were constructed under the *Indira Awas Yojana*. Waterbodies also resist flood; however, their maintenance depends upon the choice of the community and government. For example, filling the waterbodies in the municipality area requires the permission from Government. Land use planning is an important tool to escape from the higher magnitude of flood vulnerability (Cilliers 2019). However, it also depends upon the community traits and their willingness. Crop and house insurance also depends upon the mutual understandings of the people and Government. If people invest money to save their crops and house, the government may take responsibility for the loss of their resources. The flood detection map is also prepared by the Government or by other agencies with the help of the local people.

12.4.5 Rural–Urban Difference in Community Preparedness for Flood Management

Flood in the *Rarh* tract in the Murshidabad District is recurrent throughout history (Mollah 2016). However, virtually all the respondents are reluctant to move elsewhere leaving this territory. It has been found that more than 50% of villages and wards have more than 50% of respondents in favour of complete agreement (7 of 7-point rating scale) regarding living with the flood. Similarly, under the category of 'strongly agree' (6 of 7-point rating scale), all the villages have a fair share of respondents ranging from about 20 to 80% (Fig. 12.6a). Moreover, under the category 'agree' there are also some respondents (0–100%) in some villages in favour of the statement. If 'completely agree' is taken as the deep agreement, 'agree' is taken as shallow

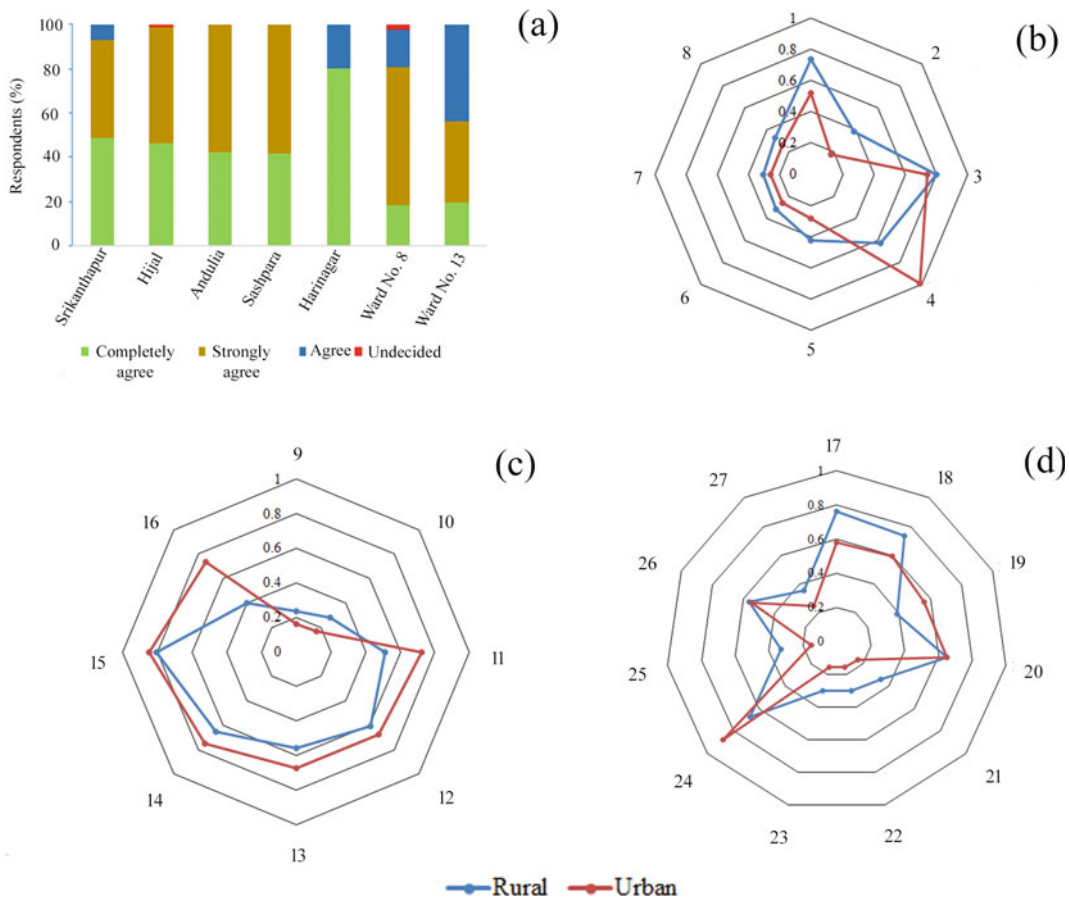


Fig. 12.6 Choice of the rural and urban people to a 'living with the flood' Flood preparedness strategies. **b** Self-help. **c** Assistance from others **d**. Joint ventures (Note 1. Selling off assets, 2. Monetary savings for flood, 3. Indigenous knowledge about flood, 4. Local emergency plan, 5. Flood awareness programme, 6. Local emergency rescue team, 7. Training of rescue team members, 8. Efficacy of rescue team members, 9. Help from NGO, 10. Help from close relatives, 11. Help from local political leaders, 12. Flood awareness by the teachers, 13. Teachers

help to the student, 14. International help, 15. Flood forecasting, 16. Loan for the reconstruction of broken house, 17. Construction of embankment, 18. Maintenance of embankment, 19. Flood resilient building, 20. Maintaining of water bodies, 21. Land use planning in practices, 22. Crop insurance, 23. House insurance, 24. Detection of flood-prone areas, 25. Having flood-prone areas map, 26. Construction of shelter for environmental refugees, 27. Association with the National Disaster Management Organization after a regular interval)

agreement. In the study area, most of the villages (RII 0.953) and also urban (0.881) people like to live there in spite of the flood.

The perception survey of rural and urban people regarding the flood preparedness activities taken by the community shows that only local emergency plan in the urban area (0.988) have higher RII (relative importance index) than the rural (0.627) (Fig. 12.6b). People agree to the

selling off assets, indigenous knowledge about the flood, and local emergency plans for both rural and urban areas. The RII is also higher (> 0.5) regarding these three parameters. The comparatively lower RII (< 0.4) for the local emergency rescue team, training of emergency rescue team, and efficacy of local emergency rescue team are found in this study. To find out the statistically significant difference between urban and rural

Table 12.4 ANOVA showing the variations in community preparedness (self) between rural and urban areas

Parameters	F	P-value	F crit	Remarks
Selling of assets	4.44159	0.0889	6.60789	Null
Monetary savings for flood	18.0073	0.00814	6.60789	Alternatives
Indigenous knowledge about flood	4.46103	0.08838	6.60789	Null
Local emergency plan	78.5953	0.0003	6.60789	Alternatives
Flood awareness programme	7.62489	0.03977	6.60789	Alternatives
Local emergency rescue team	0.09348	0.77212	6.60789	Null
Training of rescue team members	0.01652	0.90275	6.60789	Null
Efficacy of rescue team members	1.6098	0.26038	6.60789	Null

areas regarding flood preparedness of community, ANOVA was applied. At 1 degree of freedom and 0.05 significance level, the *f* critical is 6.607 for the 8 parameters of flood preparedness and there is a statistically significant difference in the three parameters, i.e., monetary savings for flood, local emergency plan, and flood awareness programme (Table 12.4). Though the intensity of the flood is slightly higher for the rural area, their propensity to save money to mitigate the effect of the flood is less because they are more accustomed to the recurrence of flood events and hence they do not emphasize monetary savings for flood, unlike the urban population. Similarly, the urban people go for more awareness programme than that of the rural because the majority of the urban people are engaged in the non-agricultural practice and naturally the experience of flood in relation to agricultural distress is less perceived by the urban people.

Regarding the assistance from others, rural people have agreed more regarding help from NGOs and help from close relatives (Fig. 12.6c). ANOVA was applied for the parameters of assistance from others. At 1 degree of freedom and 0.05 significance level, the *f* critical is 6.607 for the 8 parameters of flood preparedness and there is a statistically significant difference for five parameters, i.e., help from close relatives, help from local political leaders, teachers help to the students, and international help and loan for the reconstruction of the broken house (Table 12.5). However, as the magnitude of the flood is higher in the rural area, to combat the disastrous effect of the flood rural people often make the necessary arrangements. It is noteworthy that the majority of the parameters in the self-adjustment category do not show a significant difference between rural and urban areas because flood management by self-help strategy often results in subjectivity

Table 12.5 ANOVA showing the rural–urban variations in flood preparedness (others)

Parameters	F	P-value	F crit	Remarks
Help from NGO	2.22168	0.19628	6.60789	Null
Help from close relatives	10.4524	0.02313	6.60789	Alternatives
Help from local political leaders	35.9796	0.00185	6.60789	Alternatives
Flood awareness by the teachers	3.16998	0.13512	6.60789	Null
Teachers help to the student	8.1196	0.03585	6.60789	Alternatives
International help	11.2255	0.02032	6.60789	Alternatives
Flood forecasting	0.0476	0.83592	6.60789	Null
Loan for the reconstruction of broken house	17.1067	0.00903	6.60789	Alternatives

within the group than between the group. Contrary to the self strategies, flood abatement measures by others show that the majority of parameters (5 out of 8) show a significant difference. This is because of the varying nature of political consciousness and people’s responses. In a rural area, help from the relatives and contribution of NGOs is relatively better received which makes significant differences. On other hand, urban people are politically more conscious and hence the majority of the benefits from the other groups reach directly to the urban group while the relatively lower political consciousness of the rural people induces malpractices in the distribution of benefits that make a significant difference in some parameters like a loan for the reconstruction of a broken house, and help from local political leaders, etc.

The opinion polls depict that among the joint ventures of flood preparedness activities, rural people emphasize the construction and maintenance of embankment and the RII value is 0.762 and 0.733, respectively, while urban community gives more emphasis on the detection of flood-prone areas and the RII value is 0.88 (Fig. 12.6 d). An ANOVA was applied for the parameters of assistance from others. At 1 degree of freedom and 0.05 significance level, the f critical is 6.607 for the 11 parameters of flood preparedness and there is a statistically significant difference of seven

parameters, i.e., construction of embankment, flood resilient building, land use planning in practices, crop and house insurance, detection of the flood-prone area, and having flood-prone areas map (Table 12.6). Regarding the flood mitigation measures of joint initiatives of the local people and others (Govt.), the majority of the parameters (7 out of 11) have a significant difference between rural and urban areas. Construction of embankment is a vital issue to save the crops from flooding, and this makes a significant rural–urban difference. Similarly, flood resilient building is comparatively higher in the urban area because of structural urbanization. The practice of land use planning, crop insurance, house insurance is remarkably higher in the rural area than that of urban area. This makes a significant statistical rural–urban difference. Moreover, the availability of flood-prone maps is significantly lower in both rural and urban areas. However, the flood-prone area has been detected with a higher emphasis in the urban area than the rural area.

The single linkages of nearest neighbour cluster analysis portray that helps from NGOs, house and crop insurance, land use planning in practices, having the flood-prone map, helps from relative and monetary savings for flood make the large cluster of lower level in the urban area and the smallest cluster appears with a single variable of the local emergency plan (Fig. 12.7a, b). However,

Table 12.6 ANOVA showing the rural–urban variations in flood preparedness (joint ventures)

Parameters	F	P-value	F crit	Remarks
Construction of embankment	20.1107	0.00649	6.60789	Alternatives
Maintenance of embankment	5.61898	0.06392	6.60789	Null
Flood resilient building	16.1875	0.01009	6.60789	Alternatives
Maintaining of water bodies	0.1742	0.69372	6.60789	Null
Land use planning in practices	17.1043	0.00903	6.60789	Alternatives
Crop insurance	25.1609	0.00405	6.60789	Alternatives
House insurance	44.3038	0.00115	6.60789	Alternatives
Detection of flood-prone areas	9.10334	0.02951	6.60789	Alternatives
Having flood-prone areas map	95.4189	0.00019	6.60789	Alternatives
Construction of shelter for environmental refugees	0.19949	0.67381	6.60789	Null
Association with the National Disaster Management Organization after a regular interval	0.64375	0.45878	6.60789	Null

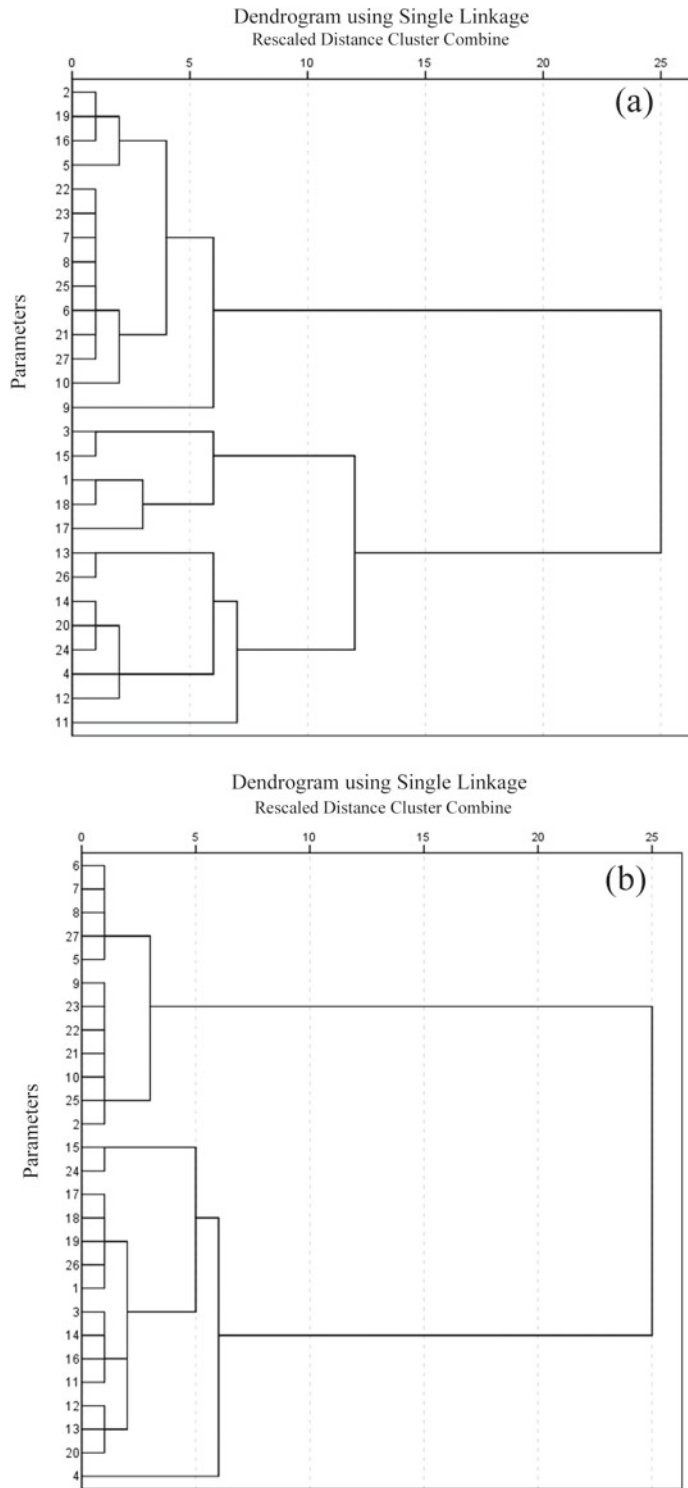


Fig. 12.7 Cluster analysis of flood preparedness. a Rural. b Urban

for the rural area, a more complex hierarchy has been found. One large cluster and twelve small clusters of parameters have been observed. The large cluster consists of the local emergency rescue team, training of emergency rescue team members, efficacy of team members, land use planning in practices, crop, and house insurance, having flood-prone areas map and association with NDMO (National Disaster Management Organization).

Apart from the overall scenario, regarding self initiatives of flood preparedness in rural areas four clusters have been found while for urban areas five clusters have been found, i.e., flood awareness programme, local emergency rescue team, training of rescue team members, the efficacy of rescue team members, and another four variables that do not make any cluster at the lower level. Regarding assistance from others, five clusters have been observed for the rural area and the largest cluster of three parameters, i.e., help from political leaders, flood awareness by the teachers, and teacher help to the student while for urban areas two clusters have been noticed and the large cluster has been formed by six parameters, i.e., help from local political leaders, flood awareness by the teacher, teacher help to the student, international help, flood forecasting, and loan for the reconstruction of the broken house. Regarding the joint initiatives of flood preparedness parameters, rural area has one large cluster consisting of flood resilient building, land use planning in practices, crop, and house insurance, having flood-prone areas map and association with NDMO while in urban area four clusters have been found (Fig. 12.8a–f).

12.5 Conclusion

The flood of urban and rural areas of C.D. Block Kandi is mainly triggered due to the overflow of Mayurakshi and its tributaries coupled with the

heavy rainfall or sudden releases of water from the reservoir. The flood magnitude and flood vulnerability between rural and urban areas do not differ significantly. The colossal flood of 2000 diversified the rural occupational structure of the severely flood-affected villages of the C.D. Block Kandi. From 1998 to 2018, the percentage of farmers in rural areas is found to decline. For example, Hijal exhibits a transformation from 84.7% (1998) to 60.13% (2018) and Srikanthapur from 69.09 to 50.36%. However, the labour force is increasing. For example, Hijal exhibits a change from 10.68 to 30.06% and Srikanthapur from 19.51 to 27.38%. Thus, during this period of observation, about 25% of farmers were transformed into labours and servicemen while in municipality wards the transformation is negligible (transformation of 2% of farmers). About 24% of the working population from Hijal have migrated to middle east countries and the migration is observed mainly from the village area. Thus, the receipt of the monthly per capita remittances is about INR 1200 and INR 571 for the villages and municipality wards respectively. On the other hand, the urban area has a higher non-agricultural income compared to the rural counterpart. This typical balancing mechanism induces a similar income profile of the rural and urban areas. Regarding flood preparedness initiatives, the local political party is more active in an urban area, and also different government initiatives are enjoyed by the urban community. However, the rural people are keen on promoting self-help strategies than taking assistance from others.

Acknowledgements The first author (Dr. Aznarul Islam) as the Principal Investigator of the Major Research Project acknowledges the financial support given by the Indian Council of Social Science Research (ICSSR), Government of India vide reference number F.NO. -02/295/16-17/RP to carry out this work.

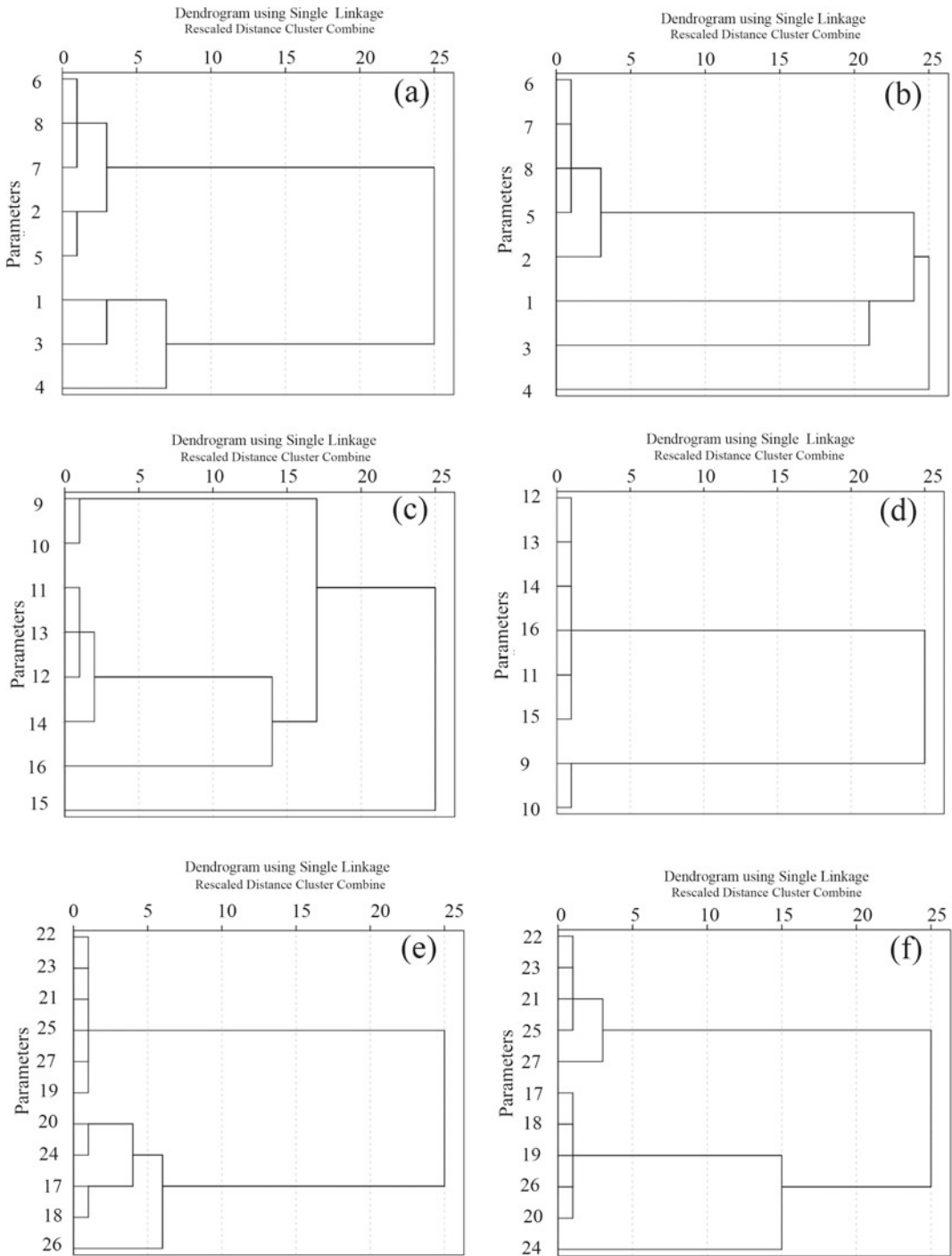


Fig. 12.8 Cluster analysis of flood preparedness. **a** Rural self-help. **b** Urban self-help. **c** Rural others. **d** Urban others. **e** Rural joint ventures. **f** Urban joint ventures

References

- Adebayo W, Arohunsoro JS (2014) Environmental Effects of Urbanization of River Ajilosun Drainage Basin in Ado-Ekiti, Ekiti State, Nigeria. *J Nat Sci Res* 4(2):113–124
- Buciega A, Pitarch MD, Esparcia J (2009) The context of rural–urban relationships in Finland, France, Hungary, The Netherlands and Spain. *J Environ Planning Policy Manage* 11(1):9–27
- Chakraborty L, Rus H, Henstra D, Thistlethwaite J, Scott D (2020) A place-based socioeconomic status index: measuring social vulnerability to flood hazards in the context of environmental justice. *Int J Disast Risk Reduct* 43:101394
- Cilliers DP (2019) Considering flood risk in spatial development planning: a land use conflict analysis approach. *J Disast Risk Stud* 11(1):1–9
- Cutter SL, Barnes L, Berry M, Burton C, Evans E, Tate E, Webb J (2008) A place-based model for understanding community resilience to natural disasters. *Glob Environ Change* 18(4):598–606
- District Census Handbook (2011) Murshidabad District Directorate of Census operation, West Bengal Part XII B Series 20
- Ghosh KG, Mukhopadhyay S (2015) Hydro-statistical analysis of flood flows with particular reference to Tilpara barrage of Mayurakshi River, Eastern India. *ARPN J Earth Sci* 4(2)
- Gupta K (2020) Challenges in developing urban flood resilience in India. *Phil Trans R Soc A* 378(2168):20190211
- Jha VC, Bairagya H (2012) Floodplain planning based on statistical analysis of Tilpara Barrage discharge: a case study on Mayurakshi River Basin. *Caminhos de Geografia* 13(43)
- Islam A et al (2020) Role of human interventions in the evolution of forms and processes in the Mayurakshi. In: Das et al (eds) *Anthropogeomorphology of Bhagirathi-Hooghly River System in India*. CRC Press
- Islam A, Barman SD (2020) Drainage basin morphometry and evaluating its role on flood inducing capacity of tributary basins of Mayurakshi River, India. *SN Appl Sci*. <https://link.springer.com/article/10.1007/s42452-020-2839-4>
- Islam A, Sarkar B (2021) Analysing flood history and simulating the nature of future floods using Gumbel method and Log-Pearson Type III: the case of the Mayurakshi River Basin, India. *Bull Geogr. Phys Geogr Ser* 19(1):43–69
- Islam A, Ghosh S (2021a) Economic transformation in the wake of flood: a case of the lower stretch of the Mayurakshi river basin. *Env Dev Sustain, India*. <https://doi.org/10.1007/s10668-021-01310-6>
- Islam A, Ghosh S (2021b) Community-based riverine flood risk assessment and evaluating its drivers: evidence from rural plains of India. *Appl Spat Anal Policy*. <https://doi.org/10.1007/s12061-021-09384-5>
- Jamshed A, Birkmann J, Feldmeyer D, Rana IA (2020) A conceptual framework to understand the dynamics of rural–urban linkages for rural flood vulnerability. *Sustainability* 12(7):2894
- Jamshed A, Birkmann J, McMillan JM, Rana IA, Feldmeyer D, Sauter H (2021) How do rural–urban linkages change after an extreme flood event? Empirical evidence from rural communities in Pakistan. *Sci Total Environ* 750:141462
- Jahan A, Mahdi A, Muhammad G, Chakma S (2014) Vulnerability and coping strategies of floods in Bangladesh agriculture. *ASA Univ Rev* 8(2)
- Kandi Final Report (2012) DPR for improvement of embankments and ancillary works in Kandi and other adjoining areas of district of Murshidabad. Irrigation and Waterways Directorate Govt of West Bengal
- Le KN, Tam VWY (2007) A survey on effective assessment methods to enhance student learning. *Austr J Eng Educ* 13(2):13–20
- Mahmood S, Rahman AU, Sajjad A (2019) Assessment of 2010 flood disaster causes and damages in district Muzaffargarh, Central Indus Basin, Pakistan. *Environ Earth Sci* 78(3):63
- McMinn WR, Yang Q, Scholz M (2010) Classification and assessment of water bodies as adaptive structural measures for flood risk management planning. *J Environ Manage* 91(9):1855–1863
- Mollah S (2013) Flood hazard in Murshidabad district of West Bengal—an environmental appraisal. An unpublished Ph.D. thesis, Department of Geography, University of Calcutta, Kolkata
- Mollah S (2016) Assessment of flood vulnerability at village level for Kandi block of Murshidabad district, West Bengal. *Curr Sci* 81–86
- Pal S (2015) Assessment of spatial hydrological potentiality: A study on a sub tributary of Mayurakshi river, West Bengal. *Indian J Reg Sci* 47(2):56–63
- Pal S (2016) Impact of Massanjore dam on hydrogeomorphological modification of Mayurakshiriver, Eastern India. *Environ Dev Sustain* 18(3):921–944
- Pal S (2017) Impact of Tilpara barrage on backwater reach of Kushkarni River: a tributary of Mayurakshi River. *Environ Dev Sustain* 19(5):2115–2142
- Rhoades SA (1993) Efficiency effects of horizontal (in-market) bank mergers. *J Bank Financ* 17:411–22
- Satterthwaite D, Tacoli C (2002) Seeking an understanding of poverty that recognizes rural–urban differences and rural–urban linkages. In: *Urban livelihoods: a people-centred approach to reducing poverty*, p 52, 70
- Sahoo SN, Sreeja P (2017) Development of flood inundation maps and quantification of flood risk in an urban catchment of Brahmaputra River. *ASCE-ASME J Risk Uncertain Eng Syst Part A: Civil Eng* 3(1):A4015001
- Suriya S, Mudgal BV (2012) Impact of urbanization on flooding: the Thirusoolam subwatershed—a case study. *J Hydrol* 412:210–219
- Surminski S, Aerts JC, Botzen WJ, Hudson P, Mysiak J, Pérez-Blanco CD (2015) Reflections on the current debate on how to link flood insurance and disaster risk

- reduction in the European Union. *Nat Hazards* 79 (3):1451–1479
- Sanyal J, Lu XX (2006) GIS based flood hazard mapping at different administrative scales: a case study in Gangetic West Bengal India. *Singapore J Tropical Geography* 27(2): 207–220
- Tingsanchali T (2012) Urban flood disaster management. *Procedia Eng* 32:25–37
- Twigger-Ross C (2005) The impact of flooding on urban and rural communities. Environment Agency, Bristol
- UNFCC (2020) Guidelines for Sampling and Surveys for CDM Project Activities and Programme of Activities. EB 69 Report Annex 5. https://cdm.unfccc.int/Reference/Guidclarif/meth/meth_guid48.pdf
- Wesselink A, Warner J, Syed MA, Chan FK, Tran D, Huq H, Huthoff F, Thuy NL, Pinter N, Staveren MV, Wester P, Zegwaard A (2015) Trends in flood risk management in deltas around the world: are we going 'soft'? *Int J Water Govern* 3(4):25–46
- Wu SY, Yarnal B, Fisher A (2002) Vulnerability of coastal communities to sea-level rise: a case study of Cape May County, New Jersey, USA. *Climate Res* 22 (3):255–270



Application of Geospatial Techniques for Urban Flood Management: A Review

13

Biraj Kanti Mondal and Satiprasad Sahoo

Abstract

The present world is fond of urbanization and the rapid urban growth often gave birth to so many new problems, like urban flood and that leads to several other challenges which can be managed with the use of geospatial technology. The urban communities in most of the urban areas of the world are often exposed to vulnerable condition to a greater risk by witnessing urban flood as it has amplified its incidence and magnitude in the current era and India is not an exception. As a consequence, the spatial distribution, extensive mapping, zonation of flood, vulnerability, risk proneness, and risk zonation have now become popular, irrespective of boundaries to deal with the question of urban flood monitoring and management. In this context, the geospatial technology coupled with the Remote Sensing (RS), Geographic Information System (GIS), and Global Positioning System (GPS) has become the powerful and key tool for urban flood management and thus gaining attention in both developed and developing

countries. The Optical to Microwave remote sensing have provided the data of flood mapping analysis in all weather conditions and GIS helps to map the flood hazard, potential areas, vulnerable areas, core attention areas, etc.; therefore, both become vigorously imperative. The remotely sensed hydrological data, geomorphological information, weather information, and Digital Elevation Model (DEM) have becoming more effective, and they furnish the high accuracy of flood estimation derived from the high-resolution remote sensing data and they are powerfully employed to manage urban flood more efficiently and effectively. The current effort is an attempt to highlight the reviews which already worked in various cities of the world, addressing the diverse issues of urban flood management with the application of geospatial techniques, to provide scientific information for the city planners and policy-makers to formulate the resilient urban flood management strategy.

Keywords

Urban • Geospatial techniques • Urban flood • Flood management • Resilient • Strategy

B. K. Mondal
Department of Geography, Netaji Subhas Open
University, Kolkata, West Bengal, India

S. Sahoo (✉)
Department of Geography, Jadavpur University,
Jadavpur West Bengal, India

13.1 Introduction

Flood occurs worldwide in various locations and in diverse magnitudes, and thus this widespread hazard plays a marked and significant role in shaping the environment, economy, and society. Heavy rainfall, uneven distribution of rainfall, improper drainage system, decreasing and decaying of wetlands, etc. are often aggravated together with the uncontrolled urban population growth and density leads to urban flood. Flood is a widespread devastating phenomenon as it affected more than 2 billion people worldwide between 1998 and 2017; loss of life, damages of property, and health hazards are the immediate effects of such incidences. Worldwide, people belong to low-lying areas and floodplains are the most vulnerable, but the urban areas are not an exception to fetch such incidences for diverse reasons. Urban flooding is considered as a type of pluvial flooding caused by surface run-off, and thus this concept is different from fluvial or coastal flooding. The physical characteristics and concrete infrastructure of the urban area and the rate of urbanization are the factors that increase the chances of water logging problem in a larger scale and enhance the occurrences of flood. The flood management especially in urban areas is often becoming very challenging and a tough mission for the urban planners and policy-makers because it must enclose the wellbeing of the inhabited people, maximize the use of resources along with the minimization of human and economic loss and damages caused by the flood. Recently, the geospatial technology coupled with the Remote Sensing (RS), Geographic Information System (GIS) and Global Positioning System (GPS) has become the dominant and solution tool for flood mitigation and management. The vulnerability, risk proneness, flood-affected zones, and attainable areas could easily be found out and mapped through the GIS. Moreover, the advancement from optical to microwave remote sensing has developed in this field, which provides the all-weather capable data for mapping and analysis of flood hazard. The quantification

and reduction of the damages, precaution and assessment of flood, identification of vulnerable areas and prediction of such events through the RS and GIS helps to minimize the harmful effects of flood and superior management can be provided with the diverse applicable ways by geospatial technology. Furthermore, the troubles of socio-economic motion together with transport and communication, contamination of drinking water, unavailability of food and loss of property, aftermath illness along with the structural damages are the consequences of urban flood (Hewitt and Burton 1971). The urban area located in the flat surface or low-lying terrain often have to adjust with the poorly built drainage and sewerage system which often have been blocked by disposed municipal waste. The unplanned or poorly planned urbanization makes the densely concentrated inhabitants vulnerable to urban flood, and therefore the damages become extra-passionate and complex to manage (Jha et al. 2011). Urbanization often found in turn of the switch of wetland, natural vegetation, agricultural land to build up setting, structure and infrastructural enlargement (Adoeye et al. 2009), which has a strong connection with the occurrence of urban flood. Thus, many factors are responsible for the occurrence of urban flood, such as duration and intensity of precipitation, clearance of natural vegetation, land use pattern, natural, quasi-natural and man-made impediments. All of these enhances the occurrence of flood, its frequency, duration of stay, magnitude, inundation and areal expansion which are needed to judge for the mitigation and management, and the application of geospatial technology is the key apparatus for such effort. Different statistical and geospatial techniques have been successfully used for qualitative and quantitative analysis of urban flood to uncover the vulnerable and risk proneness, and thus it contributes a lot in the planning and formulation of appropriate flood management strategies. The magnitude of urban flood can be reduced if adequate emergency prevention, preparedness, response, and sustainable recovery measures are implemented in a timely manner.

Some important studies have been found describing the collision of urbanization and meteorological changes and its connection with the increasement of rainfall in urban area (Guhathakurata et al. 2011; Ghosh et al. 2009; De et al. 2005; De Roo 2000; Rao et al. 2004; Khole and Dey 2001; Roy et al. 2001; De and Rao 2004; Goswami et al. 2006; Sinha et al. 1999); rapport between urbanization and hydrological features like decrease in infiltration, incensement of runoff, increase the number and height of flood occurrence (Alaghmand et al. 2010). Some studies have found RS and GIS as very effectual in identifying the spatial section of flood management as it supplies adequate geographical information (Lowery et al. 1995; Smith 2001); GIS made the flood hazard identification, vulnerability assessment, monitoring and forecasting easier (Roy et al. 2001); while RS intended a synoptic attitude of spatial information, allocation and dynamism of hydrological episode employed to determine and monitor the flood, and quantification of the areal extend easily (Izinyon and Ehiorobo 2011). Currently, greater than 50% population of the world live in the urban area and this is going to accomplish two-thirds by 2050 (IFRC 2010; WHO 2010) and this could be very alarming so far the management of urban flood is concern. Furthermore, the urban flood is considered as dangerous catastrophic events across the globe and ranked as the commonest event with some serious consequences ranging from trivial to foremost accidental (Liu and Li 2017; Gharagozlou et al. 2011; Clement 2013; Ramlal and Baban 2008; Mark et al. 2004). Moreover, the flood risk is increasing with an escalation of hydrological and climatic variables (Masser 2001; Mathew et al. 2012; Messner and Meyer 2006; Mohit and Aktar 1998; Yi et al. 2010; Heywood et al. 1993; Huong and Pathiran 2013), thus and need of the hour is to reduce such urban flood risk in urban areas of the world. In most of the urban areas, the harsh nature of urban flood is exasperated by the predominantly occurred heavy rainfall; stumpy infiltration due to impervious facade, poor and unmaintained prior urban drainage infrastructure, accelerated surface runoff, and related inundation

of low-lying areas (Liu and Li 2017; Few 2003; Chen et al. 2009; Fernandez and Lutz 2010). Such urban flood events are often amplified by the consequences of climate change and unplanned and extensive urban expansion, and therefore diverse techniques have to be employed for effective and efficient management. In this regard, the prologue exercise of geographical information systems (GIS) has improved the estimation of urban floods, identifying poor zones, finding risk-prone zones using diverse analysis and modelling of flood-causing essentials like precipitation, river discharge, drainage systems, depth of groundwater table, and slope to deal the perilous nature of urban floods for resilient management. Different aspects of urban flood elements have been analyzed using multi-criteria spatial analysis, overlay analysis, employment of different models using GIS techniques, and with the help of systematic integration of structural and non-structural events with the community level, flood risk can be lessened to some extent or to an acceptable level.

13.2 Common Concepts in Flood and Flood Management

The relevant and important terms that are closely associated with the urban flood and its management are mentioned in the form of a flowchart (Fig. 13.1).

Flood hazard: In a specific time within an area, the occurrence of an urban flood event showing its potentiality and magnitude and the several factors dependent on it (Crichton 2002; Kron 2005; Dang et al. 2010). The frequency of occurrence, warning time, rate, and increase of water levels, flood depth, duration, velocity, etc. are very important in flood management.

Flood vulnerability: The physical, economic, social, environmental conditions that make the population more susceptible to urban flood hazard is known as flood vulnerability, which has been judged in numerous studies (Alcantara-Ayala 2002; Pelling 2003; ISDR 2004; Barroca et al. 2006; Adelekan 2011). This vulnerability should be studied as vulnerability indicators,

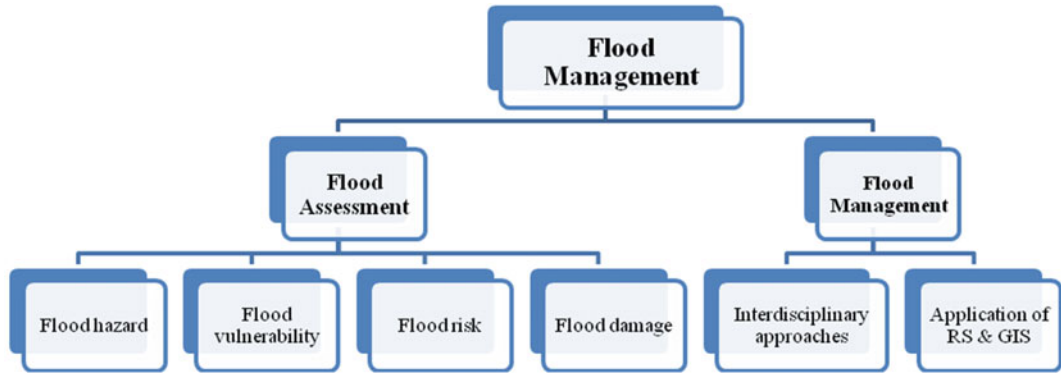


Fig. 13.1 Flowchart of concepts of flood management

susceptibility, exposer, and coping indicators (Weichselgartner 2001; Adelekan 2011) and such kind of information is paramount in determining the flood risk.

Flood risk: The hazards and its potential loss is generally amounted by the flood risk (Crichton 2002; Kron 2005) which signifies the overall effects of urban flooding including the treats of life, danger, evacuating of people, potential damages to the structure, buildings, social disruption, loss of production and community belongings, etc. Thus the flood risk is often expressed by the formula: Flood Risk = Flood hazard x Flood vulnerability (Dang et al. 2010; Karim et al. 2005; Kron 2005; Apel et al. 2009).

Flood damage: The impact of flood damage can be assessed by the amount of flood damage both in tangible and intangible form, which includes agricultural and environmental damages, business interruption, health, etc. (Pielke and Downton 2000; Munich and Topics 2005; Dutta et al. 2003).

Flood management: Urban flood has been gaining increased attention over the years because of the increased rate of urbanization and its connections with the hazards, and significant damages caused to populace, livestock, health, assets, bridges, buildings, communication, homes, and business (Ramlal and Baban 2008; Chen et al. 2009; Few 2003; Mark et al. 2004). In the developed countries, these hazards are devastating to the cities in diverse ways mostly due

to notably extreme precipitation events coupled with dilapidated drainage system generated by over urbanization. The urban flood management reducing its potentiality includes proper and timely analysis of risk assessment employing interdisciplinary approaches with the help of RS and GIS (Barbosa et al. 2012; Chen et al. 2009). The application of RS and GIS techniques in all the four stages (Prediction, Preparation, Prevention and Mitigation and Damage Assessment) of flood management is incredibly effective and fruitful as it has updated and potential appliances.

13.3 Flood Management with the Application of RS and GIS

RS and GIS can provide information about predicted flood events in order to facilitate early prediction and planning and to build up an improved management system. Thus, effective and efficient planning with the help of some models and methods by using geospatial techniques for urban flood management was well adopted in some urban areas of the world. Some of the models like, WetSpa, HYDROTEL, LIS-FLOOD, TOPMODEL, SWAT, (Wang et al. 2011; De Smedt et al. 2000; Fortin et al. 2001; De Roo et al. 2000; Quinn et al. 1991; Arnold et al. 1998; De Smedt et al. 2002); Digital Elevation Model (DEM) and hydrological models were increasing popularity as these models

include the data of land use and land cover, river discharge, rainfall amount, rainfall frequency, surface roughness, spatial and temporal information, etc. Some have used multispectral RS data for employing GIS-based models like Normalized Difference Vegetation Index (NVDI), DEM (Townsend and Walsh 1998; Konadu and Fosu 2009); while several studies worked on different GIS-based hydrological models (De Roo et al. 2000; De Smedt et al. 2000; Usul and Tarun 2006; Batelaan et al. 2007; Chormanski et al. 2008; Stancalie et al. 2009; Kabir et al. 2011) in a more simplified manner to predict flood. The application of geospatial technology in urban flood management is grouped into a single frame (Fig. 13.2).

13.3.1 Flood Hazard Mapping

The identification of potential urban flood-prone area, risk-prone area and probable threat area is very essential in flood management, and this helps the planner, government, and even Non-Governmental Organizations (NGOs) to concentrate on the priority areas, allocating resources in

proper areas. In this regard, the application of geospatial technology have proved powerful in predicting potential flood risk, vulnerability, and hazard (Islam and Sado 2000; Brivio et al. 2002; Hardmeyer and Spencer 2007; Singh and Sharma 2009; Stancalie et al. 2009; Konadu and Foshu 2009; Davor et al. 2016; Farnandez and Lutz 2010; Joy et al. 2019; Patel and Srivastava 2013; Singh and Kanga 2017; Sowmya et al. 2015) as the maps provide simplified information on the flood depth, velocity, direction of flow, inundated area, etc. The season wise (dry and wet) analysis of remote sensing-based satellite data can easily be comparable with the flood inundation models (Samarasinghea et al. 2010) and hydrological models, and helps to validate the accurate information of flood simulation and flood risk mapping in any urban area. The application of recent RS data like Landsat Enhanced Thematic Mapper Plus (ETM +) and ERS (European Space Agency) SAR(Synthetic Aperture Radar) imageries to recognize and categorize the flood depth, flooded zones, and non-flooded areas (Sanyal and Lu 2004; 2005; Solheim et al. 2001) helps to predict floods (Ramlal and Baban 2008; Correia et al. 1999) and build up urban flood resilient strategies.

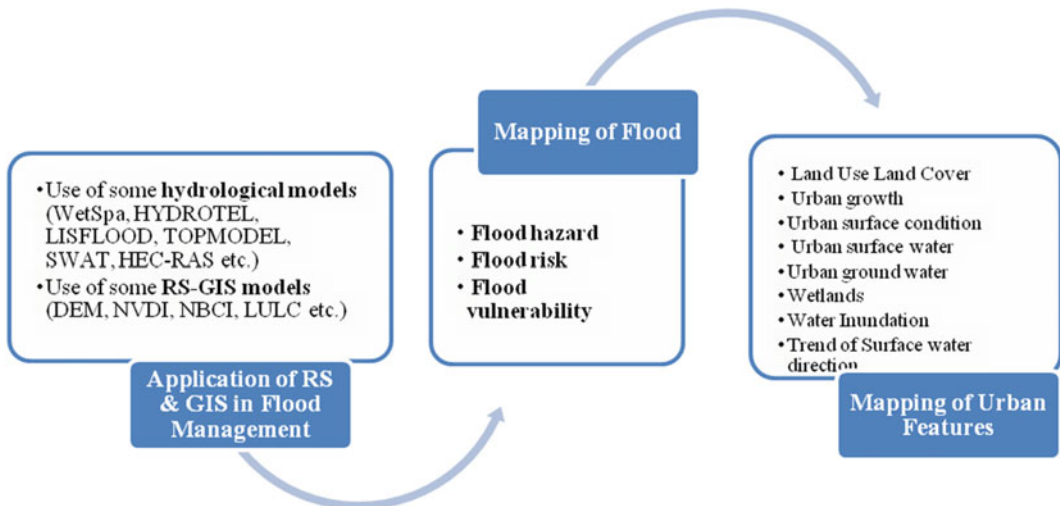


Fig. 13.2 Application of geospatial techniques for flood management

13.3.2 Mapping of Urban Features

As the anthropogenic inputs are very prompt in urban areas and have a larger contribution in occurrence of flood, various factors including urban growth scenarios are needed to consider, and this is the importance of geospatial technology. Urbanization enhances the trend of urban flood and it is anticipated that more than five billion people athwart the globe will inhabit the mega urban areas by the year 2025, which could aggravate the occurrences of urban flood (Masser 2001; Sorensen et al. 2016; Fernandez and Lutz 2010). Therefore, worldwide urban planner, civil engineers, architects, scientist, and environmentalist come forward together for updated and sustainable city planning to reduce the diverse effects of dissimilar hazards like urban flood and other issues. In this context, the geospatial technology easily pointed out the complex network of urban infrastructure, both natural and man-made features using various RS-GIS methods. Similarly, the changes of Land Use Land Cover (LULC) have some serious and valuable non-stop and indirect contributions in the discrepancy and disruption of hydrological cycle and which awkwardly later causes urban flood (Dai et al. 2001; Correia et al. 1999; Betel and Moghanm 2011; Weng 2001; DeVantier and Feldman 1993), and this could be addressed by the application of geospatial technology. Moreover, the spatio-temporal changes of urban expansion can be studied using this technology, which is very effective and necessary to formulate resilient flood management plans. Moreover, it is imperative to note that geospatial technology helps in site selection for waste disposal, location of wetlands, concentration of build up areas and ground water assessment (Dai et al. 2001; Chen et al. 2009; Correia et al. 1999) and facilitate new avenues in building 3D urban mapping models (Esri 2014) for appropriate urban ecosystems

environment, urban land use planning, natural hazards identification, etc.

13.3.3 Preparation of Hydrological Models

In most of the urban areas, the developmental works affect the hydrological setting and water system, and the parameters like rainfall amount, duration, frequency, infiltration, surface runoff, water discharge, water stagnation, inundation, water balance, etc. can effectively be incorporated in building hydrological models for urban flood management with the application of geospatial technology. Thus, with employment of advanced, affordable, available RS and GIS software, the planner can fruitfully develop the proficiency to manage, manipulate, analyze, and display spatial information of urban flood (Sample et al. 2001; Mark et al. 2001; Lekuthai and Vongvisessomjai 2001; Meyer et al. 1993; Tsihrintzis et al. 1996; Lee and Heaney 2003; Diaz-Nieto et al. 2008). The employment of such models helps to attenuate urban flood, quick assessment of sinks, and probable areas of urban flooding for building sustainable resilient strategies. In this regard, the open-source RS data, like Google Earth permits to be updated by the users which could be greatly applied in urban planning, land use planning, infrastructural planning, and fed into an integrated urban flood management plan as it depicts the ground-level scenario (Penanowski et al. 2007; Patterson 2007; Schumann et al. 2007; Liu et al. 2005; Smith and Lakshmanan 2006; Shepard and Cizek, 2009; Whitmeyer 2012; Yu et al. 2008; Chien and Tan 2011; Yu and Gong 2012). Moreover, despite some challenges in the utilization of geospatial technology, many researchers, planners, and government officials are using this sophisticated technology, and thus it gained sombre attention from the users to analyze the

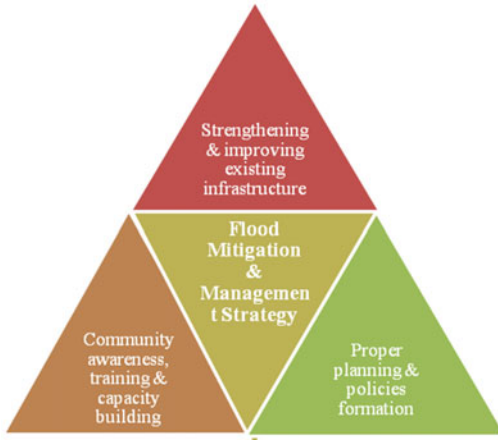


Fig. 13.3 Strategies of urban flood management

miscellaneous and imperative spatial and geo-referenced datasets for the superior urban flood management integrating the local plans, diverse systems, and framework.

13.3.4 Flood Management Strategies

The flood management strategies, especially for the urban area has some solemn methodological

consequences and steps to be followed. In this process, strengthening and improving the existing flood management infrastructure, proper planning, policies formation and community awareness, training, capacity building are considered as the pillars (Fig. 13.3).

It is also imperative to collect the historical records, secondary data, and information from various sources and websites about the flood occurrences; and for the minute observation of the flood scenario, primary survey needs to be completed for the statistical analysis of the ground level urban flood scenario of an urban area. The groundwater data have to be acquired from different sources, and groundwater zonation map, identification of the low-lying areas using Digital Elevation Model (DEM), flow direction map of running water, zonation of water inundation level, Land Use Land Cover (LULC) maps, etc. should be analyzed and mapped and finally statistical methods have been applied for hazard and risk zonation map of urban flood. Moreover, the post-incident part is also important and the employment of geospatial techniques in all phases is becoming powerful for the formation of proper mitigation and to build

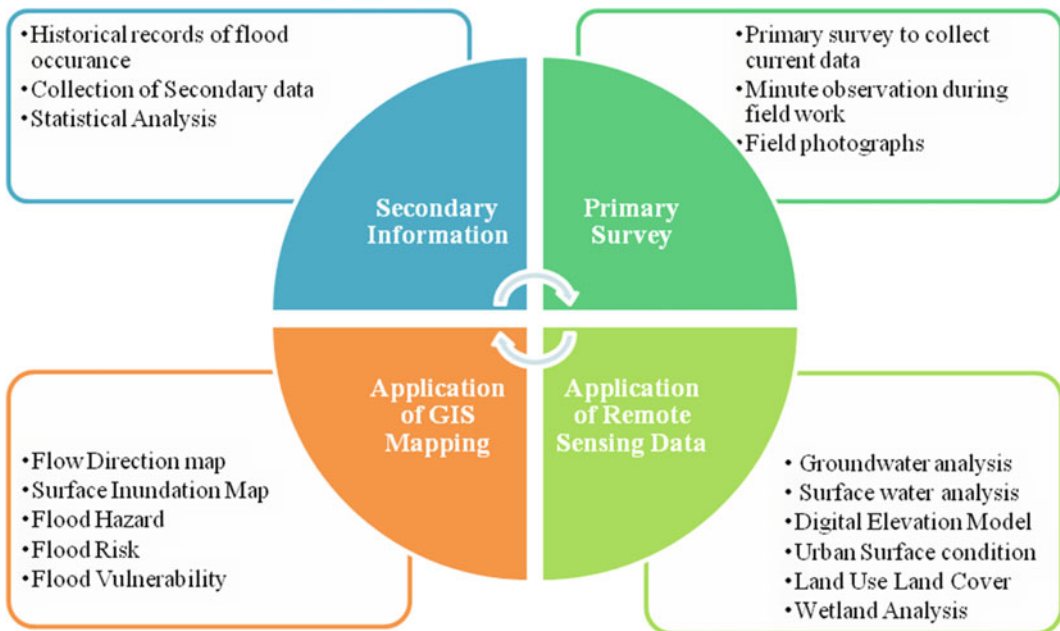


Fig. 13.4 Application of geospatial technology in flood risk assessment for monitoring management

up resilient strategies for superior management. The methodological steps that usually follows in the application of geospatial technology in urban flood risk assessment and monitoring the management is mentioned systematically in the form of a diagram (Fig. 13.4).

A number of recommended measures for the formulation of flood management strategies as recognized in various studies in the context of Indian cities, in combination of the National Disaster Management Guidelines (2010) are grouped into a single window (Fig. 13.5).

13.4 Conclusion

The urban flood occurred primarily due to long-term anthropological reasons and natural situation, still everywhere the anthropological causes are largely highlighted; but the physical settings, climatic conditions, geological, and geomorphological characteristics of the area is also responsible to large extent. The existing review works demonstrate how the urban flood be triggered according to the location, physical setting, and anthropogenic upshots, and all these are

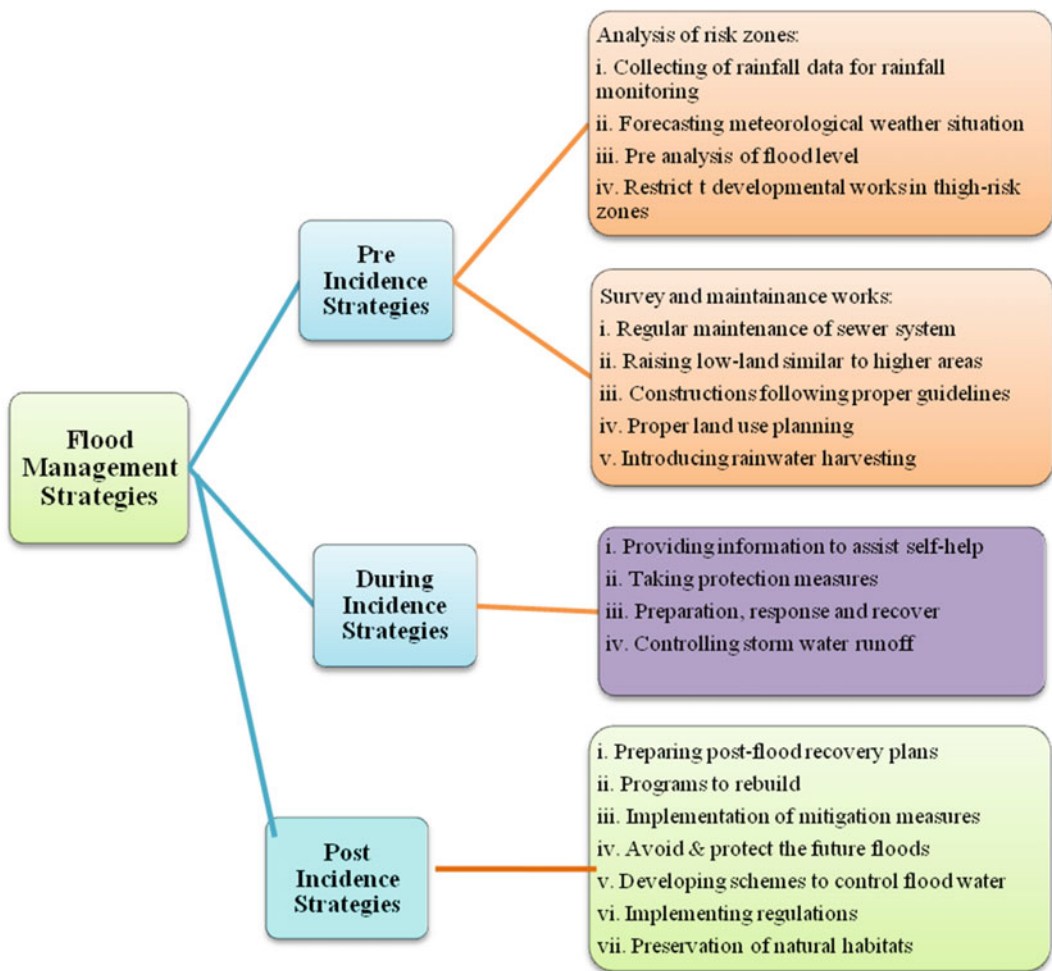


Fig. 13.5 Flood Management Strategies

efficiently explained with the application of geospatial technology. This geospatial technology with the combination of RS and GIS techniques deals with the various aspects of flood issues and holds best to manage the urban flood by prevention, preparedness, and relief management. It also helps to take the appropriate, location-specific flood management strategies, and policies, and if the remedial measures are taken accurately, the effect of such disaster can straight forwardly be reduced and confined into a reduced amount of valuable hazard in near future. Furthermore, this geospatial technology is capable to update and amend the existing flood management system by supplementing or complementing with the combination of various mapping and employment of hydrological (WetSpa, HYDROTEL, LISFLOOD, TOPMODEL, SWAT, HEC-RAS etc.) and RS based models/methods (DEM, NVDI, NBCI, LULC etc.), and thus, this technology has enormous prospect in preparedness in flood proneness, risk assessment, and relief management of every urban spot. Finally, it reveals that the current review effort definitely helps to sketch future research on flood risk analysis and management matters, strategy building, and finding innovative approaches in any urban vicinity employing the geospatial technology.

References

- Adelekan OI (2011) Vulnerability assessment of an urban flood in Nigeria: Abeokuta flood 2007. *Nat Hazards* 56:215–231
- Adeoye NO, Ayanlade A, Babatimehin O (2009) Climate change and menace of floods in Nigerian Cities: socio-economic implications. *Adv Nat Appl Sci* 3(3):369–377
- Alaghmand S, Bin Abdullah R, Abustan I, Vosoogh B (2010) GIS-based river flood hazard mapping in urban area (a case study in Kayu Ara River Basin, Malaysia). *Int J Eng Technol* 2(6):488–500
- Alcantara-Ayala I (2002) Geomorphology, natural hazards, vulnerability and prevention of natural disasters in developing countries. *Geomorphology* 47:107–124
- Apel H, Aronica GT, Kreibich H, Thielen A (2009) Flood risk assessments: How detailed do we need to be? *Nat. Hazards* 49:79–98
- Arnold JG, Srinivasan S, Muttiah RS, Williams JR (1998) Large area hydrologic modeling and assessment. Part 1: Model development. *J Am Water Res Assoc* 34: 73–87
- Barbosa AE, Fernandes JN, David LM (2012) Key issues for sustainable urban stormwater management. *Water Res* 46(20):6787–6798
- Barroca B, Bernardara P, Mouchel JM, Hubert G (2006) Indicators for identification of urban flooding vulnerability. *Nat Hazards Earth Syst Sci* 6:553–561
- Batelaan O, Chormanski J, Canters F, Van de Voorde T (2007) Improved distributed runoff modelling of urbanised catchments by integration of multi-resolution remote sensing. *Proceeding of the geoscience and remote sensing symposium, IGARSS, IEEE* 23–28 July 2007, pp 5021–5024
- Belal AA, Moghanm FS (2011) Detecting urban growth using remote sensing and GIS techniques in Al Gharbiya governorate. *Egypt Egyptian J Remote Sens Space Sci* 14(2):73–79
- Brivio PA, Colombo R, Maggi M, Tomas R (2002) Integration of remote sensing data and GIS for accurate mapping of flooded areas. *Int J Remote Sens* 23:429–441
- Chen J, Hill AA, Urbano LD (2009) A GIS-based model for urban flood inundation. *Journal of Hydrology* 373 (1):184–192
- Chien NQ, Tan SK (2011) Google Earth as a tool in 2-D hydrodynamic modeling. *Comput Geosci* 37(1):38–46
- Chormanski J, Van de Voorde T, Deroeck T, Batelaan O, Canters F (2008) Improving distributed runoff prediction in urbanized catchments with remote sensing based estimates of impervious surface cover. *Sensors* 8:910–932
- Clement AR (2013) An application of Geographic Information System in mapping flood risk zones in a north central city in Nigeria. *Afr J Environ Sci Technol* 7(6):365–371
- Correia FN, da Graca Saraiva M, Da Silva FN, Ramos I (1999) Floodplain management in urban developing areas. Part II. GIS-based flood analysis and urban growth modelling. *Water Resour Manag* 13(1):23–37
- Crichton D (2002) UK and global insurance responses to flood hazard. *Water Int* 27:119–131
- Dai FC, Lee CF, Zhang XH (2001) GIS-based geo-environmental evaluation for urban land-use planning: a case study. *Eng Geol* 61(4):257–271
- Dang NM, Babel MS, Luong HT (2010) Evaluation of food risk parameters in the day river flood diversion area, Red River Delta, Vietnam. *Nat Hazards* 56:169–194. <https://doi.org/10.1007/s11069-010-9558-x>
- Davor KV, Roger AF, Michaela B (2016) Flood Hazard assessment for extreme flood events. *Nat Hazards* 84:1569–1599. <https://doi.org/10.1007/s11069-016-2501-z>
- De Roo APJ, Wesseling CG, Van Deursen WPA (2000) Physically based river basin modeling within a GIS: the LISFLOOD model. *Hydrol Process* 14:1981–1992

- De Smedt F, Liu YB, Gebremeskel S (2000) Hydrologic Modeling on a catchment scale using gis and remote sensed land use information. In: Brebbia CA (ed) Risk Analysis II. WTI Press, Southampton, Boston, pp 295–304
- De Smedt F, Liu YB, Qiao Y (2002) Prediction of floods with the WetSpa model. *Ann Warsaw Agric. Univ SGGW Land Reclam* 33:71–80
- De US, Rao PGS (2004) Urban climate trends—the Indian scenario. *J Indian Geophys Union* 8(3):199–203
- De US, Dube RK, Prakasa RGS (2005) Extreme weather events over India in the last 100 years. *J Indian Geophys Union* 9(3):173–188
- DeVantier BA, Feldman AD (1993) Review of GIS applications in hydrologic modeling. *J Water Resour Plann Manag* 119(2):246–261
- Diaz-Nieto J, Blanksby J, Lerner DN, Saul AJ (2008) A GIS approach to explore urban flood risk management. In: Proceedings of the 11th international conference on urban drainage, Edinburgh, UK (Vol 31)
- EM-DAT (Emergency Events Database) (2006) Disaster profile for floods. International Disaster Database, Retrieved from: <http://www.em-dat.net/disasters/profiles.php>. Retrieved February 16, 2021
- ESRI (2014) 3D urban mapping: from pretty pictures to 3D GIS, An Esri® White Paper. [online] New York, USA: esri. Available at: <https://www.esri.com/library/whitepapers/pdfs/3d-urban-mapping.pdf>. Retrieved May 7, 2021
- Fernández DS, Lutz MA (2010) Urban flood hazard zoning in Tucumán Province, Argentina, using GIS and multicriteria decision analysis. *Eng Geol* 111(1):90–98
- Few R (2003) Flooding, vulnerability and coping strategies: local responses to a global threat. *Progr Dev Stud* 3(1):43–58
- Gharagozlou A, Nazari H, Seddighi M (2011) Spatial analysis for flood control by using environmental modeling. *J Geogr Inf Syst* 3(4):367
- Ghosh S, Luniya V, Gupta A (2009) Trend analysis of Indian summer monsoon rainfall at different spatial scales. *Atmos Sci Lett* 10(4):285–290
- Goswami BN, Venugopal V, Sengupta D (2006) Increasing trend of extreme rain events over India in a warming environment. *Science* 314:1442. <https://doi.org/10.1126/science.1132027>
- Guhathakurta P, Sreejith OP, Menon PA (2011) Impact of climate change on extreme rainfall events and flood risk in India. *J Earth Syst Sci* 120(3):359–373
- Hardmeyer K, Spencer MA (2007) Using risk-based analysis and geographic information systems to assess flooding problems in an urban watershed in rhode island. *Environ Manag* 39:563–574
- Hewitt K, Burton I (1971) The hazardousness of a place: a regional geology of damaging events. Department of Geography Research Publication, University of Toronto, Toronto
- Heywood I, Oliver J, Tomlinson S (1993) Building an exploratory multi-criteria modeling environment for spatial decision support. *Int J Geogr Inform Sci*. <http://libraries.maine.edu/Spatial/gisweb/spatdb/egis/eg94072.html>
- Huong HTL, Pathirana A (2013) Urbanization and climate change impacts on future urban flooding in Can Tho city. Vietnam. *Hydrol Earth Syst Sci* 17:379–394
- IFRC (2010) World Disaster Report 2010: Focus on urban risk. International federation of red cross & red crescent societies, Retrieved February 16, 2021, from: <https://www.ifrc.org/Global/Publications/disasters/WDR/WDR2010-full.pdf>
- ISDR (International Strategy for Disaster Reduction) (2004) A global review of disaster reduction initiatives. Retrieved February 16, 2021, from: http://www.unisdr.org/eng/about_isdr/bd-lwr-2004-eng.htm
- Islam MM, Sado K (2000) Satellite remote sensing data analysis for flood damaged zoning with GIS for flood management. *Ann J Hydraul Eng JSCE* 44. Retrieved February 16, 2021, from: <http://www.un-spider.org/content/4461/satellite-remote-sensing-data-analysis-flood-damaged-zoning-gis-flood-management>
- Izinyon O, Ehiorobo J (2011) Measurements and documentation for flood and erosion monitoring and control in the Niger Delta states of Nigeria. TS07E. Engineering Survey, Marrakech, Morocco, Retrieved February 16, 2021, from: https://www.fig.net/resources/proceedings/fig_proceedings/fig2011/papers/ts07e/ts07e_ehiorobo_izinyon_5126.pdf
- Jha A, Lamond J, Bloch R, Bhattacharya N, Lopez A, Papachristodoulou N, Bird A, Proverbs D, Davies J, Barker R (2011) Five feet high and rising: cities and flooding in the 21st century, policy research working paper 5648, The World Bank, East Asia and Pacific Region, Transport, Energy and Urban Sustainable Development Unit
- Joy J, Kanga S, Singh SK (2019) Kerala flood 2018: flood mapping by participatory GIS approach. *Meloor Panchayat Int J Emer Technol* 10(1):197–205
- Kabir A, Mahdavi M, Bahremand A, Noora N (2011) Application of a geographical information system (GIS) based hydrological model for flow prediction in Gorganrood river basin. Iran. *Afr J Agric Res* 6:35–45
- Karim MF, Minura N, Nobuoka H (2005) Management of storm surge flood risk in the coastal region of Bangladesh. In: Proceedings of the 1st international conference on coastal zone management and engineering in the Middle East.
- Khole M, De US (2001) Socio-economic impacts of natural disasters. *WMO Bull* 50:35–40
- Konadu DD, Fosu C (2009) Digital elevation models and gis for watershed modelling and flood prediction—a case study of Accra Ghana. Appropriate technologies for environmental protection in the developing world, pp 325–332. Retrieved February 16, 2021, from: books.google.com/books?isbn=1402091397
- Kron W (2005) Flood Risk = Hazard · Values · Vulnerability. *Water Int* 30(1):58–68

- Lee JG, Heaney JP (2003) Estimation of urban imperviousness and its impacts on storm water systems. *J Water Resour Plan Manag* 129(5):419–426
- Lekuthai A, Vongvisessomjai S (2001) Intangible flood damage quantification. *Water Resour Manag* 15(5):343–362
- Liu C, Li Y (2017) GIS-based dynamic modelling and analysis of flash floods considering land-use planning. *Int J Geogr Inf Sci* 31(3):481–498
- Liu YB, De Smedt F, Hoffmann L, Pfister L (2005) Assessing land use impacts on flood processes in complex terrain by using GIS and modelling approach. *J Environ Model Assess* 9(4):227–235
- Lowry JH, Miller HJ, Hepner G (1995) A GIS-based sensitivity analysis of community vulnerability to hazardous contaminants on the Mexico/US Border. *Photogramm Eng Remote Sens* 61(11):1347–1359
- Mark O, Apirumanekul C, Kamal MM, Praydal G (2001) Modelling of urban flooding in Dhaka City. In: *Urban drainage modeling*, 333–343
- Mark O, Weesakul S, Apirumanekul C, Aroonnet SB, Djordjević S (2004) Potential and limitations of 1D modelling of urban flooding. *J Hydrol* 299(3):284–299
- Masser I (2001) Managing our urban future: the role of remote sensing and geographic information systems. *Habitat Int* 25(4):503–512
- Mathew S, Truck S, Henderson-Sellers A (2012) Kochi, India case study of climate adaptation to floods. *Glob Environ Change* 22:308–319
- Messner F, Meyer V (2006) Flood damage, vulnerability and risk perception-challenges for flood damage research. In: Schanze J, Zeman E, Marsalek J (Eds), *Flood risk management-hazards, Vulnerability, Mitigation Measures*. NATO Special Series, Springer, Berlin, Heidelberg, New York, pp 149–167
- Meyer SP, Salem TH, Labadie JW (1993) Geographic information systems in urban storm-water management. *J Water Resour Plan Manag* 119(2):206–228
- Mohit MA, Akther S (1998) delineation of flood damaged zones of Dhaka city based on the 1998 flood by using GIS. In: Ali MA, Seraj SM, Ahmad S (Eds), ISBN: 984–823–002–5
- Patel DP, Srivastava PK (2013) Flood hazards mitigation analysis using remote sensing and GIS: Correspondence with town planning scheme. *Water Resour Manag* 27:2353–2368
- Patterson TC (2007) Google Earth as a (not just) geography education tool. *J Geogr* 106(4):145–152
- Pelling M (2003) *The vulnerability of cities: natural disasters and social resilience*. Earthscan Publications, London
- Pezanowski S, Tomaszewski B, d MacEachren AM (2007) An open geospatial standards-enabled google earth application to support crisis management. *Geomatics Solutions for DisasterManagement*. Springer, Berlin Heidelberg, pp 225–238
- Quinn P, Beven K, Chevallier P, Planchon O (1991) The prediction of hillslope flow paths for distributed hydrological modeling using digital terrain models. *Hydrol Process* 5:59–79
- Ramlal B, Baban SM (2008) Developing a GIS based integrated approach to flood management in Trinidad, West Indies. *J Environ Manage* 88(4):1131–1140
- Rao GSP, Jaswal AK, Kumar MS (2004) Effects of urbanization on meteorological parameters. *Mausam* 55:429–440
- Roy L, Leconte R, Brissette F, Marche C (2001) The impact of climate change on seasonal floods of a southern Quebec River basin. *Hydrol Processes* 15:3167–3179
- Roy AH, Wenger SJ, Fletcher TD, Walsh CJ, Ladson AR, Shuster WD, Thurston HW, Brown RR (2008) Impediments and solutions to sustainable, watershed-scale urban stormwater management: lessons from Australia and the United States. *Environ Manage* 42(2):344–359
- Samarasinghea SMJS, Nandalalb HK, Weliwitiyac DP, Fowzed JSM, Hazarikad MK, Samarakoond L (2010) Application of remote sensing and GIS for flood risk analysis: a case study at Kalu-Ganga River, Sri Lanka. *Int Arch Photogr Remote Sens Spatial Inform Sci* 38(8), Kyoto Japan
- Sample DJ, Heaney JP, Wright LT, Koustas R (2001) Geographic information systems, decision support systems, and urban storm-water management. *J Water Resour Plann Manag* 127(3):155–161
- Sanyal J, Lu XX (2004) Application of remote sensing in flood management with special reference to Monsoon Asia: a review. *Nat Hazards* 33:283–301
- Sanyal J, Lu XX (2005) Remote sensing and GIS-based flood vulnerability assessment of human settlements: A case study of Gangetic West Bengal, India. *Hydrol Process* 19:3699–3716
- Schumann G, Hostache R, Puech C, Hoffmann L, Matgen P, Pappenberger F, Pfister L (2007) High-resolution 3-D flood information from radar imagery for flood hazard management. *IEEE T Geosci Remote Sens* 45(6)
- Sheppard SR, Cizek P (2009) The ethics of Google Earth: crossing thresholds from spatial data to landscape visualisation. *J Environ Manage* 90(6):2102–2117
- Singh AK, Sharma AK (2009) GIS and a remote sensing based approach for urban flood-plain mapping for the Tapi catchment, India. *Hydroinformatics in hydrology, hydrogeology and water resources*. Proceeding of the symposium of JS.4 at the Joint IAHS and IAHR Convention, Hyderabad, India
- Singh SK, Kanga S (2017) Mapping of salt affected and waterlogged areas using geospatial technique. *Int J Recent Innov Trends Comput Commun* 5(5):1298–1305
- Sinha Ray KC, Mukhopadhyay RK, De US (1999) Meteorological disasters during last twenty two years. *Natural disasters some issues and concerns*. Natural disaster management cell. VisvaBharati, Santiniketan, 10–23
- Smith K (2001) *Environmental hazards: assessing risk and reducing hazards*. Third Edition. Routledge (Taylor & Francis Group), New York, USA

- Smith TM, Lakshmanan V (2006) Utilizing google earth as a GIS platform for weather applications. In: 22nd international conference on interactive information processing systems for meteorology, oceanography, and hydrology
- Solheim I, Solbo S, Indregard M, Lauknes I (2001) User requirements and SAR-solutions for flood mapping. In: 4th international symposium on retrieval of bio- and geophysical parameters from SAR data for land applications, Innsbruck, Austria
- Sorensen J, Persson A, Sternudd C, Aspegren H, Nilsson J, Nordström J, Jönsson K, Mottaghi M, Becker P, Pilesjö P, Larsson R (2016) Re-thinking urban flood management—time for a regime shift. *Water* 8(8):332
- Sowmya K, John CM, Shrivastava NK (2015) Urban flood vulnerability zoning of Cochin City, southwest coast of India, using remote sensing and GIS. *Nat Hazards* 75:1271–1286
- Stancalie GH, Craciunescu V, Irimescu A (2009) Spatial data integration for emergency services of flood management. In: Jones JAA et al (Eds), threats to global water security, pp 155–165
- Townsend PA, Walsh SJ (1998) Modeling floodplain inundation using an integrated GIS with radar and optical remote sensing. *Geomorphology* 21:295–312
- Tsihrintzis VA, Hamid R, Fuentes HR (1996) Use of geographic information systems (GIS) in water resources: a review. *Water Resour Manage* 10(4):251–277
- Usul N, Turan B (2006) Flood forecasting and analysis within the Ulus Basin, Turkey, using geographic information systems. *Nat Hazards* 39:213–229
- Wang Y, Li Z, Tang Z, Zeng G (2011) A GIS-based spatial multi-criteria approach for flood risk assessment in the Dongting Lake Region, Hunan, Central China. *Water Resour Manage* 25:3465–3484
- Weichselgartner J (2001) Disaster mitigation: The concept of vulnerability revisited. *Disaster Prevent. Manag.* 10:85–94
- Weng Q (2001) Modeling urban growth effects on surface runoff with the integration of remote sensing and GIS. *Environ Manage* 28(6):737–748
- Whitmeyer SJ (2012) Google Earth and virtual visualizations in geoscience education and research (ed. vol 492). Geological Society of America
- WHO (2010) World Disasters Report. Chapter 2 and 6: Focus on Urban Risk. Retrieved from: <http://www.ifrc.org/Docs/pubs/disasters/wdr2010/WDR2010-English-2.pdf>. Retrieved May 7, 2021.
- Yi CS, Lee JH, Shim MP (2010) GIS-based distributed technique for assessing economic loss from flood damage: Pre -feasibility study for the Anyang Stream Basin in Korea. *Nat Hazards* 55:251–272
- Yu L, Gong P (2012) Google Earth as a virtual globe tool for Earth science applications at the global scale: progress and perspectives. *Int J Remote Sens* 33 (12):3966–3986

Index

A

Analytic Hierarchy Process (AHP), 81, 82, 91, 92, 95, 97, 99–101, 105, 110, 119, 121, 126, 127, 132, 133, 137, 139

B

Brahmaputra river, 77, 78, 83, 87
Bridge failure, 196, 199

C

Community preparedness, 216, 218
Cooch Behar, 119, 121, 122, 139

D

Discharge reconstruction, 40, 47

F

Flash flood, 119–133, 135–139
Flash floods hazards, 1, 11
Flood, 15–20, 23–28, 185–196, 198, 203–205, 207, 208, 210–222
Flood control, 73
Flood hazard, 51–53, 55, 56, 58–63, 66, 71, 203, 205, 209, 211, 214
Flood intensity, 79
Flood management, 225–233
Flood risk, 11, 143, 145, 152, 158
Flood susceptibility, 105–107, 111–113, 115
Flood vulnerability index, 91, 97, 100, 101
Frequency Ratio (FR) model, 96, 161–163, 171, 172

G

Geographic Information System (GIS), 52, 53, 56, 73, 92, 94, 143, 151, 152
Geospatial techniques, 225, 226, 228, 229, 231

Geospatial technology, 15

GIS modelling, 1

H

HEC-HMS, 143, 151, 152, 154, 158
HEC-RAS, 143, 152, 155, 158
Himalayan Foreland Basin, 161, 163

L

Land Use and Land Cover (LULC), 77, 82

M

Machine learning, 105, 112, 113, 115
Machine learning algorithms, 1, 11
Modelling, 151–153
Morphometric parameters, 15–18, 20–22, 24, 27
Multi-criteria decision approach, 51, 52

N

Nyabugogo River Basin, 148

P

Palaeoflood events, 43
Palaeohydrology, 34
Palaeostage, 43, 47
Public utility, 185, 189, 191, 193–196

R

Raidak river, 91, 93, 94, 97, 99, 101
Rarh plains, 205, 208
Receiver Operating Characteristics (ROC), 161, 174, 180
Remote sensing, 106
Resilient, 225, 227, 229, 230, 232
Road network, 185, 186, 191, 193, 194, 198

ROC curve, [107](#), [111](#), [113](#), [114](#)
Rural-urban gap, [214](#), [216](#), [219](#)

S

Sensitivity analysis, [105](#), [111](#), [115](#), [116](#)
Silabati River basin, [15](#), [17](#), [18](#), [22](#)
Slackwater deposits, [33–35](#), [40](#), [41](#), [43](#), [44](#), [47](#)
Statistical technique, [92](#), [172](#), [188](#)
Strategy, [225](#), [233](#)
Sub-basin prioritization, [24](#)
Susceptibility mapping, [119](#), [120](#), [123–125](#), [127](#), [128](#),
[133](#), [139](#)
Sustainable basin management, [1](#)

T

Torsa river, [93](#)
Torsa river system, [161](#), [163](#), [164](#), [166](#), [170](#), [174](#), [175](#),
[177–180](#)
Transport infrastructure, [185–187](#), [191](#), [193](#), [196](#)

U

Urban, [225–233](#)
Urban flood, [225–227](#), [229](#), [230](#)

V

Validation, [93](#), [119](#), [120](#), [127](#), [137](#), [225](#)